1981

A study of hydrogen in coals, polymers, oxides, and muscle water by nuclear magnetic resonance; extension of solid state high resolution techniques

Larry Michael Ryan
Iowa State University

RYAN, LARRY MICHAEL

A STUDY OF HYDROGEN IN COALS, POLYMERS, OXIDES, AND MUSCLE WATER BY NUCLEAR MAGNETIC RESONANCE; EXTENSION OF SOLID STATE HIGH RESOLUTION TECHNIQUES

Iowa State University PH.D. 1981

A study of hydrogen in coals, polymers, oxides, and muscle water by nuclear magnetic resonance; extension of solid state high resolution techniques

by

Larry Michael Ryan

A Dissertation Submitted to the
Graduate Faculty in Partial Fulfillment of the
Requirements for the Degree of
DOCTOR OF PHILOSOPHY

Department: Chemistry
Major: Physical Chemistry

Approved:

Signature was redacted for privacy.

In Charge of Major Work

Signature was redacted for privacy.

For the Major Department

Signature was redacted for privacy.

For the Graduate College

Iowa State University
Ames, Iowa

1981

TABLE OF CONTENTS

CHAPTER 1. INTRODUCTION

Many physical methods have been developed during the last forty years which have greatly extended chemists' ability to probe microscopic properties of matter (1); among them, nuclear magnetic resonance (NMR) spectroscopy (2,3) has become one of the most important. Operating in the MHz radio frequency region of the electromagnetic spectrum, NMR measures extremely small energy differences which reflect details of molecular structure and conformation (4-6). To achieve this molecular insight, NMR exploits the nondegeneracy of the nuclear spin states of spin > 0 nuclear isotopes when subjected to a strong, static magnetic field, and the dependence of NMR transition frequencies upon the electronic surroundings (chemical shift), direct (static dipole-dipole) and indirect (J-J coupling) dipolar interactions, and other interactions (quadrupolar, etc.) of nuclei in matter. Also, NMR spectral lineshapes and spin relaxation times are sensitive to dynamic molecular processes (7). As a consequence, nuclear magnetic resonance can provide unique information about molecular motions in roughly the 10^{-2} to 10^{10} Hz range.

Although NMR spectroscopy is a relatively mature field, advances within recent years have led to exciting new applications of NMR in many areas of chemistry. For example, the development of high field, large homogeneity

superconducting magnets and the growth of pulse Fourier transform NMR techniques (7,8) have made it possible for low-sensitivity, low-natural abundance nuclei, e.g., ^{13}C, ^{17}O and ^{15}N, to be measured in a routine manner (9). Those nuclei and others are finding much use in the rapidly growing area of biochemical applications of NMR (10-12). Similarly, nuclei such as ^{113}Cd, ^{119}Sn and ^{207}Pb, which are of interest to inorganic and organometallic chemists, can now be readily studied by NMR (9). Carbon-13 NMR, most notably, has in recent years assumed a major role in organic structure elucidation (13,14) and polymer studies (13-16), where it offers the possibility of direct investigation of molecular backbones. Also, the large chemical shift range of ^{13}C results in highly resolved spectra, in which each carbon atom in the molecular framework typically corresponds to a separate peak in the spectrum (13,14).

Another developing area of NMR research which is of considerable current interest, is high resolution NMR of solids (17-19). It is well known that NMR spectra of solids measured by conventional cw or normal Fourier transform methods are typically broad and usually featureless, with widths of up to about 60 KHz (4,6). In contrast, NMR lines in liquids are usually several orders of magnitude narrower, on the order of 0.1 to 1 Hz, and spectral line separations

of less than 0.1 Hz can be measured. In liquids, this permits the observation of small, high resolution spectral features such as chemical shifts and spin-spin splittings, which identify molecular environments and make NMR a broadly useful analytical and structural tool. In solids, on the other hand, the nuclear resonance behavior is usually dominated by magnetic dipole-dipole interactions among neighboring nuclei, resulting in severe line broadening and the obscuring of chemical shifts (17-19). In addition, anisotropic interactions such as the chemical shift anisotropy, and quadrupolar interactions for nuclei with spin greater than 1/2, can lead to broad complex lineshapes in solids even when dipolar broadening is absent or eliminated (17-19).

In principle, all of these line broadening mechanisms are also present in liquids, but fortunately are attenuated by the rapid, random, translational and reorientational motions of molecules in that state. Artificial, experimental manipulations of nuclear spins can similarly produce spectral line narrowing in NMR (17-19), and during the last decade, a number of sophisticated multiple pulse and sample spinning experiments have been designed to reduce the intrinsic line broadening in solids (17-19). One bonus of these solid state methods is that by selective removal of, e.g., dipolar broadening, one can sometimes observe the

actual anisotropic character of smaller spin interactions (such as the chemical shift anisotropy) which reflect the nonspherical nature of electronic distributions in molecules; in liquids, only the isotropic part of the chemical shift is accessible. It is the purpose of the studies presented in this work to further extend the experimental techniques developed to achieve state-of-the-art resolution in NMR of solids and to apply those and conventional pulse NMR techniques to problems in solid state chemistry.

Following a brief introduction to the basic theory of NMR and NMR line narrowing in solids, Chapter 3 describes the simultaneous application of multiple pulse sequences (17-19) and magic-angle sample spinning (20) to protons in strongly dipolar broadened solids. That method develops the possibility of resolved isotropic hydrogen chemical shifts in such materials. Experiments have been devised for the observation of high resolution chemical shifts in many solids (17-19), but they have not yet been generally available for hydrogen resonances. Carbon-13 and other low abundance isotopes can be observed at high resolution in solids, and recently the resolution of chemically shifted fluorines has been reported (21), but prior to the work described here, it was generally assumed that samples to be studied by proton NMR had to be liquids of low viscosity.

A major impetus for the initiation of the above work was the desire to obtain resolved proton spectra from solid organic fossil materials. Characterization of solid fossil fuels by solid state ^{13}C NMR methods has become an important part of fossil fuel research in recent years (22-30). To compliment those studies, a knowledge of the hydrogen as well as the carbon chemical distributions in fuels is desirable. High resolution ^{1}H and ^{13}C liquid state NMR and solid state ^{13}C NMR is currently providing compositional data on solid fossil fuels and coal derived liquifaction products (31). Such information is important to an understanding of the mechanism of liquifaction processes and in evaluating fuels for their intended end uses (31). As initially conceived, combined multiple pulse and spinning sample NMR would allow hydrogen lines with widths of 60 KHz to be reduced to lines of 10 Hz width. The development of characteristic spectra of model compounds might then allow spectra of coals to be characterized in terms of known compounds. In practice, proton lines obtained in this manner are typically an order of magnitude broader (Chapter 3), and chemical entities in coals and other fossil fuels can not be individually identified. Characterization of aromatic/aliphatic differences is possible and estimates of the average degree of condensation of the aromatic rings

in coals can also be made. Chapter 4 describes those applications of high resolution ^{1}H solid state NMR to solid fossil fuels. This work was greatly enhanced by collaborative measurements using Fourier transform IR spectroscopy by Dr. Peter R. Solomon of Advanced Fuels Research, Inc. Previous ^{13}C NMR measurements of coals by Dr. P. D. Murphy (32) were also helpful.

Chapter 5 is a report of experimental work done in collaboration with A. Cirillo of the University of Wisconsin, Milwaukee and Dr. Jose Fripiat of the Centre National de Recherche Scientifique, CROSCI, Orleans Cedex, France, in which protons in the catalyst $H_{1.65}MoO_3$, were studied. Also, NMR measurements of hydrogens in γ-Al_2O_3 are described.

Finally, Chapter 6 discusses NMR experiments performed in collaboration with Dr. Bing Fung of the University of Oklahoma, to investigate the nature of water in muscle.

CHAPTER 2. BACKGROUND AND LITERATURE SURVEY

Basic Theory

Nuclear magnetic resonance (NMR) is a technique for studying nuclear spin environments using the absorption of radio frequency energy as a probe. The method was first developed in 1946, at Harvard, by Purcell, Torrey, and Pound (2), and independently at Stanford by Bloch, Hansen, and Packard (3). Because the details are well known (4-6), only a brief review is given.

An atomic nucleus with spin $\vec{I}$ has an associated magnetic moment $\vec{\mu}$, given by

$$\vec{\mu} = \gamma\hbar\vec{I} \ , \tag{1}$$

where γ, the magnetogyric ratio, is a constant for a given nucleus. A magnetic moment placed in a static magnetic field $\vec{H}_0$, directed along an arbitrary z axis, will have an interaction described by the Zeeman Hamiltonian

$$H_z = -\vec{\mu}\cdot\vec{H}_0 = -\gamma\hbar\vec{I}\cdot\vec{H}_0 = -\gamma\hbar I_z H_0 \ . \tag{2}$$

I_z is the component of $\vec{I}$ resolved along $\vec{H}_0$. Since I_z can assume any of $2I + 1$ values, specified by the magnetic quantum number $m = I, I-1, \ldots -I$, the possible Zeeman energy levels of the nuclear system are

$$E_m = -\gamma\hbar H_0 m \ . \qquad (3)$$

Thus, the energy separation between adjacent levels is

$$\Delta E = -\gamma\hbar H_0 = \hbar\omega \ . \qquad (4)$$

The selection rule for transitions between energy levels is $\Delta m = \pm 1$, and in nuclear magnetic resonance, transitions are induced between these levels by application of a radio frequency field, H_1, perpendicular to H_0, with a frequency in the region of

$$\vec{\omega}_0 = -\gamma\vec{H}_0 \ , \qquad (5)$$

called the Larmor frequency.

Of course, in a real NMR experiment, we do not deal with an isolated nucleus, but rather an assembly of identical nuclei. At equilibrium, these nuclei are distributed among the available spin energy levels according to a Boltzmann distribution, resulting in a net macroscopic magnetization along z, $\vec{M} = M_z$. F. Bloch first developed (33,34) a set of phenomenological equations to describe the behavior of $\vec{M}$ following any perturbation which disturbs the spin equilibrium. Application of H_1 tips $\vec{M}$ away from H_0 (4), so that transverse components M_x and M_y are generated. These decay to zero ($\vec{M}$ returns to M_z) with characteristic relaxation times (33,34) T_2, the transverse or <u>spin-spin</u>

relaxation time, and T_1, the longitudinal or spin-lattice relaxation time. T_2 is the characteristic time for the exponential decay of the nuclear spin system toward equilibrium within itself (7,8). This time also governs linewidths in the NMR frequency spectrum, since the free induction decay (FID) signal generated by the transverse decay components in a pulse NMR experiment (i.e., following a pulse radio frequency excitation by H_1) is the Fourier transform of the normal NMR absorption line (7,8). T_1 is the characteristic time for the spins to come to equilibrium with the surrounding "lattice," and controls the rate at which a pulse NMR experiment may be repeated (7,8).

High Resolution NMR in Solids

From Equation 5, it is seen that the resonance frequency of a particular nucleus depends on the magnetic field it experiences. In a molecule, a nucleus is not isolated, but rather interacts with surrounding nuclei and electrons, so that the field it experiences is generally different from the applied field, $\vec{H}_0$. In general, the NMR spectrum of a nucleus is governed by a series of interaction Hamiltonians. Those which will be of concern to us are given by

$$H = H_z + H_D^{II} + H_D^{IS} + H_\sigma + H_{rf} \tag{6}$$

where

$$H_z = -\sum_i \gamma I_{zi} H_0 = -\sum_i \omega_0^i I_{zi} \tag{7}$$

$$H_D^{II} = \sum_{i<j} \frac{\gamma^2}{2r_{ij}^{-3}} (\vec{I}_i \vec{I}_j - 3I_{zi}I_{zj}) \times (1-3\cos^2\theta_{ij}) \tag{8}$$

$$H_D^{IS} = \sum_{i<j} \frac{\gamma_i\gamma_j}{2r_{ij}^{-3}} (I_{zi}S_{zj})(1-3\cos^2\theta_{ij}) \tag{9}$$

$$H_\sigma = \sum_i \omega_0^i \sigma_{zzi} I_{zi} \tag{10}$$

and

$$H_{rf}(t) = -\omega_1 I_x \cos\theta t + \omega_1 I_y \sin\theta t \ . \tag{11}$$

H_z is the Zeeman Hamiltonian for the entire nuclear spin system. H_D^{II} is the secular portion of the homonuclear dipolar Hamiltonian, corresponding to direct dipole-dipole interactions between like nuclear spins. H_D^{IS} is the secular portion of the heteronuclear dipolar Hamiltonian.

H_σ is the chemical shift Hamiltonian due to the magnetic shielding produced at a nuclear site by the motion of its orbiting electrons, and finally, $H_{rf}(t)$ is the time dependent interaction between the nuclear spin system and a radio frequency pulse of magnitude H_1.

Each of these Hamiltonians contains information about the nuclear spins being studied, and hence, about the molecular system under study. For example, the direct magnetic dipole-dipole interactions, H_D^{II} and H_D^{IS}, are strongly dependent upon the separation (r) and orientation (θ) of nuclei, and thus may be used to obtain geometrical information on the locations of atoms in solids. r_{ij} is the internuclear distance between nucleus i and nucleus j, while θ_{ij} is the angle between their internuclear vector and H_0. Pake (35) first demonstated many years ago that analysis of dipole-dipole splittings can provide detailed information about molecular geometries in materials where the natural occurance of small numbers of spins in isolated groups produces a relatively simple Hamiltonian, e.g., for protons in H_2O groups in crystalline hydrates (35). In polycrystalline solids, the angles θ are randomly oriented, producing a smearing of the spectral lineshape, and often giving a broad spectrum with no structure at all (4). In such cases, the moments of the resonance line can give information on the microscopic structure of the system (36), and partial

averaging of dipole-dipole interactions by molecular reorientation and diffusion resulting in the narrowing of the resonance can yield information about the nature of molecular motions (4). In any case, dipolar linewidths are generally much greater than the entire range of possible values for smaller interactions such as the chemical shift, effectively preventing their observation in NMR spectra of solids (4). In recent years, a number of solid state NMR techniques have been developed involving methods to alter the nature of the dipolar interactions (17-19).

The first attempts to overcome the dipolar broadening in solids were made independently by E. R. Andrew et. al. (37,38) and I. J. Lowe (39) using high speed sample rotation about a rotation axis inclined at the "magic-angle" of $54^0 44'$ with respect to H_0. It is seen from Equations 8 and 9 that the dipolar interaction between any two nuclei is proportional to $(1-3\cos^2\theta)$. In turn, if the nuclei are rotated about an axis at an angle α with respect to the static field, all of the dipole-dipole interactions aquire a multiplicative term $(1-3\cos^2\alpha)$ (17,18), which becomes zero at the magic-angle. The caveat that goes with this technique is that the rotational speed employed must be comparable to the dipolar linewidth being attacked. For nuclei such as ^1H, ^{13}C, and ^{19}F, which often experience strong dipolar couplings (and which are among the most commonly studied

NMR active nuclei), the rotational speeds required (tens of kilohertz) are prohibitively large (but have been approached by Andrew et al. (40) and by Zilm et al. (41)). Over the past twenty years, a number of uses of this method have been reported (37-62), including the measurement of Knight shifts in metals (49-51), applications to polymer structure determination (52-57, 60-62), and the observation of ^{19}F spin multiplets in KPF_6, $NaPF_6$, and $KSbF_6$ (48). In the latter sample, scalar spin-spin interactions of ^{19}F with both ^{121}Sb and ^{123}Sb were also observed. A review of magic-angle spinning techniques with a description of sample spinning devices has been published by Andrew (63).

Although high speed sample rotation has had moderate success in producing high resolution NMR in some solids, the more recent development of multiple pulse (17-19) and dilute spin double resonance (18,19) methods has made that goal routinely possible for many samples. The basic idea underlyling these techniques is the manipulation of the nuclear spin portion of the dipolar Hamiltonians in a manner analogous to the motional averaging of the geometric term produced by magic-angle spinning. In this case, however, the sample remains stationary, and if a single crystal, in some preferred orientation with respect to the static field (17-19). The spin operators are manipulated by applying short repetetive radio frequency pulse sequences

consisting of pulses with various rf carrier phases and spacing between pulses as described below. In rough analogy with sample rotation, the pulse sequence repetition frequency must be greater than the static dipolar linewidth to achieve a significant degree of line narrowing (17-19). However, with modern pulse spectrometers, pulse spacings of a few μsec are easily achieved (7), so that dipolar linewidths of nearly 100 KHz can now be averaged (17-19). Thus, it becomes possible to consider high resolution NMR in a much wider class of materials, including rigid solids containing hydrogen (17-19).

The first successful multiple pulse sequence applied to improving NMR resolution in solids was the four pulse WAHUHA cycle (64) due to Waugh, Huber, and Haeberlen. The utility of this cycle, which can be represented by $P_{-y}-(\tau-P_x-2\tau-P_{-x}-\tau-P_y-2\tau-P_{-y})_n$, was first demonstrated by the measurement of the chemical shift of the ^{19}F nuclei in a single crystal of CaF_2 (64). P_α here represents a 90^0 rf pulse applied along the α axis in the rotating frame (i.e., $\omega_1 t = -\gamma H_{1\alpha} t = \pi/2$), and τ is a unit of time. In this experiment, the dipolar linewidth of CaF_2 was reduced from tens of kilohertz to 120 Hz (64).

Since the introduction of the WAHUHA by Waugh et. al. in 1968 (64), it has been realized that the effectiveness of this sequence is limited by its sensitivity to H_1 field

inhomogeneities (17,18). In response, a number of more complex multiple pulse sequences have been devised (17-19). The Haeberlen and Waugh eight pulse cycle (65) eliminates the residual broadening produced by coupling of dipolar interactions with H_1 inhomogeneities, but not that produced by chemical shifts or resonance offsets (17,18). Mansfield (66) reported a pulse cycle suitable for line narrowing, described as a four pulse 6τ cycle. Haeberlen et al. (67) described the effect of resonance offsets on 4-pulse, 6-pulse, and phase-altered tetrahedral-angle pulse sequences. Kessemeir and Rhim (68) reported a line narrowing experiment which averages inhomogeneities in the static magnetic field, as well as in H_1. Finally, Rhim, Elleman, and Vaughan (69,70) and, independently, Mansfield (71) developed an eight pulse cycle with further reduction of rf inhomogeneity effects, and also compensation for small errors in pulse phasing and timing. This MREV-8 pulse cycle was able to further reduce the linewidth of CaF_2 from 120 to 17 Hz (69). Figure 1 shows a schematic representation of this sequence. Recently, Haeberlen (17) has suggested that MREV-8 and similar eight pulse cycles might be combined to form compound cycles which even more efficiently eliminate the effects of dipolar interactions in solids. Such compound cycles of 24 and 52 pulses have been recently introduced by Burum and Rhim (72-74) which have substantially more resolving power than previously available sequences.

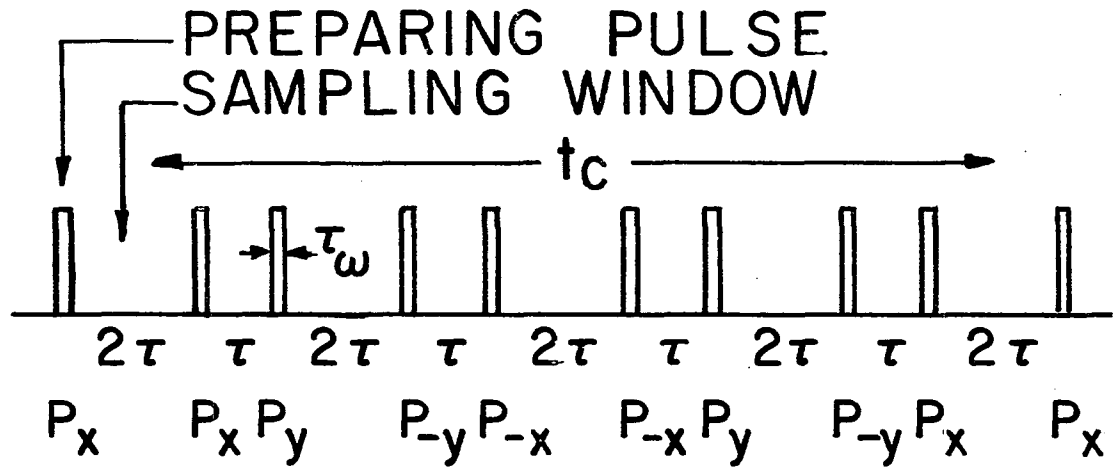

Figure 1. The MREV-8 multiple pulse sequence used for removal of homonuclear dipolar broadening. The cycle time of the sequence is t_c and the pulse width is t_ω

In addition to these multiple pulse cycles, which suppress the effects of homonuclear dipolar interactions in solids, dilute spin double resonance methods have also been described (74-78) for the observation of dilute spins, e.g., ^{13}C or ^{15}N, without the effects of heteronuclear broadening. In this thesis, we will be concerned primarily with hydrogen in solid materials, and therefore, with multiple pulse NMR.

In order to discuss these multiple pulse experiments, a theoretical framework has been developed by Waugh and others (64,65,70,71,74, 79-85) which is well-adapted to interpreting experimental results and developing new methods. The starting point for this "Average Hamiltonian Theory" is a description of the nuclear spin system in terms of the density matrix, ρ (6). In a pulse NMR experiment, the signal detected is proportional to a component of the nuclear spin angular momentum operator, $\vec{I}$, in the xy plane (7), or

$$\langle I_x(t) \rangle = Tr(\rho(t) I_x) \quad . \tag{12}$$

Then, if the spin system is subjected to a train of rf pulses, the time development of the spin system is describable in terms of the time evolution of the density matrix. The equation of motion for the evolution of the density

matrix is (79)

$$i\hbar \frac{\partial \rho}{\partial t} = [H, \rho] \quad , \tag{13}$$

where H is the nuclear spin Hamiltonian. In the interaction frame of the Zeeman interaction (i.e., the rotating frame with $\omega_0 = \gamma H_0$), H can be written as

$$H(t) = H_{int} + H_{rf}(t) \tag{14}$$

where

$$H_{int} = H_o + H_\sigma + H_D \quad . \tag{15}$$

H_o is the offset Hamiltonian ($H_o = -\gamma(\omega_0 - \omega) I_z$), H_σ the chemical shift, and H_D the truncated dipolar interaction.

It can be shown (79, 86) that the solution of Equation 13 may be written in terms of the density matrix $\rho(o)$, at some initial time $t = o$, as:

$$\rho(t) = U(t,o)\rho(o)U(t,o) \tag{16}$$

where

$$U(t,o) = U_{rf}(t,o)U_{int}(t,o) \tag{17}$$

with

$$U_{rf}(t,o) = T \exp\{-i \int_o^t H_{rf}(t')dt'\} \tag{18}$$

and

$$U_{int}(t,o) = T \exp\{-i \int_o^t \tilde{H}_{int}(t')dt'\} \qquad (19)$$

and

$$H_{int}(t) = U_{rf}^{t}(t,o) H_{int} U_{rf}(t,o) \quad . \qquad (20)$$

T is the Dyson time ordering operator, meaning that Equations 18 and 19 can be extremely complicated for an arbitrary $H_{rf}(t)$. However, simplifications occur by using a pulse sequence which is both periodic and cyclic, i.e.

$$H_{rf}(t + Nt_c) = H_{rf}(t) \qquad \text{(periodic)} \qquad (21)$$

$$\int_o^{Nt_c} H_{rf}(t)dt = 0 \quad , \qquad \text{(cyclic)} \qquad (22)$$

and by restricting observation of the spin system to integral multiples of the cycle time, t_c (35). From Equations 18 and 22,

$$U_{rf}(Nt_c,o) = T \exp(o) = 1 \quad , \qquad (23)$$

and then

$$U_{int}(Nt_c,o) = \{U_{int}(t_c,o)\}^N \quad . \qquad (24)$$

Now $U(Nt_c,o)$ can be expanded using the Magnus formula (87),

$$U_{int}(Nt_c,o) = \exp\{-iNt_c(\bar{H}_{int}^{(0)} + \bar{H}_{int}^{(1)} + \bar{H}_{int}^{(2)} + \ldots)\} \quad , \qquad (25)$$

where

$$\bar{H}_{int}^{(0)} = \frac{1}{t_c} \int_0^{t_c} \tilde{H}_{int}(t')dt' \tag{26}$$

$$\bar{H}_{int}^{(1)} = \frac{-i}{2t_c} \int_0^{t_c} dt'' \int_0^{t''} dt' [\tilde{H}_{int}(t''), \tilde{H}_{int}(t')] \tag{27}$$

$$\bar{H}_{int}^{(2)} = \frac{1}{6t_c} \int_0^{t_c} dt''' \int_0^{t'''} dt'' \int_0^{t''} dt' \{ [\tilde{H}_{int}(t'''), [\tilde{H}_{int}(t''), \tilde{H}_{int}(t')]] + [\tilde{H}_{int}(t'), [\tilde{H}_{int}(t''), \tilde{H}_{int}(t''')]] \} \quad . \tag{28}$$

The strong condition for convergence of this series is

$$t_c || \tilde{H}_{int}(t) || << 1 \quad , \tag{29}$$

where $|| \tilde{H}_{int}(t) ||$ is the magnitude of the internal interaction averaged by the particular pulse cycle used. At times $t = Nt_c$, then, the density matrix behaves as if it develops under an "effective" Hamiltonian

$$\bar{H}_{int} = \bar{H}_{int}^{(0)} + \bar{H}_{int}^{(1)} + \bar{H}_{int}^{(2)} + \ldots \quad , \tag{30}$$

which is time independent. By our choice for H_{rf}, we can thus control the Hamiltonian under which the spin system appears to evolve, and obtain results which are quite different from conventional NMR experiments. $\bar{H}_{int}^{(0)}$, the limiting Hamiltonian for short t_c, is called the "average" Hamiltonian (65, 83) of the system.

Most applications of the theory outlined above have been in the development of pulse sequences which will remove or attenuate the homonuclear dipolar broadening in solids. One such sequence is the MREV-8 pulse cycle shown in Figure 1. The average Hamiltonian for the eight pulse cycle, assuming an H_{int} given by Equation 15, is (85)

$$\bar{H}^{(0)}_{\delta\omega} = \frac{1}{3} \sum_i (\delta\omega)\{(1+2a)(I_{xi}+I_{zi}) - \epsilon_i I_{zi}\} \tag{31}$$

$$\bar{H}^{(0)}_{\sigma} = \frac{1}{3} \sum_i (\omega_o \sigma_{zzi})\{(1+2a)(I_{xi}+I_{zi}) - \epsilon_i I_{zi}\} \tag{32}$$

$$\bar{H}^{(0)}_{D} = 0 \tag{33}$$

$$a = \frac{3t_w}{t_c}\left(\frac{4}{\pi} - 1\right) \quad , \tag{34}$$

where the effects of H_1 inhomogeneity (ϵ_i being the pulse length error introduced by H_1 inhomogeneity) and finite pulse widths, t_w, were taken into account. Also, $\bar{H}^{(1)}_D$ is equal to zero for this sequence (85). Thus, the effective Hamiltonian has no contribution from the homonuclear dipolar Hamiltonian to first order.

In contrast, the dipolar average Hamiltonian under the WAHUHA four pulse sequence is

$$\bar{H}^{(0)}_{D} = \sum_{i<j} \{\frac{6}{\pi}\frac{t_w}{t_c} + \epsilon_i\} B_{ij} \{I_{yi}(I_{xj}+I_{zj}) + (I_{xi}+I_{zi})I_{yj}\} \quad , \tag{35}$$

where B_{ij} is the geometric part of the dipolar Hamiltonian. Equation 35 indicates that the WAHUHA has a contribution from both inhomogeneity induced pulse length errors and finite pulse widths.

One distinguishing feature of high resolution multiple pulse NMR spectra of solids, in comparison to NMR of liquids, is that the former allows for the observation of the anisotropy of chemical shifts. In liquids, rapid molecular motions average what is actually a tensorial quantity, $\bar{\bar{\sigma}}$, so that only the isotropic part is accessible, or

$$\bar{\sigma} = \frac{1}{3}\mathrm{Tr}(\bar{\bar{\sigma}}) = \frac{1}{3}(\sigma_{xx} + \sigma_{yy} + \sigma_{zz}) \quad , \tag{36}$$

where $\bar{\bar{\sigma}}$ is the magnetic shielding (chemical shift) tensor, and the σ_{ii} are its principal components (17, 18). While the utility of $\bar{\sigma}$ is beyond contention, and isotropic chemical shifts have been used extensively to investigate a wide variety of phenomena (5, 88), considerably more information is potentially available from a knowledge of the individual quantities that characterize $\bar{\bar{\sigma}}$ (17-19). For example, the nonspherical nature of the electronic distributions around atoms involved in chemical bonding is directly indicated by differences between the three principal values of the chemical shift tensor (17-19). In liquids, from the trace of the chemical shift one can only infer information on such anisotropy.

With the development of multiple pulse and dilute spin techniques for the suppression of dipole-dipole interactions, it has become possible to measure magnetic shielding tensors for many nuclei in a variety of compounds (17-19). For a complete characterization of $\bar{\bar{\sigma}}$, a specification of the chemical shielding along three orthogonal directions and the angles relating this system to the molecular framework is required (17, 18). This generally involves a single crystal study, although recently it has been demonstrated that a correlation of the dipolar and chemical shift Hamiltonians in a single experiment can provide detailed orientational information in polycrystalline samples as well (89-92). In randomly oriented amorphous or polycrystalline solids, because all molecular orientations are present simultaneously, a spectral distribution is typically observed (17-19). These distributions are known as powder patterns, and Figure 2 shows the theoretical powder spectrum lineshape for the general case where $\sigma_{xx} \neq \sigma_{yy} \neq \sigma_{zz}$. In the case of axial symmetry, where two of the components are equal, the lineshape appears as in Figure 3. The theoretical analysis of these lineshapes has been dealt with elsewhere (17, 18, 93).

Spectra of randomly oriented samples of all but the simplest materials, even with dipolar decoupling, can still

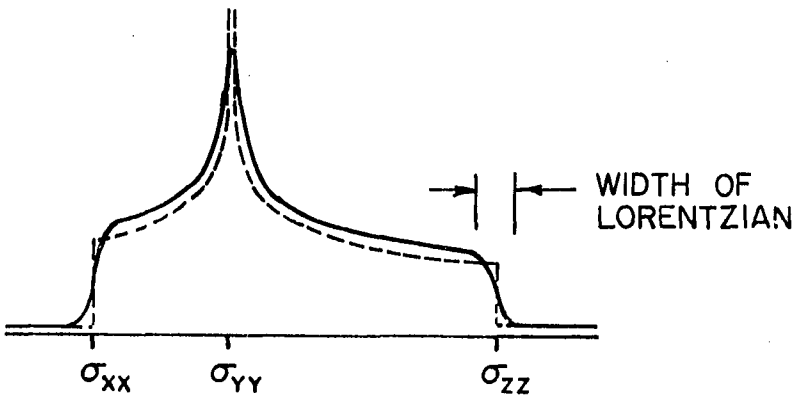

Figure 2. The theoretical powder line shape for an arbitrary chemical shift tensor. The full curve gives the experimental line shape where residual broadening is superimposed

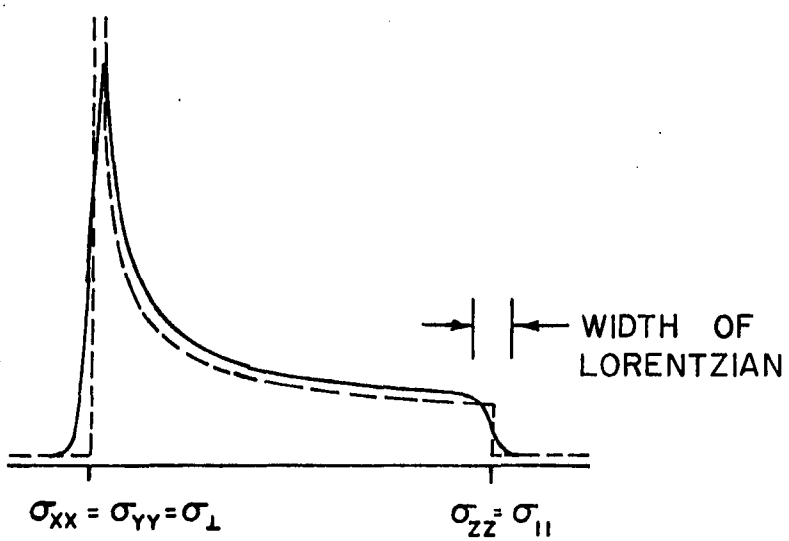

Figure 3. The theoretical and experimental line shapes for an axially symmetric chemical shift tensor

exhibit broad lineshapes which are difficult to interpret. This is because chemical shift anisotropies tend to be larger than the entire range of isotropic shifts for a given nucleus (17, 18), so that for randomly oriented solids with several chemically inequivalent nuclei (i.e., most solids), individual powder patterns may severely overlap, resulting in nondescript spectra in which the chemical shifts and smaller features are, again, entirely masked. Such spectra can be simplified by combining strong dipolar decoupling with magic-angle sample spinning (19). This is because the chemical shift anisotropy, $\Delta\sigma$, like H_D^{II} and H_D^{IS}, is proportional to $(1 - 3\cos^2\theta)$ (17-19). In this case, however, since magic-angle spinning is only required to suppress the chemical shift anisotropy, and not the dipolar broadening, the rotational speeds required are typically less than 4 KHz (at field strengths of less than about 2.5T). This approach, combining two high resolution NMR techniques, has proven to be useful for cases involving heteronuclear broadening of ^{13}C by ^{1}H, with applications to polymer (94-96) and coal (23-26) structure analysis, isomerization (97), and chemical exchange processes (98) having been reported.

Recently, it was also demonstrated that it is possible, by combining a multiple pulse experiment with magic-angle spinning, to simultaneously suppress homonuclear dipolar

broadening and magnetic shielding anisotropies (21). In that work, the resolution of chemically shifted fluorines was reported. In the following chapter is described the extension of combined multiple pulse NMR and magic-angle spinning to the separation of isotropically shifted hydrogens in randomly oriented solids with strong homonuclear dipolar interactions. Because of the relatively smaller range of isotropic shifts typical of protons, about 10 ppm compared with 200 ppm for carbon or fluorine, resolution requirements for separation of individual lines were generally found to be more severe in these systems.

CHAPTER 3. ISOTROPIC PROTON NMR SPECTRA OF RIGID, RANDOMLY ORIENTED SOLIDS

Introduction

As described in the two previous chapters, there are generally at least two major difficulties associated with obtaining high resolution nuclear magnetic resonance spectra of spin 1/2 nuclei in polycrystalline or amorphous solids. First, static dipole-dipole interactions often severely broaden spectral resonances, and second, even with strong dipolar decoupling, NMR spectra of solids may still be sufficiently broad because of overlapping chemical shift powder patterns, so that chemically important spectral features are still not observable. To obtain chemical shift information in such cases, it is necessary to suppress both dipolar broadening and chemical shift anisotropies. In this chapter are described experiments combining multiple pulse ^{1}H-^{1}H dipolar decoupling and magic-angle sample spinning for the measurement of high resolution NMR spectra of hydrogens in randomly oriented solids. High resolution spectra of protons in rigid organic solids and amorphous polymers have been recorded, and under those conditions, isotropic chemical shifts were obtained with individual linewidths varying from about 55 to 110 Hz (1-2 ppm).

Also, as shown by Dybowski and Vaughan (99), and subsequently by Lau et al. (100), it is sometimes possible to use combinations of different multiple pulse experiments to estimate the size of individual contributions to NMR linewidths from a number of different line broadening mechanisms. In addition to the production of isotropic solid state ^{1}H chemical shift spectra, part of the work described in this chapter was devoted to determining the contributions to the residual linewidths, and therefore, the current limits of resolution for proton NMR in rigid systems.

Experimental Details

The spectrometer

The pulse NMR spectrometer used in these experiments is similar to those discussed by Ellett et al. (101) and Vaughan et al. (102), and, except for the recent incorporation of a microprocessor based pulse programmer (103, 104), has been described in detail elsewhere (105). Only a brief description is given here.

A block diagram of the spectrometer is shown in Figure 4. It is a broad band unit, operating at a frequency of 56 MHz for protons. An external deuterium lock stabilizes the unit to within 30 Hz to permit signal averaging. Tuned circuits have been used wherever possible, as

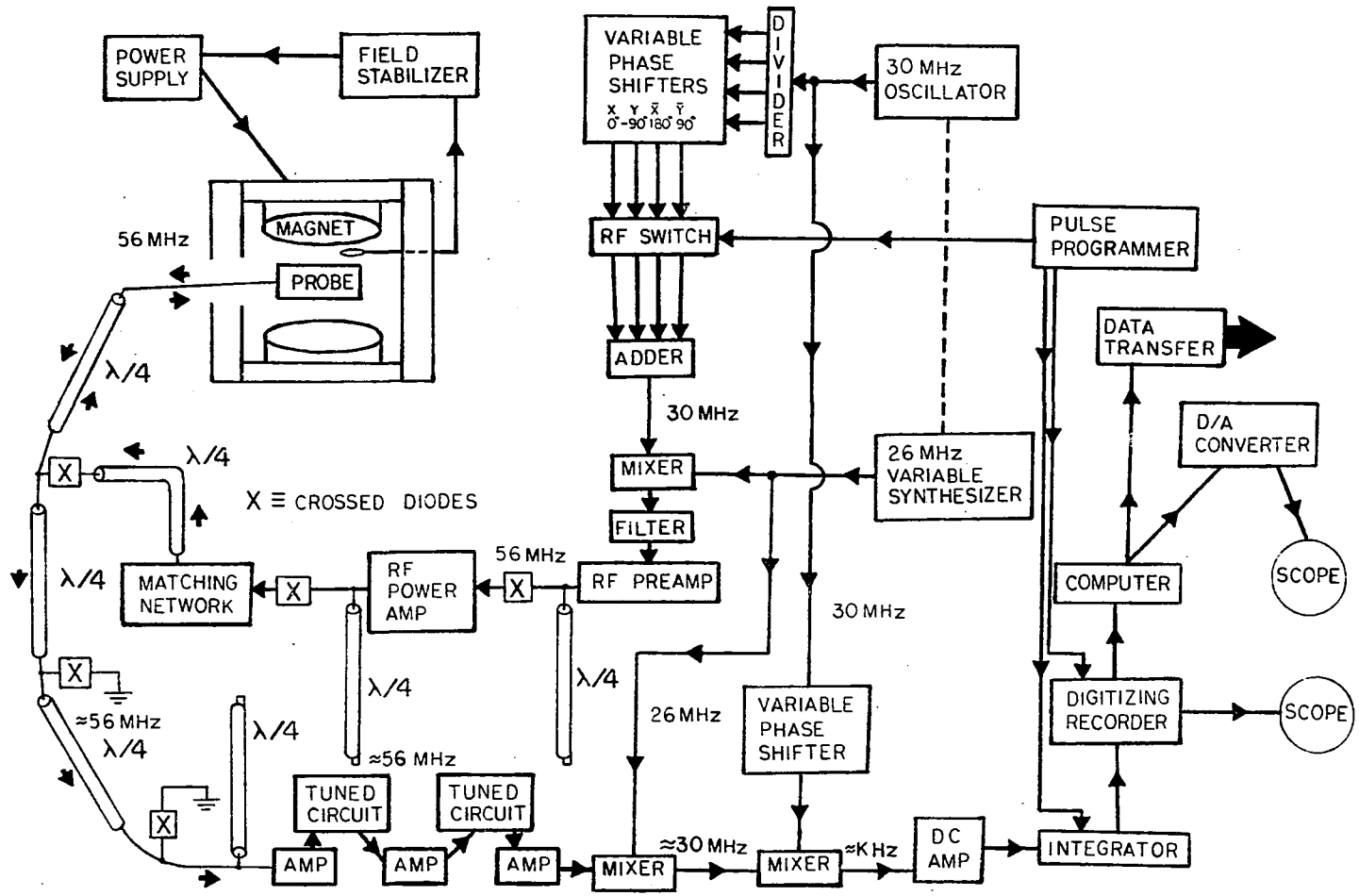

Figure 4. Block diagram of multiple pulse spectrometer used for homonuclear decoupling experiments

indicated in Figure 4, to improve signal-to-noise. However, Q's have been purposely kept low to minimize pulse transients.

The receiver consists of three stages, the first being an Avantek Model 511 amplifier, and the second two being Spectrum Microwave Model SMLD-10 limiting amplifiers, with a total gain of about 60 db. The unit was tuned to operating frequency by inserting series tuned LC circuits between the first and second, and second and third stages, and thereby, signal-to-noise was maximized. The transmitter is an IFI Model 404 distributed amplifier system, capable of 500 watts in pulsed operation. With proper matching of the transmitter to the NMR probe by a pi circuit to symmetrize and minimize phase transients, and with a probe Q of about 30, ninety degree pulses can be generated with this spectrometer in about 1 μsec. Total dead time between the start of a pulse and reception of undistorted NMR signal is approximately 3.5 μsec, with most of the recovery period following pulse overload being accountable to probe ringdown. The transient recorder is a Biomation 805, which has a minimum sampling time of 0.2 μsec per channel. The memory of the unit contains 2048 eight-bit words. It is interfaced to a PDP 11/10 computer for signal averaging and data manipulation (e.g. Fourier transformation, data smoothing, etc).

The pulse programmer is a highly versatile general purpose pulse generator, capable of generating complex pulse sequences of up to four different rf phases, for use in pulse and multiple pulse NMR applications. Pulse sequencing and timing is entered through a Decwriter keyboard, followed by interpretation and execution by internal processors. The unit has four analog controlled pulse channels with digital control to 0.1 μsec resolution and range from 1 μsec to about 100 msec. Also available are three channels for triggering of experimental events. The programmer is based on an inexpensive Motorolla (106) M6800 microprocessor system, and was designed and constructed at Iowa State University (104).

The probe

Like the spectrometer, the NMR probe used in this particular work has been described in the literature (107, 108). Figure 5 gives an indication of the probe's physical makeup. It consists of a brass tube, 31.75 mm wall, 3.81 cm o.d., machined to allow access to the probe circuitry. The tube is fitted into a brass mount which has an O-ring bearing to allow for smooth manual rotation of the tube to any desired angle. In use, the mount is fixed to an NMR probe stand centered in the air gap of a 30.5 cm electromagnet. The circuitry consists of a standard

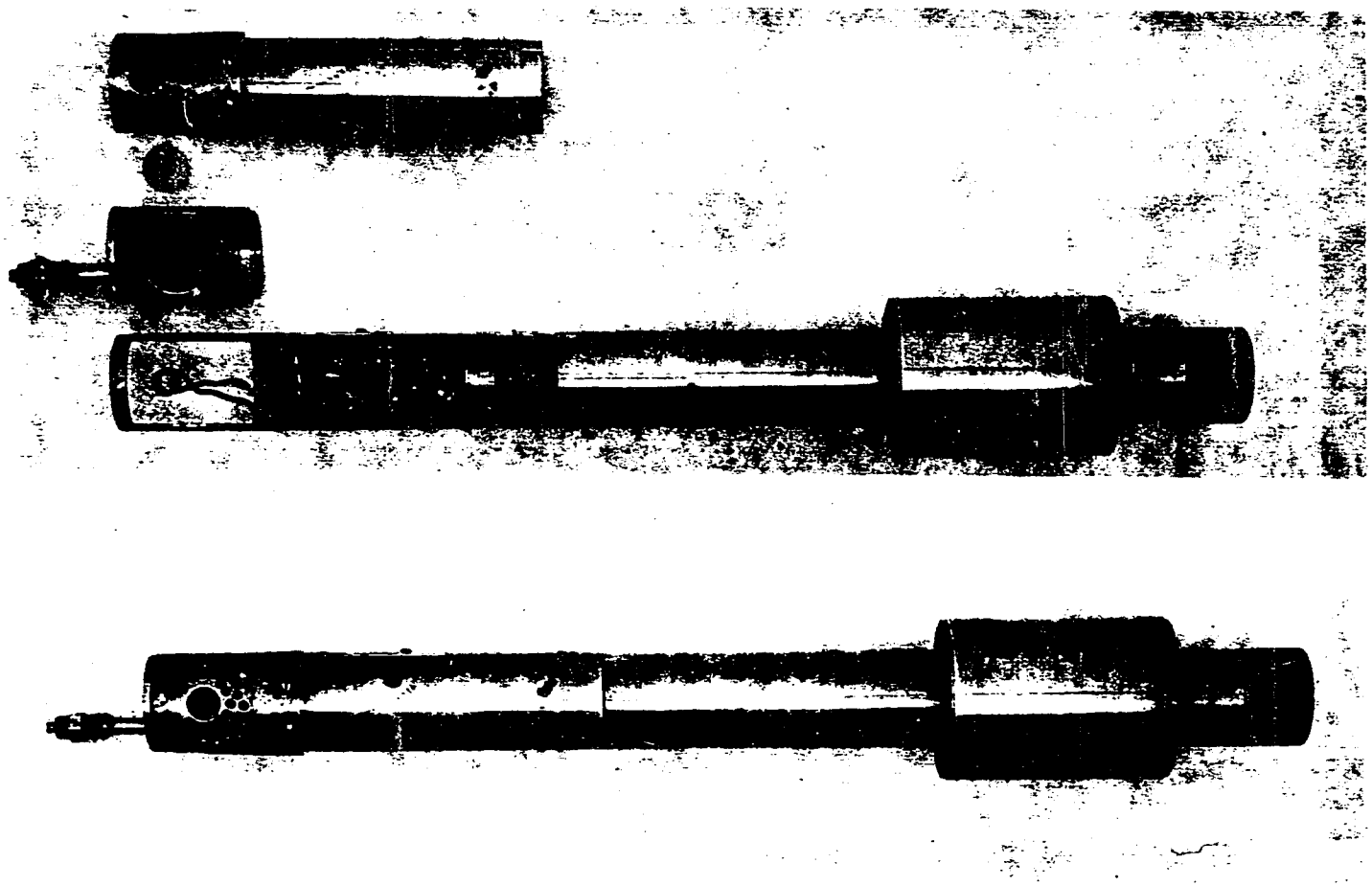

Figure 5. NMR probe for combined multiple pulse magic-angle sample spinning experiments. Top to bottom: the probe shield, rotor, stator, probe body, and assembled probe

tapped-series tuned circuit (109), shown in Figure 6. Two changes have been made in this probe since it was first described (107, 108). First, the resin insulated wire used for the sample coil L was replaced by wire with no coating. Secondly, the ceramic capacitor employed as the high voltage capacitor C_1 (107, 108) was replaced by a Polyflon VC 25-6-25 capacitor. The first change was necessary to obtain good quantitative results in ^1H measurements, since the resin coating contained protons and was therefore "seen" by the sample coil. The latter alteration improved the voltage breakdown characteristics of the probe.

Sample rotors

In order to remove chemical shift anisotropies from dipolar narrowed NMR spectra of protons at a field strength of 1.4 T, it is necessary to spin samples at the magic-angle at speeds of at least 1-2 KHz. To accomplish this, rotors of the Beams-Andrew type (40, 110-112) were machined from polychlorotrifluoroethylene (KEL-F). Three different models of rotors were designed and used.

The first model, used mainly in the experiments described in this chapter, is shown in Figure 7. Powdered samples are packed in the neck of this rotor, and may be kept in place during operation by a Teflon plug (not shown) placed above the sample. Alternatively, most polycrystal-

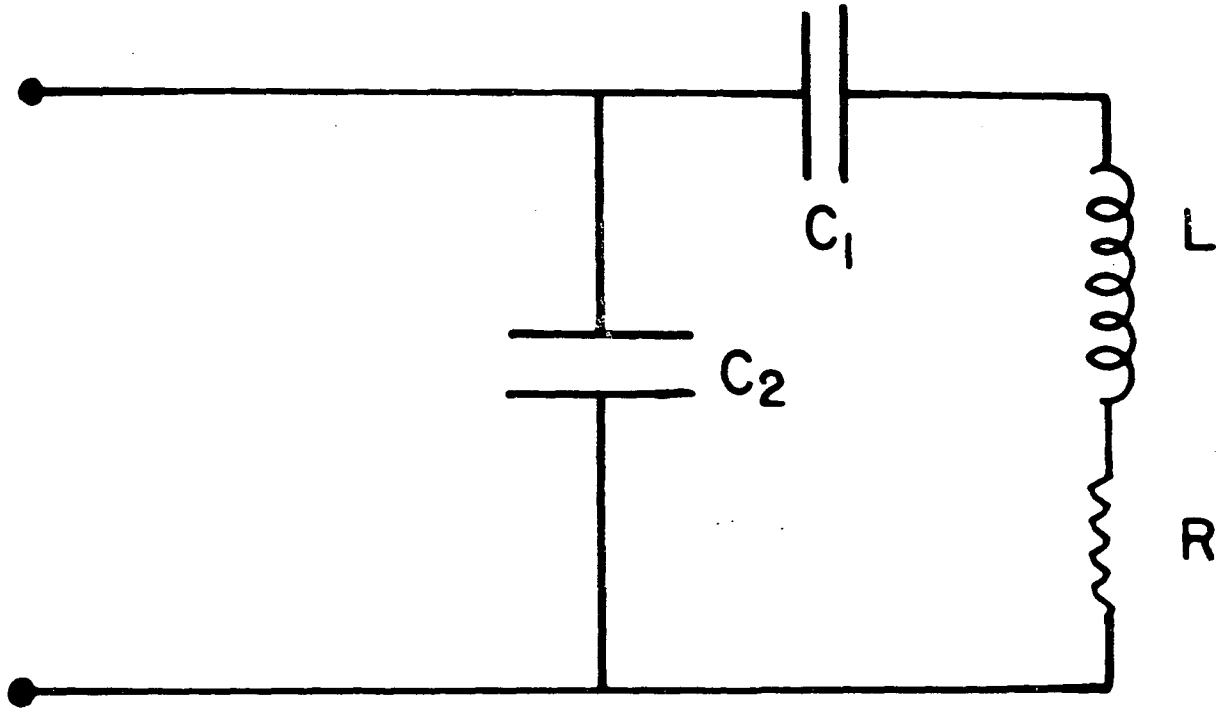

Figure 6. Tapped-series tuned circuit

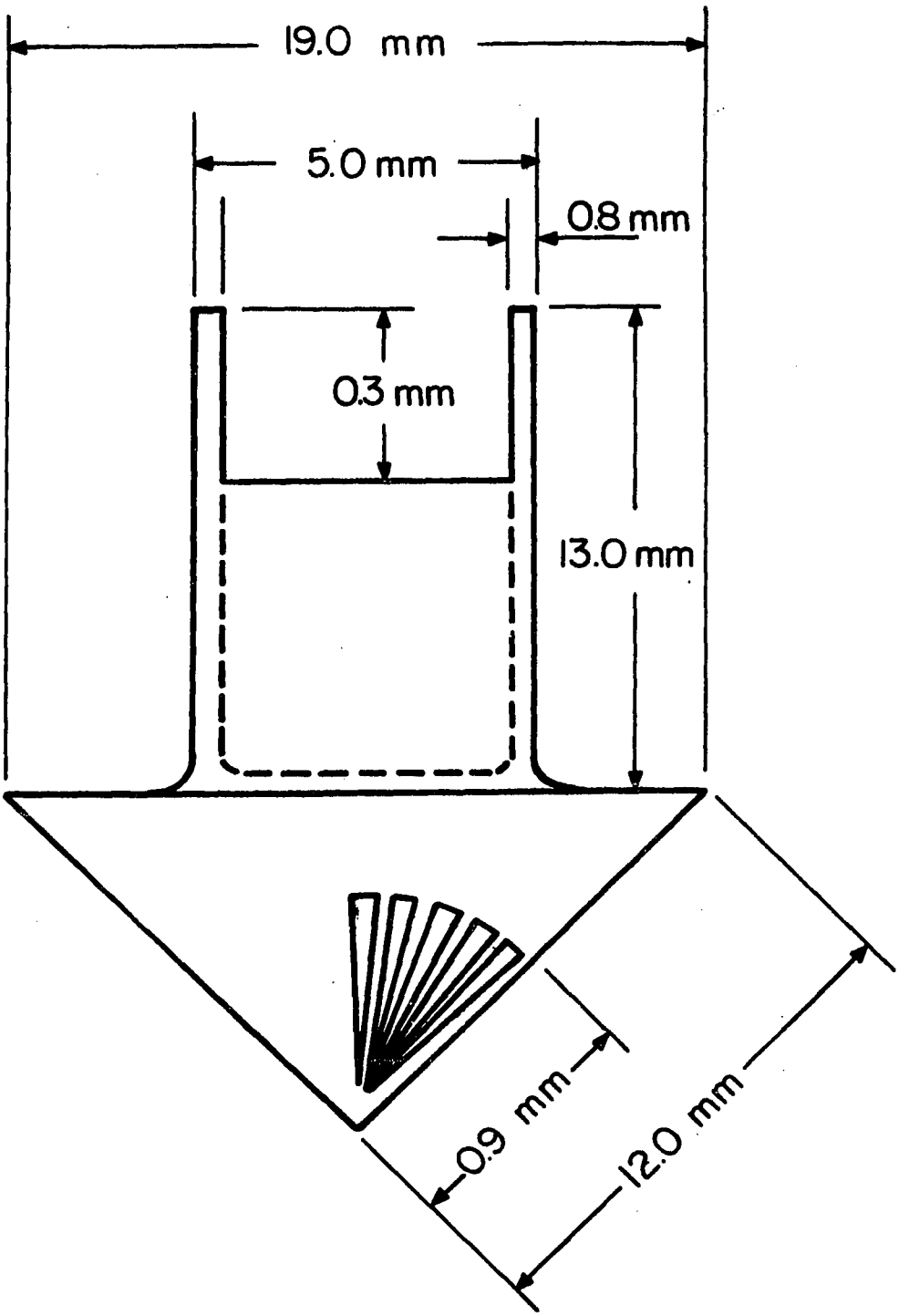

Figure 7. Dimensions of standard Beams-Andrews type rotor used for combined multiple pulse magic-angle spinning NMR experiments

line samples will remain in the sample chamber during rotation, even without the aid of this devise.

Spinning of the sample is accomplished by placing the rotor in a conical shaped stator, shown in Figure 8, which has six tangentially directed air channels connected to a compressed air source. Compressed air is forced into the stator cup, driving the rotor, while also creating an essentially frictionless air bearing for it to ride on. At the same time, Bernoulli forces are generated which prevent the rotor from leaving the stator cup (111, 112).

In the diagram shown in Figure 7, rotors of this design are indicated to be fluted. For spinning speeds above about 2.5 KHz, flutes were generally found to be necessary. For speeds below 2.5 KHz, rotors were not fluted, although in some cases, it was found that even unfluted, some rotors would run at speeds of up to 3 KHz.

The second style of rotor, designed primarily for work described in Chapters 4 and 5, is shown schematically in Figure 9. This spinner was developed for use with samples which must be maintained in nonambiant air atmospheres, e.g., hygroscopic or air-sensitive materials. As shown in Figure 9, the spinner is sealable. The sample entrance hole was drilled from the bottom of the base with a number 29 drill bit, followed by threading of the hole with a number 8 tap, 32 threads per inch. After loading

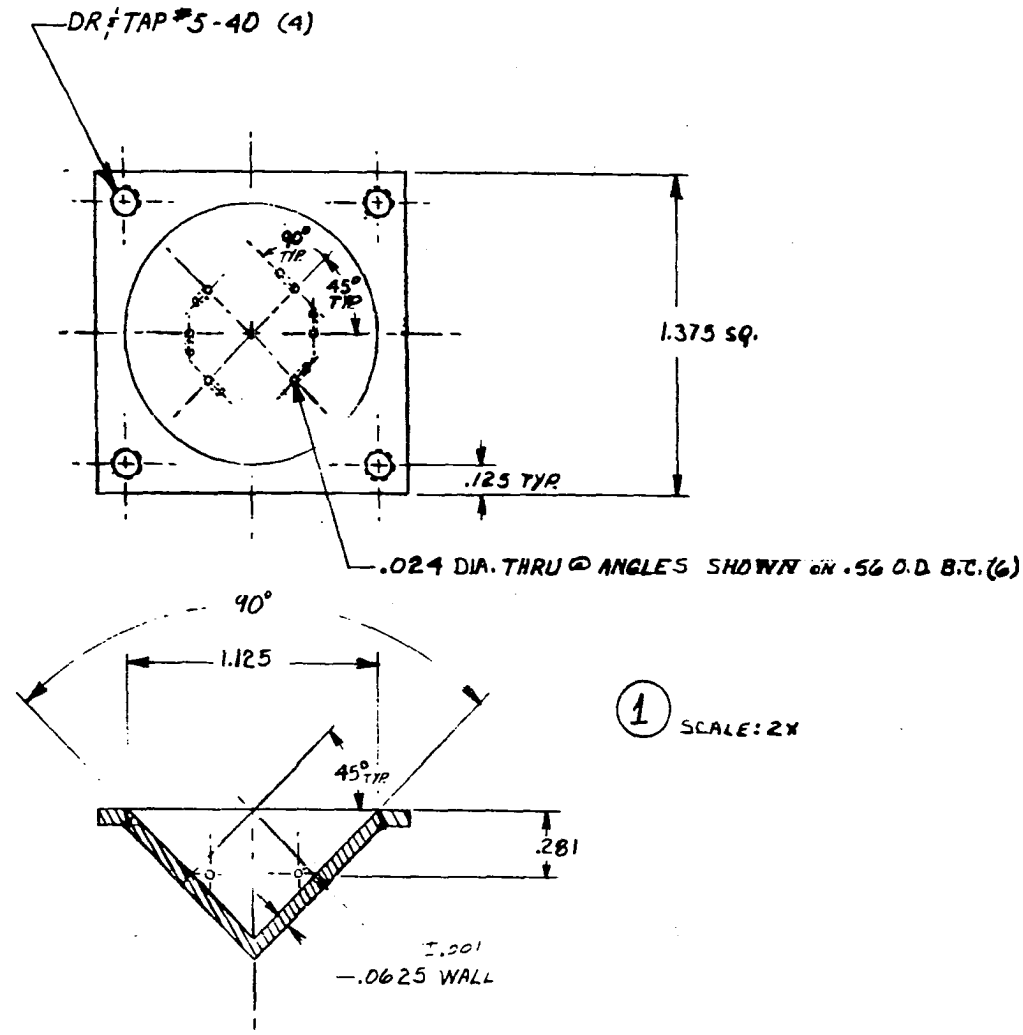

Figure 8. Design of stator used to drive rotors of the Beams-Andrew type

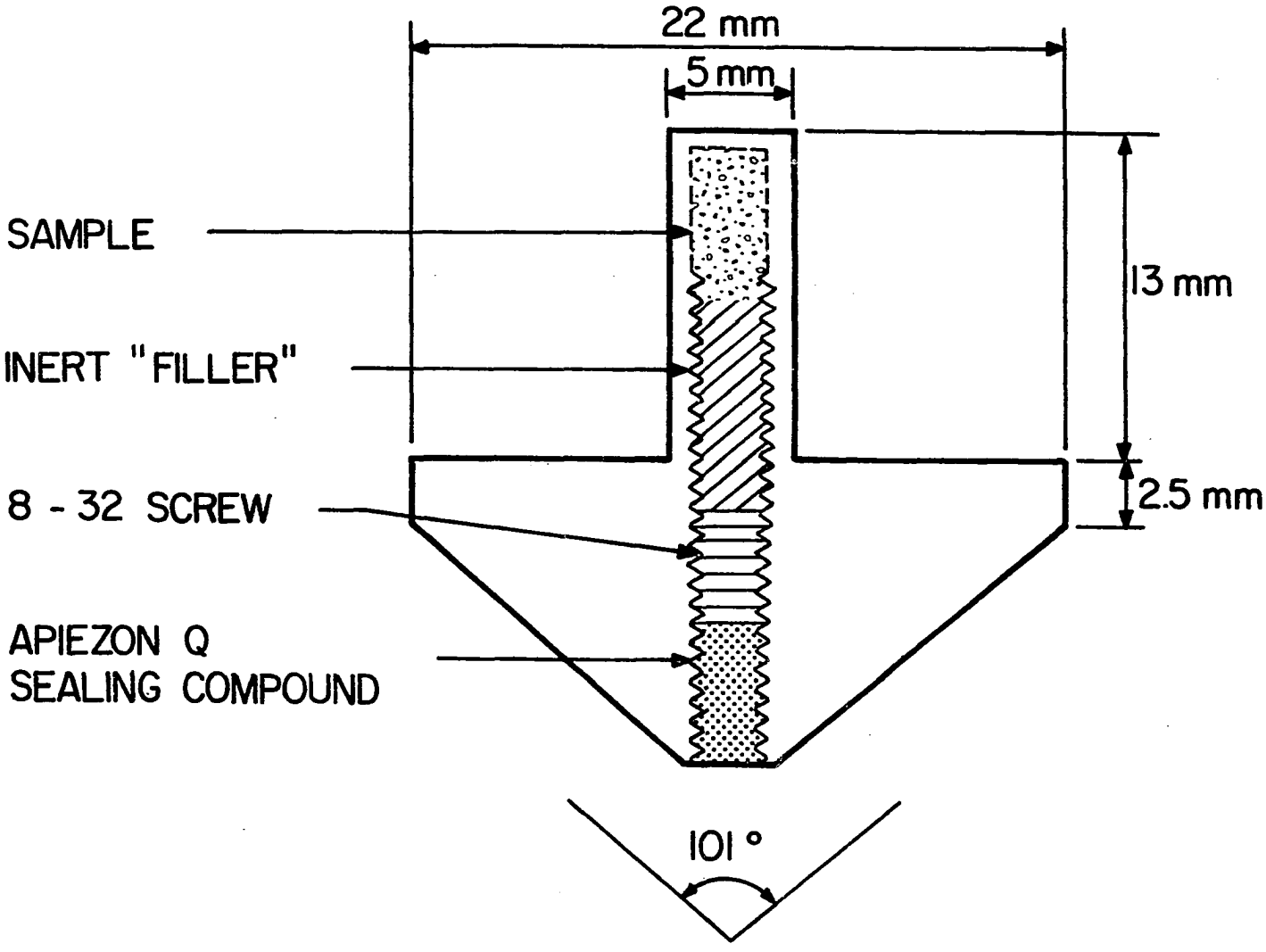

Figure 9. Sealable rotor used for air-sensitive samples

of the sample (in a dry box or dry bag), the rotor is sealed by following the sample with an inert material (if necessary), an 8-32 screw, and a suitable sealing compound, such as Apiezon Q (113). A rotor of this design was used in the study of $H_{1.65}MoO_3$ (Chapter 5), which is extremely air-sensitive (114), and after a period of several months, there was no indication of leakage. Unfluted, rotors of the dimensions indicated in Figure 9 are capable of rotational speeds up to about 2 KHz. Higher speeds should be attainable with this design by decreasing the diameter of the rotor body and/or by adding flutes to the rotor base.

Finally, Figure 10 indicates the third type of rotor, one devised for use in conjunction with a vacuum line system. Thus, rotors of this type may prove to be useful in applications of combined multiple pulse NMR/magic-angle spinning. In this case, high resolution NMR tubes are blown onto glass joints to permit initial vacuum line work. Following work-up on the vacuum line, samples are removed (while sealed off with a stopcock), and the NMR sample tubes permanently sealed at an appropriate length with a gas-oxygen torch. The sample tube is then press fit to a pre-drilled hole in a conical rotor base, thus forming the "neck" of the spinner. Samples are held in place at the top of the glass tube by a plug of glass wool initially inserted above the sample prior to attachment of the tube

Figure 10. Sealable NMR rotor for vacuum line samples

to the vacuum system. It should be noted that unlike the second-style rotor, the present spinner may be employed for samples sealed under a variety of conditions, without the need for intermediate loading in a dry box (and is therefore more versatile, and, in some ways, simpler to use).

It is worth noting that in initial work on this latter design, NMR tubes were used which were not high resolution NMR tubes, and therefore, not necessarily highly symmetrical; this approach met with mixed success. By employing tubes made for a high resolution NMR spectrometer, it was later found that stable rotation speeds up to about 3 KH_z could be routinely achieved. Also, by drilling the base hole in the rotor base to exactly match the o.d. of the NMR tube (5 mm), it was discovered that the tubes and rotor base generally have enough flexibility to allow the tube to be press fit without becoming removed during high-speed rotation. However, it is also possible, and perhaps easier, to make the hole about 0.2 mm larger than the NMR tube, and maintain the tube in place during use with a small amount of Apiezon Q putty at the bottom of the hole.

Materials studied; outline of the experiment

The materials used in this work were of two types, organic solids and semi-crystalline polymers. The specific

choice of samples was made to 1) attempt to observe ^{1}H solid state NMR spectra exhibiting a wide range of proton chemical shift differences, i.e., from less than 1 ppm to greater than 10 ppm, and to 2) provide examples which might be of interest to chemists. The organic solids were 4,4´-dimethylbenzophenone, 2,6-dimethylbenzoic acid, and acetylsalicylic acid (aspirin). The polymers were isotactic polystyrene, polymethylmethacrylate, and polyethylene terepthalate.

Both 4,4´-dimethylbenzophenone and the 2,6-dimethylbenzoic acid were prepared at the Ames Laboratory, Iowa State University, and were checked for purity via standard IR and solution NMR and found to be at least 98% pure. The acetylsalicylic acid was obtained from commercially available Bayer aspirin (trademark, the Bayer Co.) and was used without further purification. High resolution NMR in d_6-DMSO indicated that, with the exception of a small amount of adsorbed water, the sample did not contain significant amounts of proton containing impurities. The isotactic polystyrene was a powder sample obtained from the Dow Chemical Co. and has been determined by X-ray diffraction to be 27% crystalline. The polymethylmethacrylate was a rod sample from the Cadillac Chemical Co., Davenport, IA. NMR in $CDCl_3$ revealed the presence of isotactic, syndiotactic, and atactic regions in this polymer. Finally, the

polyethylene terephalate was obtained from the Eastman-Kodak Co. and was 58 ±5% crystalline.

For combined homonuclear dipolar decoupling/magic-angle spinning experiments, which we refer to as CRAMPS (Combined Rotation and Multiple Pulse NMR Spectroscopy), two different multiple pulse sequences were used to attenuate homonuclear dipolar broadening. Those were the MREV-8 pulse sequence (69-71) and the 24-pulse sequence recently introduced by Burum and Rhim (74). In each case, the sample rotation frequency at the magic-angle was approximately 3 KHz and the 90° pulse widths were 1.75 μsec. Powder samples of polystyrene, 4-4´-dimethylbenzophenone, 2,6-dimethylbenzoic acid, and aspirin were loaded into KEL-F rotors of the type shown in Figure 7. The polyethylene terepthalate was measured in a rotor of the type illustrated in Figure 10. Spectra were measured relative to an external water sample, which was also contained in a KEL-F rotor (however, in the text, many of the spectra are also referred to a high-field peak, as measured in by solution NMR). The magic-angle setting was made by manual adjustment of the probe to obtain the narrowest frequency spectrum for the polymethylmethacrylate sample, which was a solid rotor machined from that material. The estimated maximum error in setting the rotation axis to the magic-angle was less than 0.5°.

Results and Discussion

CRAMPS

Figure 11 illustrates the broad resonances typical of ^{1}H NMR in rigid, polycrystalline solids. Shown is the single pulse free induction decay Fourier transform spectrum of 4,4´-dimethylbenzophenone. The linewidth of this spectrum is on the order of several hundred parts per million, or about 30 KHz. That even with multiple pulse dipolar decoupling NMR spectra of protons may still be sufficiently broad, so that high resolution structural features are still unobservable, is further clearly demonstrated in Figure 12a, an MREV-8 pulse spectrum of the same polycrystalline sample. The multiple pulse cycle time of the MREV-8 sequence used to produce Figure 12a was 27.6 μsec and the experimental offset frequency, $\delta\omega$, was -1 KHz. These conditions were found to give the best resolution presently achievable in our spectrometer (vide infra). The experimental spectrum in Figure 12a is indicated by crosses, while the smooth line also shown in a computer generated Lorentzian fit. The spectrum is seen to consist of a featureless line, with full width at half maximum, 2 Δ f of 552 Hz, or about 10 ppm. At this level of resolution, no chemical shift structure is observable. We have similarly measured MREV-8 pulse spectra for 2,6-dimethylbenzoic acid, isotactic polystyrene, and

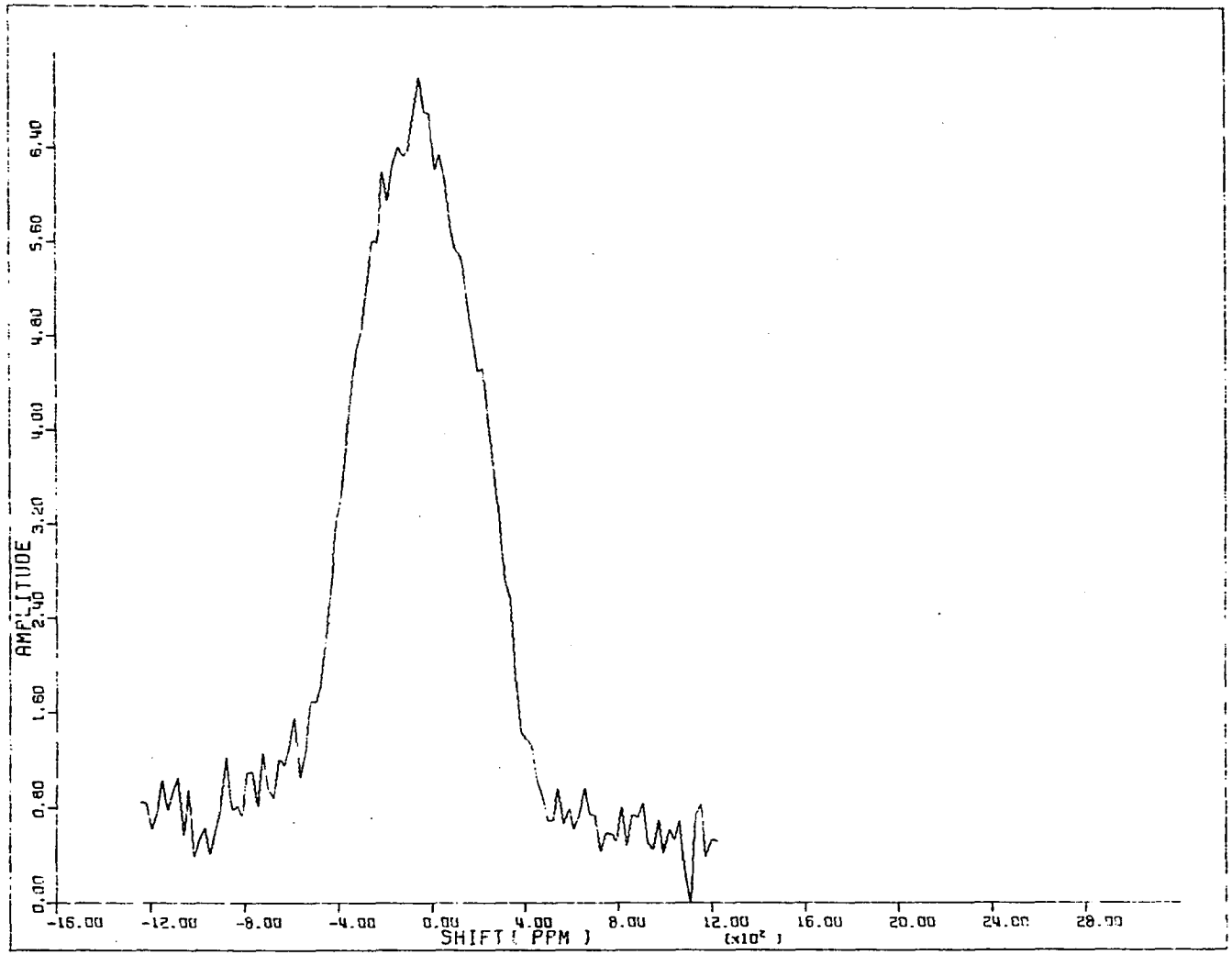

Figure 11. Single pulse, broadline NMR spectrum of 4,4´-dimethylbenzophenone

Figure 12. High resolution ^{1}H NMR spectra of solid polycrystalline 4,4´-dimethylbenzophenone. (a) The ^{1}H NMR spectrum of solid polycrystalline, 4,4´-dimethylbenzophenone, with MREV-8 dipolar decoupling. t_c was 27.6 μsec and the offset frequency was ~1 KHz. (b) the MREV-8 pulse magic-angle spinning CRAMPS spectrum of 4,4´-dimethylbenzophenone. (c) The Burum and Rhim 24-pulse sequence plus magic-angle spinning CRAMPS spectrum of 4,4´-dimethylbenzophenone. Zero ppm refers to the shift of an external water sample

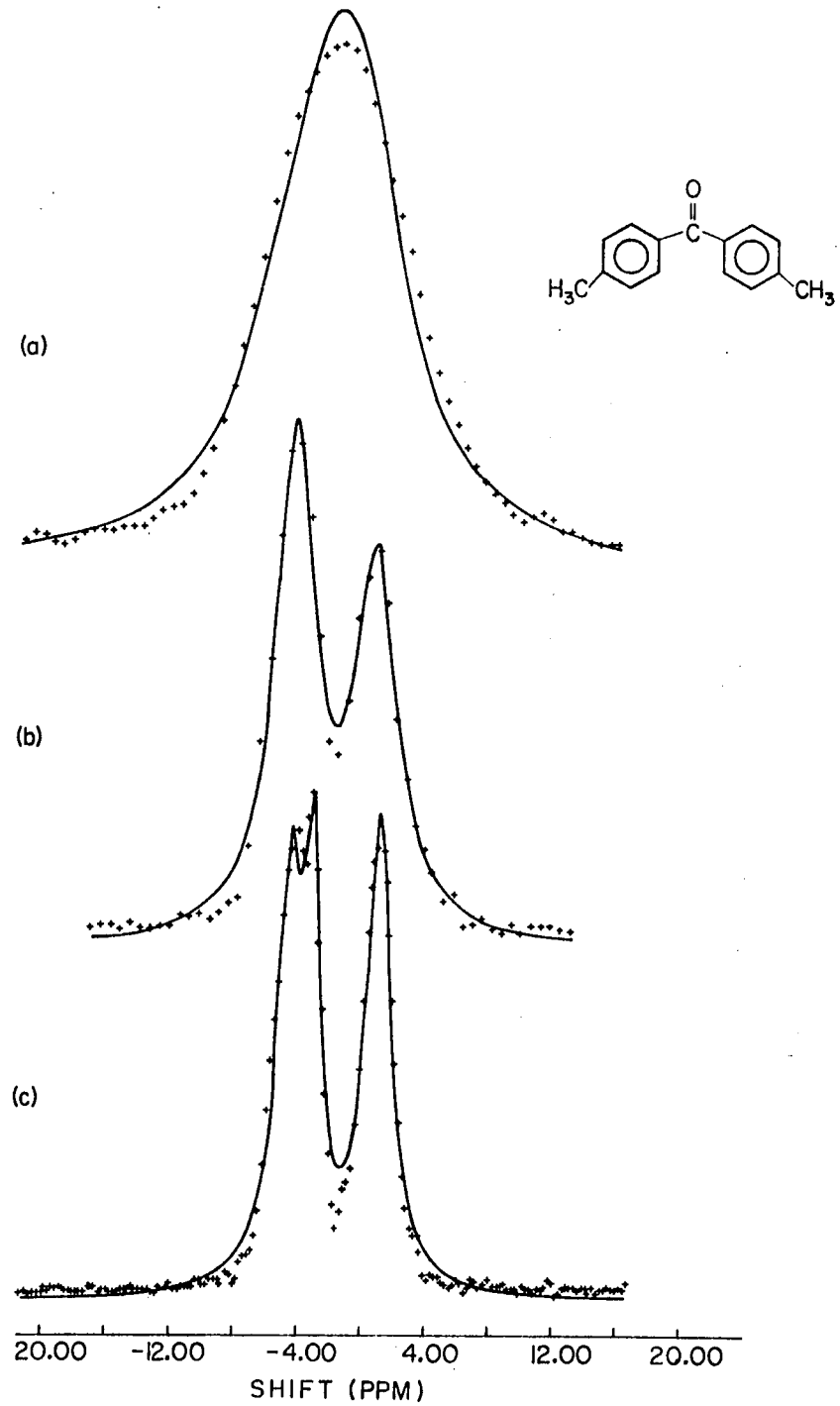
(a)
(b)
(c)
O
C
H3C
CH3
20.00
-12.00
-4.00
4.00
12.00
20.00
SHIFT (PPM)

polymethylmethacrylate (Table II), under the same conditions, and in each case, just a single broad resonance was detected. Thus, despite there being a number of chemically inequivalent protons in each of the four compounds studied, it was not possible to ascertain this using multiple pulse NMR alone.

In contrast to the results described above, Figure 12b shows the ^{1}H CRAMPS spectrum of 4,4′-dimethylbenzophenone, where magic-angle spinning has been added to the multiple pulse experiment in Figure 12a. Here, the anisotropies have been physically averaged, and two partially overlapping, but clearly distinguishable, peaks were recorded. These are separated by 5.1 ppm, and appear to correspond to the aromatic and aliphatic protons in the sample. Further evidence for this conclusion is indicated by a computer fit (115) (smooth line in Figure 12b) of the experimental spectrum to a superposition of two Lorentzian shaped lines. The integrated areas of the two peaks obtained in this fashion were 56.3% and 43.7% of the total area, in substantial agreement with the 57.1% and 42.9% anticipated from the relative number of aromatic and methyl protons, respectively, in 4,4′-dimethylbenzophenone.

Finally, the spectrum in Figure 12c was produced by substituting the recently developed (74) 24-pulse dipolar decoupling sequence of Burum and Rhim for the MREV-8 pulse

cycle used in Figures 12a and 12b. This compound cycle (74), like the MREV-8, compensates for pulse timing and phase errors (85), while removing the zeroth-order through third-order terms to the Magnus expansion for the effective dipolar Hamiltonian (65). Thus, in comparison to the MREV-8, which does not remove the second-order dipolar term (85), the BR-24 leads to enhanced resolution (74). In this case, it was found that the aromatic region was reproducibly resolved into two peaks separated by 1.4 ppm (δ=8.1 and 6.7, relative to δ_{CH_3}=2.5 determined from solution NMR in CS_2). At first consideration, these peaks would seem to correspond, respectively, to the ortho and meta aromatic protons. However, a similar low-field doublet in the solution spectrum of 4,4'-dimethylbenzophenone (Figure 13) showed a separation of only 0.4 ppm (δ_{ortho}=7.65, δ_{meta}=7.25). Furthermore, the relative areas of the solid-state aromatic shifts were determined by computer fitting (116) of the lineshapes and fitting with a Dupont 310 Curve Resolver to be approximately three-to-one (low field shift-to-high field shift, Table I), rather than the one-to-one ratio expected, and found in solution.

These incongruities might be explained by realizing that in the rigid structure of solid benzophenones (117, 118) the aromatic rings are nearly 60^{o} from coplanar, with the two rotated equally but oppositely from the plane of

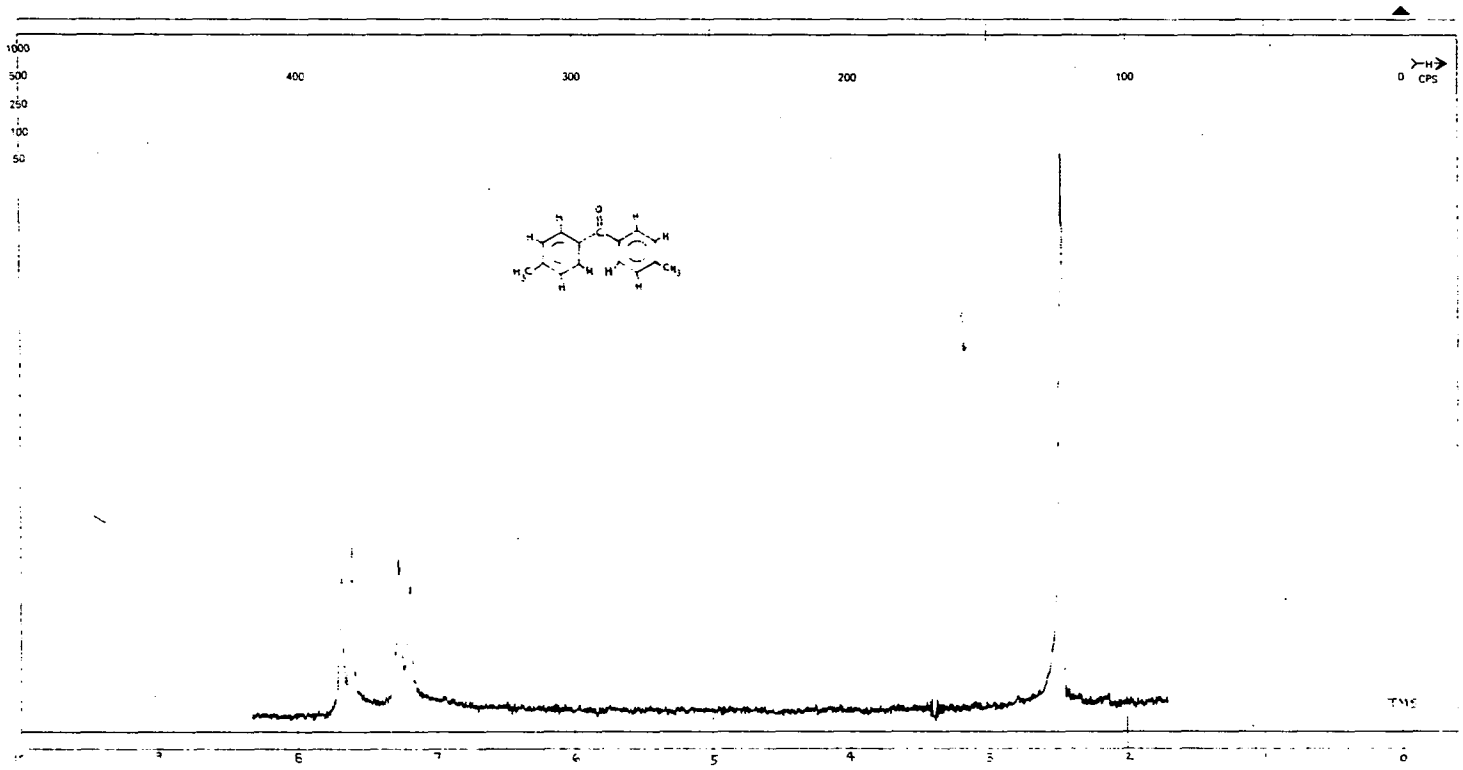

Figure 13. Solution NMR spectrum of 4,4´-dimethylbenzophenone in CS_2

Table I. Percentages of proton types in model compounds

	Experimental[a]			Theoretical
	A		B	
Polystyrene[b]				25.0
CH_2	17.1		17	12.5
CH	13.1		13	62.5
Aromatic H	69.7		70	
Polymethylmethacrylate[c]				37.5
CH_3	24.3	(30.5)	26	25.0
CH_2	25.6	(23.9)	24	37.5
OCH_3	50.1	(45.6)	50	
Polyethylene terephthalate[a]				50.0
CH_2	56.2		56	50.0
Aromatic H	43.8		44	
4,4´-DMBP				42.85
CH_3	42.8		43	14.3
High field arom H	17.6		17	42.85
Low field arom H	39.6		40	
2,6-DMBA				60.0
CH_3	56.2		56	20.0
meta-aromatic H	18.6		22	10.0
para-aromatic H	8.1		7	10.0
OH	16.9		15	
Aspirin				37.5
CH_3	40.5		40	50.0
Aromatic H	45.1		46	12.5
OH	14.4		14	

[a]A - Determined by computer fitting (115) CRAMPS spectra to Lorentzian lineshapes. B - Determined by fitting CRAMPS spectra to Lorentzian lineshapes using a Dupont 310 Curve Resolver.

[b]Theoretical value based on a single unbranched, uncross-linked polymer unit.

[c]Theoretical value based on a single unbranched, uncross-linked polymer unit. Experimental value in parentheses is from solution NMR.

the carbonyl group. In this arrangement, two of the ortho protons in 4,4'-dimethylbenzophenone may be fixed in a position where they are magnetically more shielded than the other six ring protons, whose shifts apparently overlap to give the larger low-field line. This possibility is not inconsistent with characterizations of the long-range shielding effects of the carbonyl group (119-121). In solution, of course, rapid rotation of the aromatic rings causes all four ortho protons to be equivalent, and similarly for the meta protons, leading to the 1:1 doublet.

It can be concluded, then, that we may be observing an orientational, purely solid-state effect in Figure 12c, and this suggests that one useful application of CRAMPS may be in the mapping of shielding environments of common functional groups in solids, e.g., carbonyl groups, carbon-carbon multiple bonds, etc. (although greater resolution for this experiment would be highly desirable).

Next, in Figure 14, is shown the 24-pulse ^{1}H CRAMPS spectrum of another organic solid, 2,6-dimethylbenzoic acid. Four shifts are distinguishable, corresponding, in order of decreasing shielding, to the methyl, para, ortho, and carboxylic acid protons. Table I lists the relative sizes of these peaks. Again, there are features to the spectrum that are different from those of the same compound in solution. In dilute, deuterated acetone, the chemical shift for the

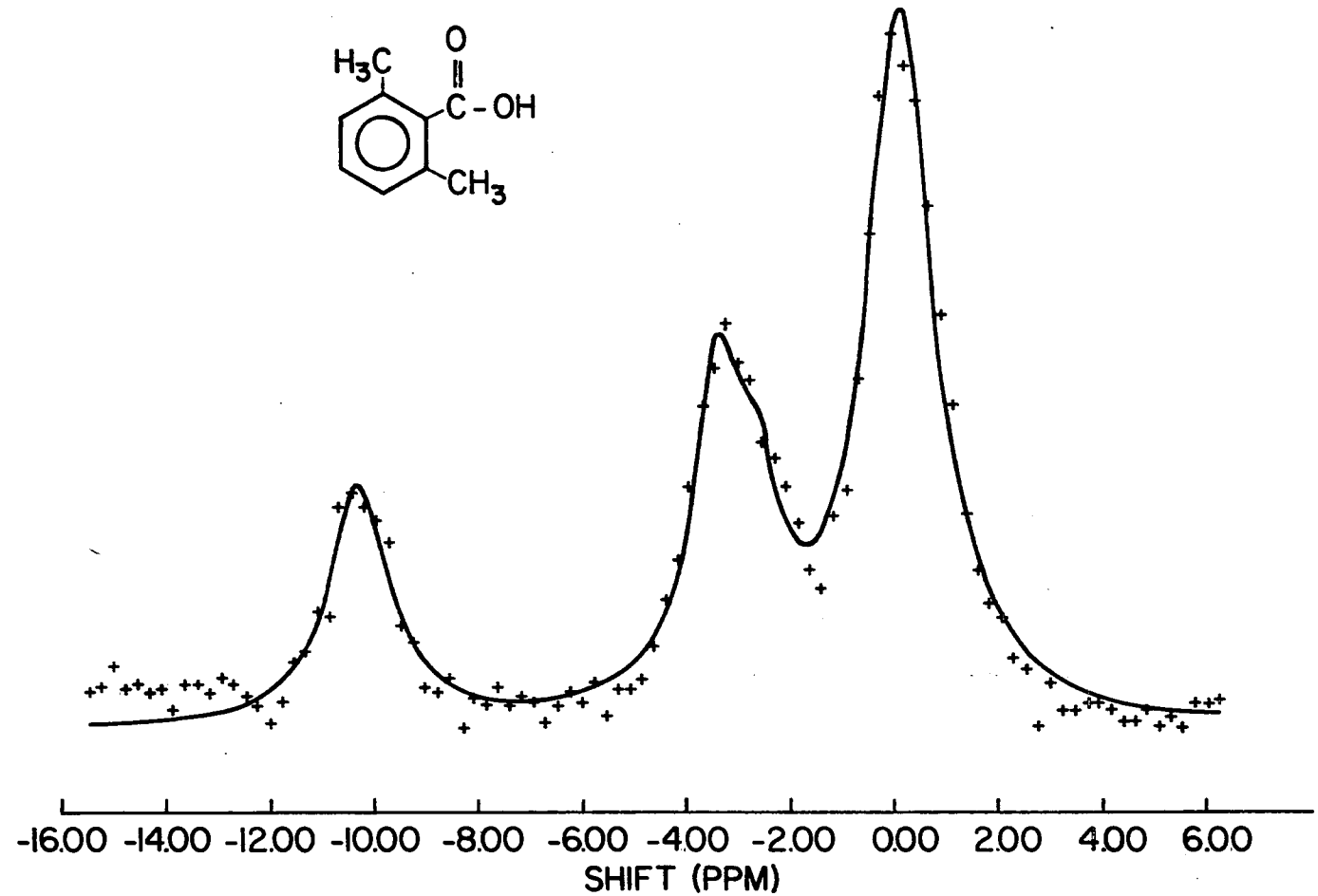

Figure 14. The BR-24 pulse CRAMPS spectrum of 2,6-dimethylbenzoic acid

acid protons occurred at 10.7 ppm downfield from TMS. For the solid, this resonance was at δ_{COOH}=14.8, using $\delta_{H_2O} - \delta_{TMS} = 4.6$, or at δ_{COOH}=14.2, using δ_{CH_3}=3.8 (from the solution spectrum). This downfield displacement of the resonance signal simply reflects the well-known formation of hydrogen-bonded dimers in the solid form of carboxylic acids (5, 122). We note that the use of an external water reference results in the neglect of the correction of the value of the acid proton shift for bulk susceptibility effects. When the position of the methyl resonance was used as an internal flag, this shift was changed by only 0.6 ppm, so that hydrogen bonding was implied in either case (15). However, it is apparent that for quantitative applications of this technique, it will be necessary to use a source of internal referencing.

Also from Figure 14, the relative peak areas in the aromatic region (given in Table I) indicate that the para proton shift in solid 2,6-dimethylbenzoic acid is apparently to higher field than is the ortho resonance (δ_{ortho}=7.4, δ_{para}=6.6, relative to δ_{CH_3}=3.8). In solution, the opposite was true, this time with the ortho shift occurring to higher field (δ_{para}=7.30, δ_{ortho}=6.65). This apparent turn-around could be the result of, for example, ring currents induced in adjacent molecules (5) held in close association in the solid state and/or solvent effects (5)

due to the acetone. Alternatively, admitting the similarity of the absolute shifts for the two cases, it is not entirely possible to discount the need for greater resolution in the solid-state experiment prior to making assignments of less than about 1 ppm difference (although the 2:1 low field-to-high field ratio was consistently reproducible).

Figure 15 shows the NMR spectrum of common aspirin (acetylsalicylic acid). Again, there is a large downfield shift, δ_{COOH}=12.6, relative to $\delta_{CO_2CH_3}$=2.2, indicative of hydrogen bonds (123). The aromatic region is relatively broad, with no visible structure, and the only unusual feature of the spectrum is an unfitted peak at about 0 ppm (δ=4.5) due to adsorbed water.

Figures 16 and 17 are the CRAMPS spectra of isotactic polystyrene and polymethylmethacrylate, respectively. While it is not obvious from a visible inspection that there are three major peaks indicated in either of these spectra, computer fits to three Lorentzian lines were better, in each case, than fits to two lines (using a linear least squares fitting criterion). Also, the line positions indicated were in good agreement with those observed in solution ($\delta_{CH_2}^{POLYSTY}\simeq1.5$, $\delta_{CH}^{POLYSTY}\simeq2.2$, $\delta_{AROM}^{POLYSTY}\simeq6.9$; $\delta_{CH_3}^{PMMA}\simeq1.0$, $\delta_{CH_2}^{PMMA}\simeq1.8$, $\delta_{OCH_3}^{PMMA}\simeq3.7$), as were the relative areas of the peaks determined by computer fitting and

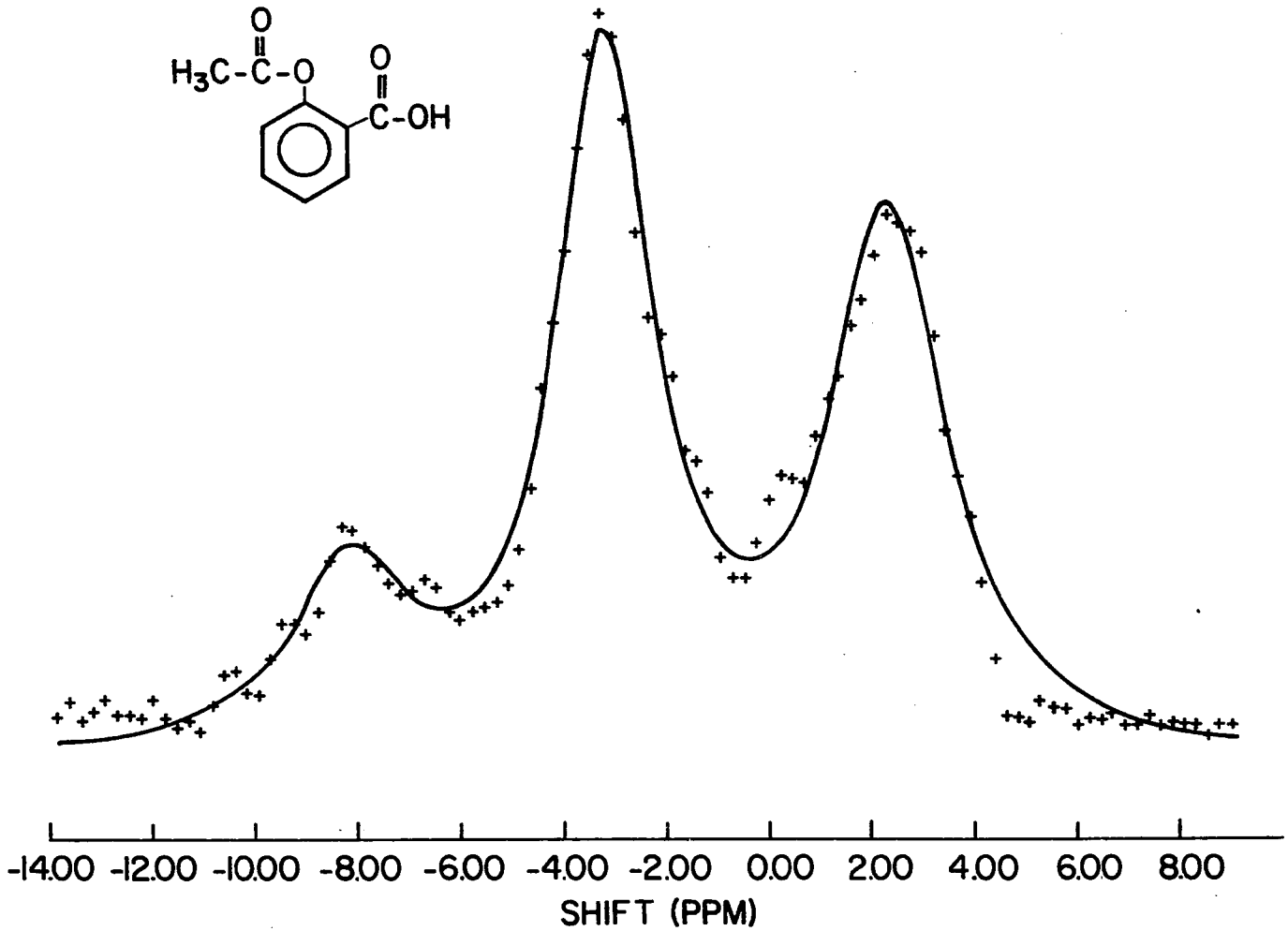

Figure 15. The BR-24 pulse CRAMPS spectrum of aspirin

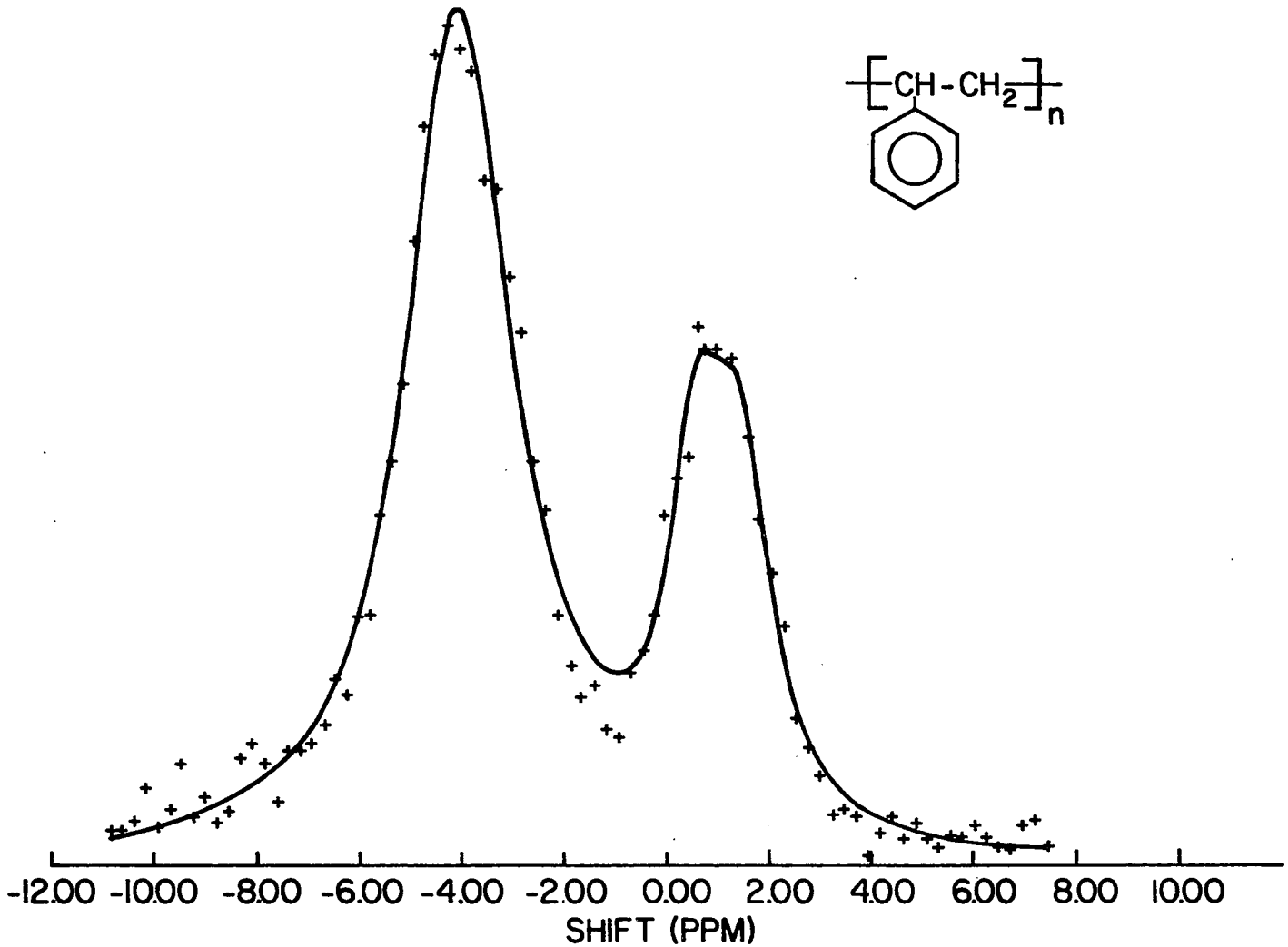

Figure 16. The BR-24 pulse CRAMPS spectrum of isotactic polystyrene

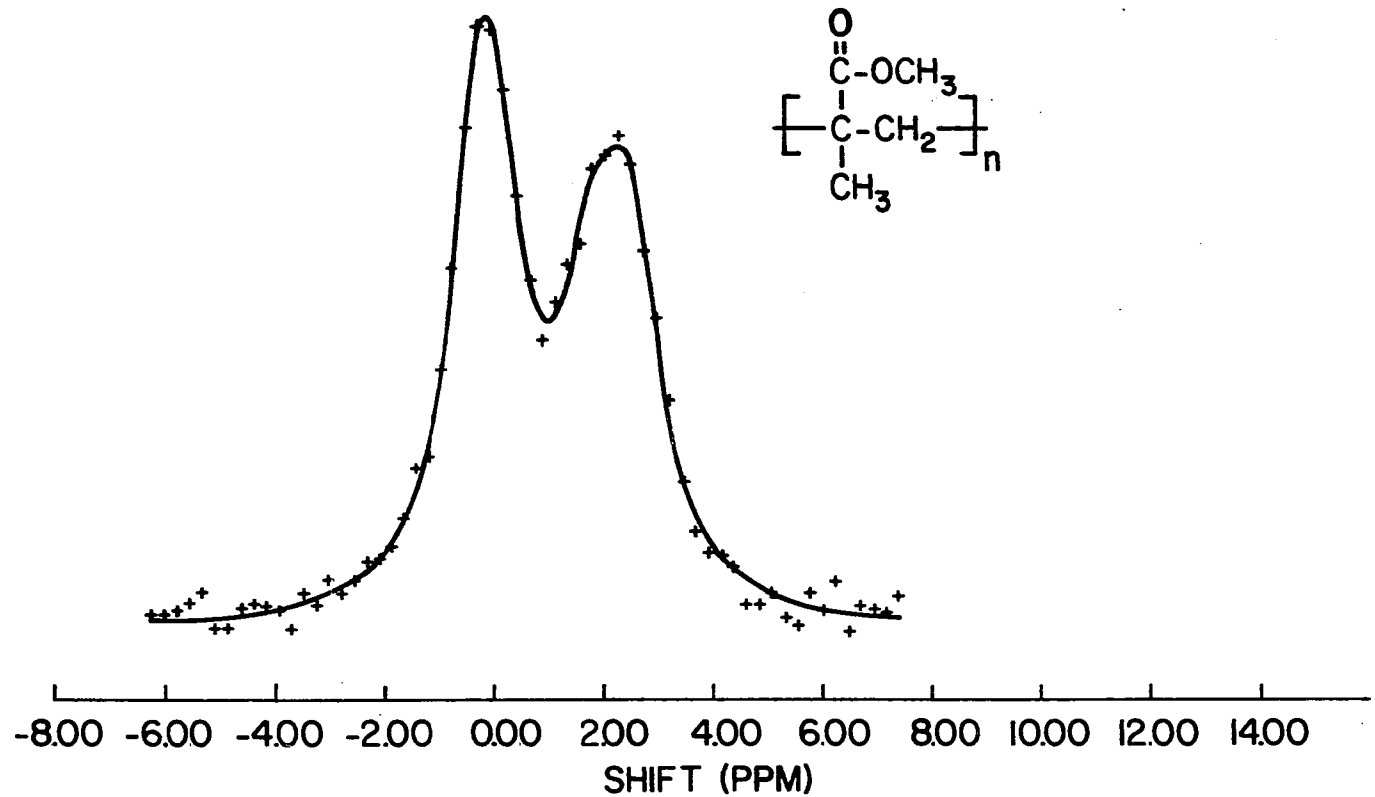

Figure 17. The BR-24 pulse CRAMPS spectrum of polymethylmethacrylate

analysis with a Dupont 310 Curve Resolver (Table I). Thus, while the linewidths in Figures 16 and 17 are not impressive by liquid-state standards (as was also the case for Figures 12, 13, and 15), the resolution is sufficient so that different chemical types may at least be distinguished.

Finally, Figure 18 shows the BR-24 pulse CRAMPS spectrum of polyethylene terepthalate (PET). As was the case for the other two polymers, the spectral linewidths observed are greater in this spectrum than for the organic solids, but the relative areas are in relatively good agreement with those anticipated (Table I). PET is prepared by reaction of either terephthalic acid or dimethyl terephthalate with ethylene glycol, and may have several percent of terminating OH groups (124). This is indicated in Figure 18 by the small, unfitted peak at about 4 ppm downfield from H_2O.

Residual linewidth contributions

We have also studied four of our samples (4,4´-dimethylbenzophenone, 2,6-dimethylbenzoic acid, polystyrene, and polymethylmethacrylate) under a variety of conditions and experiments to determine the conditions for best resolution, and the contributions accounting for the residual CRAMPS linewidths.

A single pulse free induction decay from the sample of 4,4´-dimethylbenzophenone was characterized in our

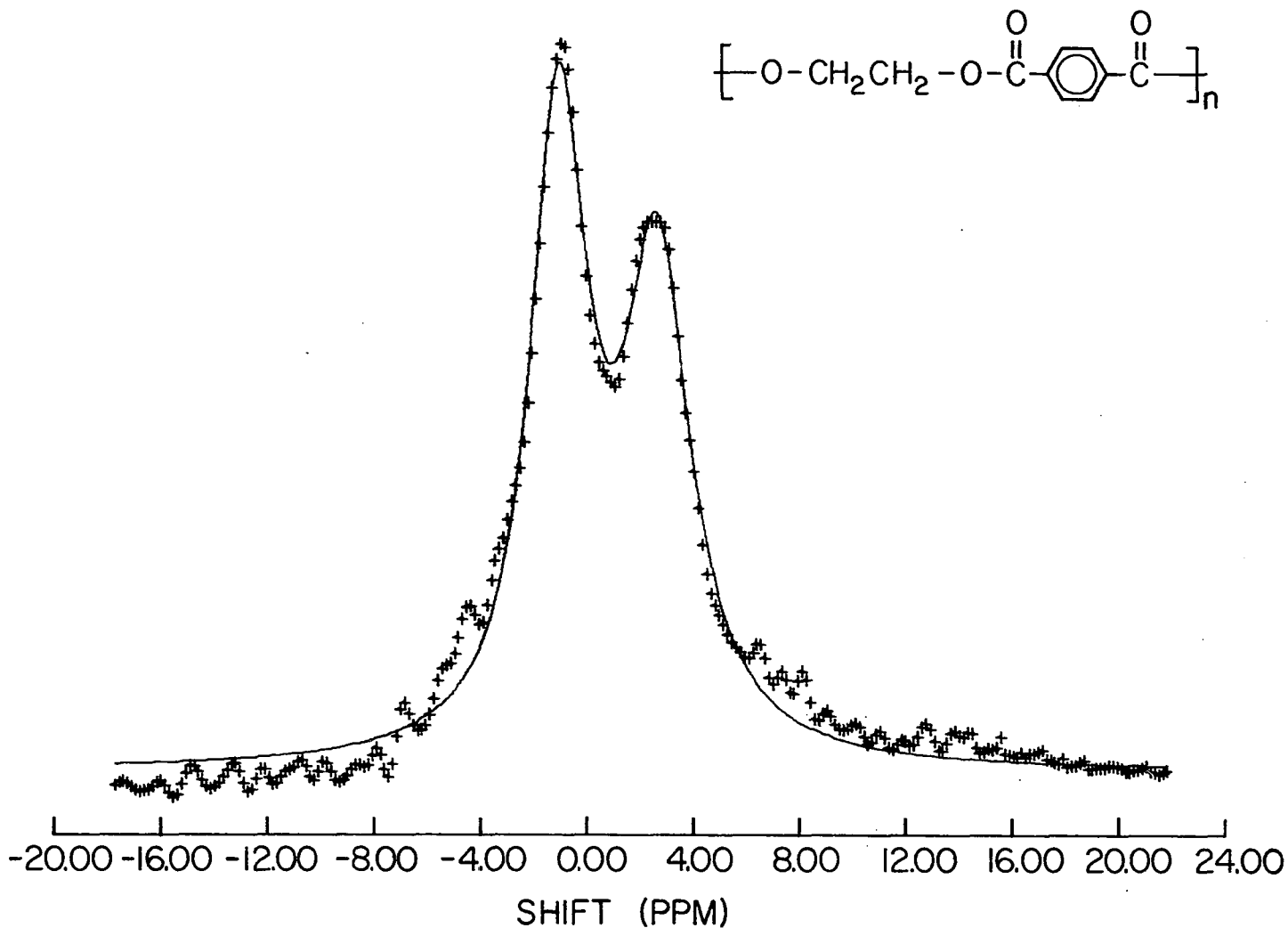

Figure 18. The BR-24 pulse CRAMPS spectrum of PET

spectrometer by an effective spin-spin relaxation constant T_2^* of 20 μsec. For multiple pulse averaging of dipolar interactions, an important criterion is (85) $t_c \|\tilde{H}_D\| << 1$, where the magnitude of the dipolar interaction may be estimated from the relation $\|\tilde{H}_D\| \simeq (\pi T_2^*)^{-1}$. t_c, in this case, is the cycle time of the multiple pulse sequence used, or some part of the sequence over which $\bar{H}_D^{(0)}$ is zero. A cycle time of 27.6 μsec, used for the MREV-8 pulse experiments (and the shortest cycle time available in our spectrometer at the magic angle) in this section (or 13.8 μsec for the four pulse subcycle of this sequence), easily satisfies the convergence criterion for 4,4'-dimethylbenzophenone; furthermore, the T_2^*'s of 2,6-dimethylbenzoic acid, isotactic polystyrene, and polymethylmethacrylate were 17, 19, and 16 μsec, respectively, so that this criterion was met for all the samples studied (and similarly for the case of the 24-pulse experiments, for which the four pulse subcycle time was also 13.8 μsec). Since under this condition the MREV-8 pulse sequence removes the zero and first-order dipolar terms from the effective Hamiltonian, the only dipolar contributions to the spectra should be due to second-order and higher even-ordered terms. For the 24-pulse cycle, the residual dipolar contributions will be fourth-order and higher-order even terms.

Correction terms to the average dipolar Hamiltonian for the MREV-8 pulse cycle generated by the coupling of the resonance offset with internal interactions or pulse imperfections reveal an offset dependency in the eight-pulse linewidth (69, 70,85). For example, the cross term between the resonance offset Hamiltonian and the dipolar interaction is given by (71)

$$\bar{H}_{DO}^{(2)} = \frac{t_c^2}{864}(\delta\omega)\,[I_x, [H_D^{(x)}, H_D^{(y)}]] + \frac{t_c^2}{432}(\delta\omega)^2 (H_D^{(z)} - H_D^{(x)}) \quad ,$$

where $\delta\omega$ is the resonance offset. The second-order correction term for the dipolar interaction along is (71)

$$\bar{H}_{D}^{(2)} = \frac{t_c^2}{648}[H_D^{(x)} - H_D^{(z)}, [H_D^{(x)}, H_D^{(y)}]] \quad .$$

Initially, as the resonance offset is increased, a process known as second averaging (67) can result in a linewidth reduction by reducing the effective size of $\bar{H}_{D}^{(2)}$. Then, as the offset is further increased, $\bar{H}_{DO}^{(2)}$ grows into dominance, and the linewidth becomes larger. This situation may be expected to apply to CRAMPS experiments as well, where the MREV-8 cycle is used for attenuation of dipolar interactions.

Figure 19 illustrates the results of varying the resonance offset relative to the tuning nucleus (^1H in H_2O) on the MREV-8 CRAMPS spectrum of 4,4´-dimethylbenzophenone. There is clearly an offset dependence to the NMR linewidths, with the greatest resolution in the region of 1 KHz below resonance. Also, positive offsets, which are not shown in

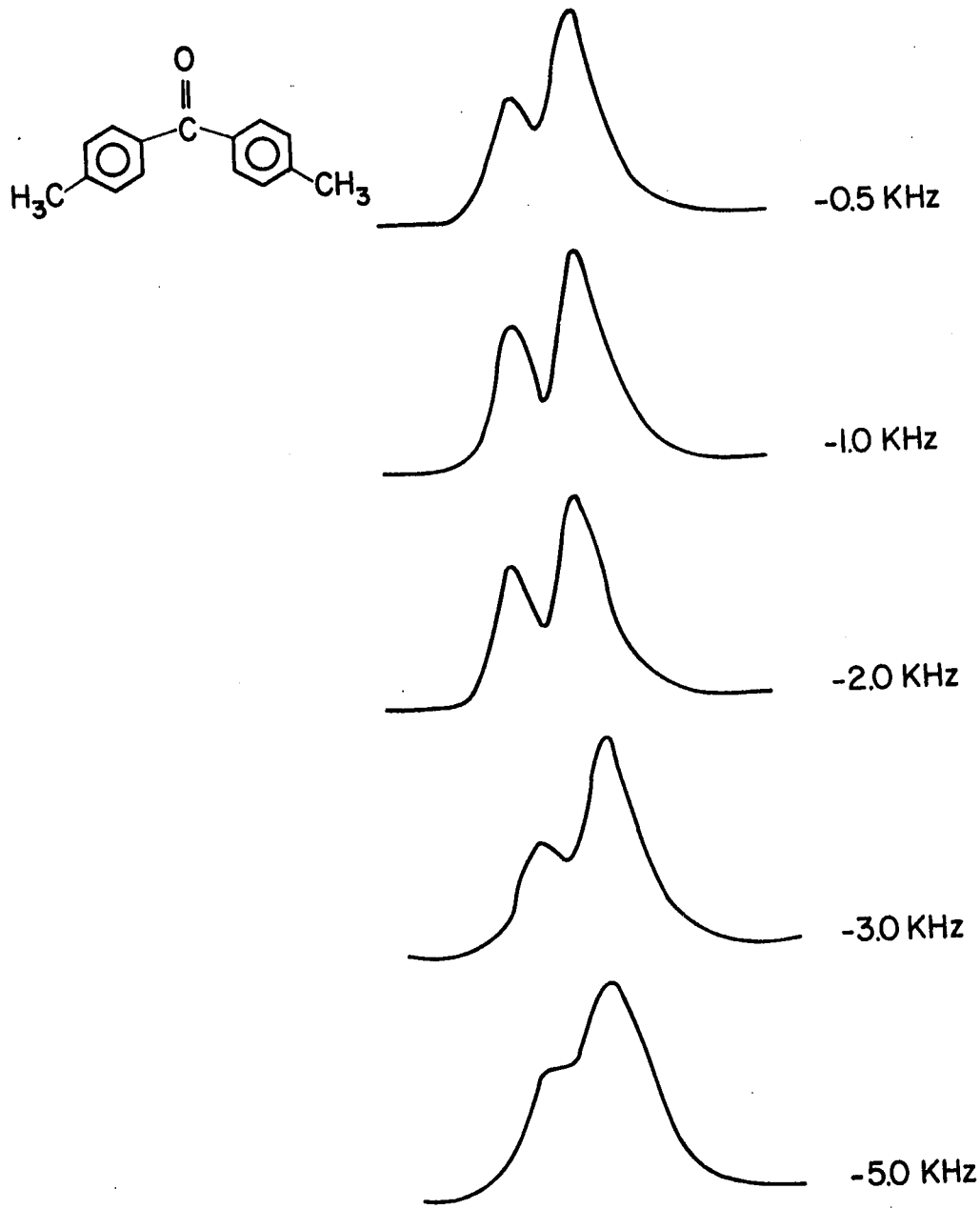

Figure 19. The effect of offset on the MREV-8 pulse CRAMPS spectrum of 4,4´-dimethylbenzophenone, at t_c=27.6 μsec

Figure 16, were found to lead to poorer resolution than negative offsets, in our spectrometer. These results were also found to hold for each of the other samples, and for the 24-pulse CRAMPS experiment.

An additional parameter whose variation may alter the resolution in a multiple pulse experiment is, of course, the cycle time of the pulse sequence, t_c. In Figure 20 is shown the effect of different cycle times on the CRAMPS spectrum of polymethylmethacrylate, where the narrowest lines were found for the shortest cycle times. Again, this result could be repeated for the other three samples and the 24-pulse CRAMPS experiment, but the latter case the cycle time dependency was not as pronounced, since the second order dipolar terms (which depend on t_c^2) are removed by this experiment, where they are not by the MREV-8.

The residual linewidth of an MREV-8 pulse spectrum, in which zero and first-order dipolar terms have been made to vanish, is generally considered to be composed of three major contributions (100). These are the static magnetic field inhomogeneity, second-order terms (plus higher-order dipolar terms, which are relatively smaller, and for purposes of discussion here, are lumped in with the second-order term), and relaxation terms. The first of these, which includes the chemical shift anisotropies, should be removed by 3 KHz magic-angle rotation, so that MREV-8

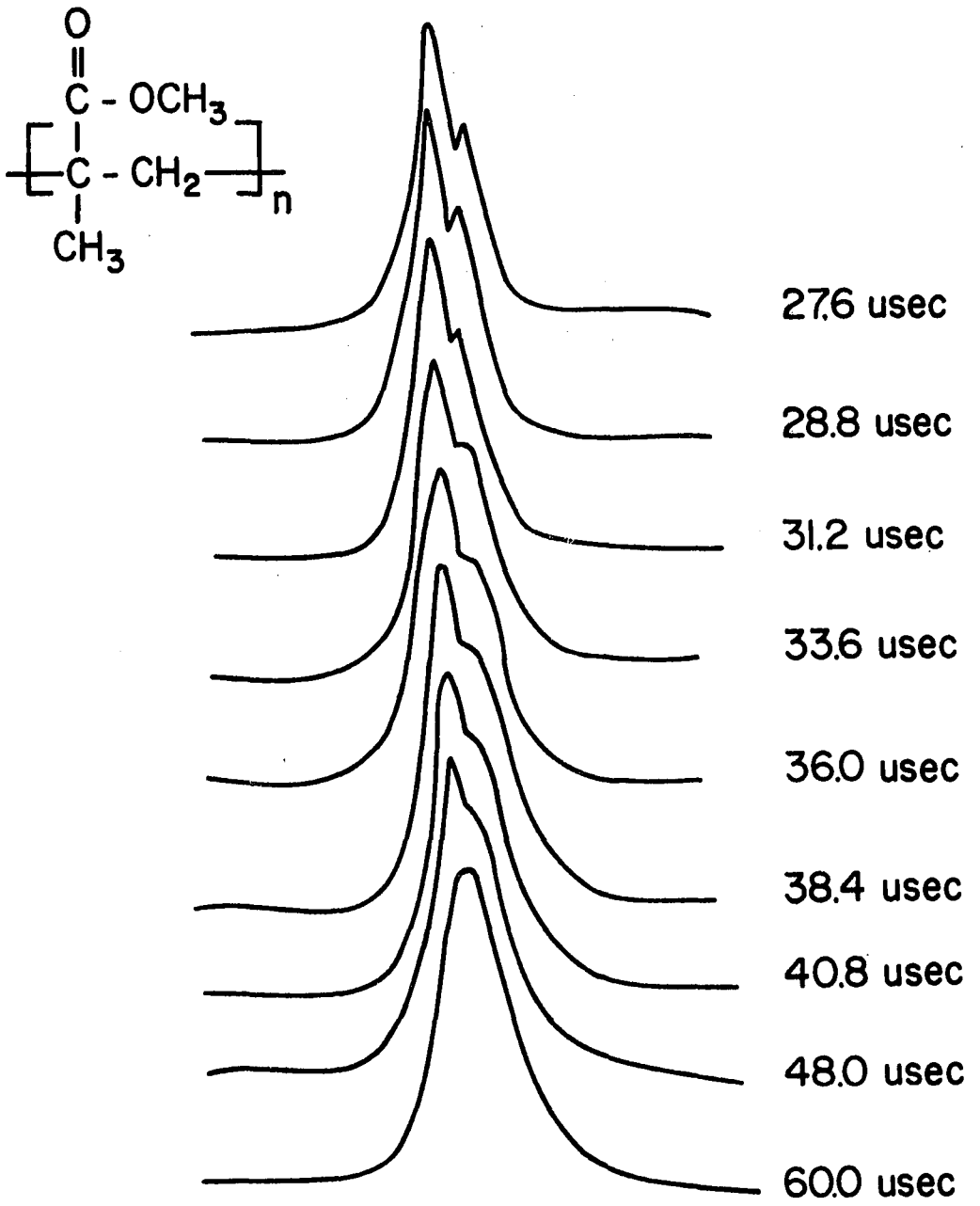

Figure 20. The effect of the cycle time on the MREV-8 pulse CRAMPS spectrum of polymethylmethacrylate, at $\delta\omega$= -1 KHz

CRAMPS linewidths should contain only second-order dipolar and relaxation broadening. The linewidths observed for such an experiment on 4,4´-dimethylbenzophenone, 2,6-dimethylbenzoic acid, isotactic polystyrene, and polymethylmethacrylate are reported in Table II.

A more exact experimental method for determining the magnitudes of these latter two terms involves the use of two additional eight-pulse sequences, the P_x-M_y (99, 100) and the $-M_x$ sequences (100). Both are versions of the MREV-8 pulse experiment in which a deliberate phase error is caused in the x pulses, thereby introducing an additional zeroth-order Hamiltonian (71)

$$\bar{H}_P^{(0)} = \frac{2}{t_c} (\phi_{\bar{x}} - \phi_x) I_y \quad .$$

In the P_x-M_y version, an x prepulse is applied, with observation of the macroscopic magnetization along the y axis in the rotating frame. This sequence removes both the magnetic field inhomogeneities (including chemical shifts) and second-order dipolar effects, so that only relaxation broadening remains. The results of applying this sequence to our four samples are also given in Table II. Relaxation broadening appears to contribute only a small amount to the multiple pulse lineshapes, particularly in the case of the molecular solids.

Table II. Linewidth results for multiple pulse and CRAMPS measurements[a]

Compound[b]	IP	PMMA	DMBP	DMBA
CRAMPS (8-pulse) Aliphatic line	157	230	156	145
CRAMPS (8-pulse) Aromatic line[c]	160	110	170	131 75[d]
CRAMPS (24-pulse) Aliphatic lines	CH CH_2 69 74^2	CH_2 CH_3 79^2 65^3	109	88
CRAMPS (24-pulse) Aromatic lines[c]	141	77	62[e] 109[f]	59[e] 65[f] 76[d]
MREV-8	586	431	552	466
$P_x - M_y$	11	15	4	3
$-M_x$	71	67	34	47

[a]Full width at half height in hertz.

[b]IP - isotactic polystyrene; PMMA - polymethylmethacrylate; DMBP - 4,4′-dimethylbenzophenone; DMBA - 2,6-dimethylbenzoic acid.

[c]OCH_3 for PMMA.

[d]OH.

[e]High field aromatic line.

[f]Low field aromatic line.

The P_x-M_x version of the phase-altered eight-pulse sequence, in which the preparation pulse is missing, and the x component of the magnetization is observed (100), removes only the inhomogeneity term, leaving both relaxation and second-order dipolar broadening. These are exactly the contributions not removed under the MREV-8 CRAMPS experiment (except that the $-M_x$ removes chemical shift difference, where the CRAMPS does not), and so represents the ultimate resolution which might be expected in an MREV-8 CRAMPS measurement. Comparison of the $-M_x$ and MREV-8 CRAMPS linewidths in Table II shows the extent of our success in this regard. The aliphatic lines for 4,4'-dimethylbenzophenone and 2,6-dimethylbenzoic acid, which correspond to a single chemical type, are of the order of 2 ppm greater than the phase-pull results. This difference is most likely due to higher-order cross terms not removed by the MREV-8, and magnetic field inhomogeneities over the sample due to field drift and demagnetization fields from the sample coil and rotor geometries, which may not be averaged by spinning around a fixed axis. We know from other work in this laboratory that this latter broadening may be as great as 60 Hz in our spectrometer (124).

Finally, also listed in Table II are the CRAMPS linewidths observed when the MREV-8 pulse cycle was substituted for by the Burum and Rhim 24-pulse cycle. It is seen that the individual linewidths were generally from 55 to 110 Hz,

and a considerable enhancement of resolution was achieved, reflecting the removal of second-order dipolar contributions. This leaves as linewidth contributions still higher-order dipolar terms, lifetime broadening, chemical shift dispersion, magnetic susceptibility and field drift induced inhomogeneities, and unresolved spin-spin couplings. This latter mechanism is typically 0 to ±20 Hz for protons, and so could be making a significant addition to residual linewidths. It is interesting to note that since these couplings are not field dependent, while the chemical shifts are, increasing the magnetic field (using, e.g., a superconducting magnet) could conceivably lead to resolving these proton-proton J-J couplings for the first time in solids (although it is important to realize that increasing the field too greatly might lead to chemical shift anisotropies of such a magnitude that they could no longer be removed by magic-angle spinning at $\leq$ 4 KHz). Also, only a small further enhancement of the resolution under the present conditions might have the same effect.

The interaction between multiple pulse homonuclear dipolar decoupling experiments and magic-angle spinning

The possibility of combining multiple pulse experiments and magic-angle spinning such as was described above was first discussed in 1968 by Haeberlen and Waugh (65). At that time, it was suggested that the interaction of the two

experiments should lead to a dependency of the line-narrowing ability of the multiple pulse sequence on the rotational cycle time, t_r, with maximum decoupling efficiency in the limit of $t_r = 0$ (thus amounting to another line broadening mechanism in the CRAMPS experiment). It has subsequently been argued that if the rotational cycle time is long compared to the multiple pulse cycle time, t_c, there is no interaction between the two experiments with regard to dipolar decoupling (108). In the work reported above, generally, $t_r > 300$ μsec and $t_c < 30$ μsec, or about an order of magnitude difference.

Figure 21 illustrates the apparent primacy of the latter argument. MREV-8 CRAMPS linewidths for ^{19}F in polycrystalline CaF_2 were measured as a function of rotation speed for two different angles of the rotation axis, the magic-axis (54^o 44') and 90^o (upright in the horizontally directed field), for t_c=36 μsec. CaF_2 is a cubic difluoride, with fluorine site symmetry T_d, so that there is no chemical shift anisotropy associated with this sample (125, 126). Thus, it is possible to observe residual dipolar broadening effects in this sample without interference from $\Delta\sigma$. It is seen that at the magic-angle there is no apparent dependency of the linewidth on t_r. Furthermore, there is also no apparent dependency on the angle of the rotation axis, α. Since under conditions of sample

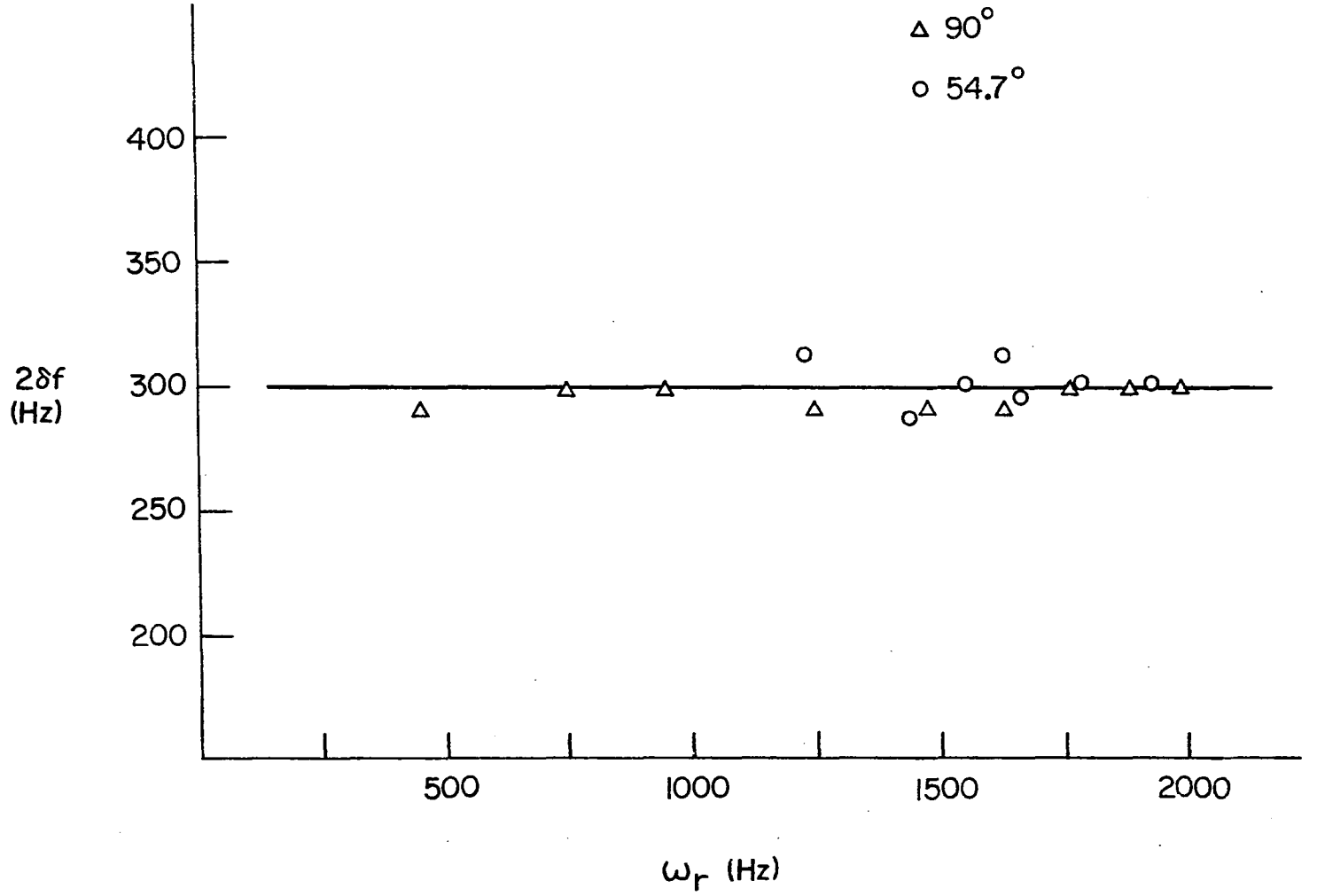

Figure 21. ^{19}F CRAMPS linewidth of CaF_2 as a function of spinning speed, ω_r $(1/t_r)$, for two angles of the rotation axis, 54°44' and 90°

rotation the dipolar contribution depends on the angular factor $(1-3\cos^2\alpha)$, it is to be expected that if there were a sizeable dipolar contribution due to the interaction of the spinning and the multiple pulse cycle, that the line-width should be significantly greater for $\alpha=90^{o}$, than for $\alpha=54.7^{o}$. Figure 21 demonstrates that this is not the case. Also, similar results were obtained for t_c=42 μsec and 48 μsec.

CHAPTER 4. ^{1}H NMR OF SOLID FOSSIL FUELS

Introduction

The combination of high-speed magic-angle sample spinning and multiple pulse homonuclear spin decoupling experiments (CRAMPS) was demonstrated in the previous chapter to be a viable method for producing relatively high resolution ^{1}H NMR spectra of rigid, chemically complex amorphous and polycrystalline solids. The spectral resolution presently achievable with that method (1-2 ppm), however, as noted, is still two-to-three orders of magnitude broader than is typically accomplished with proton NMR of liquids, thereby limiting the technique's usefulness as an analytical or research tool.

Nevertheless, it is still possible to imagine applications, involving, e.g., nonsoluble solids for which ^{1}H CRAMPS may potentially be of much practical import. Included among those might be: measurements of proton chemical shift tensors in solids with more than one distinct hydrogen chemical type (off-magic-angle CRAMPS) (127, 128), the characterization of molecular structures in solid carbonaceous materials, e.g., coals, cokes, etc. (129), and studies in relation to heterogeneous catalysis (130,131). This latter possibility is considered briefly in the following chapter.

In this chapter are described applications of proton CRAMPS in probing structural features of solid fossil fuels, and, in particular, those found in coals, coal tars, and oil shale kerogens. Specifically, in the work described, ^{1}H CRAMPS was used to infer the distribution of hydrogen atoms between aromatic and nonaromatic structures in 19 coal vitrains varying in rank from 70.9% C to 93.0% C (lignite through anthracite). Also, the H-aromaticity of a coal tar and four samples of kerogen (of different maturity or origin) were investigated. Further, the average size of polycondensed aromatic ring clusters in the above samples have been estimated on the basis of the CRAMPS data and other additional information. The latter included: 1) elemental analyses (daf) of the solid samples, 2) carbon aromaticities as determined by ^{13}C solid-state NMR (32) as well as Fourier transform infrared (FTIR) spectroscopy (132), and 3) H-aromaticities and percent hydrogen in OH groups as determined by FTIR (132). The ^{13}C NMR measurements were made at Iowa State University by P. D. Murphy and reported in an earlier thesis (32). The FTIR results are due to Dr. P. R. Solomon (Advanced Fuel Research, East Hartford, Conn.) (132)

Coal aromaticity and the chemical structure of coal (and other solid fossil fuels) are of much current interest (133), as noted earlier, in regards to devising improved

processes for conversion to substitute liquid and gaseous fuels, and chemicals (134), as an alternative to petroleum. In addition, in light of anticipated increased use of coal as an energy source and chemical feedstock, knowledge of possible sizes of polynuclear aromatic (PNA) ring clusters in coals might be useful to indicate possible physiological effects of contact with conversion products, since many PNAs are known, or suspected carcinogens (135-137).

The aromaticity of coal

Coal is a nonhomogeneous, sedimentary rock (134), primarily organic in its composition, but also incorporating many inorganic components. It is now understood that coal is the fossilized remains of terrestrial vegetation (134, 138-142), which was formed by decomposition of plants in aqueous media. The initial product was peat. Through burial, and the action of overburden pressure and heat, subsequent chemical transformations yielded coals. The initial stage in "coalification" of peat is the formation (after millions of years) of lignite, followed by subsequent transformations into subbituminous coal, and possibly (134), bituminous coal and anthracite. During this maturation process, or increasing in rank, the carbon content of coal characteristically increases (134), while the relative percentages of oxygen and (in the later stages of coalification) hydrogen decreases (134).

Since a great diversity of plant substances and diagenetic (pre-deposition) and metamorphic (post-deposition) conditions were involved in the formation of coal (134), its organic portion is chemically complex, as well as heterogeneous. Coal might be regarded as a heterogeneous polymeric structure of high molecular weight, describable by average structural characteristics (i.e., the average number of aromatic carbon atoms, average number of rings, etc.) (138). Many different techniques have been aimed at unraveling the molecular structures in coal. Included among them are: pyrolytic (143-146) and chemical (147-153) degradation of coals into smaller, more easily analyzed fragments, studies of physical properties of coals (154), such as density, molar volume, and sound velocity in coals, and spectroscopic techniques (154-158), including X-ray diffraction, infrared absorption, nuclear magnetic resonance, and ultraviolet spectroscopy. For a recent review of researches concerning the chemical structure of coal, the reader is referred to the report by Davidson (133).

The classical view of coal molecular structure considers coal to be highly aromatic, comprised of polycondensed aromatic rings with various short-chain peripheral substituents, connected largely by aliphatic and alicyclic bridges (138, 139). It is also believed that the total

aromatic fraction and the average size of the aromatic clusters increases progressively with increasing coal rank (138). This picture of coal as a predominately aromatic material has, however, been challenged in the past by several investigators (159, 160).

The following subsections review past evidence pertaining to the question of aromaticity in coal. Following that, the ^{1}H CRAMPS and related experiments discussed above, and their implications regarding coal aromaticity and the structure of coal and kerogen are described.

Early chemical degradation studies

The earliest evidence of coal aromaticity came from studies of the products of coal oxidation (161-193) and hydrogenation (151, 194-198) reactions. Mild oxidation of coal converts a large portion of the organic fraction into alkali soluble substances, termed "regenerated" humic acids. Humic acids are alkali soluble organic molecules formed by the decay of vegetable matter (199), and are thought to be precursors in coal formation. These materials are believed to have chemical functionality similar to coals (149). Continued oxidation, beyond the regenerated humic acids, produces a series of water soluble acids (149), which vary in complexity from highly complex colored acids of indefinite (but apparently (149) aromatic) composition to smaller,

identifiable acids, such as oxalic and succinic acid and, notably, a variety of benzene carboxylic acids (149, 161-193). The latter compounds have been taken as proof of the existence of aromatic substances in coal, since the conditions involved in their formation are not conducive to the development of aromatic from aliphatic material (149).

In an early study of primary coal oxidation products, Francis and Wheeler (175), in 1925, investigated the composition of regenerated humic acids by further degradation of those with hydrogen peroxide and, also, nitric acid. Identification of the simpler compounds obtained, following intermediate action of H_2O_2, showed evidence of pyromellitic acid (1,2,4,5-benzenetetracarboxylic acid). In addition, there was evidence of trimellitic acid (1,2,4-benzenetricarboxylic acid) being present. Isolated from the HNO_3 products were picric and pyromellitic acids and 4,6-dinitroresorcinol, along with a number of aliphatic dibasic acids, including oxalic and succinic acid. The observation of aromatic products was taken by Francis and Wheeler as proof of the existence of aromatic nuclei in the regenerated humic acids, and hence, in the original coal matrix, since, as they stated, "no part of [the] treatment [was believed] to cause ring formation where none previously existed."

In a later study, Fuchs and Stengel (176) also oxidized

regenerated humic acids with nitric acid and observed the formation of mellitic (benzenehexacarboxylic), benzenepentacarboxylic, pyromellitic, and trimesic (1,3,5-benzenetricarboxylic) acids. Ward (185), still later, while oxidizing regenerated humic acids with alkaline permanganate, isolated as intermediate products hydroxy-carboxylic acids, which upon further oxidation were converted into mixtures of aliphatic and benzene carboxylic acids. Ward postulated from these results that alkaline permanganate oxidations of coals (vide infra) and humic acids proceed according to the following scheme:

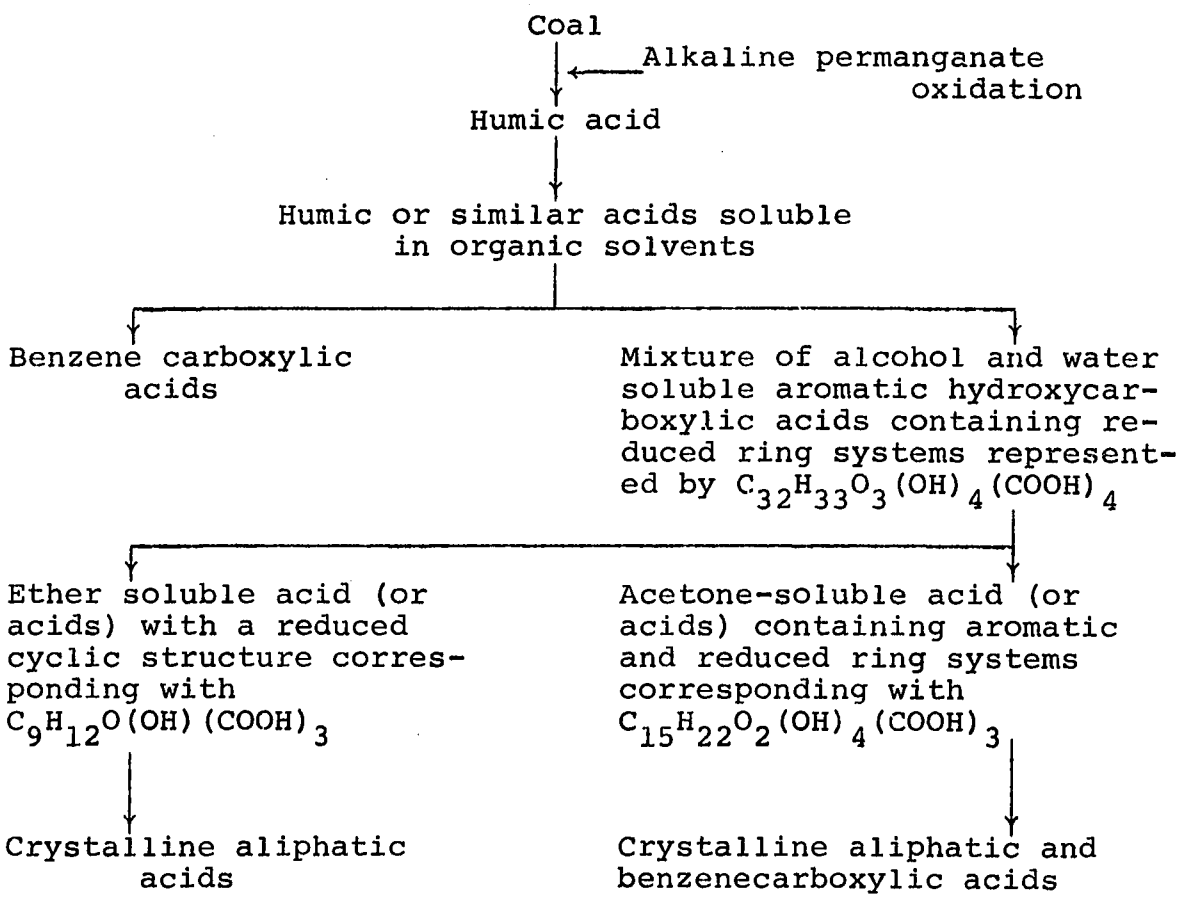

Again, from those two works, it would appear that regenerated humic acids are comprised of aromatic structures (and from the latter, that those are connected by nonaromatic linkages, possibly containing oxygen).

Other experiments in oxidations of regenerated humic acids and, especially, coals, by strong oxidizing agents, similarly produced evidence of aromaticity (149, 161-174, 177-184, 186-193). The work of Bone and coworkers (168-174), who first proposed the so-called "benzenoid ring" theory of coal structure is particularly noteworthy. By degradations of coals with alkaline permanganate, Bone and his coworkers were able to quantitatively determine the distributions of carbon among the oxidation products of a series of coals of different rank; also the carbon distributions were determined during the oxidation of a number of related model substances, including cellulose, lignin, and a number of condensed cyclic compounds.

Among the water soluble products obtained were acetic and oxalic acid and benzene carboxylic acids, along with other aromatic, and heterocyclic acids (the latter two types were not differentiated by Bone from benzecarboxylic acids (199)). It was demonstrated conclusively by these studies that benzenecarboxylic acids are produced by the degradative oxidation of condensed aromatic structures, and it was also determined that oxalic acid may similarly derive from

such materials (174). The observation of acetic acid, on the other hand, was determined to be indicative of aliphatic substances in the starting material. More importantly, it was shown by Bone et al. (172) that the aromaticity of coal (via the percentage of carbon detected in the benzenecarboxylic acids) increases progressively, beginning with coal precursors, such as lignin and cellulose, through the coal series from peat to anthracite (Table III).

Of similar importance as the work of Bone et al. in early coal structure studies by oxidation, was the work of Howard and his coworkers (177-182, 187, 188, 190), who made extensive investigations of carboxylic acid products from coals and other carbonaceous materials. In 1935, e.g., Juettner, Smith and Howard discovered evidence in bituminous coal of large condensed aromatic ring structures (177). This view was proposed on the basis of their isolation of solid aromatic hydrocarbons following decarboxylation of coal acid products, which were denser than water, and appeared in higher boiling distillation fractions than benzene. These workers later (179) reported further decarboxylation studies. The work involved examination of the methyl esters of coal acids, a substantial fraction of which did not distill at temperatures above those characteristic of the boiling range for esters of simple benzenecarboxylic acids.

Table III. Distribution of carbon among products of alkaline permanganate oxidation of coals and coal forming materials (172)

Percentage of carbon present in the original material appearing as:	Cellulose	Lignin	Peats	Brown Coals and Lignites	Bituminous Coals	Anthracite
Carbon Dioxide	48	57-60	49-61	45-57	36-42	43
Acetic Acid	3	2.7-6.0	3.1-5.6	3.0-7.5	1.7-4.6	2
Oxalic Acid	48	21-22	15-18	9-23	13-14	7
Benzenecarboxylic Acids	0	11.8-15.8	10-25	22-34	39-46	50

Again in 1937, Juettner (178, 180) studied the production of mellitic acid from samples of coal, coke, and graphite. Mellitic acid is considered especially germane to the characterization of coal aromaticity in that it can only be formed by oxidation of condensed aromatic structures, the simplest of which is triphenylene,

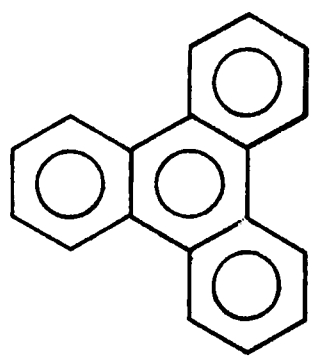

triphenylene

or from completely alkylated benzene compounds, such as hexamethylbenzene (138). Juettner discovered that in a series of carbonaceous materials, from a low rank coal through graphite, the production of mellitic acid increased progressively in order of increasing rank (Table IV). It was observed earlier that the total amount of aliphatic substance in coals decreases with increasing coal rank (172); it is, therefore, unlikely that the additional mellitic acid from the higher rank materials was due to completely alkylated benzene rings. Juettner's results, then, imply a greater proportion of polycondensed aromatic molecules as coal matures.

Table IV. Data on coal oxidations (178)

Material	Carbon per 100 g (g)	Residue after HNO_3 oxidation (g)	Total acids after permanganate oxidation	Mellitic acid recovered (g)	Mellitic acid formed per 100 g carbon (g)
Illinois no. 6	69.50	68.0	19.3	4.3	11.9
Pittsburgh	78.27	70.1	28.1	5.5	12.1
High Splint	78.70	53.2	14.4	5.0	11.4
Pocahontas no. 3	85.10	92.4	25.8	10.9	17.5
Anthracite	82.87	77.2	32.6	17.7	26.2
Natural Graphite	97.40	78.5	26.9	21.7	28.2

Interesting results were also obtained by Ward, Kirner, and Howard (182), who oxidized a number of condensed aromatic compounds, along with other more saturated compounds and a bituminous coal. The compounds studied were tetralin, dodecahydrotriphenylene, triphenylene, decacyclene, trisdecahydrodecacyclene, naphthacene, pyrene, diphenylene oxide, and carbazole. It was found that the least reactive structures among those were the nearly saturated ones, dodecahydrotriphenylene and trisdecahyrodecacyclene, followed by the aromatic hydrocarbons, decacyclene and triphenylene. Then came the heterocyclic substances, diphenylene and carbazole, while still more easily oxidized were the naphthacene, pyrene, and the bituminous coal sample. Tetralin oxidized the most rapidly. It was concluded from these results that bituminous coals are highly aromatic condensed cyclic structures (however, it may be noted that an earlier oxidation study of condensed cyclic compounds (200) led to the opposite conclusion; i.e., that coals do not contain many condensed aromatic rings).

Although studies of coal oxidation products provided much of the first evidence and details of coal aromaticity, early investigations by hydrogenation (151) also produced evidence of aromatic structures in coal. Biggs and Weiler (194-196), e.g., used mild hydrogenation at 350^{o}C with a

copper-calcium chromite catalyst to study the extract and residue from an extraction of bituminous coal by benzene at 260°C and sufficient pressure to maintain benzene in the liquid state. For both the extract and the residue, it was found that 80% of the original carbon was converted by hydrogenation into petroleum ether soluble oils. Those oils were, in turn, determined to be primarily hydrogenated polycyclic aromatic compounds. Distillation of the mixtures produced a distillable and a nondistillable fraction. Characterization of the components by means of boiling points, refractive indices, and hydrogen/carbon ratios indicated polycyclic hydroaromatic hydrocarbons comprised of from two to six rings in the distillable fractions, and of seven or more rings in the nondistillable fractions. Because of the copper-chromium oxide catalyst used, which is particularly effective in breaking cyclic and linear ether oxygen linkages (194), the moderate temperatures involved (which would seem to preclude appreciable thermal degradation of the coal structure), and the high yields obtained, it was believed that the components of the oils represented represented fundumental structural units in the coal. Additional support for Biggs' and Weiler's conclusions was later provided by coal hydrogenation experiments due to LeClaire (197).

Kreulen (198), at about this time, described the results of experiments in which humic acids were hydrogenated at

280°C and 300 atmospheres pressure of hydrogen. The oil so obtained was found to contain a large fraction of naphthenic rings linked by aliphatic bridges. Taken with the results of Biggs and Weiler, and those of Leclaire, there is again implied a progressive enrichment in cyclic-aromatic structures with increasing rank. The results of these early structural hydrogenation experiments thus supported the picture of coal aromaticity developed through oxidations of coals.

While chemical degradation studies during the first half of this century produced considerable experimental data suggesting a predominately aromatic structure for coal (vide ante), there was also criticism that because the exact reaction pathways between starting materials and end products were not well known, little could, in fact, be made of this data. It was argued that the aromaticity observed in degradation products of coal conceivably could be the result of the chemical processes involved, via secondary ring-forming reactions, and does not reflect an intrinsic characteristic of coal.

Howard (201) challenged that proposition on several points. First, he noted, aromatic products were obtained in experiments conducted at temperatures well below those at which secondary cyclizing reactions might reasonably be expected to occur. Secondly, the lack of any evidence

connecting the temperature of the experiments with the yield of aromatic products also argues against such reactions. Finally, the correlation between rank and yield of aromatic products observed by Bone et al, (172) is inconsistent with the idea of a nonaromatic coal structure, since the yield of such products, if formed by secondary reactions, would be expected to be independent of the structure of the starting material.

Howard also noted that other observations of coal point to similar conclusions; e.g., the atomic carbon to hydrogen (C/H) ratio in coals is typically greater than unity, which is suggestive of a condensed aromatic framework. Again, this also suggests an increase in aromaticity with rank, since C/H increases with rank (in recent years it has been noted that tetrahedral structures also have high C/H ratios, and those have been suggested as basic structural units in coals (vide infra)).

X-ray diffraction

Rather than analyze bits and pieces of coal structures by chemical degradation or pyrolysis, a number of workers have attempted to characterize coals by nondestructive methods (154). One of the first techniques applied in that way was x-ray diffraction (202-205).

X-ray diffraction patterns of coals characteristically exhibit a number of broad bands, whose maxima occur at positions close to, or identical with, those associated with amorphous graphite. That fact was first noted by Mahadevan (202-205) and others (206-215), and suggests that coals contain clusters of condensed aromatic rings (but see reference 216-218). Further, the diffraction patterns from coals become increasingly sharp with rank, and more exactly reproduce the detailed features of graphite (138, 211, 219-221). This includes the appearance, in high rank anthracites and meta-anthracites, or three-dimensional reflections characteristic of graphite single crystals (222-225). This implies that as coals mature, they become more graphite; i.e., the average size of the condensed aromatic clusters in coals increases as coal rank increases.

All of the above is in keeping with conclusions about coal aromaticity that were deduced from earlier chemical degradation studies (vide ante). X-ray diffraction, in addition, allows some quantitative aspects of coal aromaticity to be investigated, based on theoretical fits of the x-ray lines (154).

The diffuse nature of x-ray diffraction patterns of coals has been attributed to the relatively small crystallites present (210). However, a more complete explanation has been proposed (211), based on a "turbostratic" (226, 227) lamellar structure within coal. In this model,

graphite-like layer planes (polyaromatic lamellae) are arranged in small, essentially parallel stacks, but are more-or-less randomly oriented about layer normals (depending upon the rank of the coal). This imperfect ordering of the lamellae relative to crystalline graphite produces the broadening observed in certain portions of the x-ray spectra. For example, the (002) band, which corresponds to the interlayer spacing in graphite (154), may be associated with stacking of the lamellae, while the (10) and (11) bands are due to flat, two-dimensional ring structures in coals (154). By fitting the experimentally determined x-ray spectra with theoretical scattering curves (226, 228, 230-235), or by using the Fourier transformation of the scattering curves as a radial distribution function (229, 235), it is possible to estimate both the average diameter of the aromatic lamellae (and, hence, the number of rings in the average polyaromatic cluster), and also the average height of the parallel stacks (211, 212, 219-221, 228-236).

Blayden et al. (211), in 1944, were the first to make such determinations on coals. Those workers, using relations between linewidth and lamellae diameter worked out by Warren (226), found the average aromatic cluster size to vary from about 20 Å in coals of between 60 and 90 percent carbon, to 30 Å for coal of 95 percent carbon. Those values correspond to polyaromatic clusters of 50 to 100 fused benzene rings (211).

It is now known (138) that several important factors influencing the results in x-ray experiments on coals were not considered in that first study, and the numbers obtained, while qualitatively significant, were simply too large (138, 154). Later work, by Hirsch (219), and by Brown and Hirsch (220), indicated that in coal vitrains of between 78 and 87 percent carbon, the lamellae diameters are only about seven to eight angstroms (4 or 5 fused rings). Above that, the aromatic cluster size appeared to increase rapidly, up to 9 Å (7 fused rings) at 89% C, to about 16 Å (30 fused rings) in anthracite with 94.1% C (219,220). Further, the vertical stacking of the aromatic layers, while sometimes occuring in groups of two or more, was found to be largely limited to single lamellae (219,220).

Nelson (229), using a somewhat different approach, argued that coals with 77-89% carbon cannot contain more than four fused rings. He based his results on atomic radial distribution curves determined for vitrinites in the range from 77-89% C and comparisons with condensed aromatic hydrocarbons. Hirsch, in still later work (221, 236), using more refined techniques of analysis (230-232) than were available earlier, found results more in line with those proposed by Nelson. Amending his earlier values (219, 220), Hirsch concluded (221) that in coals with 78% C there are only

about 2 fused rings per aromatic cluster, increasing to about 4 in coal with 90% C, followed by rapid condensation to about 12 rings in anthracite with 94 percent carbon.

In addition to these evaluations of average lamellae dimensions in coals, it was also shown by Diamond (230-232) to be possible to calculate layer size distributions using information from x-ray diffraction. Diamond generated molecular size histograms for a series of coals which showed the relative proportions of various layer sizes as a function of rank. His results, and similar analyses by Hirsch (221), indicated that in coals of less than 90% C there are few aromatic clusters of greater size than three condensed benzene rings. Beyond 90 percent, highly condensed aromatic clusters appear, and increase in size and relative proportion with rank.

Statistical constitution analysis

Chemical degradations and x-ray analyses of coals, as shown above, at least up to about 1960, were consistent in their implications for coal aromaticity; i.e., that coal is strongly aromatic and the aromaticity increases with rank. Other analytical methods employed at about the same time, especially those described as "statistical constitution analysis (138, 237-241)," provided further support for those conclusions. Statistical constitution analysis methods also

produced the first consistent measures of the fraction of aromatic carbon, $f_a = C_a/C$, in coals.

Statistical constitution analysis, pioneered by van Krevelen and coworkers (138, 237-241), following the work of Vlugter et al. (242-244) on petroleum characterization, was based on the fact that many physical properties of materials are additive; i.e., the molecular values of some properties may be expressed as a summation of individual atomic contributions plus contributions from structural factors, e.g., effects of bonding between atoms (245). In such cases, it is possible to write a general expression (245) of the form

$$MF = C\phi_C + H\phi_H + O\phi_O + \ldots \sum_i X_i \phi_{X_i} \qquad (37)$$

where

M = molecular weight

MF = additive function, expressed on a per mole basis

C, H, O, etc. = number of atoms of a given type per mean structural unit

X_i = number of structural factors of the i^{th} kind per mean structural unit

and

$\phi_C, \phi_H, \ldots \phi_{X_i}$ = contributions to the additive functions by atoms and structural factors, respectively, which may be derived from data on model compounds.

Since the molecular weight of a complex material such as

coal is difficult to determine explicitly, in the sense that there is really a distribution of molecular weights, it was shown by van Krevelen and Schuyer (245) that the above equation can be written in a more useful "reduced" form by dividing it through by the number of carbon atoms, C. Thus

$$\frac{MF}{C} = \phi_C + \frac{H}{C}\phi_H + \frac{O}{C}\phi_O + \cdots \sum_i \frac{X_i}{C}\phi_{X_i} \quad . \tag{38}$$

Further, since it is possible to write

$$(\%C) = \frac{12C}{M} \times 100, \quad \text{or}$$

$$\frac{M}{C} = \frac{1200}{(\%C)} = M_C \quad , \tag{39}$$

one can write

$$\frac{1200}{(\%C)}F = \phi_C + \frac{H}{C}\phi_H + \cdots \sum_i \frac{X_i}{C}\phi_{X_i} \quad , \tag{40}$$

producing an expression in terms of %C, the carbon content of the structure of interest, or in this case, the carbon content of coals, which is obtainable from elemental analysis.

Now if one of the structural parameters on which F depends can be shown to be C_a, the number of aromatic carbon atoms, then

$$\frac{1200}{(\%C)}F = \phi_C + \frac{H}{C}\phi_H + \cdots f_a\phi_{C_a} + \sum_{i-1} \frac{X_{i-1}}{C}\phi_{X_{i-1}} \quad . \tag{41}$$

And if the additional X_{i-1} parameters can be accounted for (238, 239, 245, 246), it is possible to generate correlations between physical properties of coals and f_a, the fraction of aromatic carbon, thereby permitting f_a to be determined (245).

It was further noted by van Krevelen (245) that for pure hydrocarbon structures, the following relationship exists

$$^2\frac{R-1}{C} = 2 - f_a - \frac{H}{C} \quad , \tag{42}$$

where R is the number of rings (aromatic and alicyclic) in the hydrocarbon, and $^2\frac{R-1}{C}$ is called the "ring condensation index." For other types of structures, corrections for elements other than carbon and hydrogen may be made (245) in Equation 42 provided the nature of their bonding is known, and for polymeric substances such as coal, it is also necessary to account for the average number of bridges, B, per structural unit. Thus, e.g., for a polymeric material containing carbon and hydrogen only (245)

$$^2\frac{R-1}{C} = 2 - f_a - \frac{H}{C} - \frac{B}{C} \quad . \tag{43}$$

The point of Equation 43 is that if either f_a or R can be determined, the other can be readily deduced by empirical relations (245).

Using statistical analysis, then, van Krevelen and

coworkers (138, 237-241, 245-257) and others (258-264) via a variety of additive properties, were able to determine values for the aromaticity, f_a, in coals, as well as determine information about the average size of condensed cyclic structures present. By way of example, in one of the first applications of the method, van Krevelen and Chermin (239) used molar volumes to first determine the total number of rings per carbon atom, $\frac{R}{C}$, in a number of coals, and from those values, the corresponding f_a's. An expression for "reduced" molar volume similar to Equation 41 was first deduced, in which the only nonnegligible term involving structural factor was one for R

$$V_M = 9.9 + 3.1\frac{H}{C} + 3.7\frac{O}{C} + 1.5\frac{N}{C} + 14\frac{S}{C} - V_R \frac{R}{C} \quad . \qquad (44)$$

V_R is the molar volume contraction caused by ring formation, and was found by van Krevelen and Chermin to vary linearly with the atomic $\frac{H}{C}$ ratio (239, 245)

$$V_R = 9.1 - 3.6\frac{H}{C} \quad . \qquad (45)$$

Additionally, since the molar volume can be described by

$$V_M = \frac{M}{d} \quad , \qquad (46)$$

where d is the density, the final formula becomes

$$\frac{1200}{(\%C)d} = 9.9 + 3.1\frac{H}{C} + 3.7\frac{O}{C} + 1.5\frac{N}{C} + 14\frac{S}{C} - (9.1 - 3.6\frac{H}{C})\ \frac{R}{C} \quad . \qquad (47)$$

Values for density calculated by means of Equation 47 were compared by van Krevelen and Chermin (239) with measured densities for eighteen polymers and were found to be in excellent agreement, thereby establishing the reliability of the technique.

Next, van Krevelen and Chermin used Equation 47, together with data on the density and elementary composition of 11 coals and a graphite, to calculate the $\frac{R}{C}$ ratio for those samples (239). Their results are shown in Table V. It is seen that the number of rings per carbon atom reaches a minimum at about 85 percent C, corresponding to the characteristic minimum in the density of coal as a function of metamorphic development (239, 265, 266). Table V also indicates the values obtained by van Krevelen and Chermin for f_a. In making this determination, an expression similar to Equation 42 was used. An adjustment was made to correct for the oxygen, nitrogen, and sulfur contents of the coals (239, 245).

It must also be noted that in calculating f_a, it was assumed by van Krevelen and Chermin that $R \gg 1$, a purely experimental necessity, since only $\frac{R}{C}$ ratios were available, while Equation 42 requires the ring condensation index, $2\,\frac{R-1}{C}$. Rearranging Equation 42, we have

$$f_a = 2 - \frac{H}{C} - 2\,\frac{(R-1)}{C} \quad , \tag{48}$$

Table V. Aromaticity and number of rings per carbon atom of the coalification series (239)

Coal No.	%C	f_a	R/C
1	70.5	0.61	0.26
2	75.5	0.71	0.25
3	81.5	0.77	0.24
4	85.0	0.76	0.24
5	89.0	0.79	0.27
6	91.2	0.77	0.32
7	92.5	0.87	0.32
8	93.4	0.90	0.33
9	94.2	0.92	0.35
10	95.0	0.96	0.37
11	96.0	0.99	0.39
Graphite	(100)	1.00	0.50

or, to a first approximation

$$f_a \approx 2 - \frac{H}{C} - \frac{2R}{C} \quad . \tag{49}$$

Also, it was assumed that the number of bridges is small. The necessity of using Equation 49 to calculate f_a, rather than Equation 48, is a serious limitation for this so-called "densimetric method," and tends to produce values for the

carbon aromaticity which are smaller than those deduced by other statistical methods.

In a later paper, still involving the molar volume, van Krevelen and Chermin demonstrated that a direct correlation between that property and f_a could be found, thereby circumventing the difficulty mentioned above. Substituting a graphical description (the "graphical densimetric method") for the previous algebreic one, those workers plotted on one graph the fraction of carbon in aromatic groups versus $\frac{M_C}{d}$ and $\frac{H}{C}$ for a number of alkyl/aromatic and naphthenic/aromatic hydrocarbons. The extremes in the plot (f_a = 0 and 1) were determined from benzene and graphite (f_a = 1) and paraffinic $-CH_2-$ (f_a = 0). The f_a = 1 line was modified by investigations of pitch fractions (245, 253) and diphenylanthryl (250) and 1, 3, 5,-tri-α-naphthylbenzene (250). From the parallel, equidistant lines produced in this way it was possible to determine the aromaticity of the same series of coals studied earlier, again based on their density and elemental composition (240, 245). Table VI gives the most recent values obtained by this method (245).

In addition to the experiments described above, which employed the molar volume to calculate f_a, other physical properties have been similarly used, including molar refraction (245, 249), sound velocity in coals (255), and heat of combustion (261). Values obtained for f_a by those

Table VI. Aromaticity of vitrinites as inferred from density, molar refraction, sound velocity, and heat of combustion (245)

%C	Graphical Density	Molar Refraction	Sound Velocity	Heat of Combustion
70.5	0.70	0.67		
75.5	0.78	0.76		
80.0				∿0.82
81.5	0.83	0.83	0.79	
85.0	0.85	0.84	0.82	∿0.82
87.0	0.86			
89.0	0.88	0.89	0.85	
90.0	0.90			
91.2	0.92	0.93	0.90	
92.5	0.96	0.95	0.93	
93.4	0.99	0.97	0.97	
94.2	1.00	1.00		
95.0	1.00	1.00		1.00
96.0	1.00	1.00		

methods were all found to be in reasonable agreement (Table VI).

Conformation of the dimensions of the aromatic clusters in coals--deduced primarily by x-ray diffraction studies (subsection 2. b.), but also suggested by chemical degradations (subsection 2. a.)--was also possible using statistical constitution analysis (138, 245). The additive property of choice, in that case (238, 247, 249), was the molar refraction, expressed by

$$\frac{n^2-1}{n^2+2} \cdot \frac{M_C}{d} = R_C + \frac{H}{C} R_H + \ldots I_m \quad , \tag{50}$$

or

$$\frac{n^2-1}{n^2+2} \cdot \frac{1200}{(\%C)d} = 2.6 + 1.0\frac{H}{C} + \ldots I_m \quad , \tag{51}$$

where n is the refractive index, R is the "atomic" refraction, and I_m, the molar refractometric increment, which is seen to be the difference between the experimentally determined molar refraction and the value calculated from the atomic contributions, was assumed to be due to carbon-carbon double bonding in aromatic groups (247, 249). It could be shown theoretically (249) that I_m is directly proportional to the aromatic surface area, S, a suposition which was tested on a number of purely aromatic compounds, and found to be reliable (249). Schuyer and van Krevelen (249) used this method to determine the average aromatic surface area

for a series of vitrinites of between 70.5 and 96.0 percent carbon. Their results are shown in Table VII (from reference 138), expressed in terms of the average number of carbon atoms per aromatic lamellae. Table VII also lists complementary evidence obtained by other methods. It is observed that the values obtained by the several techniques are in general agreement; however, while the most recent x-ray diffraction results (221) suggest ~2-3 rings for coals of 87 percent carbon or less, the molar refraction data implies about 20 carbon atoms and 4-5 rings per layer.

Spectroscopic analysis

Spectroscopic techniques, e.g., IR, NMR, UV, etc., have been an important part of coal structure analysis (133), and in the past 30 years, a considerable literature has accrued in this field. Tschamler and de Ruiter (154) reviewed spectroscopic studies of coal prior to 1963. More recently, a number of extensive reviews have appeared (31, 155-158, 267, 268) which encompass subsequent work. Until recently, spectroscopic studies of coal mostly involved the qualitative detection of alkyl substituents, OH groups, or aromatic hydrogen. However, developments in the past decade, particularly in the areas of ^{13}C (31, 268) and solid-state (31, 269) NMR and Fourier transform infrared spectroscopy (145, 270), have enhanced the ability of spec-

Table VII. Size of aromatic clusters in vitrinites (138) (number of carbon atoms)

%C	Elementary Composition	X-ray Diffraction	Molar Refractive Increment	Semi-Conductivity	U.V. Spectrum
70.5			12		
75.5			13		
81.5		16	17		
84.0		17			>17
85.0		17	21		
87.0		17	(23)		
89.0		18			
90.0		18			
91.2		18			
92.5		18			
93.4	(20)	20		(45)	
94.2	22-40	(30)		(50)	
95.0	43-60			55	
96.0	85-100			>60	

troscopy to produce quantitative information, and details about the carbon skeleton of coal, as well.

IR absorption in coals recorded in the region between 650 and 4000 cm^{-1} produces spectra with ~15-20 bands (138, 271). These peaks have been assigned to various (CH), (CC), and heteroatom functionalities (138, 271). Of particular importance to coal aromaticity are the bands at 3030 and 2920 cm^{-1}, which have been assigned, respectively, to aromatic (272, 273) and aliphatic (272-275) C-H stretches. By estimating the ratio of the optical densities, D_{ar}/D_{al}, and the extinction coefficients, $\varepsilon_{ar}/\varepsilon_{al}$, for those two peaks (271), it has been shown to be possible to estimate the fraction of aromatic hydrogen in coals from their relative intensities (145, 270, 271, 274, 276). Based on the corresponding measured fraction of aliphatic hydrogen it has also been shown to be possible to estimate f_a, the fraction of aromatic carbon, using an equation derived by Brown and Ladner (277).

Nuclear magnetic resonance (NMR) is another spectroscopic technique that can be used to study the distributions of hydrogen in coals (31, 268). With recent advances in the field of Fourier transform ^{13}C NMR (13), measurement of carbon in coals by NMR has also become possible (31, 268). An inherent drawback with this method is that coal is a solid material, and as was noted before, NMR spectra

of solids are typically broad and uninteresting. Coal, unfortunately, is also not especially soluble (134, 138), although studies of solvent extracts of coals have accounted for the bulk of NMR experiments on fossil fuels (31, 268). In those experiments only about 20% or less of the original coal is investigated, and there is no guarantee that the results are representative of whole coals. Specialized solid-state techniques for high resolution ^{1}H (129, 269) and ^{13}C (31) NMR have gone far within the last few years to alleviate much of this problem.

Most early NMR studies of coals were solid state wide-line proton studies (278-284), and while it was not possible in those experiments to detect individual resonances corresponding to particular chemical types, or even chemical classes, e.g., aromatic vs. aliphatic H, analysis of the second moments could be used to make quantitative estimates of the aromatic and aliphatic functionalities in coals. In general, the second moments of NMR absorption lines from coals were found to decrease with increasing coal rank. For example, in a study of three vitrain samples of 79.2, 83.1, and 92.6% carbon, Newman et al. (278) and Bell et al. (279) observed second moments of, respectively, 21.5, 19.5, and 16 gauss^2. Those values were associated with decreasing interproton distance, i.e., increasing aromaticity with increasing rank.

While chemical information could be obtained from broadline NMR, the lack of detail in coal spectra limited its usefulness as a structural tool. Much of this non-specificity can be overcome by studying extracts of coal in solution (31, 268). Solution spectra of protons in coal extracts typically exhibit three bands--an aromatic (+ phenolic) band, a band attributed to benzylic protons, and further upfield, a group of peaks associated with hydrogen farther than alpha removed from aromatic carbons. The advantage of this approach is that hydrogen aromaticity can be directly determined based only on an integration of the associated spectral areas (31, 268). Further, it has been shown by Brown and Ladner (277) that a number of structural parameters related to the carbon skeleton of coal can also be derived from high-resolution ^1H NMR (277, 285) spectra. Their well-known set of equations are

$$f_a = \frac{\left(\frac{C}{H} - \frac{H^*_\alpha}{x} - \frac{H^*_\beta}{y} \right)}{\left(\frac{C}{H} \right)} , \tag{52}$$

$$\sigma = \frac{\left(\frac{H^*_\alpha}{x} + \frac{O}{H} \right)}{\left(\frac{H^*_\alpha}{x} + \frac{O}{H} + H^*_{ar} \right)} , \tag{53}$$

and

$$\frac{H_{aru}}{C_{ar}} = \frac{\left(\frac{H^*_\alpha}{x} + \frac{O}{H} + H^*_{ar} \right)}{\left(\frac{C}{H} - \frac{H^*_\alpha}{x} - \frac{H^*_\beta}{y} \right)} \quad , \tag{54}$$

where $H^*_\alpha = \frac{H_\alpha}{H}$, is the fraction of hydrogens which are attached to carbons α to aromatic rings, H^*_β is the fraction of other aliphatic hydrogens, and H^*_{ar} is the fraction of aromatic hydrogen. The parameter x is the atomic ratio of hydrogen to carbon at α aliphatic positions, and y is the atomic hydrogen to carbon ratio (on average) at all other positions. σ, in Equation 53, is the degree of aromatic ring substitution; i.e., that fraction of the aromatic edge carbons which are substituted. H_{aru}/C_{ar} is the H/C ratio for the hypothetical unsubstituted aromatic ring system corresponding to the polyaromatic clusters in a given coal. This latter parameter is indicative of the size of the aromatic clusters (277, 285).

Coal extracts and coal derived liquids can also be studied directly by ^{13}C NMR (31). It has been shown (286) that carbon aromaticities determined by carbon-13 NMR on coal derived liquids and those derived by ^{1}H NMR and calculations with the Brown and Ladner equation (Equation 52) are in good agreement.

Finally, in recent years, it has become possible to measure ^{13}C (22-26, 31, 32) and ^{1}H NMR (129, 269) of whole coals with moderately high resolution. Results from these

analyses indicate that coals, in accordance with the classical picture of coal molecular structure (138, 139), are highly aromatic, and that the aromaticity of coal increases with rank. These results are particularly important since, as in the case of x-ray analyses, coals were studied in their natural state, obviating many of the ambiguities introduced by dissolution or degradation. Experiments of this type will be further described in Section 3.

Hydrogen aromaticity in coals

Much of what has been said about coal aromaticity to this point has been expressed in terms of the carbon aromaticity or the number of carbon atoms in polyaromatic units in coals. Another important parameter is the fraction of aromatic hydrogen. Together with carbon data, that parameter can provide useful information on the degree of aromatic ring substitution in coals, as indicated by Equation 53 and Figure 22. Also, hydrogen aromaticity values correlate with the average size of condensed aromatic clusters (129, 277, 287).

For example, Tingey and Morrey (287) described the variation of aromatic cluster size with the $\frac{H}{C}$ ratio for completely (peri) and minimally (cata) condensed six-membered rings, as shown in Figure 23. Assuming coal to be entirely composed of condensed benzene rings, and noting

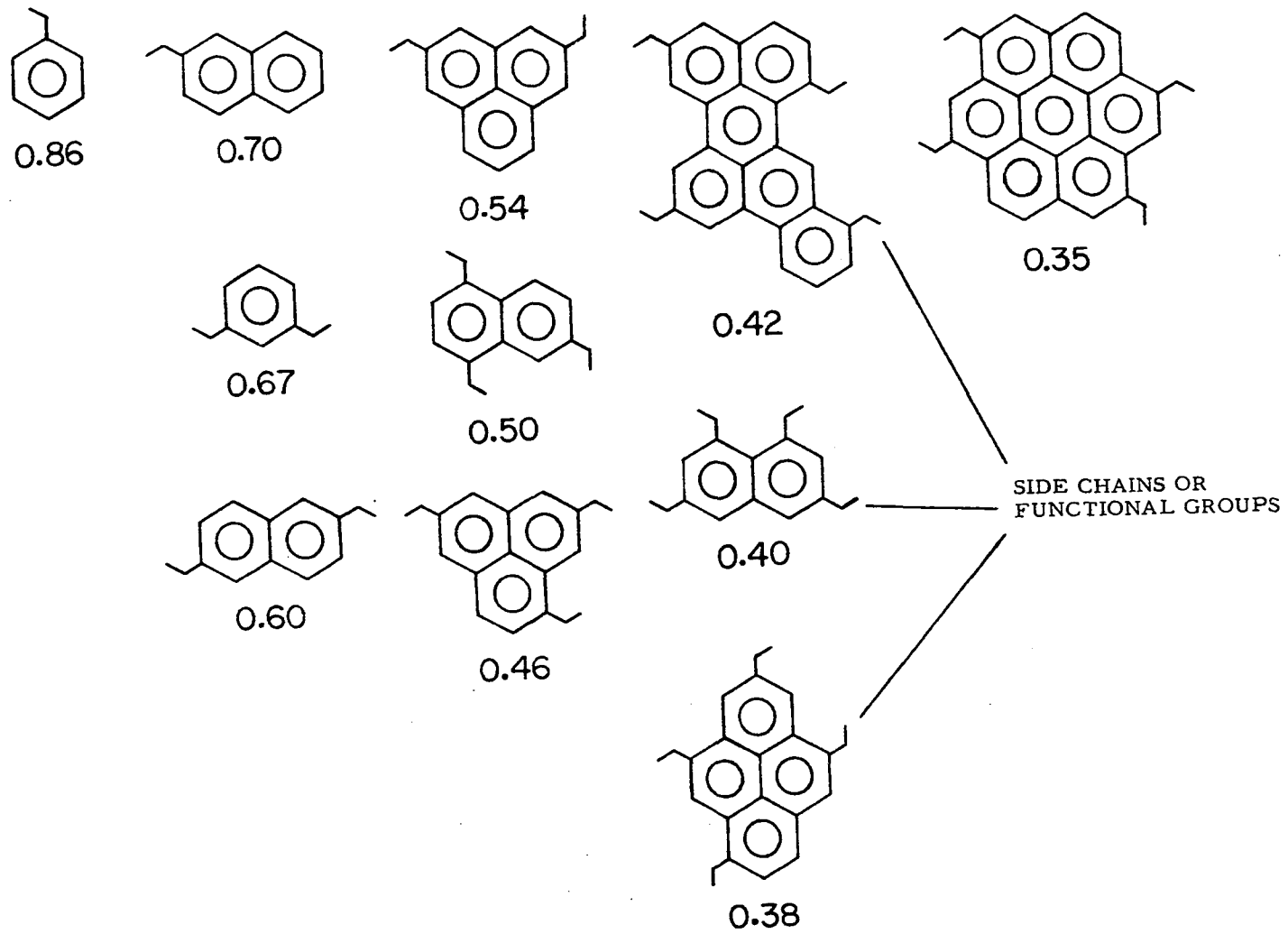

Figure 22. Average aromatic ring size as a function of H_{ar}/C_{ar} and connectivity

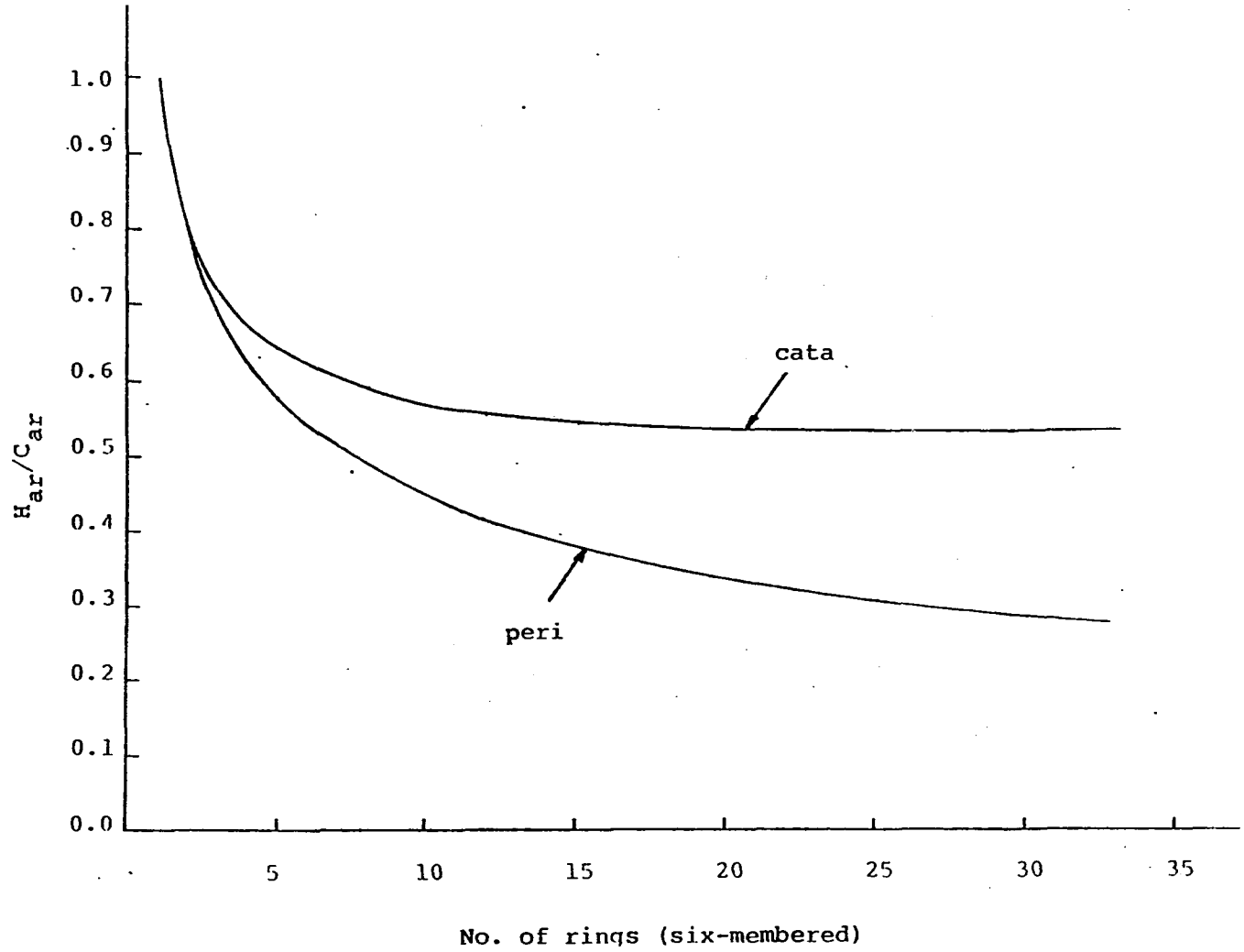

Figure 23. H/C as a function of aromatic cluster size for condensed polyaromatic compounds

the strong correlation between $\frac{H}{C}$ and the carbon content of coals (288), those authors were of the opinion that the average number of aromatic rings per cluster for coal of 70-83% carbon is 2, increasing to between 3 and 5 at 90% C, and becoming >40 for coal of 95% C. Obviously, this example involves an oversimplification of coal molecular structure, as coals are not simply a mixture of polynuclear aromatic hydrocarbons. A more complete picture would require consideration of the actual aromaticity and degree of crosslinking in coals; however, the analysis of Tingey and Morrey illustrates the potential value of hydrogen aromaticity data.

The aromatic hydrogen content of coals of varying rank has been reported by a number of investigators over the past thirty years (267, 272, 282, 283, 289-293). Figure 24 summarizes those experiments. Dryden (293) used the infrared data of Brown (272) to calculate the ratio of aromatic to aliphatic hydrogens in soluble fractions of coal vitrains containing 83 to 91 percent carbon. Ladner and Stacey (283) used IR to analyze for percent aromatic hydrogen in two coals. van Krevelen et al. (289) reported the pyrolysis of coals as a means for determining H_{ar}. Those investigators measured hydrogen in low-temperature chars of vitrinites and assumed that the residual hydrogen was entirely aromatic. In each of the cases above, it was observed that the ratio of aromatic to total hydrogen increased

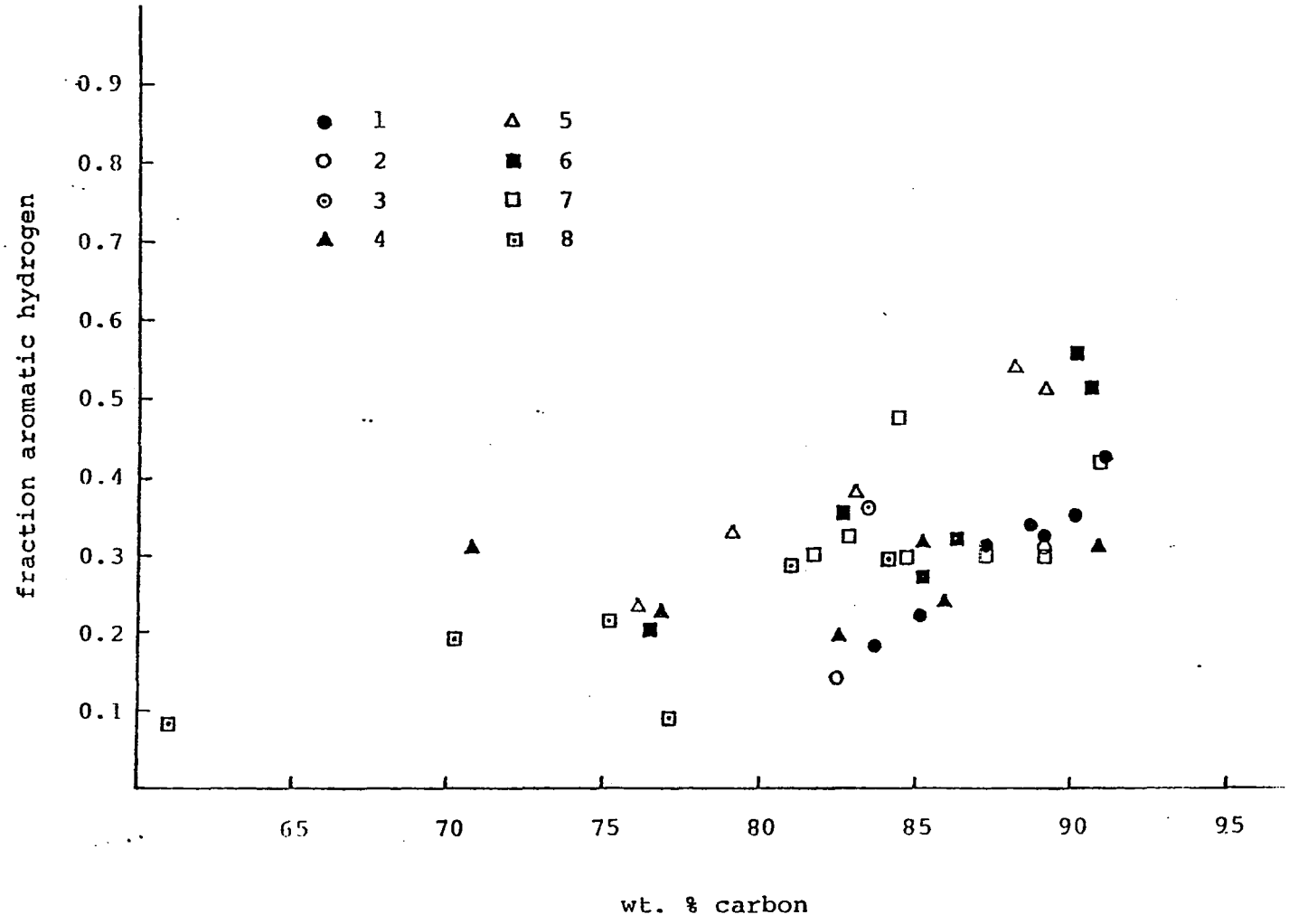

Figure 24. Aromatic hydrogen content vs. coal rank. 1. Ref. 293. 2. Ref. 283. 3. Ref. 282. 4. Ref. 290. 5. Ref. 289. 6. Ref. 267. 7. Ref. 291. 8. Ref. 292

progressively with rank. Heredy et al. (290), in contrast, measured proton NMR spectra of the soluble fractions of phenol- BF_3 depolymerized coals and found no correlation between aromatic hydrogen and rank. Takeya et al. (291), Durie et al. (292), and Retcofsky (267), however, all examined pyridine extracts of vitrains by NMR and concluded that H_{ar}/H increases with higher carbon contents.

Dissenting views; other studies of coal oxidation

There has just been presented evidence, based on chemical degradations, infrared, NMR, and x-ray analyses, and correlations with additive properties, that coal is predominately aromatic. Also, the relative degree of aromaticity and the average size of polynuclear aromatic clusters in coals were shown to increase with increasing maturity. There is still additional evidence, not explicitly mentioned, to support those conclusions, including results from halogenations (153, 294, 295) and pyrolyses of coals (238, 245), esr measurements (154) and electrical conductivity measurements (154, 296). Nevertheless, it must be pointed out that on several occasions in the past forty years the idea of extensive aromatic molecular structures in coals has been questioned (159, 160, 216-218, 297-299).

Ergun and Tiensuu (216-218) and Ergun (297), for example, compared the x-ray scattering patterns from

aromatic and alicyclic model compounds, and determined that either molecular framework could account for the diffraction bands of coals. This observation does not negate the results of Hirsch and others (subsection 2.b.), who concluded that coal is mostly aromatic; however, it does imply that the findings of those investigators are not conclusive. Friedel (159, 298) measured the ultraviolet spectrum of a bituminous coal vitrain and by comparison to UV spectra of various polycondensed aromatic compounds, concluded that polycondensed aromatic structures cannot be significant in bituminous coals. Friedel suggested that sp^3 carbons, including carbons in diamond-like structures, might be the most important type in coals. Other workers (300-305), in contrast, were not in agreement with that assessment; e.g., de Ruiter and Tschamler (303) measured UV spectra of coal solvent fractions and concluded that aromatic cluster sizes comparable with those indicated by other methods are reasonable. Ergun et al. (304, 305), from ultraviolet spectra of coals of different rank, found evidence of small aromatic nuclei in low-rank coals, and also found that the size of the aromatic clusters became larger as the coal rank increased.

More recently, Chakrabartty and coworkers (160, 299) have suggested, on the basis of oxidations of coal with aqueous sodium hypochlorite (NaOCl), that bituminous coal

is less than 50% aromatic, and that there are large amounts of diamond-like or polyamantane structures in coal. This work has been severely criticized (306-311), but the debate over polyamantane structures in coals continues (see Reference 133). There is some additional evidence to support the presence of extended cycloalkane structures in coals (312-316), although not to the extent implied by earlier studies (160, 299). Evidence from other recent oxidations of coal, employing sodium dichromate (153, 309, 310), and measurements of coals by solid-state ^{13}C and ^{1}H NMR (31, 269 - also the following section) still suggest that coals do contain aromatic structures which increase in condensation with increasing carbon content.

Results

Coals

In the previous section, an attempt was made to outline, essentially from a historical perspective, past work related to the nature and degree of aromaticity in coals. In this section are described experiments using solid state NMR which also address this problem. A series of nineteen coal vitrains varying in carbon content from 70.9 to 93% C have been studied by high resolution solid state ^{1}H NMR. Also, results from ^{13}C NMR (32) and FTIR (132) measurements have been used to characterize the coals. Table VIII lists

the elemental compositions of the coals, determined by standard analytical techniques (317). A vitrain portion of the Iowa coals--Upper Mich, Star, and Lovilia--were supplied by D. L. Biggs of the Iowa State University Department of Earth Sciences, and the Ames Laboratory of the U.S. Department of Energy. Pocahontas #4 and Powellton, two Virginia vitrains, were obtained from H. L. Retcofsky of the Pittsburg Energy Research Center. The remaining coals were supplied by P. H. Given, Fuel Science Section, Material Sciences Section, the Pennsylvania State University.

Figures 25-34 show the high resolution ^1H NMR spectra obtained for the nineteen coals described in Table VIII. The spectra were referenced to an external H_2O sample, and no corrections for bulk susceptibility shifts were made. Combined rotation and multiple pulse spectroscopy (CRAMPS), described in Chapter 3, was used to narrow the NMR spectra of ^1H in these coals. Homonuclear dipolar decoupling was accomplished by means of the MREV-8 pulse sequence (69-71), and the cycle time employed in these experiments, 36 μsec, was adequate for proton dipolar narrowing in coals (105). The magic-angle rotation rate was 2-3 KHz, and samples were spun in a rotor of the design shown in Figure 10.

For the spectra in Figures 25-34, the samples were air-dried, but otherwise untreated. Because of concern that residual water in the coals might interfere with

Table VIII. Major constituent analysis of coals, wt. % (daf)

COAL	C	H	N	S	O
Anthracite	93.0	2.5	-	-	-
Pocahontas #4	90.3	4.43	1.28	0.85	3.14
PSOC 268	86.5	5.28	1.53	0.94	5.78
Powellton	85.1	4.49	1.54	0.79	8.08
PSOC 124	83.8	6.89	1.38	0.66	7.26
PSOC 351	83.5	6.1	1.76	1.45	7.22
PSOC 501	83.4	5.6	1.44	0.54	9.03
PSOC 103	82.9	5.08	1.65	0.65	9.72
PSOC 640	82.7	5.6	1.40	1.45	8.81
PSOC 330	82.0	5.14	1.63	0.50	10.75
PSOC 170	82.0	5.36	1.42	1.89	9.36
Bumik 40660	81.3	5.57	1.56	1.50	10.04
Upper Mich	81.0	5.01	0.98	5.53	7.48
PSOC 212	79.4	5.11	1.65	0.83	13.04
PSOC 155	77.9	6.9	1.44	1.00	12.72
Star	77.0	5.46	1.17	5.02	11.35
PSOC 308	76.6	5.13	1.61	1.15	15.51
Lovilia	75.0	4.77	1.36	2.64	16.23
Savage Lignite	70.9	3.6	-	-	-

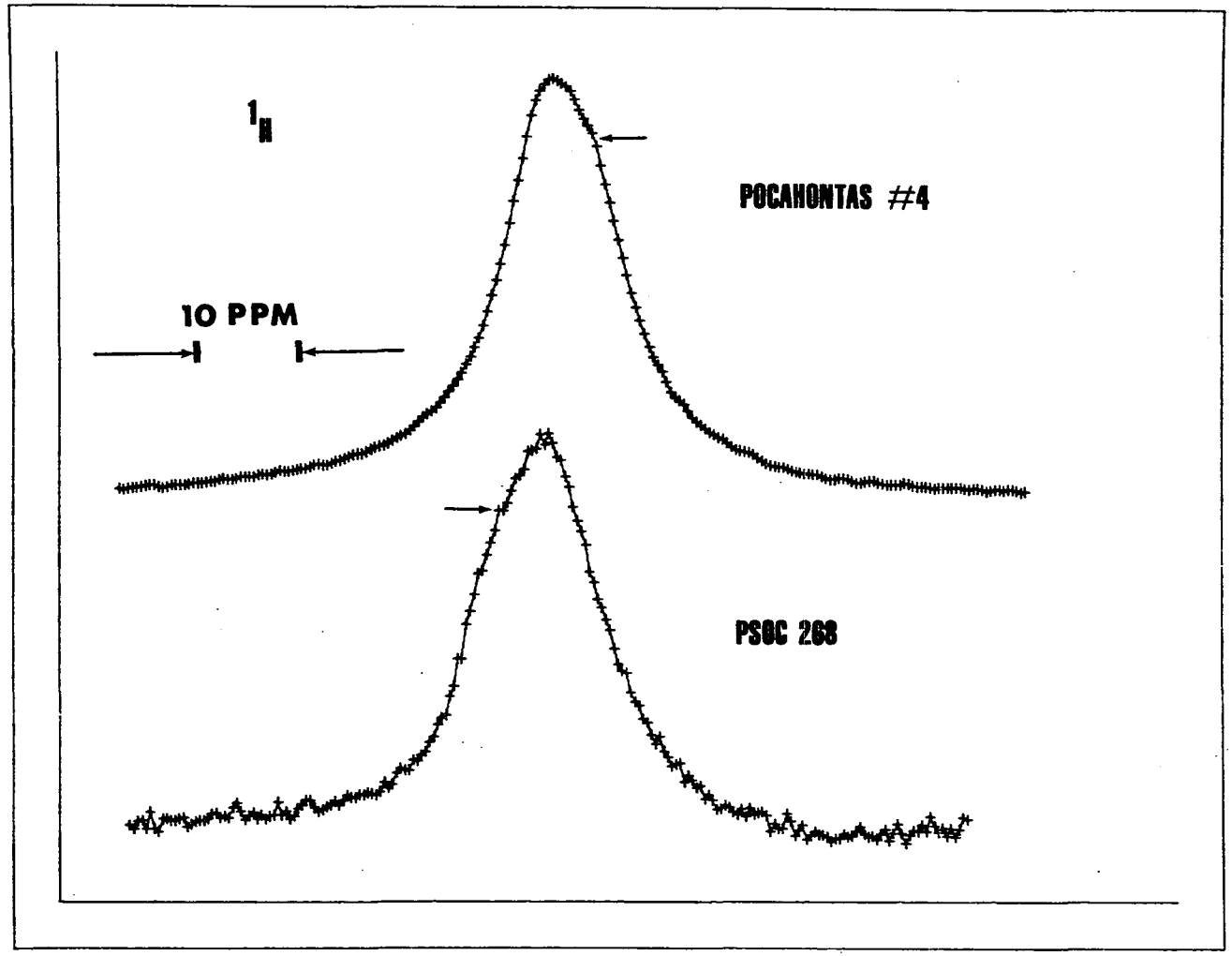

Figure 25. High resolution ^{1}H CRAMPS spectra of Pocahontas #4 and PSOC 268

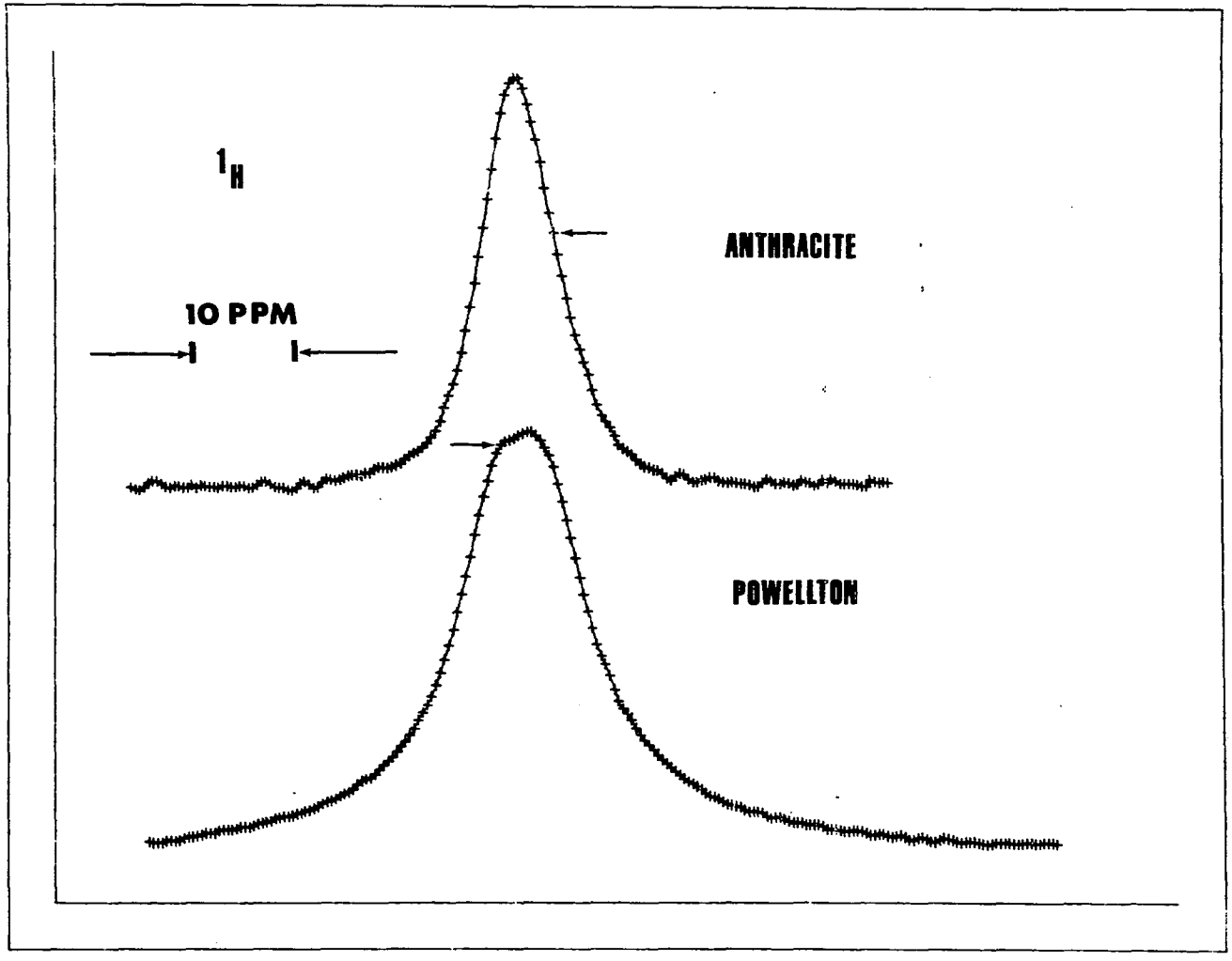

Figure 26. High resolution ^1H CRAMPS spectra of anthracite and Powellton coals

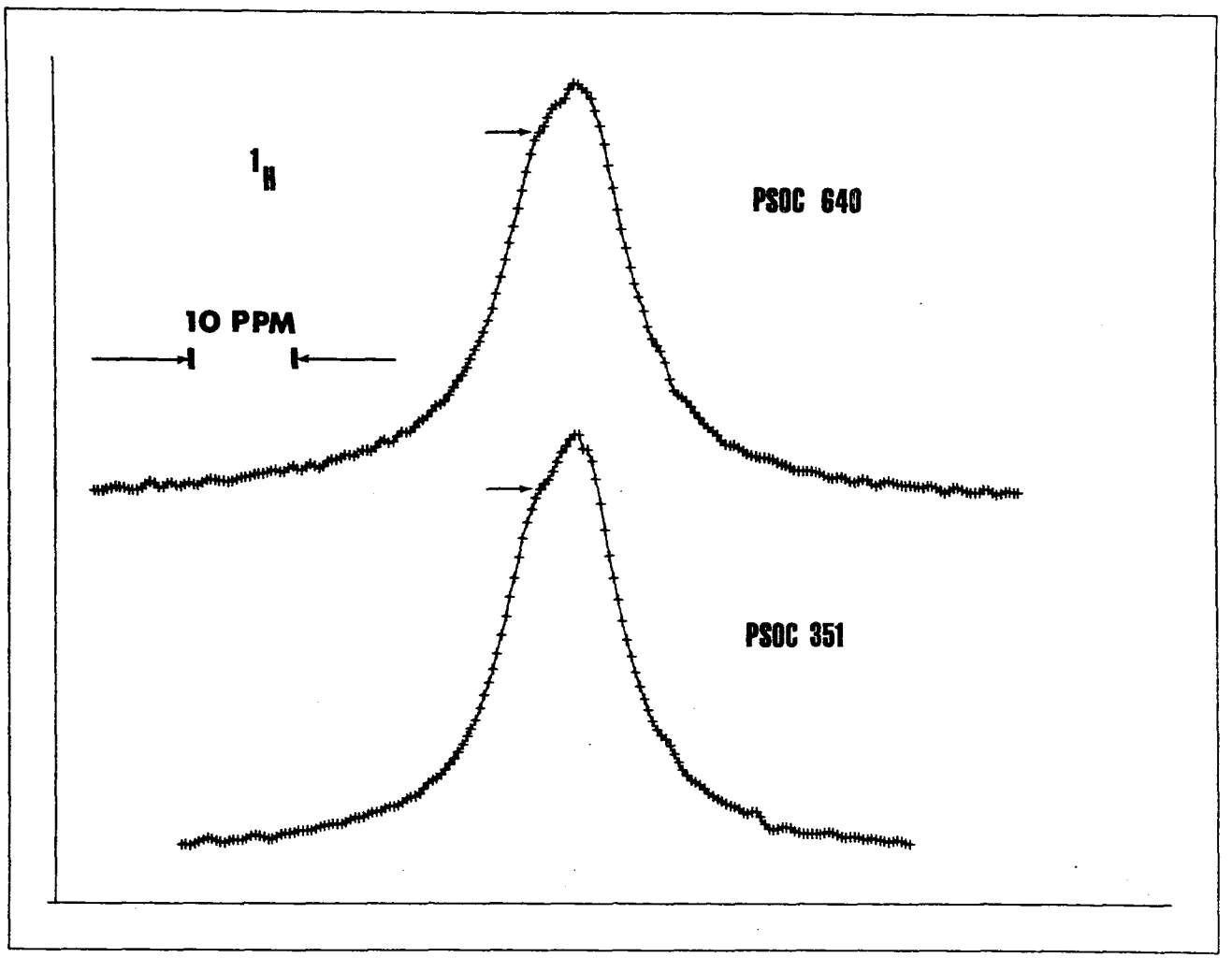

Figure 27. High resolution ^{1}H CRAMPS spectra of PSOC 640 and PSOC 351

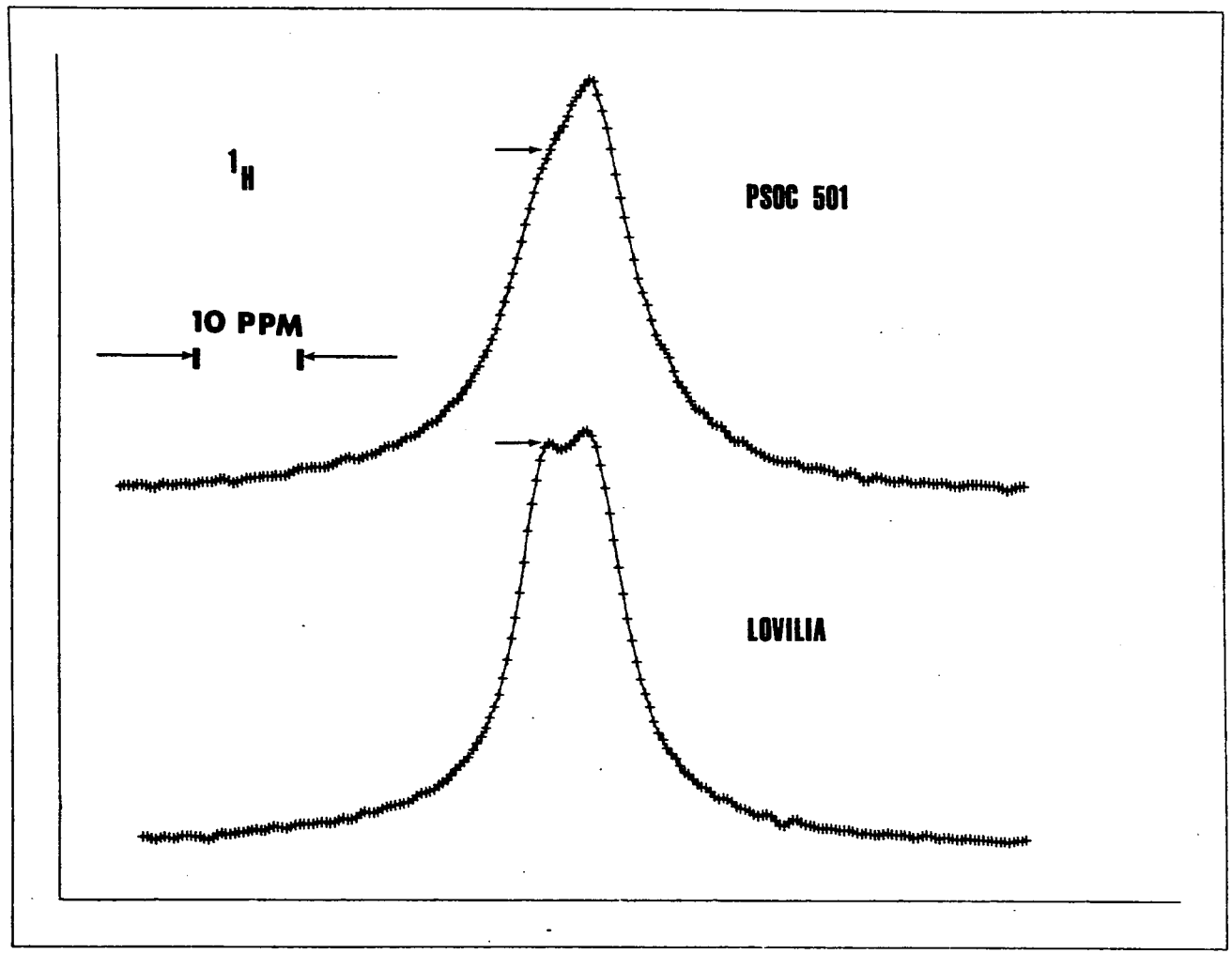

Figure 28. High resolution ^1H CRAMPS spectra of PSOC 501 and Lovilia vitrains

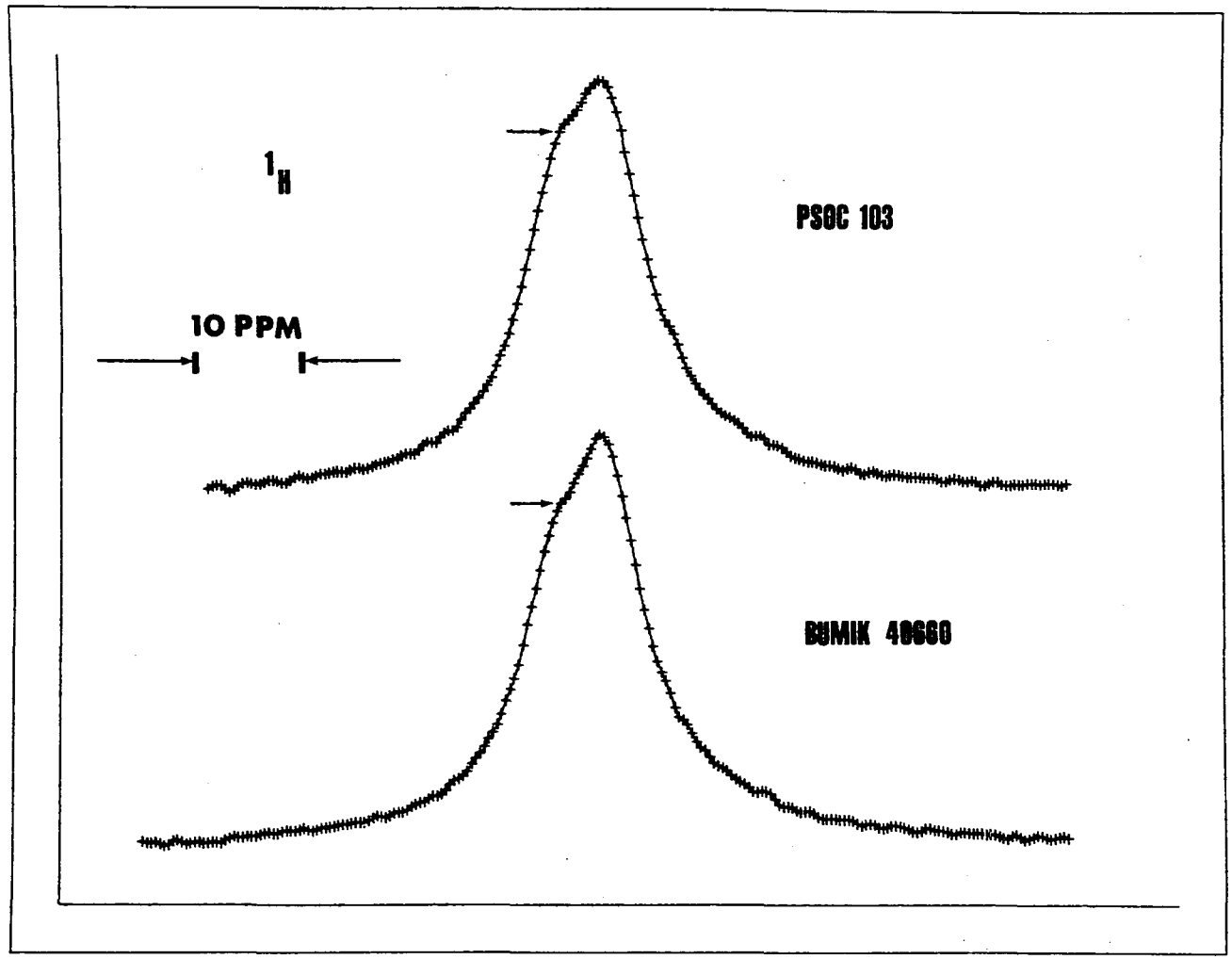

Figure 29. High resolution ^{1}H CRAMPS spectra of PSOC 103 and Bumik 40660

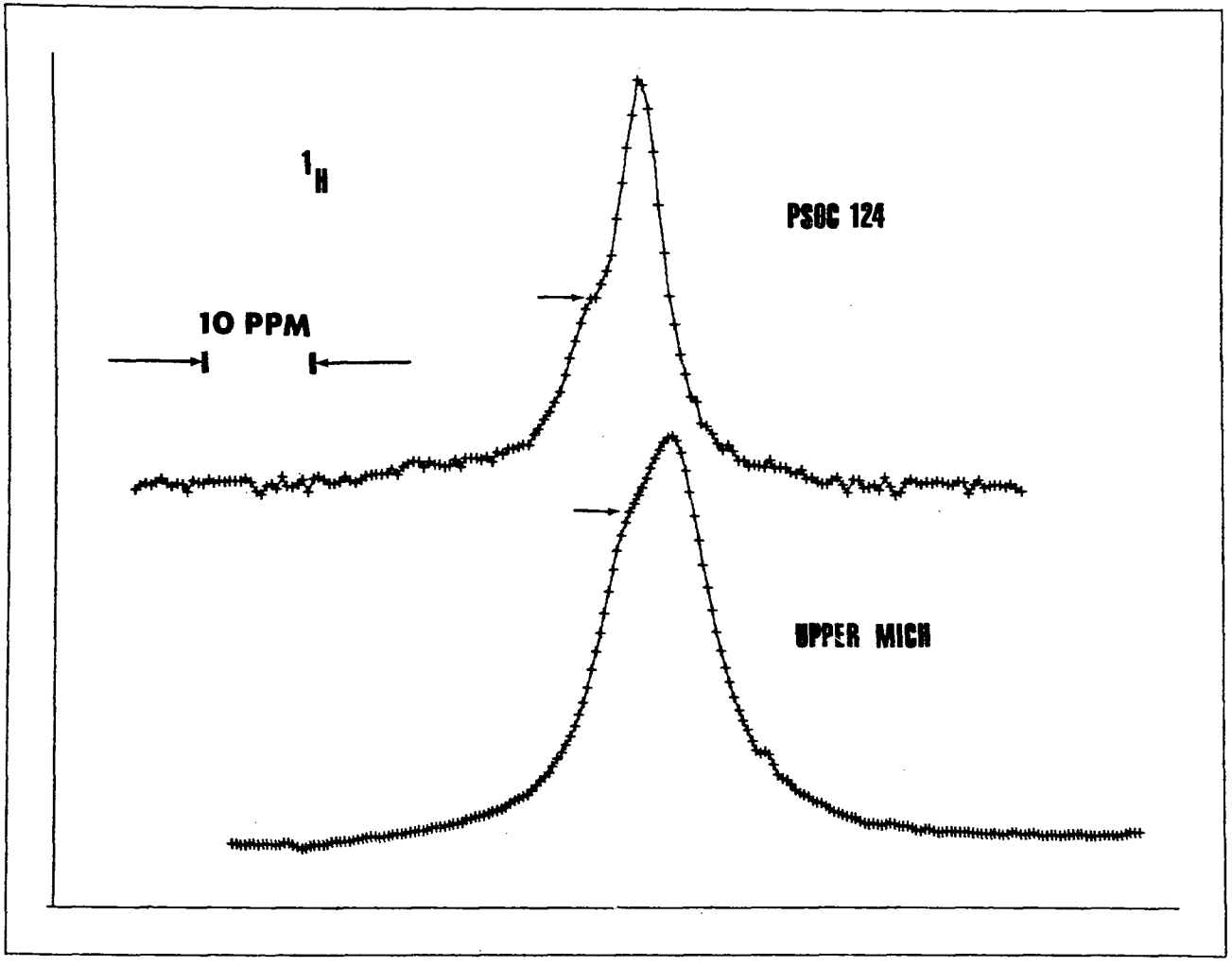

Figure 30. High resolution ^{1}H CRAMPS spectra of PSOC 124 and Upper Mich vitrains

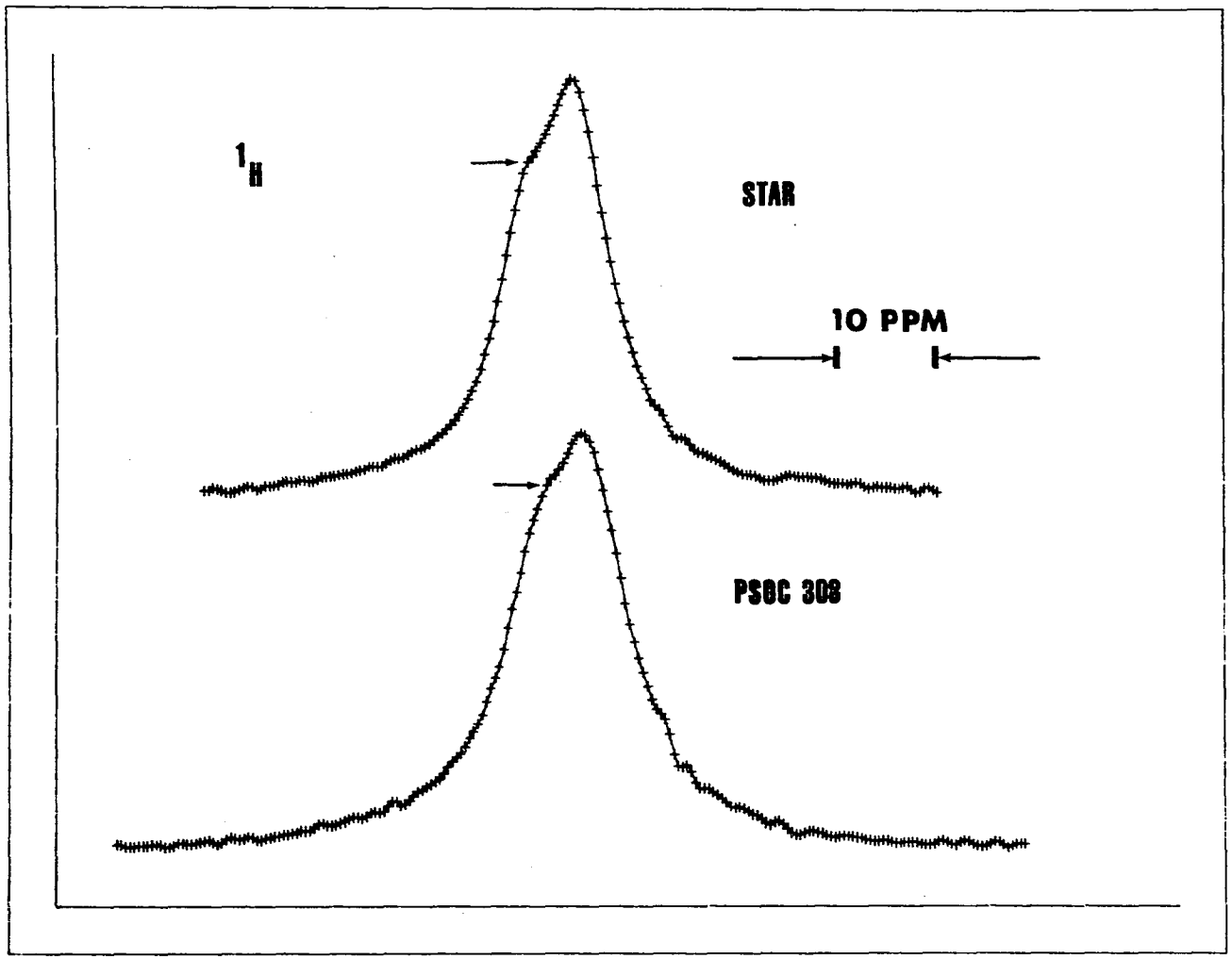

Figure 31. High resolution ^{1}H CRAMPS spectra of Star and PSOC 308 vitrains

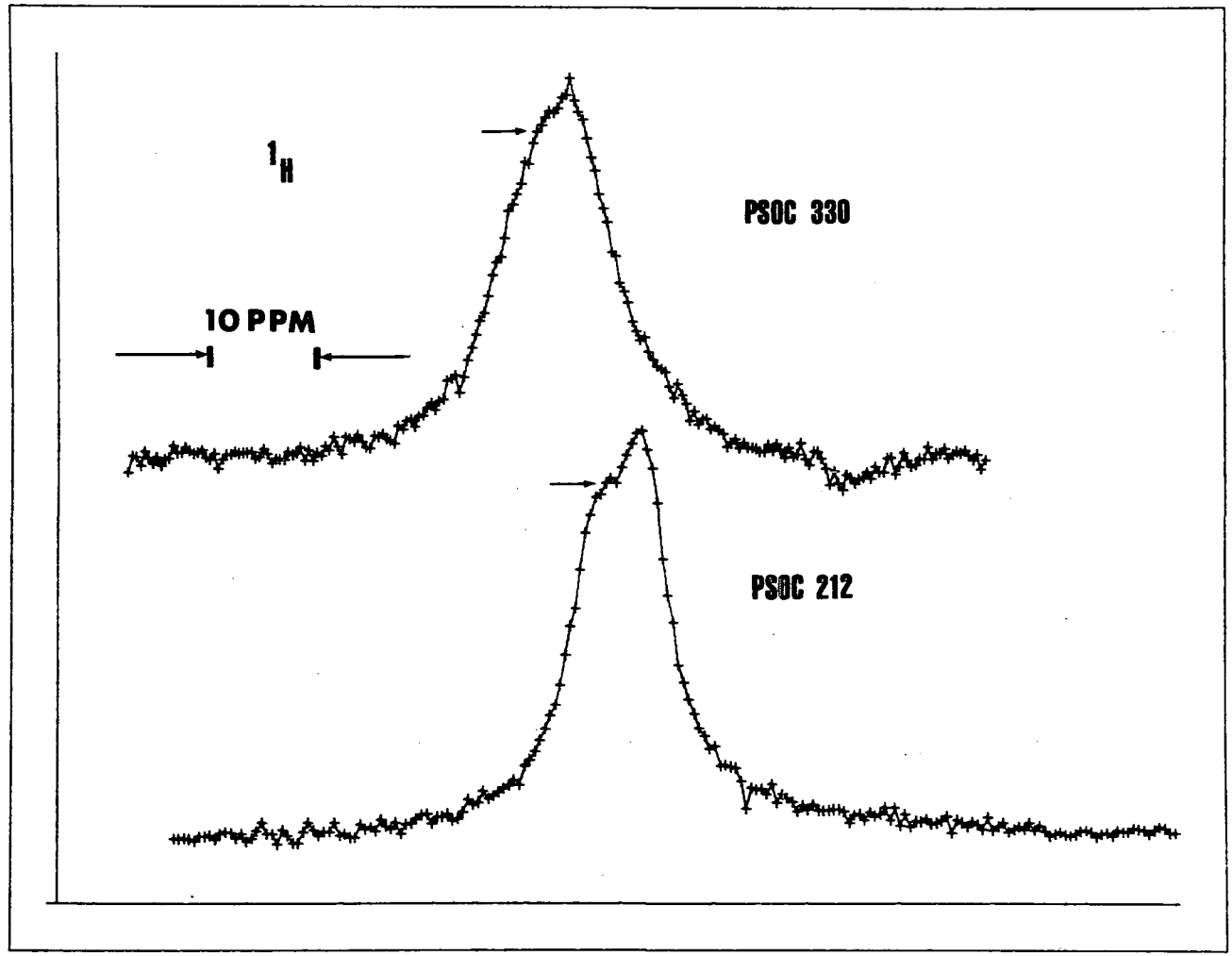

Figure 32. High resolution ^1H CRAMPS spectra of PSOC 330 and PSOC 212

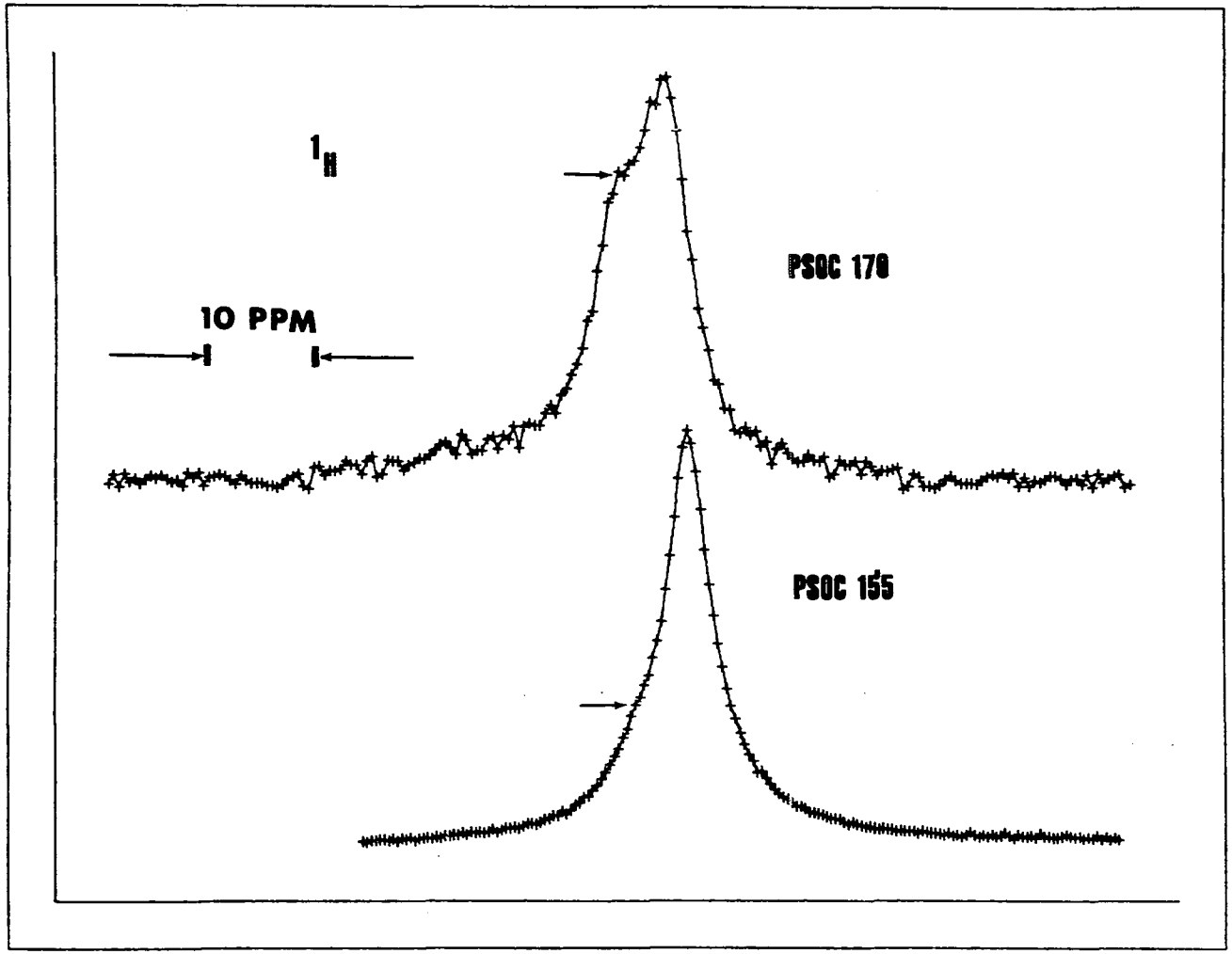

Figure 33. High resolution ^{1}H CRAMPS spectra of PSOC 170 and PSOC 155

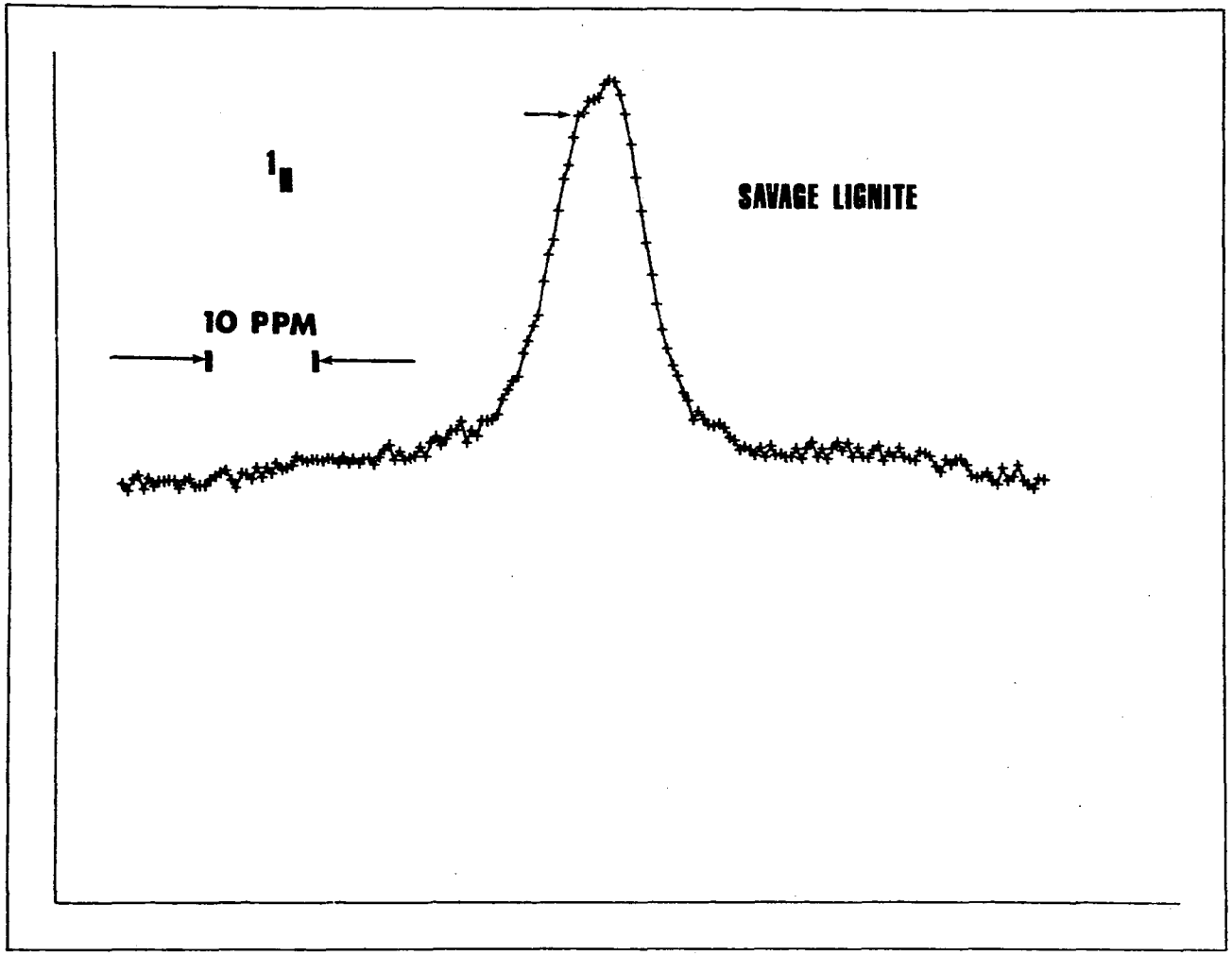

Figure 34. High resolution ^{1}H CRAMPS spectrum of Savage Lignite

quantitative measurements, several coals were also examined in sealed rotors after being dried at 105° C and 10^{-7} torr for eight hours. Figure 35 illustrates the typical result; dried coals produced broader ^{1}H spectra than undried coals. These increased linewidths following heating and pumping were also observed by Gerstein et al. (105) in static multiple pulse experiments on coals. Characterization of aromatic/aliphatic proton contents by curve fitting (vide infra) produced identical results within experimental error for dried and undried samples.

Spin counting of protons with, and without strong homonuclear dipolar decoupling, after correction for finite pulse widths (318), indicated that at least 95% of the protons in the present samples were detected under the high resolution solid state techniques used in this work.

It will be noticed in Figures 25-34 that all spectra exhibit a skewed appearance which may be associated with two major contributions, roughly 5 ppm apart. The assumption was made with one caveat (vide infra) that these two features represent contributions from predominately aromatic and aliphatic protons. In order to extract the relative fractions of aliphatic and aromatic protons from these spectra, three admittedly ad-hoc procedures were used. The first was to use a computer least squares fitting routine (115) in which a superposition of two Lorentzians was

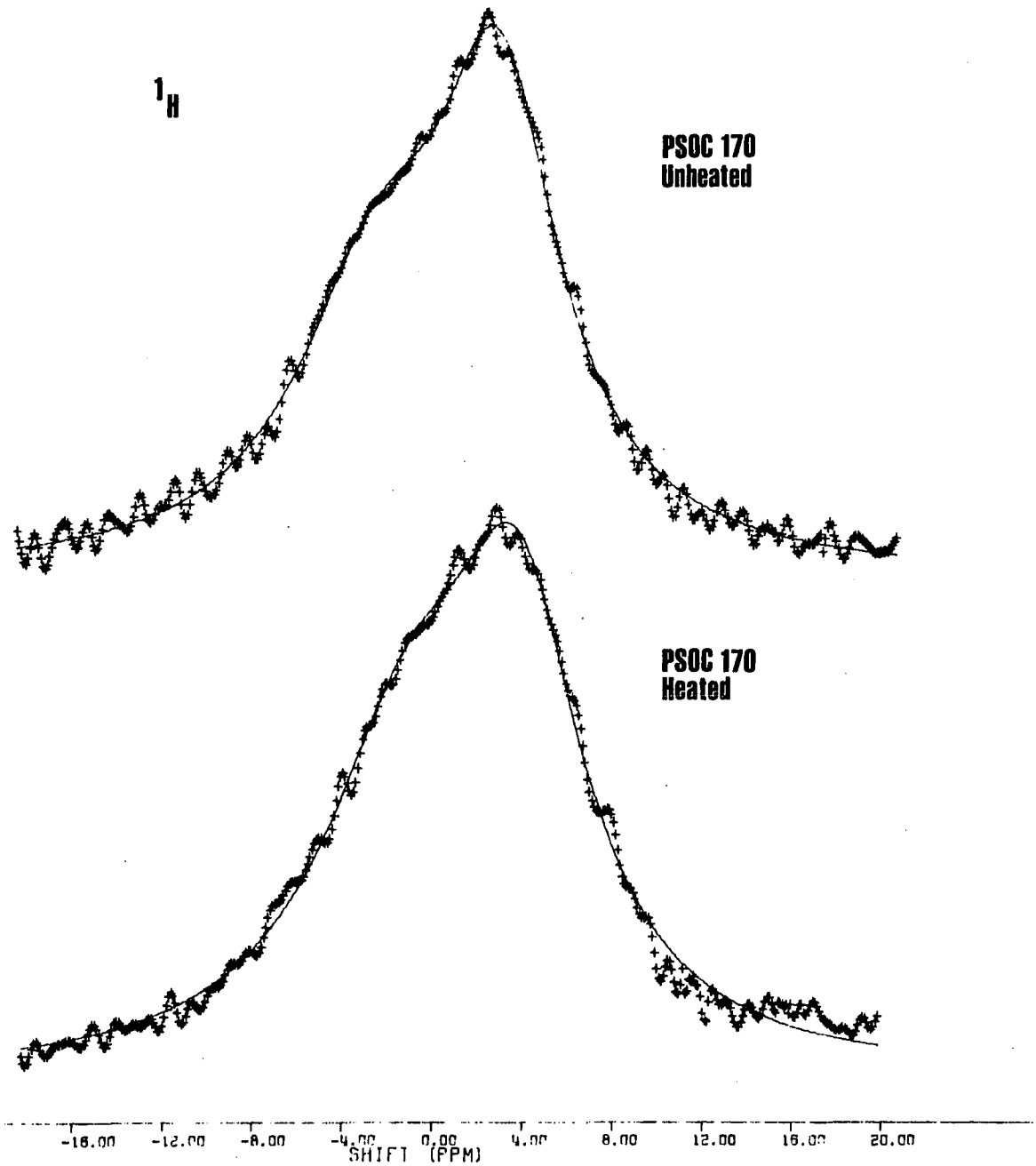

Figure 35. ^1H CRAMPS spectra of PSOC 170 vitrain. Top: Untreated coal. Bottom: Spectrum of coal after heating at 105° C and 10^{-7} torr for 8 hours

fit to the experimental data. The least squares search allowed the positions, widths, and relative amplitudes of the two Lorentzians to vary for a best fit. In order to check the applicability of this procedure, a number of model mixtures were made, containing a variable amount of aromatic, aliphatic, and hydroxyl protons. Specifically, mixtures containing polystyrene, polyethylene, 2, 6-dimethylbenzoic acid, naphthalene, anthracene, chrysene, and perylene were prepared. Figure 36 shows a typical proton spectrum for a mixture in which 22% of the hydrogens were aromatic, 73% aliphatic, and 5% were in acid or OH groups. The unrestricted Lorentzian fit gave values of 26, 70, and 4%, respectively. Fitted values for other mixtures were also within 5% of the measured fractions.

When applied to coals, this procedure resulted in fits which agreed well with the fractions of aromatic hydrogen, f^H_{AR}, as inferred from FTIR (132) in the manner described by Solomon (270) for, e.g., PSOC 124, PSOC 351, and Upper Mich, as shown in Table IX. Since hydroxyl protons would be expected to occur in the same chemical shift region as aromatic species, the NMR results have been corrected by adjusting the aromatic region for hydroxyl content. These hydroxyl values were also determined by FTIR (132)(Table X).

On the other hand, in some cases the unrestricted least squares fit appeared to result in aromaticities which were

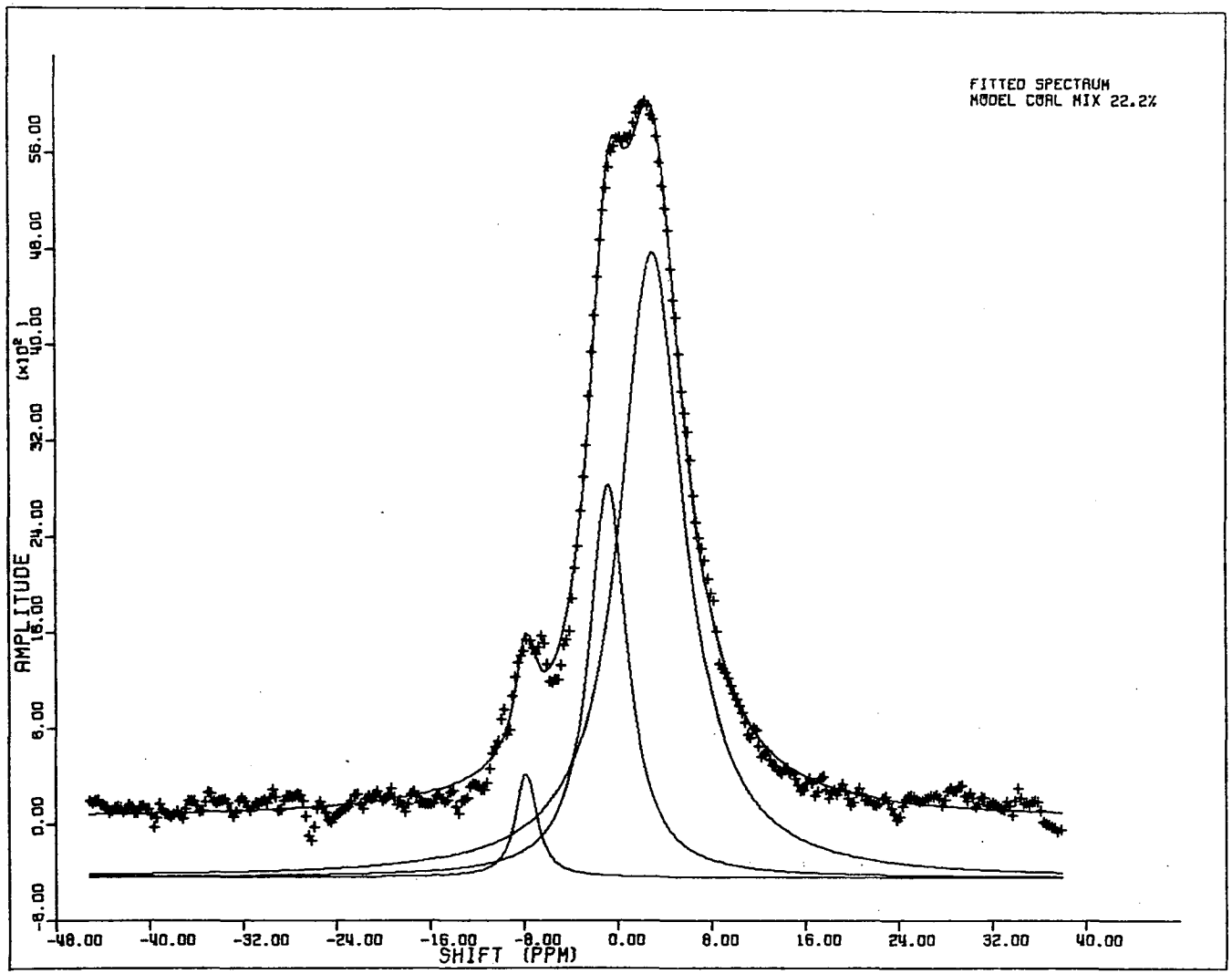

Figure 36. High resolution ^{1}H NMR spectrum of model mixture

Table IX. Fraction of aromatic hydrogen in coals as determined by NMR (via least squares Lorentzian fits) and FTIR

COAL	% C	f_{AR}^{H} (NMR)	f_{AR}^{H} (FTIR)
Anthracite	93.0	0.59	-
Pocahontas #4	90.3	0.73	0.50
PSOC 268	86.5	0.09	0.42
Powellton	85.1	0.00	0.45
PSOC 124	83.8	0.15	0.16
PSOC 351	83.5	0.32	0.29
PSOC 501	83.4	0.73	0.29
PSOC 103	82.9	0.11	0.39
PSOC 640	82.7	0.67	0.29
PSOC 330	82.0	0.18	0.31
PSOC 170	82.0	0.55	0.32
Bumik 40660	81.3	0.07	0.36
Upper Mich	81.0	0.34	0.34
PSOC 212	79.4	0.25	0.31
PSOC 155	77.9	0.00	0.14
Star	77.0	0.23	0.24
PSOC 308	76.6	0.39	0.33
Lovilia	75.0	0.38	0.31
Savage Lignite	70.9	0.00	0.31

Table X. f_{OH}^{H} in coals as determined by FTIR (132)

COAL	f_{OH}^{H}
Anthracite	~0.00 (assumed)
Pocahontas #4	0.03
PSOC 268	0.05
Powellton	0.06
PSOC 124	0.04
PSOC 351	0.05
PSOC 501	0.06
PSOC 103	0.07
PSOC 640	0.09
PSOC 330	0.08
PSOC 170	0.06
Bumik 40660	0.08
Upper Mich	0.09
PSOC 212	0.12
PSOC 155	0.08
Star	0.07
PSOC 308	0.11
Lovilia	0.10
Savage Lignite	0.20

unreasonable. For example, for Powellton, the Lorentzian sum, after correction for OH, implied no aromatic hydrogen, while FTIR suggested a relatively large f_{AR}^{H} (Table IX). Unlike the case of fitting a rather well defined mixture of aromatic, aliphatic, and hydroxyl components, it appears that the unrestricted least squares fit is not a procedure that could be uniformly applied to coals.

It is seen that, in general, proton aromaticities inferred by FTIR and an unrestricted least squares superposition of Lorentzians to ^{1}H CRAMPS lineshapes do not agree (319). In particular, many of the values obtained by NMR using the Lorentzian superposition are physically unreasonable in light of, e.g., information derived from ^{13}C NMR on these same coals (32). It must be noted, however, that since the Lorentzian superposition appears to be a valid technique for model compounds and mixtures, and that the results inferred using this technique agree well with FTIR on roughly a third of the coals studied, it may be the case that with a small improvement in resolution, computer linefitting might become routinely possible.

The second approach to analyzing the coal ^{1}H spectra was simply to use the peak heights as a measure of quantitative amounts of chemical types in the coals. This, of course, required the assumption of approximately equal spectral widths for the two supposed shift regions. In

Figures 25-34, the arrow indicates the peak height for the smaller peak in each spectrum. Table XI reports the results obtained by this method. Again, the results have been corrected for OH. By this method of analysis, the results from the NMR and FTIR experiments are seen to be in good agreement throughout the series of coals. Of course, with a complex material such as coal there is no a priori reason for expecting the width of the "aromatic" and "aliphatic" spectral regions to be identical, therefore, the accuracy of this method is highly suspect. Inspection of ^{1}H NMR spectra of extracts of coals (31, 320) suggests that these spectral widths may, in fact, be nearly equal. The good agreement between FTIR and NMR in Table XI indicates that peak height comparisons within ^{1}H CRAMPS spectra may be a reliable method for rapid estimation of hydrogen aromaticities of coals.

The final method of interpreting the spectra in Figures 25-34 was by resolving the spectra into components using a Dupont 310 Curve Resolver (The Dupont 310 is a modified analog computer specifically designed for resolving overlapped curve envelopes into component bands and measuring their relative areas. To accomplish this the 310 utilizes a series of function generator channels, each capable of generating peak shapes corresponding to Gaussian, Lorentzian, or other distributions. Individual peak

Table XI. Fraction of aromatic hydrogen in coals as determined by NMR (from peak height comparisons)

COAL	% C	f_{AR}^{H} (NMR)	f_{AR}^{H} (FTIR)
Anthracite	93.0	0.62	-
Pocahontas #4	90.3	0.50	0.50
PSOC 268	86.5	0.40	0.42
Powellton	85.1	0.43	0.45
PSOC 124	83.8	0.26	0.16
PSOC 351	83.5	0.41	0.29
PSOC 501	83.4	0.40	0.29
PSOC 103	82.9	0.40	0.39
PSOC 640	82.7	0.38	0.29
PSOC 330	82.0	0.38	0.31
PSOC 170	82.0	0.35	0.32
Bumik 40660	81.3	0.38	0.36
Upper Mich	81.0	0.34	0.34
PSOC 212	79.4	0.34	0.31
PSOC 155	77.9	0.16	0.14
Star	77.0	0.36	0.24
PSOC 308	76.6	0.35	0.33
Lovilia	75.0	0.39	0.31
Savage Lignite	70.9	0.27	0.31

parameters of height, width, and horizontal position are independently varied until the resulting summation curve from all channels exactly matches the curve being fit.) Again, both Lorentzian and Gaussian lineshapes were considered in attempting to reproduce the ^{1}H coal spectra, although the long leading and trailing edges and sharp maxima in Figures 25-34 clearly suggest Lorentzian lines. Gaussian lines were found not to be able to reproduce any of the coal spectra, while the summation of two Lorentzian lines accurately did in each case to within several percent. Table XII reports the values of f_{AR}^{H} determined using the Dupont 310 Curve Resolver and, again, compares those with Solomon's FTIR results. Figure 37 plots the hydrogen aromaticity for the FTIR measurements and the latter NMR results as a function of coal rank. It may be observed that f_{AR}^{H} shows considerable scatter about a value of approximately 0.3 up to about 85 percent carbon, at which point it rises rapidly. This is consistent with earlier observations of coal aromaticity described in Section 2. Also, the values indicated are consistent with values determined by ^{1}H NMR of pyridine extracts of coals (Figure 24). It has recently been observed that pyridine extracts of coals are probably representative of overall coal molecular structure (321), so that this correspondence is reasonable.

Using the values in Table XII and results for the carbon aromaticity in the same series of coals measured by

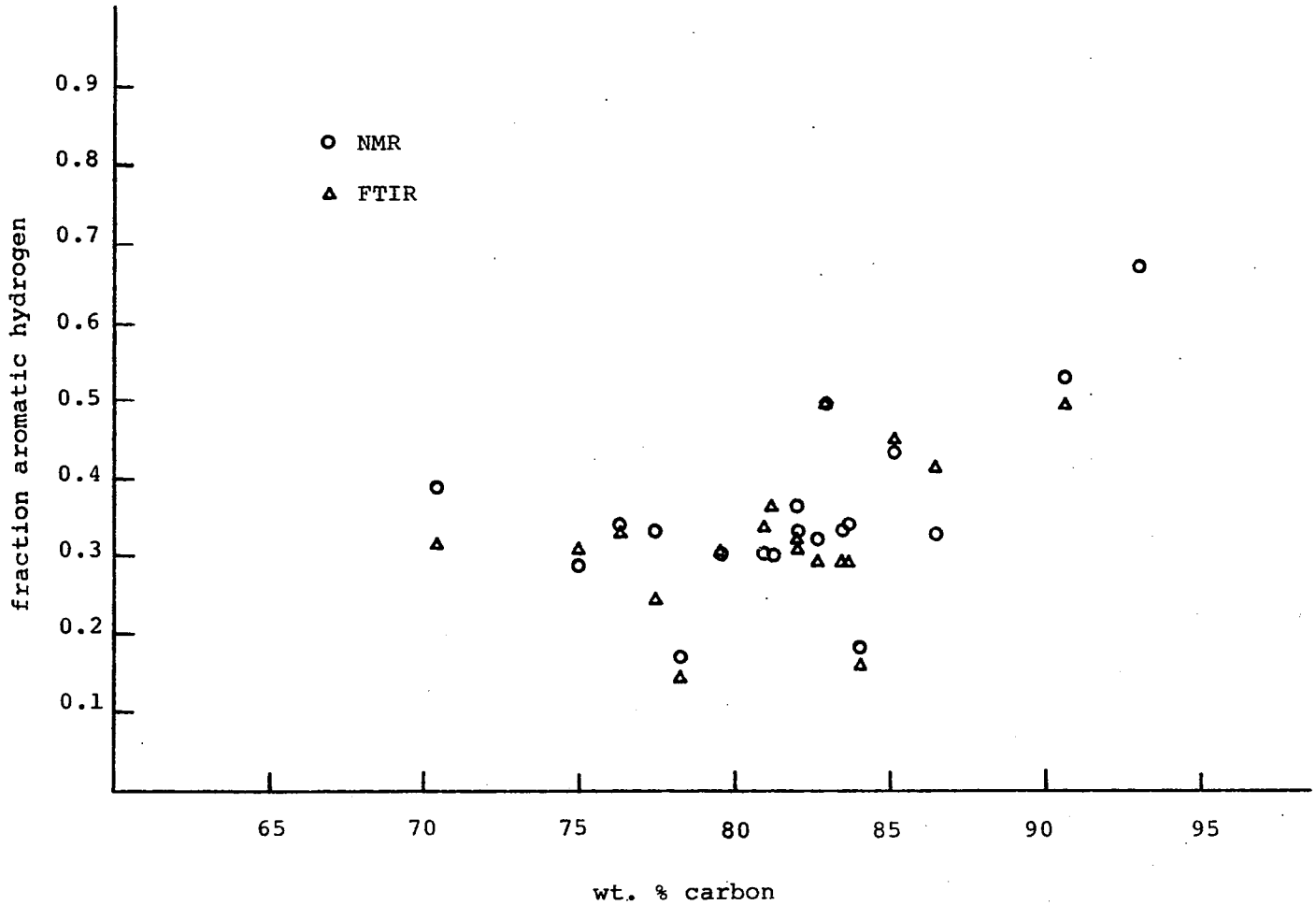

Figure 37. Hydrogen aromaticity vs. coal rank as determined by ^{1}H CRAMPS and FTIR

Table XII. Hydrogen aromaticity values (f_{AR}^{H}) in coals determined by solid state ^{1}H NMR (using the Dupont 310 curve resolver) and FTIR

COAL	% C	f_{AR}^{H} (NMR)	f_{AR}^{H} (FTIR)
Anthracite	93.0	0.68	-
Pocahontas #4	90.3	0.53	0.50
PSOC 268	86.5	0.33	0.42
Powellton	85.1	0.43	0.45
PSOC 124	83.8	0.18	0.16
PSOC 351	83.5	0.34	0.29
PSOC 501	83.4	0.33	0.29
PSOC 103	82.9	0.39	0.39
PSOC 640	82.7	0.32	0.29
PSOC 330	82.0	0.33	0.31
PSOC 170	82.0	0.36	0.32
Bumik 40660	81.3	0.30	0.36
Upper Mich	81.0	0.31	0.34
PSOC 212	79.4	0.31	0.31
PSOC 155	77.9	0.16	0.14
Star	77.0	0.33	0.24
PSOC 308	76.6	0.34	0.33
Lovilia	75.0	0.29	0.31
Savage Lignite	70.9	0.38	0.31

other workers (Table XIII -- the value reported for f_{AR}(NMR) of Savage Lignite was measured by the author at 200 MHz using a Varian XL-200 spectrometer and differs from that reported in Reference 32. This is because at higher fields it becomes possible to discriminate between aromatic and carbonyl carbons. The latter being of significant proportion in lignites.), it is possible to calculate the mole ratios of aromatic hydrogen to aromatic carbon (H_{AR}/C_{AR}) in the coals. Those values are reported in Table XIV. To avoid a circular argument, only the f^C_{AR} values determined by NMR were used in this calculation, since the f^C_{AR}(FTIR) values were determined using a method suggested by Brown and Ladner (277). That method determines C_{AR} by difference, with $C_{AR}=C_{TOTAL}-C_{AL}=C_{TOTAL}-(12/x)H_{AL}$. In this case, x, which describes the stoichiometry of the aliphatic material (CH_x), was assumed to be 1.8 (145,270). An average of the NMR and FTIR results was used in Table XIV to represent f^H_{AR}.

Also, from the values in Tables X, XII and XIII, and material balance, it is possible to calculate the H/C ratio in the aliphatic portion of the coals; those ratios are also given in Table XIV. Finally, on the basis of the following data, which we now have at hand: i) the weight percent of carbon and hydrogen in the coals, ii) f^C_{AR}, f^H_{AR}, f^H_{OH}, and iii) H_{AR}/C_{AR}, it is possible to place some limits on the average size of the polynuclear aromatic clusters in the coals. In particular, it is at least possible to determine the

Table XIII. Carbon aromaticity values (f_{AR}^{C}) in coals determined by solid state ^{13}C NMR (32) and FTIR (132)

COAL	% C	f_{AR}^{C} (NMR)	f_{AR}^{C} (FTIR)
Anthracite	93.0	0.95	---
Pocahontas #4	90.3	0.86	0.84
PSOC 268	86.5	0.76	0.78
Powellton	85.1	0.77	0.80
PSOC 124	83.8	0.54	0.56
PSOC 351	83.5	0.77	0.69
PSOC 501	83.4	0.78	0.69
PSOC 103	82.9	0.75	0.79
PSOC 640	82.7	0.79	0.73
PSOC 330	82.0	0.74	0.76
PSOC 170	82.0	0.78	0.73
Bumik 40660	81.3	0.77	0.74
Upper Mich	81.0	0.70	0.69
PSOC 212	79.4	0.77	0.77
PSOC 155	77.9	0.38	0.49
Star	77.0	0.71	0.65
PSOC 308	76.6	0.75	0.75
Lovilia	75.0	0.69	0.72
Savage Lignite	70.9	0.84	0.82

minimum allowable ring size consistent with the above information. Those numbers are reported in the last column of Table XIV.

In order to effect this latter calculation, the following procedure was employed. Peri condensed atomic ring structures connected by aliphatic chains with average stoichiometry CH_x ($x = H_{AL}/C_{AL}$) were assumed as skeletal models for coal structure. Starting with benzene, these were increased in size until the minimum ring size consistent with the known data was determined.

From the number of aromatic carbon atoms, C_{AR}, in any model ring, the number of aliphatic carbon atoms, C_{AL}, required in the model for consistency with a given coal was determined from the relation $C_{AL} = \left(\frac{1}{f^C_{AR}} - 1\right)C_{AR}$, where f^C_{AR} is the NMR determined fraction of aromatic carbon in the coal (Table XIII). Next, the total molecular weight required of the model average molecular structure could be calculated according to M.W. = $[(C_{AR} + C_{AL}) \times 12/\text{wt. \% C}] \times 100$, with wt. % C being the weight percent of carbon in the coal (Table XIII). From the molecular weight for the average molecular structure, it is possible to determine the total number of hydrogen atoms required in the model from the relation H_{TOTAL} = M.W. x wt. % H/100. This total hydrogen could be further divided according to chemical types (H_{AR}, H_{AL} and H_{OH}) on the basis of the average of the NMR and FTIR hydrogen

Table XIV. Structural parameters of coals

COAL	% C	H_{AR}/C_{AR}	H_{AL}/C_{AL}	Minimum Avr. Aromatic Cluster Size
Anthracite	93.0	0.23	2.06	30
Pocahontas #4	90.3	0.35	1.91	6
PSOC 268	86.5	0.36	1.75	3
Powellton	85.1	0.36	1.38	3
PSOC 124	83.8	0.31	1.69	1
PSOC 351	83.5	0.36	2.42	3
PSOC 501	83.4	0.32	2.31	3
PSOC 103	82.9	0.38	1.59	3
PSOC 640	82.7	0.31	2.34	3
PSOC 330	82.0	0.33	1.74	3
PSOC 170	82.0	0.34	2.14	3
Bumik 40660	81.3	0.35	2.11	3
Upper Mich	81.0	0.34	1.45	2
PSOC 212	79.4	0.31	1.91	3
PSOC 155	77.9	0.42	1.32	1
Star	77.0	0.34	1.89	2
PSOC 308	76.6	0.36	1.78	2
Lovilia	75.0	0.33	1.48	2
Savage Lignite	70.9	0.25	1.73	6

results. The values generated in this manner are consistent with what is known about the coals. For example, for Lovilia vitrain, if the average ring size is presumed to be unity, the average molecular structure for the aromatic portion will be represented by benzene, which has six aromatic carbon atoms. The number of aliphatic carbons in the model, C_{AL}, is then calculated to be $C_{AL} = \frac{1}{0.69} - 1)6 = 2.7$, and the molecular weight is $(8.7 \times \frac{12}{75}) \times 100 = 139.2$. The total number of hydrogen atoms is given by $139.2 \times \frac{4.77}{100} = 6.6$, and of those $H_{AR} = 0.30 \times 6.6 = 2.0$, $H_{AL} = 0.60 \times 6.6 = 4.0$, and $H_{OH} = 0.10 \times 6.6 = 0.6$.

At this point, the model average molecular may be fully constructed. The minimum possible ring size (minimum average polynuclear aromatic cluster size in the coal) is obtained if all aliphatic carbon is alpha to aromatic rings; i.e., only peripheral CH_3 groups and alkyl or naphthenic bridges with two carbon atoms were considered (322). To check for self-consistency, the H_{AR}/C_{AR} ratio of the model is then compared with that of the coal, as inferred by NMR/FTIR (Table XIV). For example, for one ring on average in Lovilia vitrain, the average repeating unit may be represented by

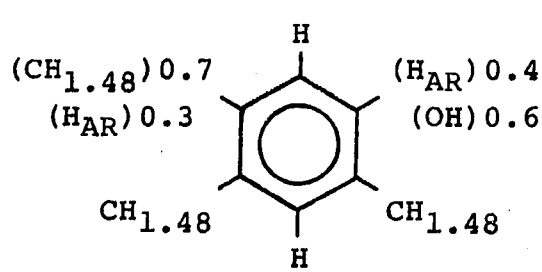

$C^{AR}_{6.0}C^{AL}_{2.7}H^{AR}_{2.0}H^{AL}_{4.0}(OH)_{0.6}$, or as the unit and $(H_{AR}/C_{AR})_{MODEL}$ = 0.45. This value is greater than the experimentally determined 0.33 for Lovilia (Table XIV), and, therefore, the average cluster size in that coal must be greater than 1.

The process described above is continued, employing progressively larger aromatic backbones, until $(H_{AR}/C_{AR})_{MODEL} \leq (H_{AR}/C_{AR})_{COAL}$. Values for the model which are less than that of the coal can be reconciled by considering some aliphatic bridges to be greater in length than two carbon atoms. The minimum possible cluster size becomes the smallest polyaromatic ring structure for which the above inequality is satisfied.

Table XIV lists the results of this type of analysis for the 19 coals examined in this work. While it is not possible to conclude that the condensed aromatic clusters indicated are necessarily the actual average ring sizes in the coals, it is interesting to observe that most of the coals have smallest possible ring sizes of at least two, and many are three or more. Further, in agreement with work described earlier in Section 2, the aromatic clusters appear to be smallest for coals of less than about 85 percent carbon. Above 85% C the size of the clusters increases significantly, with coal becoming nearly graphitic by 93% carbon.

Also interesting is the fact that the ring sizes shown in Table XIV are in generally good agreement with those determined by other methods (Section 2) despite the assumption of only relatively short aliphatic attachments to the aromatic backbones, and our ignoring of heteroatom functionalities except for OH. It is perhaps noteworthy that in recent years, Deno et al. (323, 324) have been able to study selectively the aliphatic portion of coals by oxidation with aqueous hydrogen peroxide in trifluoroacetic acid. Those workers have determined that much of the aliphatic material in coals is present in relatively short structures, including particularly Ar CH_2CH_2Ar (323, 324).

Further, oxygen existing in coals is for the greater part considered to occur mostly in hydroxyl groups, ether groups, and heteroatom functionalities, while nitrogen and sulfur are relatively minor components of coal (134, 138). This explains how the H_{AR}/C_{AR} ratio and the average cluster sizes in coals may be nearly equal to that of the hydrocarbon with identical average molecular structure, except with the heteroatoms eliminated (i.e., our average structural model).

Coal tar

In a complementary experiment to those described above, the proton aromaticity of a coal tar produced by vacuum

devolatilization of PSOC 170 at low temperature was also measured (325). Coal tars are an important source of raw materials for the production of solvents, pharmaceuticals, plastics and synthetic fibers (134), and while the chemical structure of coal has been an important subject in coal research, because combustion and most coal conversion processes involve thermal decomposition (134) of coal, understanding that step has also been of considerable interest in coal studies.

Recently, Solomon (146) studied the vacuum pyrolysis behavior of a number of coals at temperatures between 300° and 1,000° C. Evidence from that work led to the development of a kinetic model for the time and temperature evolution of products in coal devolatilizations (146). This model was based on the belief that in vacuum, secondary product-char and product-product reactions are minimal. Coal tar produced under those conditions is thus presumed to be formed from relatively large primary fragments of coal structure. It may be expected, then, that coal tars produced by vacuum devolatilization should be chemically similar to the organic part of their parent coals. This resemblence of vacuum pyrolysis tars to original coal has been inferred in the past by several investigators (245, 326-329). It would seem that solid state ^{1}H NMR might be a useful method for investigating this assumption.

The coal tar studied in this work was prepared by Dr. P. R. Solomon by vacuum devolatilization of PSOC 170 vitrain (Table VIII) on an electrically heated wire grid (146) of the type described by Anthony et al. (330, 331). The final sample temperature was 595°C, achieved at a heating rate of 600°C/sec. This temperature was maintained for 20 seconds. Coal tar produced was then collected from glass and steel liners in the devolatilization chamber (146).

The elemental composition of the tar was found to be nearly identical to that of its parent coal, except for an increase of about 10% in hydrogen (146). This is presumed to be the result of hydrogen abstraction from the residual coal char to stabilize free radical sites produced during the coal decomposition (134, 146). Figure 38 compares the ^{1}H CRAMPS spectra of PSOC 170 and PSOC 170 tar, where the BR-24 multiple pulse sequence (74) was employed for ^{1}H-^{1}H homonuclear dipolar decoupling. It may be observed from Figure 38 that the ^{1}H spectra of coal and tar are essentially identical. Analysis of the spectra using the Dupont 310 Curve Resolver indicates that the hydrogen aromaticity of both samples is 35% (in comparison with 36% obtained earlier for PSOC 170 (Table XII)).

Since coal tar, unlike coal, is completely soluble in some solvents, it is also possible to obtain high resolution solution NMR spectra of tars in many cases. Figure 39 shows

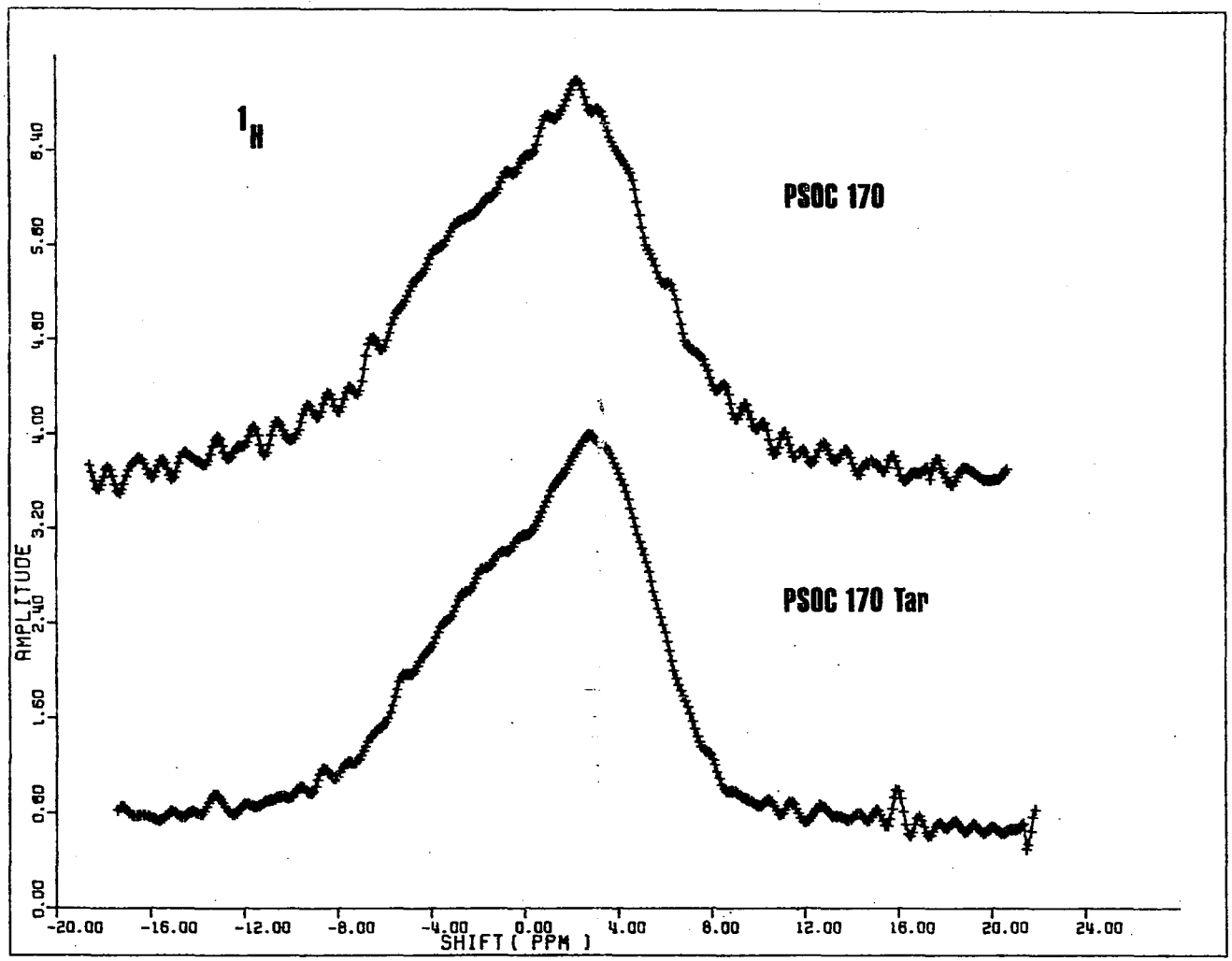

Figure 38. High resolution ^1H CRAMPS spectra of PSOC 170 coal and PSOC 170 tar

the ^{1}H NMR spectrum of PSOC 170 tar dissolved in 99% per-deuterated pyridine. The broad envelope of resonances centered near 7.5 ppm is assignable to aromatic and phenolic protons, while the three narrow resonances superimposed are due to residual protons in the solvent. Benzylic hydrogens are observed at ~1.8-3.0 ppm, while the peaks at still higher field are due to nonbenzylic aliphatic hydrogens. Integration of the spectral areas in Figure 39, after correction for the solvent peaks, indicates that PSOC 170 tar has approximately 33% aromatic hydrogens, in good agreement with the solid state proton results.

Kerogens

Oil shale is another organic/inorganic fossil material which may become a primary source of liquid fuel to future generations. The organic portion of oil shale, termed "kerogen," is a mixture of complex chemical compounds, similar to coal. In addition to the experiments described in subsections a and b, ^{1}H CRAMPS measurements were also made on four kerogens and one whole shale to attempt a characterization of hydrogen aromaticity in those substances.

Samples were kerogens from an immature (shallow depth) Green River shale and its laboratory matured counterpart (260^{o} C for 1 yr.), and naturally matured Green River and North Sea (Kiminerdgean) shales. Also, a sample of

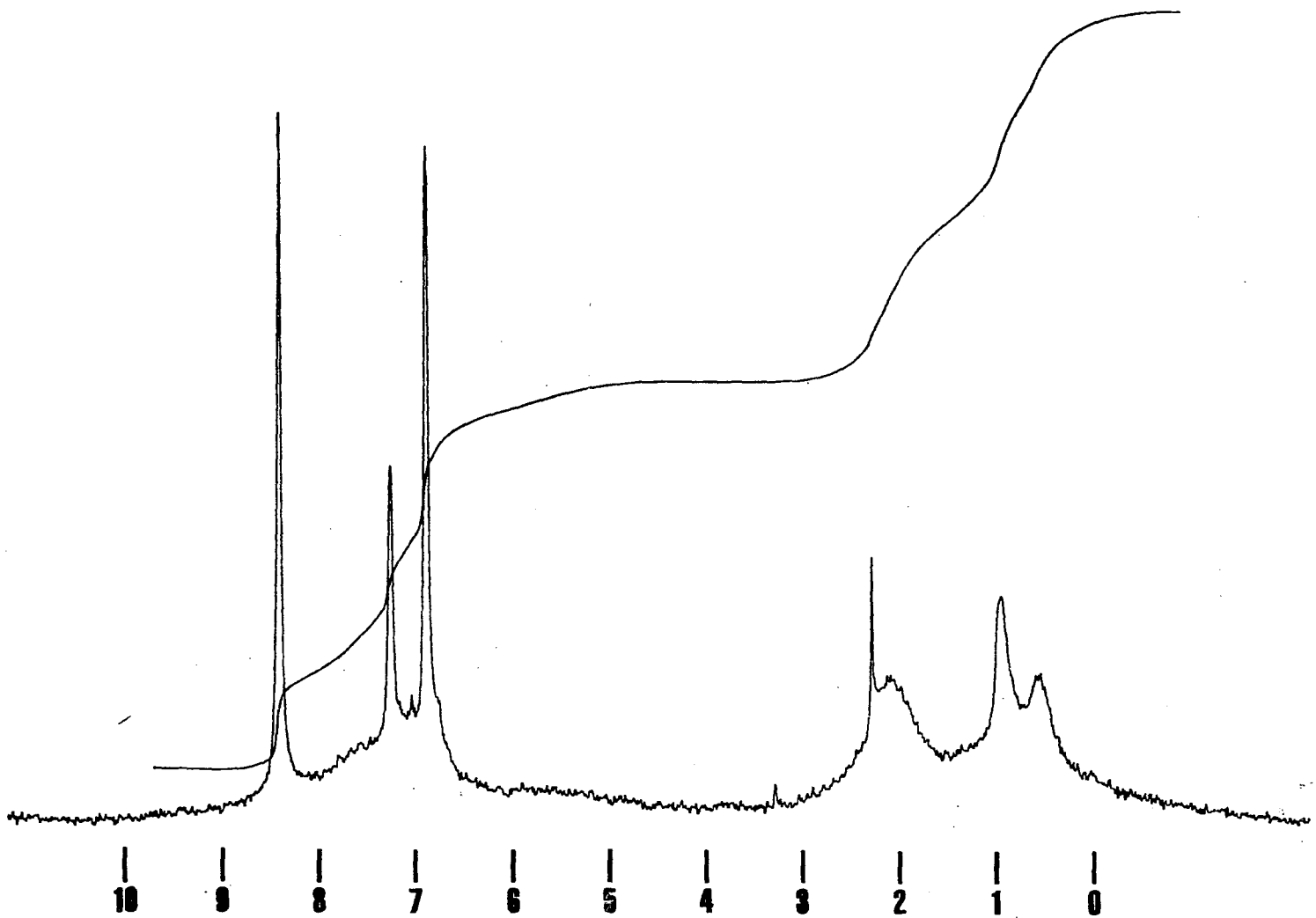

Figure 39. ^{1}H NMR spectrum of PSOC 170 tar in perdeuterated pyridine

naturally matured Green River shale which was not demineralized was examined, but no NMR signal could be detected, probably due to the paramagnetic substances in the shale. All samples were supplied by Dr. Don M. Wilson, Chevron Research Company, Richmond, CA, and were analyzed for hydrogen and carbon elemental compositions by Dr. P. R. Solomon, Advanced Fuels Research, East Hartford, Connecticut.

Table XV gives the kerogen compositions for percent carbon and hydrogen. Also given are the percentages of aromatic carbon in the samples, as determined by solid state ^{13}C NMR (332). Figures 40 and 41 show the high resolution proton CRAMPS spectra of the kerogens, under magic-angle spinning and MREV-8 dipolar decoupling (69-71). Resolution of the aromatic and aliphatic regions is poor, but it is apparent that the hydrogen aromaticities in these samples are relatively small. Table XVI reports the f_{AR}^{H} values obtained from the spectra by Lorentzian linefitting using the Dupont 310 Curve Resolver, after correction for hydroxyl hydrogens (132). It was found that approximately 90% of the hydrogens in the kerogens are in aliphatic groups.

A small difference in aromaticity was observed between immature Green River shale kerogen, and a sample of the same kerogen matured in the laboratory for one year. This diference, however, was approximately equal to our probable error limit (±5%), and so cannot be viewed as significant.

Table XV. Carbon and hydrogen compositions and aromatic carbon content of kerogens

KEROGEN	Wt. % C	Wt. % H	f_{AR}^{C}
S3917-A00 GRS Kerogen Extract (immature)	68.55	8.80	0.22
S30845 GRS Kerogen Extract (high maturity)	77.9	9.27	0.34
S3917-011B GRS Kerogen Extract (immature; lab matured)	75.88	8.00	0.31
S31516-3 KIMINERDGEAN Kerogen Extract	64.81	6.47	0.35

Table XVI. Hydrogen aromaticities in kerogens

KEROGEN	f_{AR}^{H}
S3917-A00 GRS Kerogen Extract (immature)	0.09
S30845 GRS Kerogen Extract (high maturity)	0.05
S3917-011B GRS Kerogen Extract (immature; lab matured)	0.16
S31516-3 KIMINERDGEAN Kerogen Extract Extract	0.08

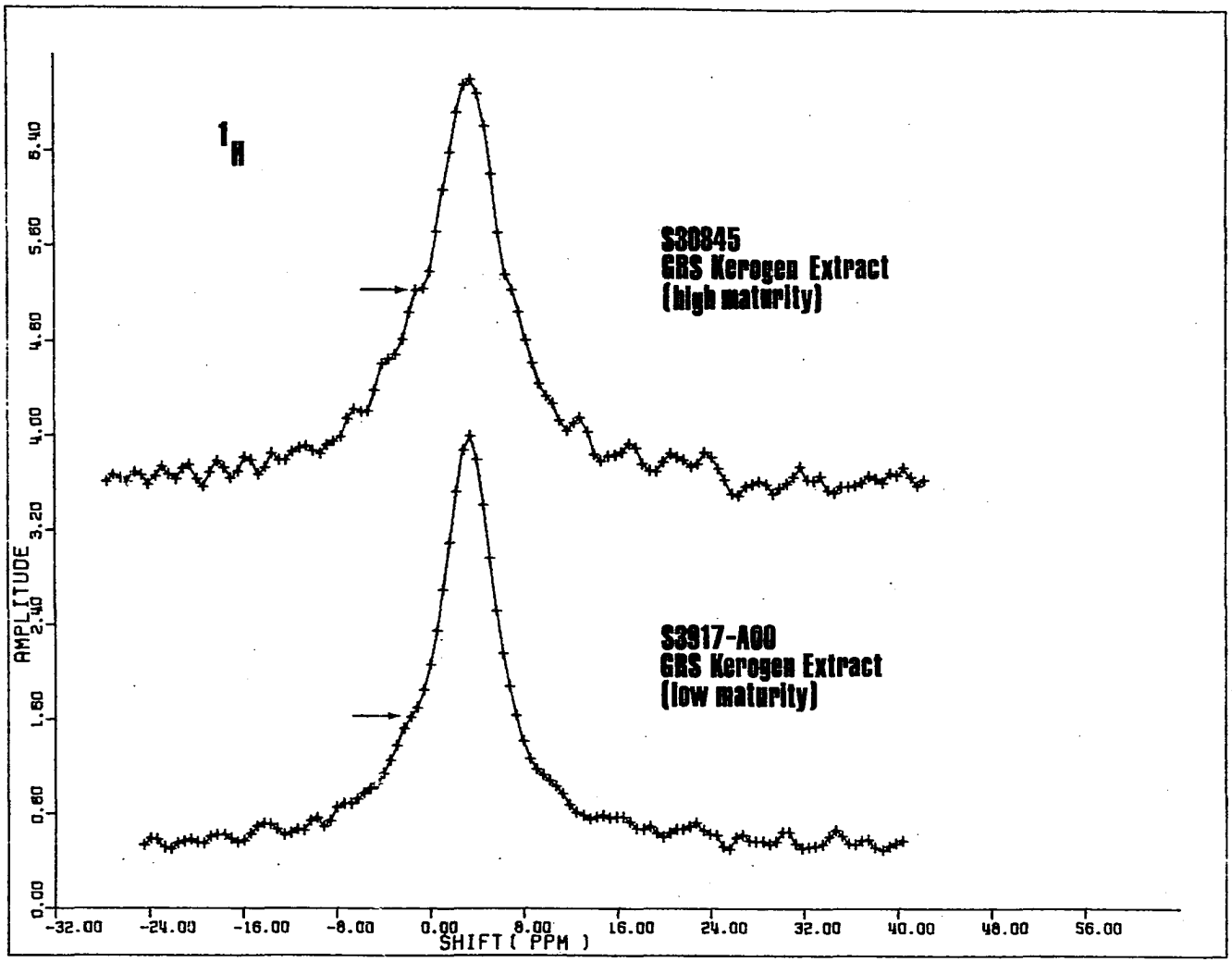

Figure 40. High resolution ^{1}H CRAMPS spectra of Green River oil shale kerogens

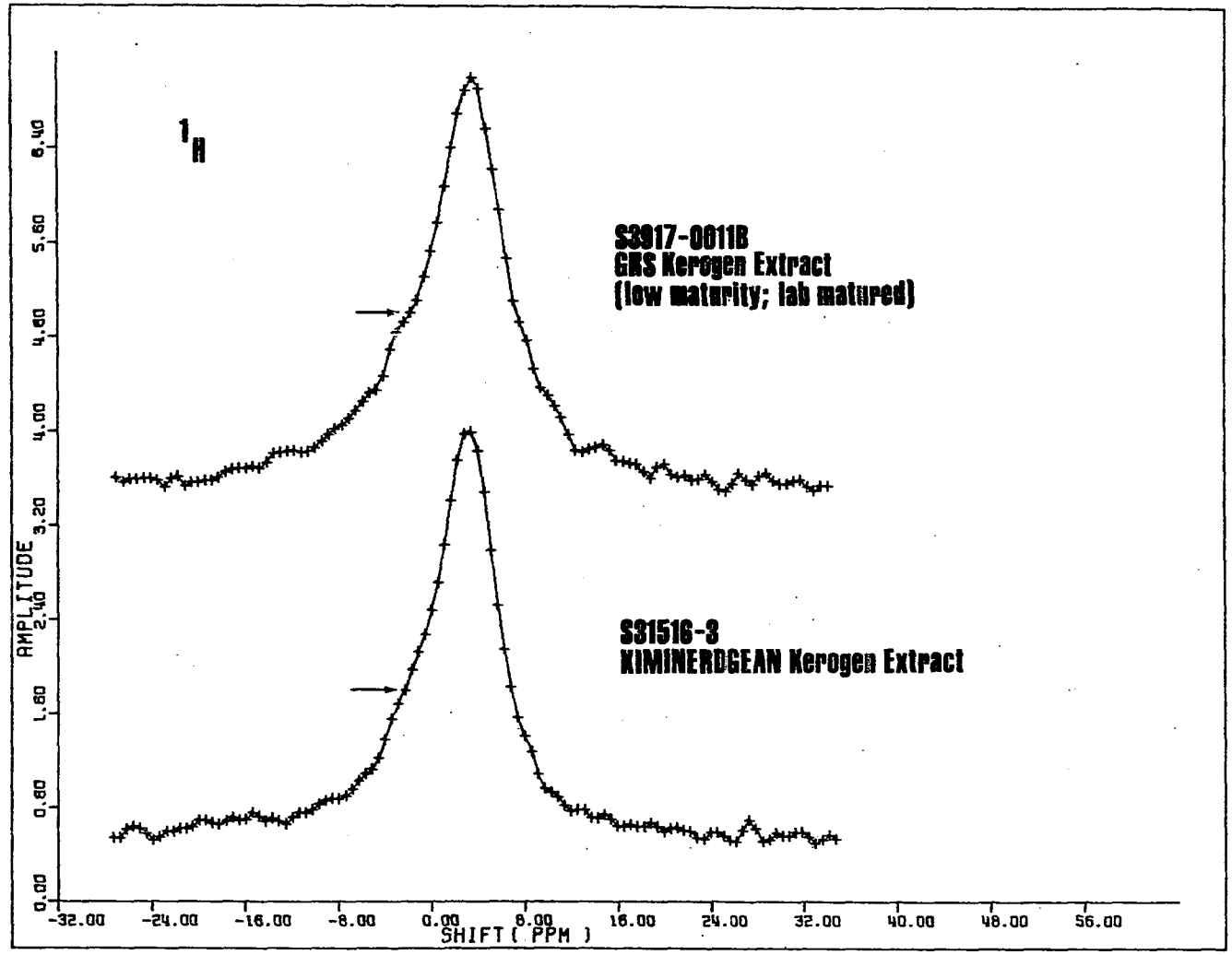

Figure 41. High resolution ^{1}H CRAMPS spectra of Green River and Kiminerdgean kerogens

Further work in developing this technique may at some time in the future show ^{1}H CRAMPS to be useful for evaluating procedures for the recovery of oil from shale, and in targeting new developments that would be fruitful.

CHAPTER 5. NMR OF HYDROGEN IN A HYDROGEN MOLYBDENUM BRONZE AND γ-ALUMINA

Introduction

Studies of hydrogen associated with oxide catalysts are important since it is generally conceded that hydroxyl groups are cardinal to the activity of oxides for many important catalytic reactions, including cracking and reforming reactions in the petroleum industry (333). In this chapter the nature of hydrogen in a hydrogen molybdenum bronze, $H_{1.64}MoO_3$, is investigated by conventional and solid state NMR methods. Hydrogen in $H_{1.64}MoO_3$ may potentially model the reduction of industrially important supported molybdena catalysts (334), which are used in the petroleum industry for hydrotreating and hydrodesulfurization, and more recently for coal hydrogenation (335, 336).

In the second section of the chapter an unsuccessful attempt to observe the up to five possible OH configurations proposed to be present on the surface of γ-alumina (337), using solid state ^1H NMR techniques is described.

These experiments were made in collaboration with A. C. Cirillo of the University of Wisconsin, Milwaukee and Dr. J. J. Fripiat of the Centre National de Recherche Scientifique, CROSCI, Orleans Cedex, France.

Proton NMR in a Hydrogen Molybdenum Bronze

Recently, the proton structure and mobility in a hydrogen molybdenum bronze were investigated by nuclear magnetic resonace (338). The bronze was prepared by exposing gaseous hydrogen to microcrystalline MoO_3 which was covered with small particles of Pt, the so-called hydrogen spillover technique (339). The NMR line observed was asymmetric and was displaced from that detected for water absorbed on the oxide. The lineshape became more symmetric upon cooling the bronze below about 230 K. The bronze behaved as a metallic conductor and, from the point of view of nuclear spin relaxation, was comparable with metal hydrides. The longitudinal relaxation rate was proposed to have three main contributions: one from the interaction between protons and conduction electrons $(T_1)_e^{-1}$, and the others from proton-proton dipolar $(T_1)_{II}^{-1}$ and proton-paramagnetic center $(T_1)_{IS}^{-1}$ interactions, respectively. Since these latter interactions may be modulated by proton mobility in the oxide lattice, their temperature dependence was treated using the theory of Torrey, modified by Krüger (340).

The present work extends that first study by presenting new experimental data which allows a better understanding of the physical nature of the bronzes. The cause of the asymmetry of the NMR lineshape was investigated using solid state

NMR techniques (L. M. R.), and a further investigation of the relaxation properties was made (A. C. C. and J. J. F.).

Related studies

Preliminary x-ray studies (341) on the same bronze used in this work have shown that the $H_{1.64}MoO_3$ bronze has a structure which is different from that of pure MoO_3, and that this structure does not change when the material is cooled to 78 K. A bronze with lower proton content can also be prepared (338), but was found (341) to be heterogeneous, as its diffraction pattern is composed of a superposition of that of MoO_3 and $H_{1.64}MoO_3$.

Birtill and Dickens (342) have stated that the bonze formed using the hydrogen spillover technique has the same structure as one formed in solution, viz. the red monoclinic phase (338); however, Taylor et al. (128, 131) have demonstrated that subtle differences exist between bronzes prepared by the two methods.

Magnetic susceptibility measurements (343) showed an increase in the paramagnetic character of the oxide upon transformation into the bronze. Moreover, at high temperatures (220-300 K), Pauli-type behavior was found, whereas at low temperatures (below ~220 K), χ increased as the temperature was lowered, suggesting Curie behavior. This work also showed that the Fermi velocity of the electrons is in the range of Pauli conducting metals at room temperature.

A small number of Mo^{+5} centers were observed by EPR of MoO_3 carefully outgassed to 10^{-6} torr at 100 °C (g = 1.93 with a concentration of 10^{16}-10^{17} spins/gram). In the bronze, Mo^{+5} was not detectable by EPR although XPS measurements (343) showed a distribution of about 30% Mo^{+5} and 30% Mo^{+4}, with the balance as Mo^{+6}. A maximum was observed (343) in the optical spectrum of the bronze around 18,000 cm^{-1}, very near that from Mo_4O_{11}, in which Porter et al. (344) have suggested 0.5 d-electrons per Mo cation. These authors assumed that one electron was shared by two cations with an exchange rate of greater than 10^{15} Hz. This interpretation agrees with the bronze data since Mo^{+5} centers having such a short lifetime would not give rise to a detectable EPR signal, but would be seen by XPS.

Experimental

Preparation of the bronze using the hydrogen spillover technique has been described in detail elsewhere (338, 339). The bronzes used in this study contained 0.25% Pt by weight, and had a surface area of 0.6 m^2/g (BET, N_2). All samples were prepared at 60 °C.

The relaxation measurements were performed at Orleans, France on a Brucker SXP pulse spectrometer operating at 90 MHz, using samples contained in sealed 10 mm pyrex NMR tubes.

The single and multiple pulse solid state NMR experiments and those involving magic-angle spinning were made at Iowa State University on the spectrometer described earlier in Chapter 3.

Results

Figure 42 offers a comparison of the single pulse lineshapes between the fully protonated $H_{1.64}MoO_3$ bronze and the heterogeneous $H_{1.0}MoO_3$ at room temperature. The temperature dependence of these lineshapes and that of a bronze with composition $(H+D)_{1.66}MoO_3$ were described elsewhere (338). In the partially deuterated sample, the stoichiometry was determined both by NMR and by volumetric measurements to be $H_{0.5}D_{1.1}MoO_3$. The salient features of the lineshape data are: 1) for the $H_{1.64}MoO_3$ bronze, the lineshape at room temperature is that of an axially symmetric tensor with $\sigma_{\parallel} - \sigma_{\perp} = -23$ ppm. At lower temperatures, the line becomes more symmetric, until at about 180 K it appears Lorentzian (Figure 43), and at 80 K it broadens to a width of about 60 KHz. 2) Dilution of the bronze with deuterium had no effect on the lineshape at room temperature, but the line for the deuterated sample broadened more rapidly than for the undeuterated sample as the temperature was lowered.

The lineshape of $H_{1.64}MoO_3$ under the MREV-8 multiple pulse sequence in the temperature region between 190 and

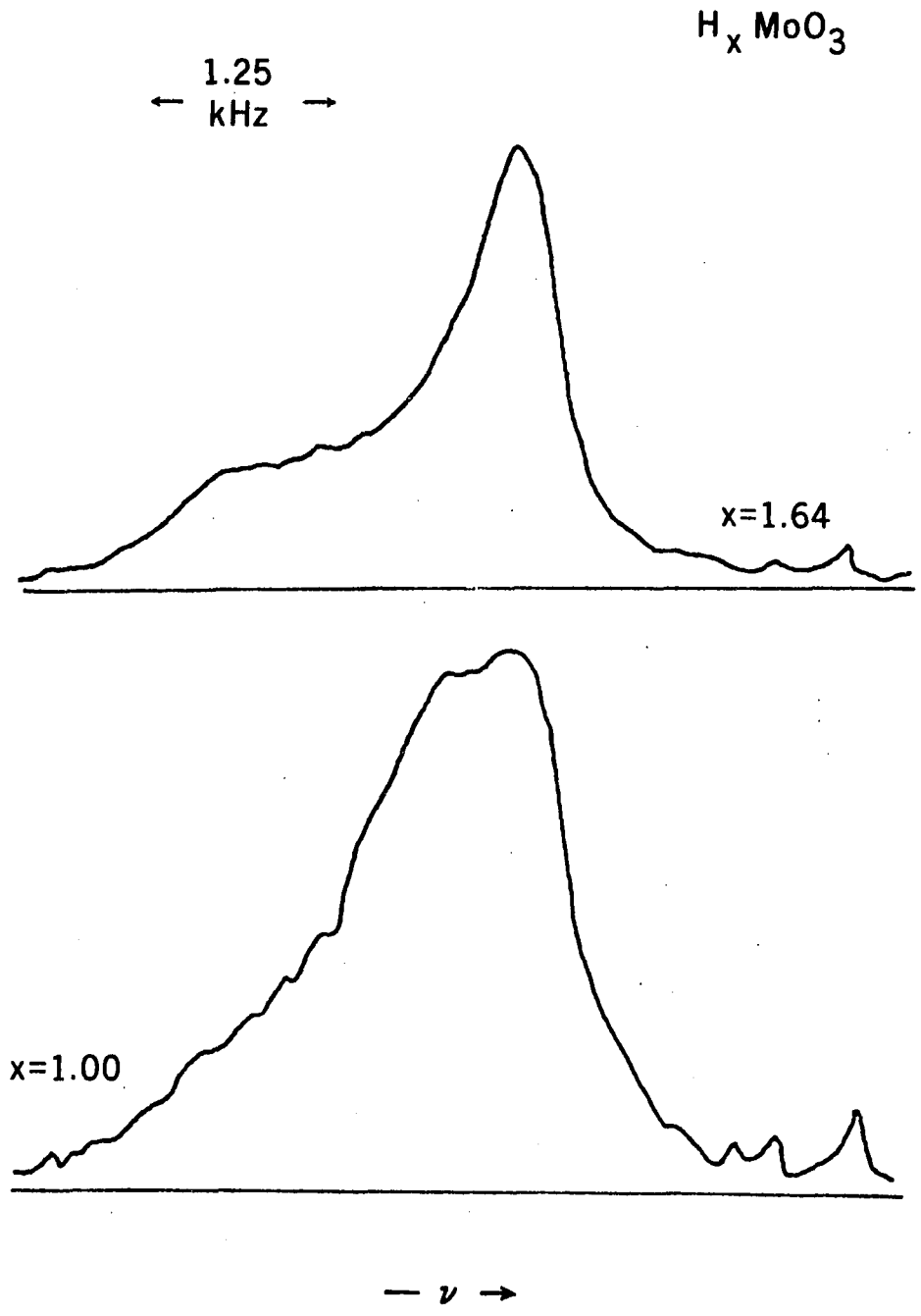

Figure 42. A comparison of NMR spectra of protons in $H_{1.64}MoO_3$ and $H_{1.0}MoO_3$ at room temperature and H_0 = 90 MHz

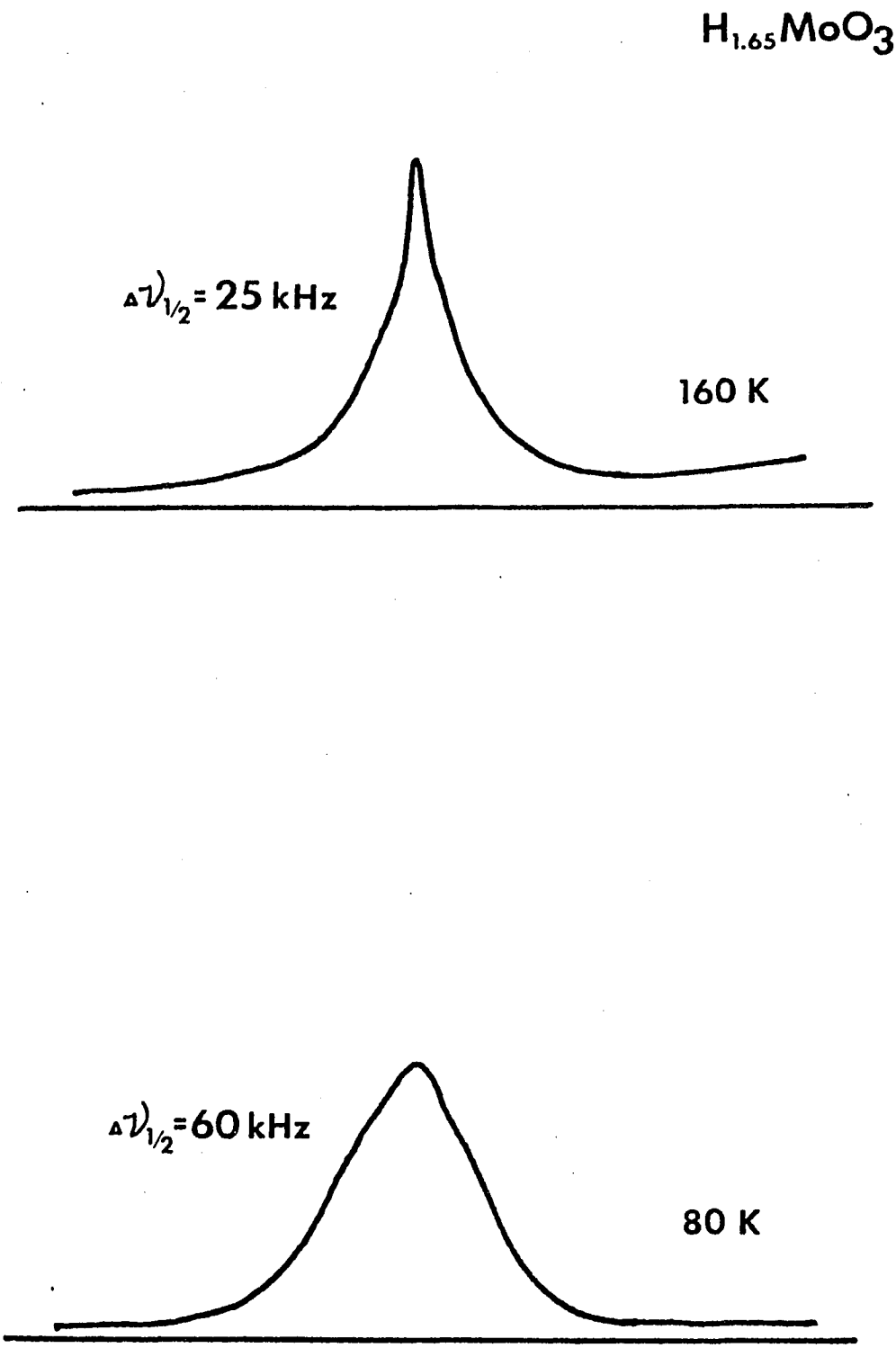

Figure 43. NMR spectra of hydrogen in $H_{1.64}MoO_3$ at 80 and 160 K and H_0 = 56 MH_z

300 K is compared in Figure 44 with the lineshape obtained under a single pulse excitation. In this figure, the single pulse result (solid line) has been superimposed on the multiple pulse result with frequency scaling accounted for (17,18). Figure 45 compares lineshape data for the $H_{1.64}MoO_3$ bronze obtained at 56 MHz under various experimental conditions. In this figure, a) is the Fourier transform of an FID observed following a single 90° pulse, showing a total anisotropy of -23 ppm, b) is the result of an MREV-8 experiment, with t_c = 36 μsec, c) is the FT of the decay following a single 90° pulse with the sample spinning at 2 KHz perpendicular to the applied field, and d) is the result of magic-angle spinning at 2 KHz, again using only single pulse excitations. All spectra were obtained at room temperature. Spinning perpendicular to the field inverts the sign of the anisotropy and scales the magnitude by 0.5 (17, 18). The effect of magic-angle spinning is to completely average the chemical shift tensor, resulting in a final linewidth of about 2 ppm. This spectrum indicates that at room temperature there is one major and one minor species of hydrogen in the bronze, as indicated by the two central peaks. The outer lines are spinning sidebands due to 2 KHz sample rotation.

Relaxation data taken for the $H_{1.64}MoO_3$ bronze are compared with data obtained for the similar, but partially deuterated sample, in Figure 46. The longitudinal (T_1),

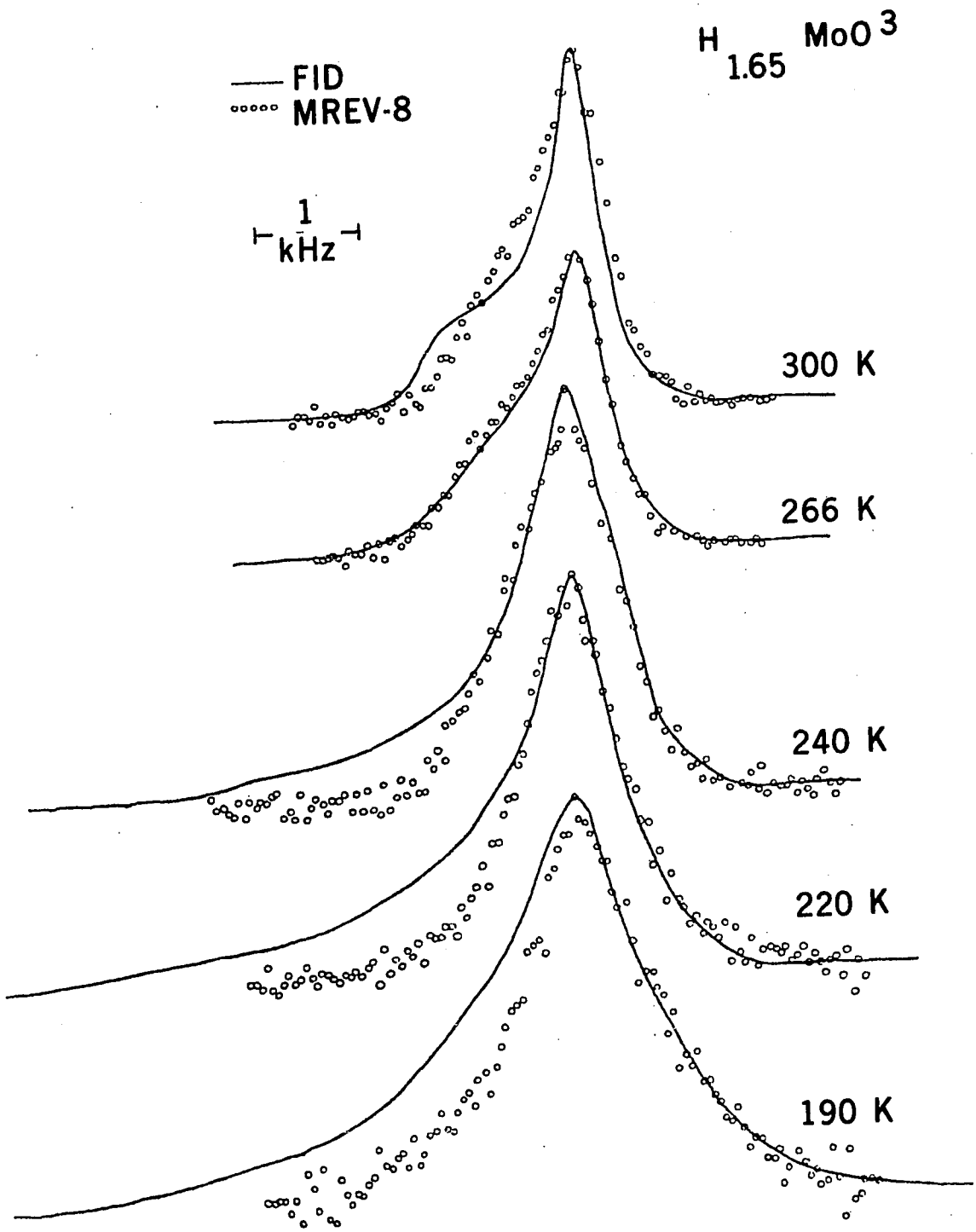

Figure 44. A comparison of the NMR spectra of hydrogen in $H_{1.64}MoO_3$ taken under conditions of single pulse excitation (solid line) and homonuclear dipolar decoupling (circles) as a function of temperature

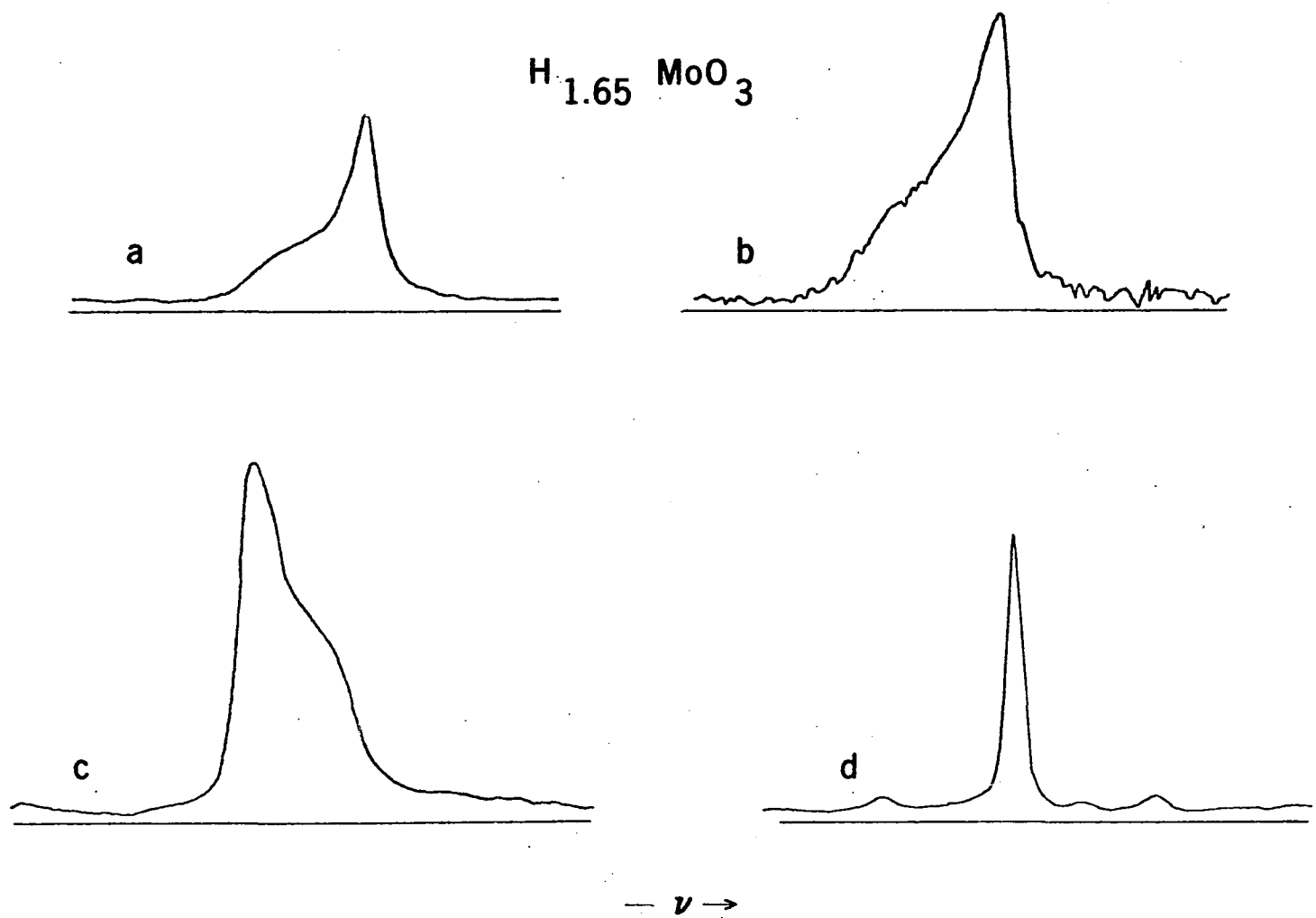

Figure 45. Comparison of NMR spectra of hydrogen in $H_{1.64}MoO_3$ taken under a) a single pulse excitation, b) multiple pulse homonuclear decoupling, c) 2 KHz sample spinning perpendicular to H_0, and d) magic-angle spinning

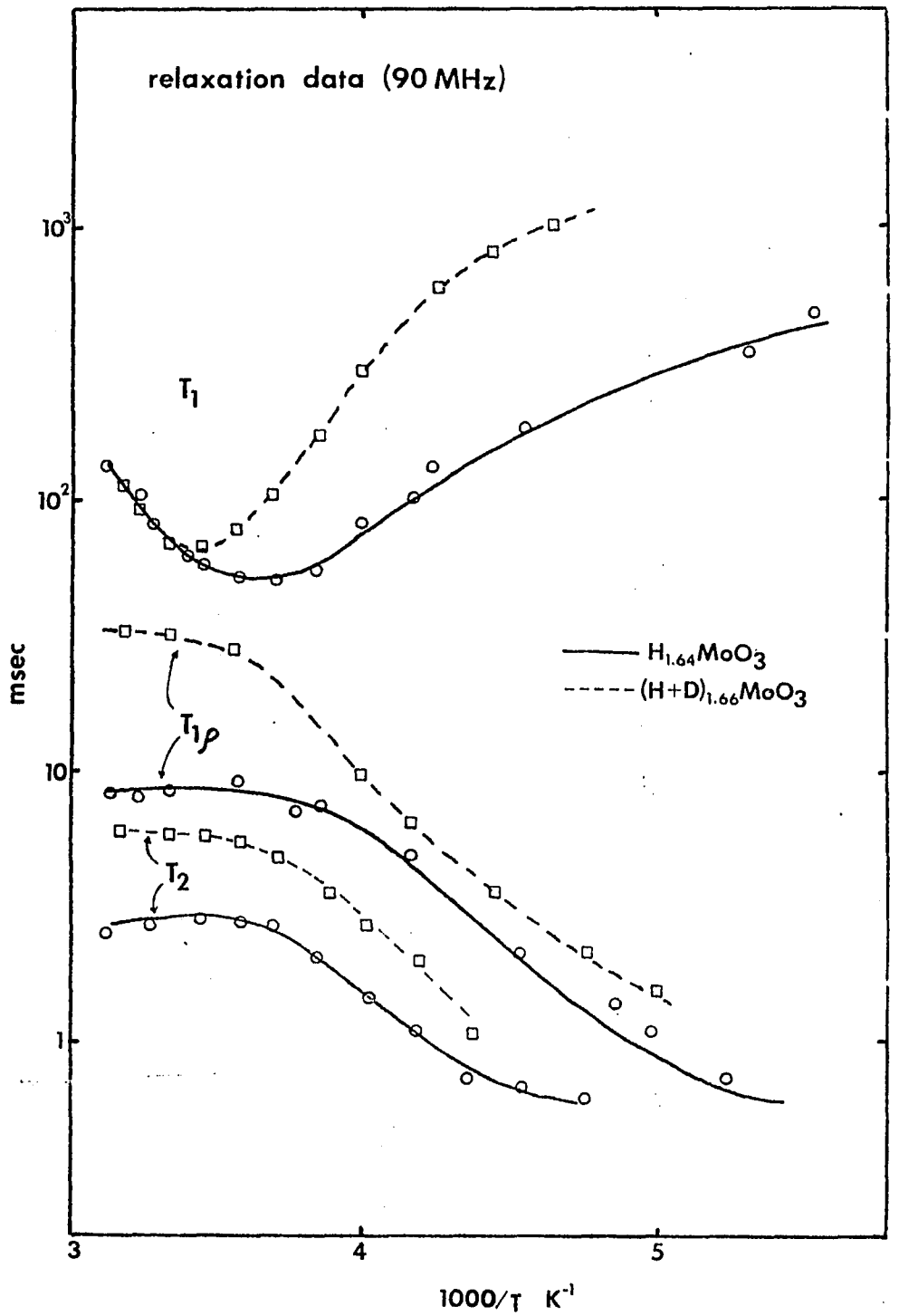

Figure 46. T_1, T_2, and $T_{1\rho}$ of hydrogen in $H_{1.64}MoO_3$ (solid lines) and $(H + D)_{1.66}MoO_3$ as a function of temperature

transverse (T_2), and rotating frame ($T_{1\rho}$) (7) relaxation times were measured at 90 MHz using appropriate pulse sequences (7). The values of T_2 were obtained from spin-echoe data (7) and $T_{1\rho}$ was measured using an H_1 field of 25.5 Gauss. Changing H_1 to 7.4 Gauss had no effect on $T_{1\rho}$ in the temperature region between 190 and 300 K, suggesting that $\omega_1\tau << 1$ for those temperatures (7) and that the minimum in $T_{1\rho}$ versus 1000/T should occur at a temperature below those used in these measurements.

Finally, the transverse relaxation time was measured for the $H_{1.64}MoO_3$ bronze using both the spin-echo and Carr-Purcell-Meiboom-Gill techniques (7). The temperature dependence of those results are given in Figure 47.

Discussion

A fundumental question concerning the hydrogen molybdenum bronzes is the nature of the interaction between the inserted hydrogen and the lattice oxygen atoms. Birtill and Dickens (342) have prepared bronzes by reducing MoO_3 in an aqueous medium using nascent hydrogen. They observed different crystal phases for various hydrogen contents, and they have proposed the formation of OH groups on the basis of elastic and inelastic neutron diffraction studies (345). Those authors also state that the bronze formed by hydrogen spillover has the identical structure as those prepared in solution, viz., the red monoclinic phase (342).

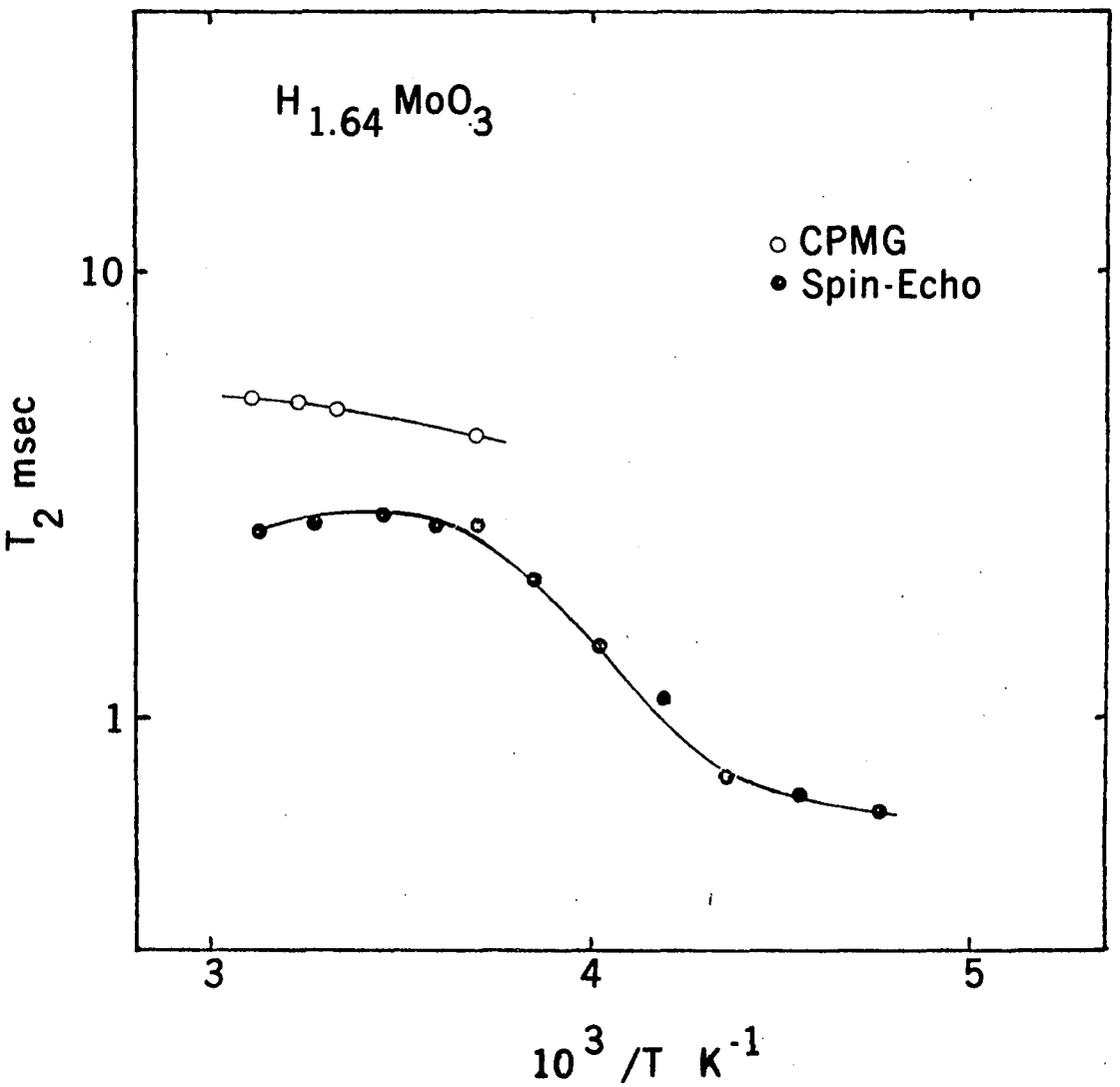

Figure 47. T_2 vs. 1000/T for protons in $H_{1.64}MoO_3$ measured by the Hahn spin-echo (solid circles) and the CPMG (open circles) techniques

This proposal of a hydroxide structure for the bronze prepared by the spillover technique is inconsistent with several experimental observations: 1) the bronze reacts quantitatively with O_2 to produce a stoichiometric amount of water and the resulting oxidized sample can be reduced with H_2 to its original state, 2) the heat of formation of the bronze is 25 kcal/mole (346), whereas the heat of formation of OH groups in hydroxides is typically on the order of 100 kcal/mole, 3)the bronze reacts with ethylene to form C_2H_6, and the amount of hydrogen used for this reaction can be replaced stoichiometrically by titration with H_2 gas (347), and 4) the metallic character of the bronze (338) is difficult to explain if only OH groups are formed.

Although it is likely that hydroxyl groups do form on the surface of the oxide, the surface area of the bronze samples used in this work were less than $1m^2/g$, so that the surface OH content must be negligible with respect to the total amount of hydrogen in the samples.

In discussing the structure of the bronze, ambiguity exists concerning the oxidation states of molybdenum, thereby suggesting the incorporation of hydroxyl groups into the lattice. Since the data suggest that the lifetime of these species is extremely short (on the order of 10^{-16} seconds), a model of delocalized electrons seems preferable. This

delocalization may result from the overlap of Mo d-orbitals with oxygen 2p-orbitals, as suggested by Goodenough (348). This view is supported by XPS measurements which show oxygen in the bronze to be more electron rich than oxygen in MoO_3 (343).

NMR data The identical values of shielding anisotropy exhibited by the $H_{1.64}MoO_3$ and $(H + D)_{1.66}MoO_3$ bronzes at room temperatures support the assumption that the two have the same structure. Moreover, this indicates that the important contributions to the lineshape at around 300 K do not arise from the nearest-neighbor interactions between protons. This evidence does not disallow, however, the possible existence of associated pairs of protons at low temperatures, as have been suggested to exist by Birtill and Dickens (342), and as perhaps evidenced by the greater linewidth of the deuterated bronze in this region (338).

The results of the MREV-8 multiple pulse experiments shown in Figure 44 indicate that homonuclear dipolar interactions make little or no contribution to the observed lineshape at room temperature, and at temperatures as low as perhaps 266 K, in accordance with the data from the deuterated bronze. In the low temperature region, an apparent increase in dipolar broadening gave the line a more symmetrical

appearance, although the asymmetric tensor was still contained within the signal envelope, at least down to around 220 K. Below this temperature, other evidence (vide infra) suggests a change in the electronic structure of the bronze which could remove at least part of the shielding anisotropy.

The MREV-8 data show that the lineshape of the bronze is determined by two competing interactions. Around room temperature, the shielding anisotropy is greater than the dipolar broadening. As the temperature is lowered, this circumstance is reversed, until at about 80 K the lineshape is completely dominated by the dipolar interaction. Some motion, most probably rotational, remains below 180 K, as indicated by the pseudo-Lorentzian lineshape in the intermediate temperature region (Figure 43). Even this motion apparently "freezes out" at about 110 K, although the shoulders on the spectrum obtained at 80 K could possibly be due to a molecular reorientation about some preferred axis (4).

There are several possible causes for the asymmetric NMR lineshape at high temperatures. The most probable are either Knight shift anisotropy or chemical shift anisotropy. The hydrogen molybdenum bronze behaves as a metal (338); the conduction band is occupied by electrons produced by the ionization of hydrogen atoms invading the MoO_3 lattice (348). If the extent of ionization should be temperature dependent,

the electron content and thus the distribution of the s and d character may change. If the symmetry of the hydrogen environment is lower than cubic, the term describing the electron-nuclear coupling will not be a scalar quantity, and the resulting Knight shift will depend on the direction of the applied field with respect to the crystalline axes. Thus, Knight shift anisotropy seems the most likely cause of the asymmetry at room temperature.

Norberg (349) has observed an asymmetric proton signal in PdH which was attributed to a skin depth effect. The presence of a dispersive component of the resistive nuclear signal was considered to be provoked by protons contained in the metallic conductor and a phase shift of $\pi/2$ was attained at a depth equal to the skin depth. Since the conductivity of the bronze is unknown, a calculation of the skin depth was performed using the values known for copper metal, on the assumption that this procedure would give a lower limit for the skin depth. At room temperature and 90 MHz, the calculated skin depth was slightly greater than 800 μm which was much greater than the average particle size (10 μm). This does not discount the fact that good ohmic contact between particles may be generated by the metallic platinum on the surface, thereby increasing the effective particle size. However, a bronze containing no platinum exhibited the same proton asymmetry as the bronze with platinum (350).

Since, as previously mentioned, a hydroxide structure has been propsed for the bronze (345), it is instructive to compare its room temperature linewidth with that measured earlier for ice at 173 K (351). Both measurements were made at 56 MHz on the same instrument. The values of the shift anisotropy $\sigma_{\parallel} - \sigma_{\perp}$ were -23 ±2 and +34 ±1 ppm for the bronze and ice samples, respectively. The large positive value observed for ice is one of the largest observed for hydrogen atoms bonded to oxygen (17, 18), and is in characteristic agreement with theoretical studies of magnetic shielding (352, 353), which show the unique axis of the σ tensor to be parallel to the OH bond. While reorientation of molecules about a unique axis can invert the sign of the shift anisotropy (17, 18), no angle of the reorientation axis can convert $\Delta\sigma = +34$ ppm or less into $\Delta\sigma = -23$ ppm (17, 18). The large negative value found for the bronze is, thus, further evidence that the proton resonance at room temperature is not due to hydroxyl groups.

Relaxation data The temperature behavior of longitudinal relaxation in conducting materials has been described by Abragam (4) and may be summarized as follows: T_1 will be proportional to T for a metallic conductor and proportional to $T^{\frac{1}{2}}$ for a semiconductor. Unfortunately, it was not possible to distinguish between these two cases for

the bronzes. At high temperatures (above 440 K), decomposition to a lower oxide began to occur, thereby preventing an accurate assessment of the electronic contribution to T_1. In the low temperature region (below 200 K), it is unclear whether the electronic term remains since magnetic susceptibility measurements (343) have shown a transition from Pauli to Curie-like behavior as the temperature is lowered through 230 K. Thus, at low temperatures, the magnetic and electronic properties of the bronze seem to change in such a way as to suggest that interactions other than those with conduction electrons are responsible for T_1. In the region of the minimum of T_1, the electronic contribution cannot dominate T_1 (4) and is assumed to be negligible. Therefore, there was no temperature range accessible to these studies in which the electronic contribution is believed to dominate T_1.

The fact that both the line shape and the behavior of T_1 around room temperature did not change as the bronze was diluted with deuterium does not mean that the two parameters are controlled by the same interaction. In fact, although the anisotropic line shape is believed to arise from electronic interactions, measurements of T_1 versus temperature at various frequencies clearly show that in this region of temperature T_1 is independent of ω_0^2, and thus is not dominated by this mechanism. In summary, although the bronzes

are believed to be electronic conductors, the interaction between the proton nuclei and the conduction electrons does not dominate the spin-lattice relaxation over the temperature region between 190 and 320 K.

The observation of a minimum in the plot of T_1 versus temperature suggests (4) that dipolar interactions modulated by motion are responsible for the spin-lattice relaxation in the temperature region shown in Figure 46. Moreover, a comparison between the values observed for the X = 1.64 bronze and those obtained from the partially deuterated sample indicates the presence of at least two types of interactions, one which is sensitive to the average proton-proton distance and a second which is not. Assuming a random occupation of protons in both samples, the average distance between proton nearest neighbors is increased by a factor $(1.64/0.56)^{1/3}$ when the bronze is diluted with deuterium in the manner described above.

The difference between the values of $(T_1)^{-1}$ for the two bronzes may be defined as

$$\Delta = (T_1)^{-1}_{1.64} - (T_1)^{-1}_{0.56} \qquad (55)$$

The temperature dependence of this parameter is shown in Figure 48. This function represents the component of T_1 which is a function of the homonuclear dipolar interaction, assuming that dilution with deuterium changes only the

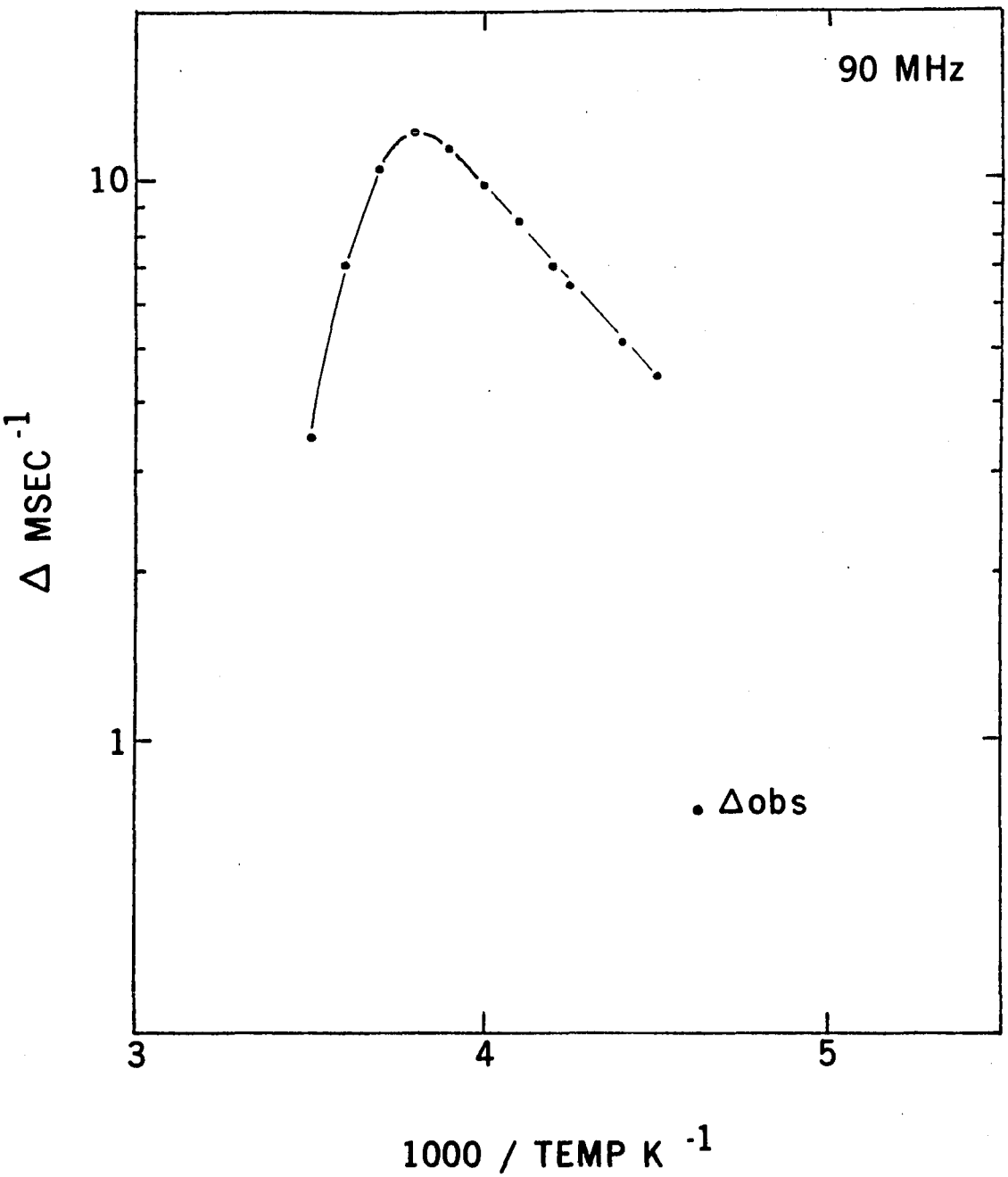

Figure 48. $(T_1)^{-1}_{1.64} - (T_1)^{-1}_{0.56}$ vs. 1000/T; observed values

distance between proton nearest neighbors.

The theory describing the spin-lattice relaxation rate due to dipolar interactions modulated by proton motion has been derived by Torrey and Resing (354, 355), and modified by Krüger (340). The relevant expression for the hydrogen molybdenum bronze, in terms of the two types of interactions, is

$$(T_1)_{obs}^{-1} = (T_1)_a^{-1} + (T_1)_b^{-1} \qquad (56)$$

where the subscripts "a" and "b" refer to the interactions which are sensitive or not sensitive to dilution with deuterium, respectively. If $(T_1)_a^{-1}$ is assumed to be due to homonuclear dipolar interactions, then

$$(T_1)_a^{-1} = \frac{8\pi}{15} \gamma^4 \hbar^2 I(I+1) \frac{N}{\omega d^3} g_{1,\ like}(\alpha,y) \qquad (57)$$

where N is the number of protons per cm^3, d is the distance of closest approach between two interacting spins and the function $g_{1,\ like}(\alpha,y)$ has been tabulated previously (340) and gives the relationship between the relaxation rate and the correlation time for the motion; the other constants have their usual meaning. Combining Equations 55 and 57 we obtain

$$\Delta = 1.89 \times 10^{-45} \frac{N_{1.64} - N_{0.56}}{d^3} g_{1,\ like}(\alpha,y) \qquad (58)$$

where

$$N_{1.64} = 3.1 \times 10^{22} \text{ protons per cm}^3$$

$$N_{0.56} = 1.0 \times 10^{22} \text{ protons per cm}^3$$

and it has been assumed that although dilution with deuterium will change the average interproton distance, the distance of closest approach remains unchanged.

The magnitude of the slope of the curve shown in Figure 48 is greater for $\omega\tau<1$ (high temperature region) than for $\omega\tau>1$. This behaviour is similar to that for $\alpha=0$ in the Krüger treatment for like spin interactions.

$$\alpha = \frac{\langle r^2 \rangle}{12d} \tag{59}$$

where $\langle r^2 \rangle$ is the mean square jump distance. A value of α which is small suggests localized motion, e.g., rotation, since the average jump distance will be small compared with the distance of closest approach.

At the maximum of $g_{1,\ like}\ (\alpha,y)$ vs. $10^3/T$ for $\alpha=0$, the value of g_1 is 0.963 (34). Equation 58 then allows the calculation of d^3 from a knowledge of Δ at the maximum of Δ vs. $10^3/T$ (Table XVII). Similarly it is now possible to calculate $g_{1,\ like}\ (\alpha,y)$ as a function of temperature, to obtain the contribution to T_1 due to interactions depending upon internuclear distances, i.e. to calculate $(T_1)_a^{-1}$, using Equation 57. This behavior is shown in Figure 49, indicated by the line through the crosses (x). Furthermore, $\omega\tau_a$

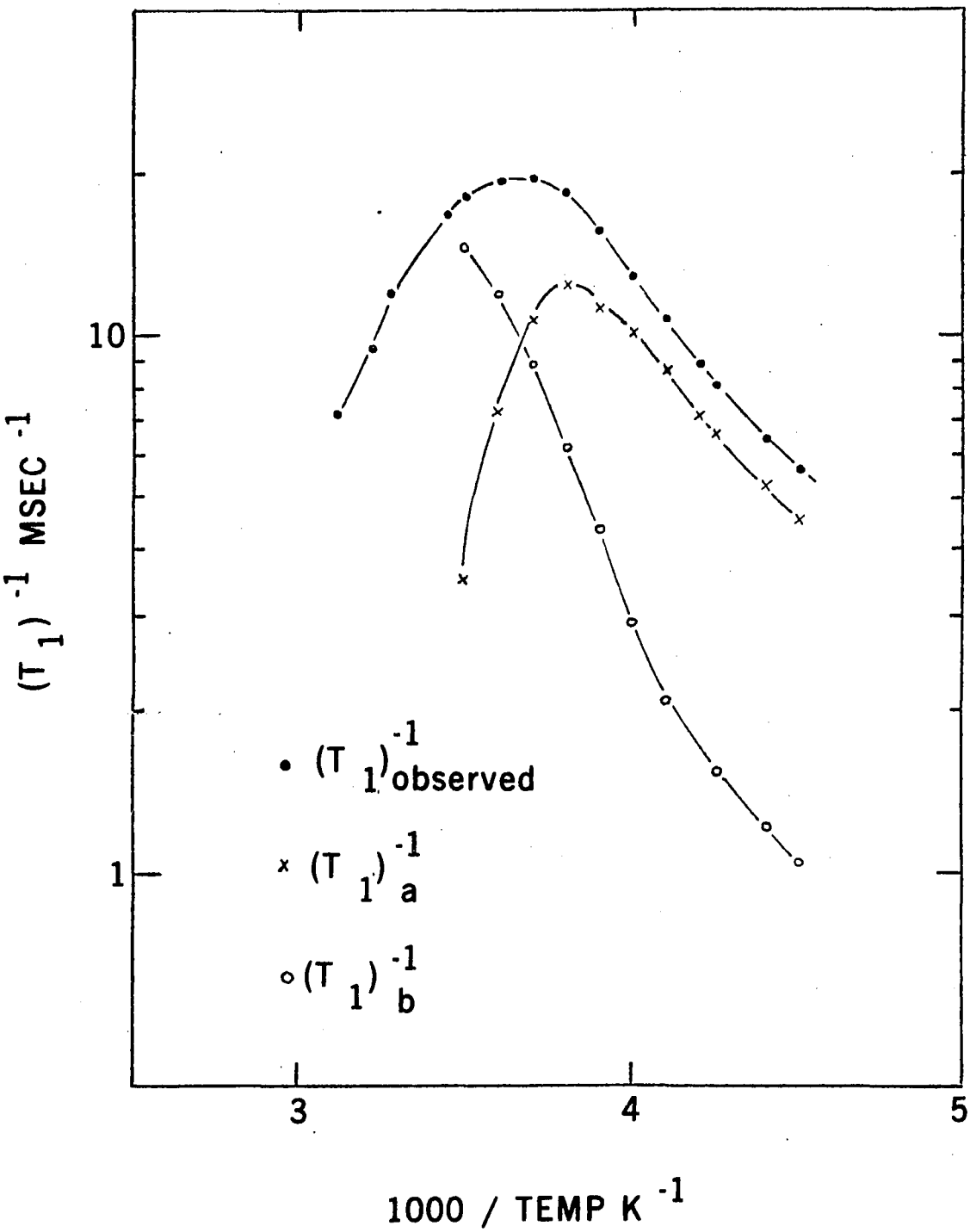

Figure 49. A plot showing the $(T_1)_a^{-1}$ and $(T_1)_b^{-1}$ components for protons in $H_{1.64}MoO_3$ at 90 MHz. Values were calculated from the observed values of $(T_1)^{-1}$

can be calculated as a function of $10^3/T$ to obtain an activation energy of motion for those contributing to T_1 via interactions dependent upon internuclear distance. These results are shown in Figure 50, as the line through the solid points. The value obtained was E_a = 15 Kcal mol^{-1}.

Substituting the values determined for $(T_1)_a^{-1}$ at each value of $10^3/T$ into Equation 56 gives the corresponding $(T_1)_b^{-1}$ values, also shown in Figure 49 (open circles). The behavior of the "b" portion of T_1 is similar to the Krüger treatment for $\alpha = \infty$, i. e., the interactions which are spin-other spin in nature appear to have a very delocalized character. Again, using the Krüger treatment for spin-other spin interactions, $g_{1,\ like}\ (\alpha,y)$ was calculated as a function of $10^3/T$, for $\alpha = \infty$, leading to $\omega\tau_b$ as a function of $10^3/T$, shown in Figure 51 as the line through the open circles. The activation energies obtained from the slopes of both lines in Figure 50 are the same to within experimental error.

Table XVII. Parameters obtained from the maximum of Δ versus 1000/T, K^{-1} for X = 1.64

Δ, sec^{-1}	1000/Temp, K^{-1}	g_1, like (α,y)	d(Å)
12.2	3.82	0.963	1.5

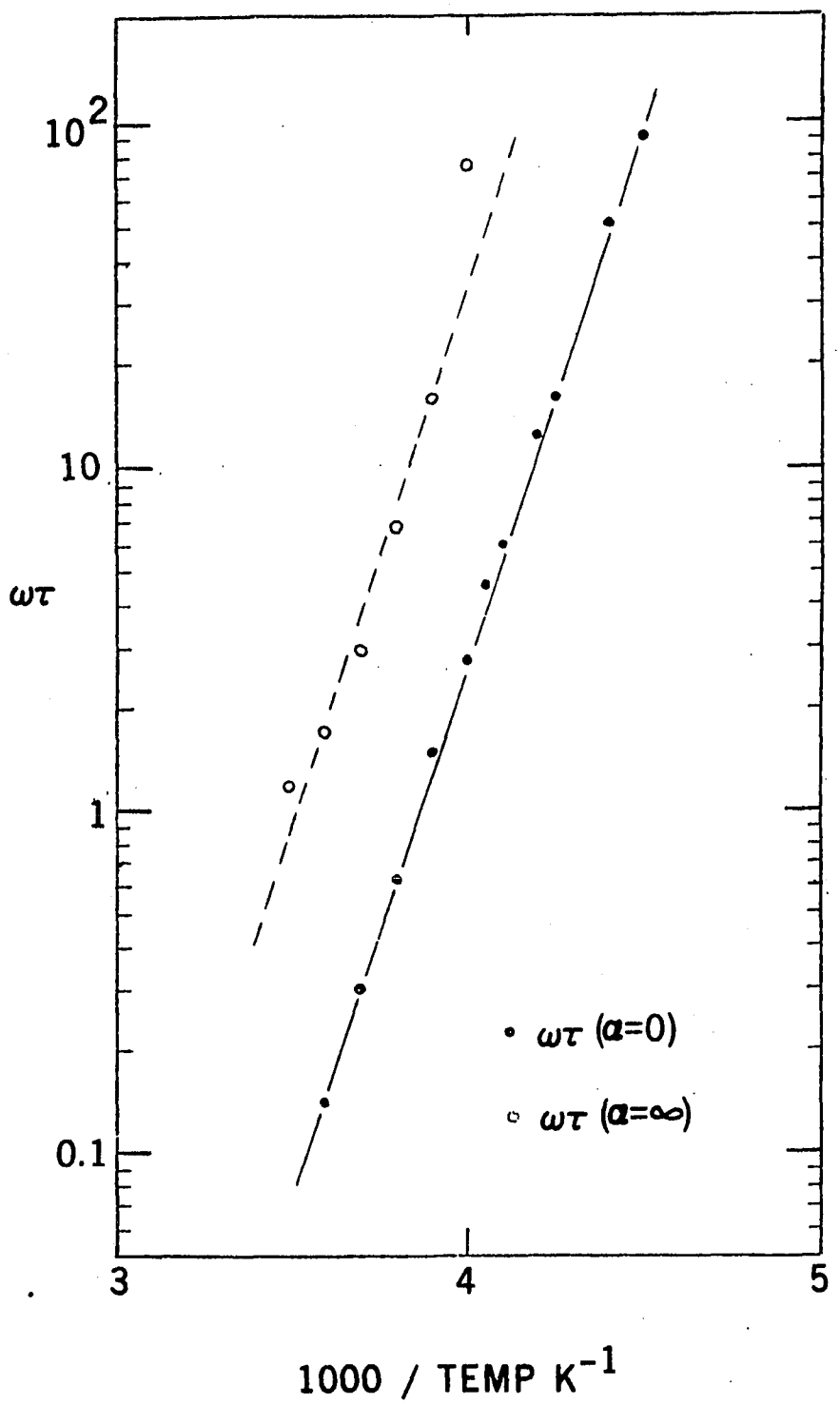

Figure 50. A plot of $\omega\tau$ vs. 1000/T to determine the activation energy for motion of protons in $H_{1.64}MoO_3$

In summary, the $(T_1)^{-1}$ values result from two contributions, one which depends upon the average proton-proton distance, $(T_1)_a^{-1}$, and a second one which does not, $(T_1)_b^{-1}$. The correlation times for both interactions led to the same activation energy of about 15 kcal/mole but τ_b was found to be about 10 times larger than τ_a. Finally, the distance of closest approach was calculated as 1.5 Å.

Transverse relaxation time The spin-spin relaxation time was obtained using the Hahn spin echo technique (7). The result thus obtained is dependent upon diffusion of the detected species. This effect depends upon the spatial magnetic field gradients (G), the diffusion coefficient (D) and the time during which diffusion is able to occur (2). The amplitude of the echo for a pulse sequence with a separation may be expressed as

$$A \text{ (echo at } 2\tau) \alpha \text{ Exp } \left[- \frac{2\tau}{T_2} - 2/3\, \gamma^2 G^2 \, D \tau^3 \right] \qquad (60)$$

Due to the τ^3 dependence in the second term of the exponential, the effect of diffusion is particularly pronounced for large values of τ and thus effects most measurements of long T_2's.

Carr and Purcell (356) showed that a simple modification of Hahn's spin-echo technique would reduce the effects

of diffusion. For a Carr-Purcell sequence, the expression for the echo amplitude is

$$A \text{ (echo at } \tau) \propto \exp\left[-\frac{t}{T_2} - \left(\frac{1}{3}\right)\gamma^2 G^2 D \tau^2 t\right] \qquad (61)$$

and thus by making τ small, the second term can be made as small as experimentally feasible. Furthermore, by doing both experiments and solving Equations 60 and 61 simultaneously, it is possible to estimate the magnitude of the internal field gradient (G) using values of the diffusion co-efficient (D) obtained from T_1 measurements.

A plot of ln A (Carr-Purcell) versus t is shown in Figure 52 for various experimental temperatures. The deviation from linearity occurred in the same region of temperature as the strong change in lineshape (vide ultra), the break in the magnetic susceptibility curve (343) and the occurrence of a singularity in the heat capacity data (357). As the temperature is lowered through this region (about 230 K), the electronic and magnetic parameters of the system are changing, but x-ray data show that no change is occurring in the structure of the bronze (341). One possible explanation, which is consistent with all the data accumulated to date, is that the degrees of freedom of the proton system are reduced in this range such that the homonuclear dipolar interaction is becoming dominant at low temperatures. There seem to be two aspects to this change, one concerning

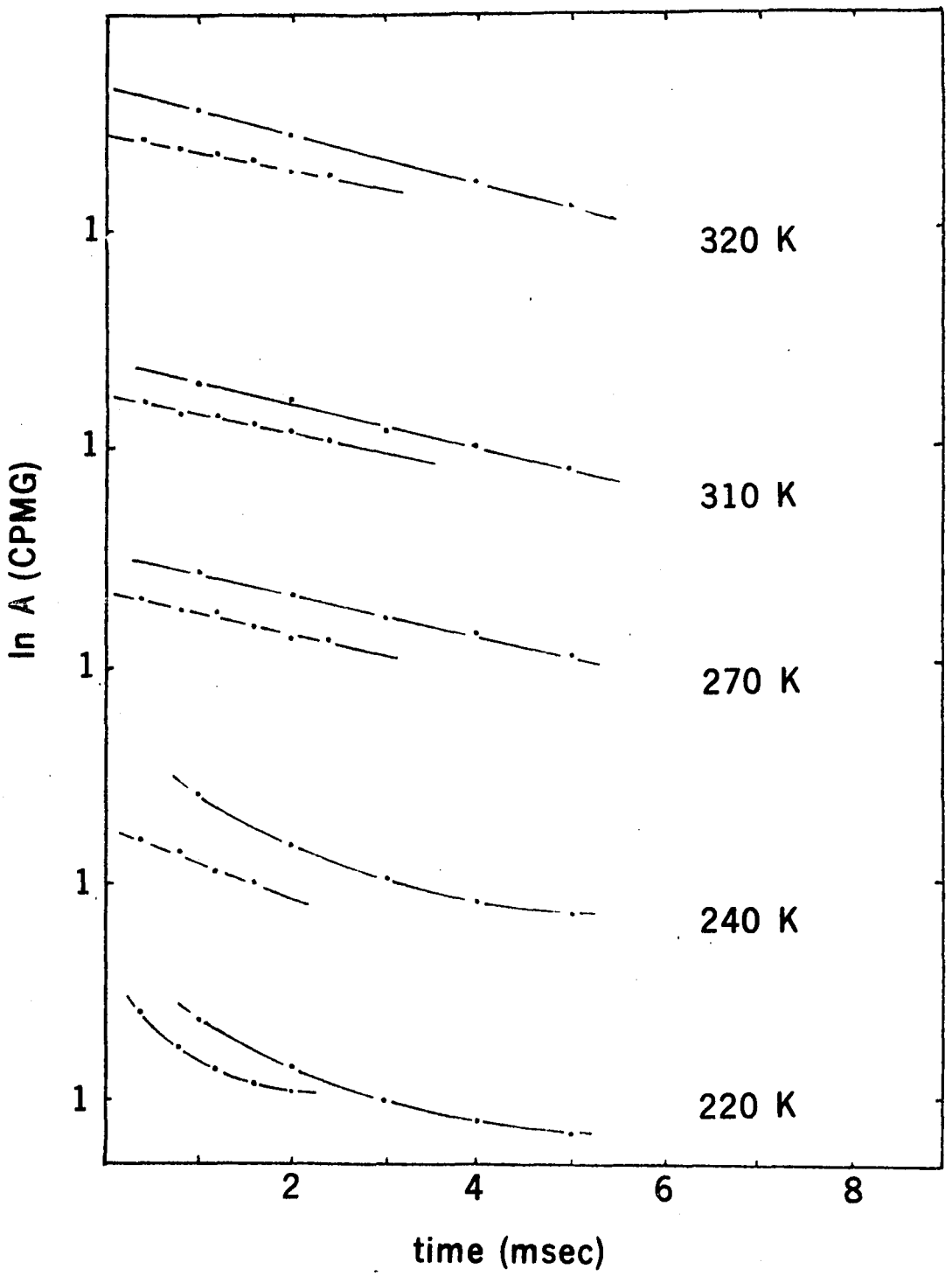

Figure 51. A plot of ln A vs. time for the CPMG sequence at 90 MHz as a function of temperature for protons in $H_{1.64}$ MoO_3

the reduced mobility of the proton system as the temperature is lowered and a second concerning a change in the electronic and magnetic properties of the bronze such that at low temperatures the electronic conductivity no longer dominates either the NMR lineshape or the bulk magnetic susceptibility. Conductivity measurements should indicate the presence of a conductor-to-semiconductor transition, if one exists in this region.

The difference between T_2 (spin-echo) and T_2 (Carr-Purcell) for the X = 1.64 bronze is shown in Figure 47. Using these data and Equations 60 and 61 in the temperature range between 310 and 320 K, the product G^2 D was found to be between 1.3×10^{-7} and 2.8×10^{-7} gauss^2 sec^{-1}. Since the diffusion coefficient calculated from the correlation time of T_1 was on the order of 4×10^{-7} cm^2 sec^{-1}, the field gradient will be between 0.6 and 0.9 gauss cm^{-1}. The diffusion constant from the T_1 measurements is in disagreement with that obtained by Taylor et al. (358) using a pulsed field gradient technique, viz $\sim 7 \times 10^{-6}$ cm^2 sec^{-1}. Since the value obtained from the T_1 measurement was calculated with the assumption of isotropic motion, the difference between the two values may give an indication of the degree of anisotropy in the proton motion within the bronze.

Spin-lattice relaxation time in the rotating frame

As shown in Figure 46, $T_{1\rho}$ levels off in the high temperature region in a manner similar to T_2, with the values for the $H_{1.64}MoO_3$ bronze being smaller than those for the partially deuterated sample. As the temperature is lowered, the two curves merge. Homonuclear dipolar interactions, which become important as T falls below 220 K, are not refocused under the simple spin echo sequence, so a measurement of T_2 at temperatures where a minimum should occur were not available by use of the Hahn spin-echo technique.

Using the BPP theory, $T_{1\rho}$ is normally expressed assuming a sample system of two interacting protons with only one correlation time. In the presence of two or more spin species, this treatment no longer applies, since $T_{1\rho}$ becomes a complicated function of the longitudinal relaxation time of the differing species. In particular, if there are contributions from paramagnetic species, the T_1 of the paramagnetic center may dominate $(T_{1\rho})^{-1}$.

$T_{1\rho}$ was found to be independent of H_1 over the temperature range shown for values of H_1 equal to 7.4 gauss and 25.5 gauss, which suggests $\omega_1\tau_c < 1$ in this region. Furthermore, the values of $T_{1\rho}$ in the low temperature region could be derived from the T_1 values using reference 359.

$$(T_{1\rho})^{-1} \simeq K \sum_{j=1}^{N} g_{ij}(0) \frac{2\tau_c}{1 + (\omega_1\tau_c)^2} \qquad (62)$$

where $K \sum_{j=i}^{N} g_{ij}^{(0)}$ is a numerical constant for a powdered sample which for the bronze was assumed equal to the second moment. Substituting the observed constant and the correlation times calculated from the $(T_1)_b^{-1}$ data into Equation 62, the theoretical values shown in Figure 52 were found. There is reasonable agreement between the T_1 and $T_{1\rho}$ data below 220 K. Above this temperature, the $T_{1\rho}$ data level off in a manner similar to T_2 and another mechanism not effective in T_1 becomes dominant.

NMR of Hydrogen Associated with γ-Alumina

Aluminas have been used extensively for many years as adsorbents, active catalysts, and as catalyst supports (333). Among the applications of aluminas in catalytic processes are for hydrocracking and hydrodesulfurization, the conversion of paraffins to olefinic hydrocarbons, and many others (333). Despite the widespread interest in catalytic aluminas and the great importance of their surface structure in determining the structure of supported catalytically active phases (333), the nature of the alumina surface is still only partially understood.

The presence of hydroxyl groups on the surface of alumina catalysts has been demonstrated by infrared spectroscopy (360, 361), by deuterium exchange (362, 363), and by chemical analysis (364); similar methods have shown that

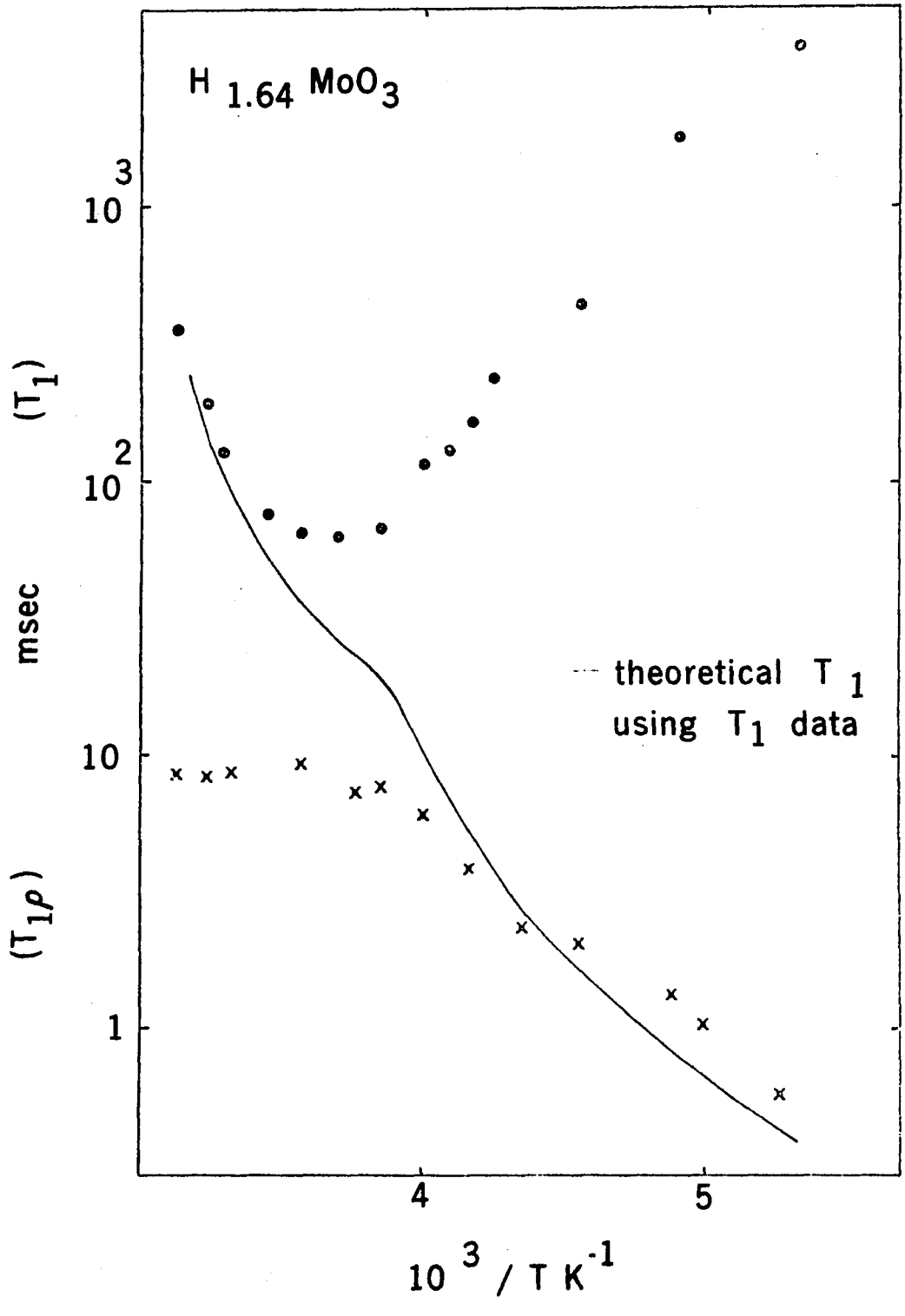

Figure 52. A comparison of T_1 (solid circles), $T_{1\rho}$ (crosses), and $T_{1\rho}$ calculated from T_1 (line)

hydroxyl groups are also present on molybdena-alumina catalysts. The latter systems are active for catalytic reforming, for making toluene and other aromatics from saturated hydrocarbons, and many other economically important reactions (333). Currently, much effort is being made to study the surface chemistry of these molybdena-alumina catalysts (334, 365).

Several models have been proposed for the surface of aluminas (361, 363, 366, 367), and five different configurations of OH have been identified by IR (360, 361). Knözinger and Ratnasamy (361) describe those as

Type Ia 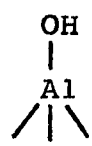

,

a terminal OH group coordinated to a single tetrahedral Al^{+3} cation

Type IIa 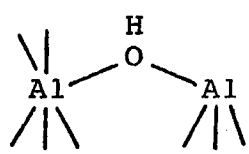

,

a bridging OH group which links a tetrahedral and an octahedral cation

Type IIb 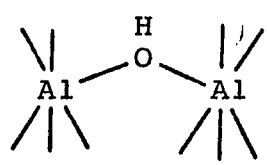

,

an OH group which links two cations in octahedral positions

Type III 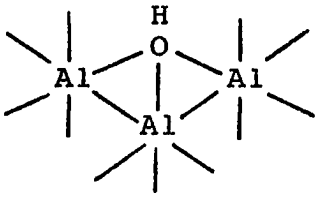

,

which is coordinated to three cations in octahedral interstices, and

Type Ib 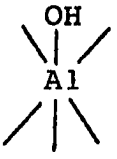

,

in which the OH group is coordinated to a single cation in an octahedral interstices.

Cirillo (334) has attempted to construct a model of alumina and molybdena-alumina surfaces on the basis of NMR and IR studies of catalyst dehydroxylations. Unfortunately, the data could not distinguish which types of hydroxyl groups are affected when molybdenum is supported on alumina as an epitaxial layer. To that end, ^{1}H CRAMPS (Chapter 3) measurements were planned to see if that technique could distinguish between some or all of the various types of hydroxyls, and if differences could be detected between aluminas and supported molybdena-aluminas.

A sample of γ-alumina (Ketchen CK-300) was prepared by A. Cirillo of W. Keith Hall's group at the University of Wisconsin, Milwaukee, by the following pretreatment: evacuation at room temperature for 30 minutes; evacuation

at 120° C for 2 hours; evacuation at 230° C for 2 hours; then the temperature was slowly raised to 550° C and the sample evacuated for 4 hours. Dry O_2 was flowed over the sample overnight to remove organic impurities and the catalyst was further evacuated at 500° C for 1 hour. The alumina was then exposed to dry H_2 at 500° C for 30 minutes and sealed under 100 ton of H_2 at 500° C.

Figure 53 shows the ^1H CRAMPS spectrum of this sample, where the MREV-8 pulse sequence was employed, with t_c = 36 μsec. The sample was contained in a rotor of the type shown in Figure 9. Approximately 10,000 scans were accumulated over a period of three days at a repetition rate of 20 seconds. The linewidth is seen to be extremely broad, ~20 ppm, possibly due to interactions with quadrupolar ^{27}Al. No evidence of more than one peak was observed.

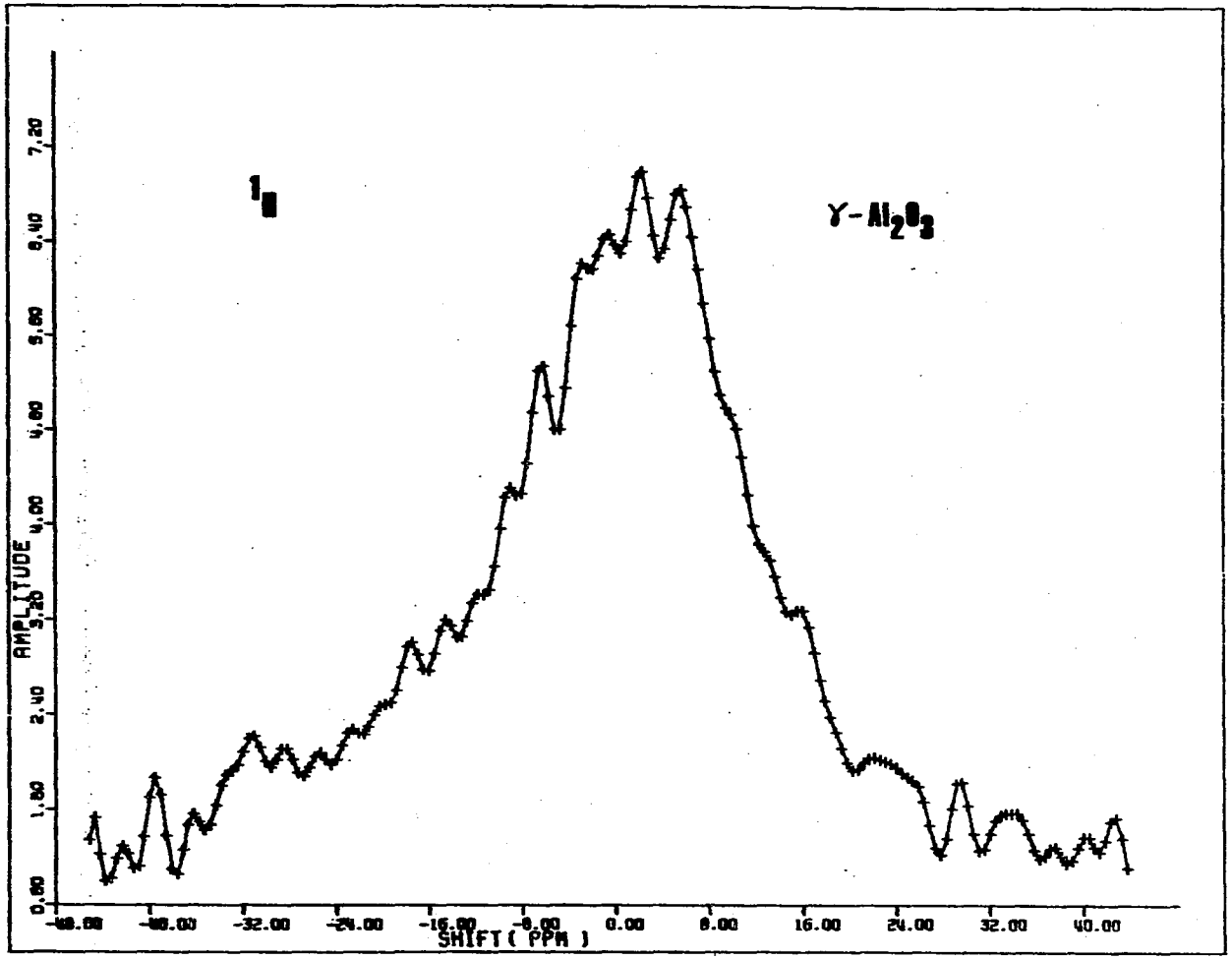

Figure 53. ^{1}H CRAMPS spectrum of hydrogen on γ-alumina

CHAPTER 6. VARIED MAGNETIC FIELD, MULTIPLE PULSE, AND MAGIC-ANGLE SPINNING PROTON NMR STUDY OF MUSCLE WATER

Introduction

Water constitutes a significant portion of all biological systems, and is important to their proper functioning (368). Thus, the state of water in biological substances has been the subject of much interest, and notably, the question of ordering of intercellular fluids has commanded much attention (369). NMR is one technique that has been used extensively in this area (370-372).

For example, in some systems in which biological macromolecules are oriented, such as collagen (373, 374), oriented DNA (375, 376), silk fibroin (375), and keratin (375, 377), dipolar splittings from H_2O ($\Delta\upsilon_H$) and quadrupolar splittings from D_2O ($\Delta\upsilon_D$) have been observed by NMR. These splittings indicate bound, ordered (or at least not isotropically mobile) water. On the other hand, the existence of dipolar or quadrupolar order for water in biological cells has not been unequivocally demonstrated.

An observation of orientation-dependent NMR patterns for water protons in nerve fiber was later attributed to the effect of demagnetization fields (378, 379). Recently, Fung (380) reported changes in the linewidths of both protons

and deuterons in muscle water as a function of the angle between the muscle fiber and the static magnetic field. However, the interpretation of the results as an indication of water orientation was also questioned (372), and it was suggested that the change in proton lineshape of muscle water may also be the result of anisotropy in the magnetic susceptibility of the sample.

In collagen (373, 374, 381), Li-DNA (376), and nonbiological materials such as clay (382) and rayon (383), $\Delta\upsilon_H/\Delta\upsilon_D \sim 0.3$. However, the observed linewidths for H_2O in nerve (378, 379) and muscle (380) are larger than those for D_2O. $\Delta\upsilon_H$ and $\Delta\upsilon_D$ in hydrated collagen decrease as the water content increases (374, 384-387). Native collagen contains about one gram of water per gram of dry protein. At this water content, the proton doublets overlap each other and are not resolvable (373). Skeletal muscle contains about 75% water, or three grams of water per gram of dry muscle. Since the water contents in muscle and nerve are much larger than in native collagen, it is surprising that their proton NMR peaks should show apparent splittings (378, 380). These comparisons seem to favor the interpretation that the multiple proton peaks in these cellular systems are due to dispersion of the demagnetization fields (372, 379), rather than true dipolar splittings. It has been suggested (372) that the argument can be settled by

examining the proton linewidth as a function of the strength of the external magnetic field, H_0 (since dispersion is directly field dependent, while dipolar splittings do not depend on the field (4)).

As has been noted throughout this thesis, homonuclear dipolar couplings in solid or partially ordered systems can be reduced or eliminated by sample spinning at the magic-angle, by using multiple pulse sequences, or by a combination of both. In this chapter, those techniques and a measurement of the variation of proton linewidth with H_0 have been used to investigate structural ordering of water in muscle. These studies were done in collaboration with Dr. Bing Fung of the University of Oklahoma.

Experimental Details

Muscles of frogs (Xenopus laevis) were used in this study. Immediately after a frog was killed, the tibialis muscle was excised from the leg and a striated piece was cut and aligned on a Teflon plug, which was then inserted into an upside down NMR sample tube. The sample was then placed in the magnetic field, and was rotated so that the axis of the muscle fibers could form specific angles with respect to H_0. A proton NMR study at $H_0 = 23,487$ gauss was made using a Varian XL-100 spectrometer operating in the continuous wave mode with an external ^{19}F lock.

Measurements of H_0 = 11,744, 5.872 and 2,936 gauss were made on a home-built pulse spectrometer with a Brucker high resolution (unshimmed) magnet at the University of Oklahoma. The total time required for studying each sample at four frequencies was 2 to 3 hours. Except at 23,487 gauss, the linewidth was defined as $\Delta\upsilon = 1/ T_2^*$, where T_2^* is the decay constant for the free induction decay. Since at exact resonance the FID signal is sensitive to small drifts of H_0 for a system without field-frequency lock, T_2^* was determined from the envelope of the FID when the frequency was set at 1 KHz off resonance. $\Delta\upsilon$ determined in this manner was probably not exactly the same as the half width of the Fourier transform of the FID. However, the error introduced was much smaller than uncertainties due to the variation of the sample shape and size, and the lack of perfect alignment. The values of $\Delta\upsilon$ reported are the average of two measurements for the same relative θ (0^o and 180^o, 30^o and 150^o, etc.). Multiple pulse and magic-angle spinning experiments were performed at Iowa State University on the spectrometer described in Chapter 3. Five mm (o.d.) oriented samples were used in the multiple pulse experiments, and unoriented samples were used for the magic-angle spinning experiments. The spin-spin relaxation time, T_2, was obtained by using the Carr-Purcell-Meiboom-Gill sequence (7).

Results

In a previous study of oriented frog muscle at H_0 = 23,487 gauss (380), the sample size was large, fitting a 12 mm o.d. tube. Considerable variations of proton linewidth and small changes in the peak center with the angle between the fiber axes and H_0 (θ) were observed (380). In the present work, samples of smaller size (fitting a 5 mm tube) were studied. The spectra differed somewhat from sample to sample, but the maximum linewidth $\Delta\upsilon$ (for $\theta = 0^{\circ}$) was generally smaller than that observed for the larger samples and there was less variation in $\Delta\upsilon$ with respect to θ. The spectra of one sample are shown in Figure 54. The maximum variation in the position of the peak is 1.2 ppm. The maximum variation in linewidth is 30 Hz. Changes in the center of the spectrum and linewidth with orientation also were observed in the proton spectra for a sample of liquid water which was placed in a rectangular container roughly 5 mm x 2 mm x 7 mm, constructed by shaping a 5 mm NMR tube. The results of this experiment are given in Figure 55, which shows the NMR spectra observed with the long side of the rectangular parallelpiped at angles of 0°, 55°, and 90° to the external field. The variation in the linewidth is 25 Hz.

To determine whether the line broadening of protons in muscle water is due only to dispersion of the demagneti-

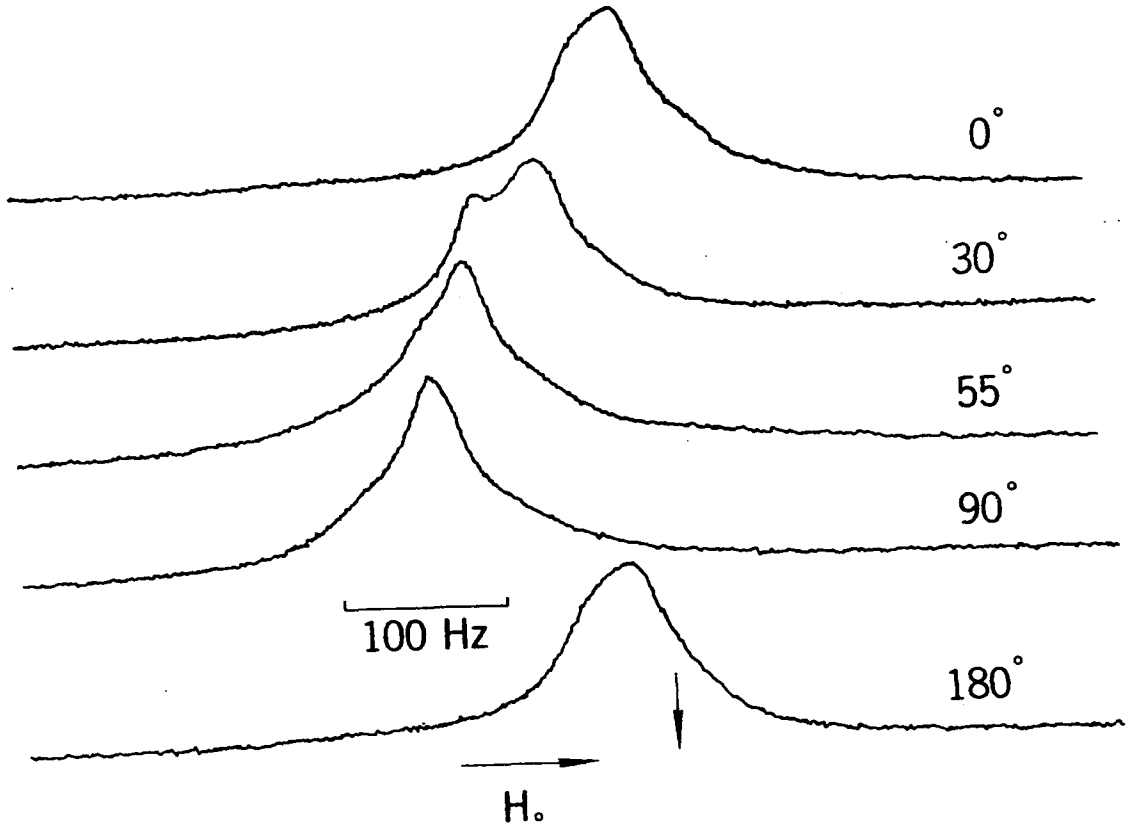

Figure 54. Proton NMR spectra of frog muscle oriented at different angles with respect to H_0. The sample was placed in a 5 mm (o.d.) tube and the spectra were taken at 100 MHz and 25 C. The arrow indicates the peak position for liquid water

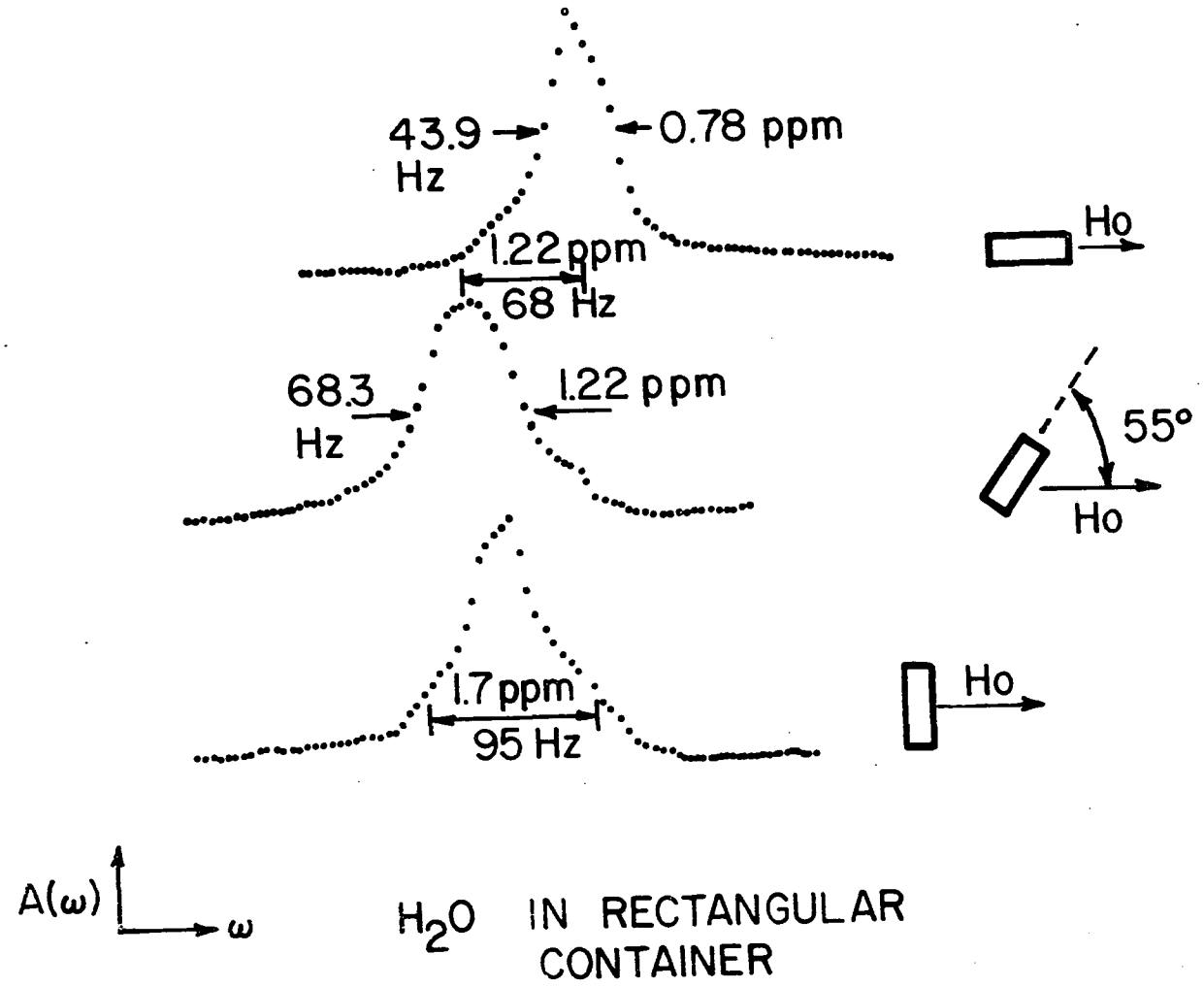

Figure 55. Lineshape of a rectangular water sample as a function of orientation to the static field. Note change in linewidth due to dispersion of demagnetization field, and the change in center of the spectrum due to change in average demagnetization field

zation, a study of the proton linewidth of muscle water was conducted as a function of magnetic field. The results for two samples at four different fields are given in Table XVIII.

In another set of experiments, the possible existence of dipolar broadening in the proton spectrum of muscle water was studied using the MREV-8 multiple pulse sequence (69-71). Under optimum conditions, the static homonuclear dipolar interaction is removed by this cycle to first order, and interactions involving H_0 (chemical shift, magnetic susceptibility, and H_0 inhomogeneity) are scaled by roughly $3/\sqrt{2}$ in the resulting spectrum (69-71). This scaling factor was indeed observed in comparing the Fourier transformed spectra of liquid water under a single pulse and for the MREV-8 sequence. The results for a muscle sample are given in Table XIX.

It is well-known (20) that dipolar interactions can be removed by sample spinning at the magic-angle, at a speed greater than the dipolar splitting (both expressed in hertz). Anisotropy in chemical shifts and in magnetic susceptibility will also be averaged to their respective isotropic values provided that the spinning rate is comparable to the anisotropy. The spectra in Figure 56 show the effect of magic-angle spinning on a sample of randomly oriented muscle. The linewidth was reduced from 128 to 23 Hz under magic-angle

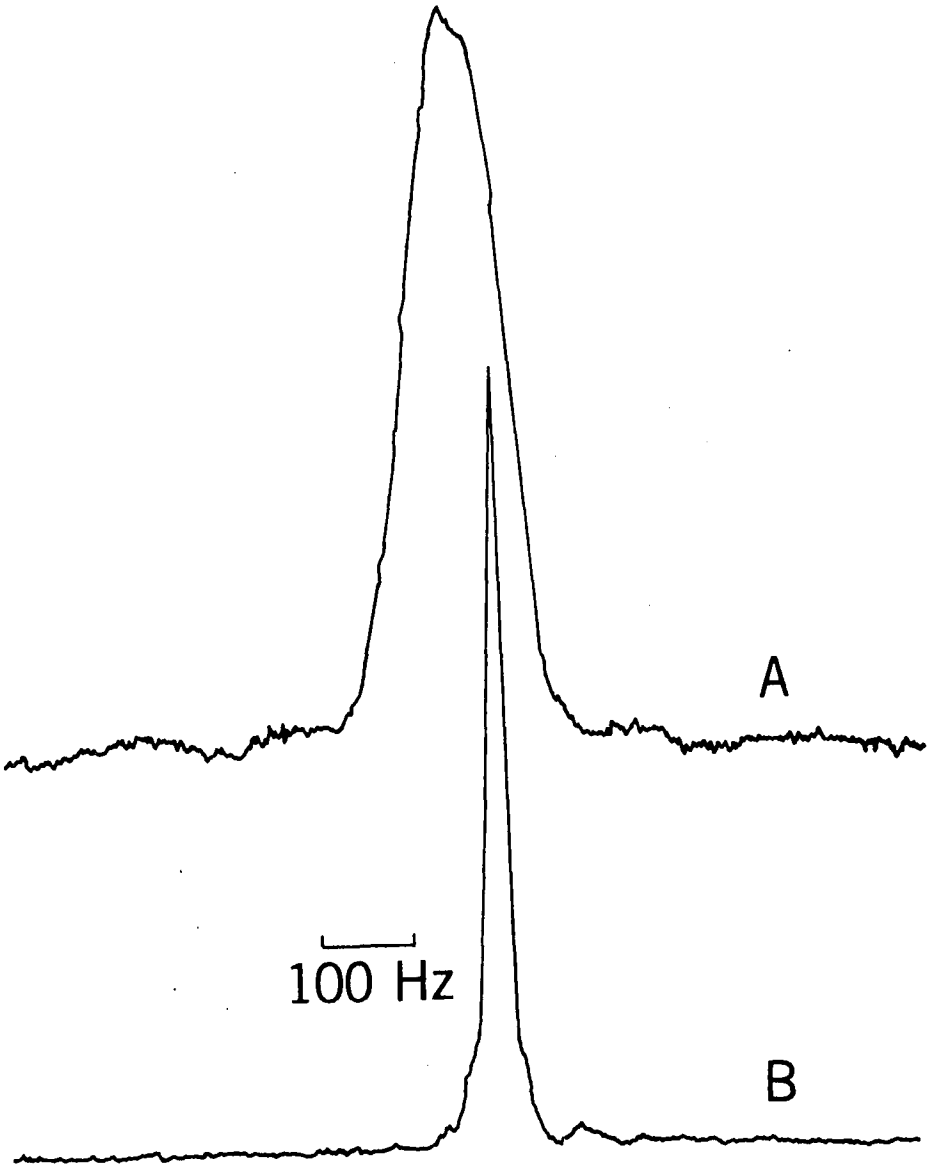

Figure 56. Proton NMR spectra of frog muscle at 56 MHz and 25° C. (A) Without spinning. (B) With magic angle spinning at a rate of 2 kHz

Table XVIII. Proton linewidth (Hz) of water at different values of H_0 at 25° C. The orientations of the muscle axes with respect to H_0 are shown

H_0, gauss	Muscle sample A				Muscle sample B				Liquid water, spherical
	0°	30°	55°	90°	0°	30°	55°	90°	
23,487	76	82	70	62	130	160	180	132	4
11,744	53	47	41	56	132	83	74	55	30
5,872	46	42	28	33	53	39	34	39	20
2,936	25	27	21	28	27	24	20	25	16

Table XIX. Proton line width (Hz) of a sample of muscle water at 56 MHz and 25° C

Orientation versus H_0	0°	30°	55°	90°
Single pulse linewidth $\Delta\nu_1$	100	97	90	83
REV-8 linewidth $\Delta\nu_2$	41	39	37	31
$\Delta\nu_1/\Delta\nu_2$	2.4	2.5	2.4	2.7

spinning. When the sample was spun at the same rate (2 KHz) about an exis perpendicular to H_0, the linewidth was reduced only by a factor of 2. A study of the spin-spin relaxation

time, T_2, with magic-angle spinning, was also made. For randomly oriented muscle sample, T_2 for the water protons at 56 MHz and 25° C was 35 ±3 μsec without spinning, and 43 ±4 μsec with magic-angle spinning. The corresponding results for another sample were 36 ±3 and 35 ±3 μsec, respectively.

Discussion

Spectra at high field

To discuss the results of the proton linewidth study, it is necessary to realize that the effective magnetic field at a given proton in a sample within an external field consists of a number of contributions

$$\vec{H}_{eff} = \vec{H}_0 + \vec{H}_{demag} + \vec{H}_{shielding} + \vec{H}_{dipolar} \qquad (63)$$

$\vec{H}_0$ is the external field of the magnet. $\vec{H}_{demag}$ is the demagnetization field associated with the surface geometry of the sample. $\vec{H}_{shielding}$ is the field associated with the currents induced in the local electronic environment by the external field, $\vec{H}_0$. $\vec{H}_{dipolar}$ is the field due to the through space interaction with all other nuclear magnetic moments in the sample.

In terms of the demagnetization factor, n, the volume susceptibility tensor, $\bar{\bar{\chi}}_v$, the shielding tensor, $\bar{\bar{\sigma}}$, the nuclear magnetogyric ratio, γ, and the internuclear vector,

r_{ik}, between the i^{th} moment and the k^{th} moment, the field at the i^{th} nucleus is given by

$$\vec{H}^{i}_{eff} = \vec{H}_0 \ (\bar{\bar{I}} - n\rho\bar{\bar{\chi}}_v - \bar{\bar{\sigma}}_i) \ - \sum_k [3\vec{r}_{ik}(\vec{\mu}_k \cdot \vec{r}_{ik})/r^5_{ik} - \vec{\mu}_k/r^3_{ik}] \quad (64)$$

For a sample with the appropriate geometry, e.g., an elipsoid of revolution, n is exactly calculable. For a needle with H_0 parallel to the needle axis, $n = 0$; for a needle with H_0 perpendicular to the needle axis, $n = 2$. A sample with nontractable boundary conditions, e.g., a cube, will have the effect of an external field inhomgeneity, and will result in a corresponding broadening of the NMR spectrum associated with dephasing of the transverse components of spin throughout the sample. For a particular sample geometry and orientation with respect to the external field, the dispersion of the demagnetization field within the sample may be calculated by, e.g., relaxation techniques applied to solutions of the appropriate Maxwell equations. Alternatively, in the absence of exact knowledge of the boundary conditions for the sample in question, one may choose to estimate this dispersion via an experiment on an appropriately chosen model system.

The experiment of the rectangular cell (Figure 55) shows the effect of sample geometry on the spectrum. In general, the average value of the demagnetization field determines the center of the spectrum and dispersion of the

field determines the lineshape and width. Muscle cells are elongated and highly anisotropic. By comparing the spectra in Figures 54 and 55, it is possible to conclude that the main contribution to the linewidth and the change in the peak position for muscle water is the demagnetization field. The larger linewidth and the splitting previously observed (380) were most likely due to the larger size of samples used.

Variation of linewidth with magnetic field

To determine whether there are other contributions to the proton linewidth of muscle water, we studied the linewidth at different magnetic field strengths (Table XVIII). If the line broadening is due to the dispersion of the demagnetization only, $\Delta\upsilon$ would be directly proportional to H_0 for each sample. The data in Table XVIII show that $\Delta\upsilon$ does decrease with the decrease of H_0, but the change in $\Delta\upsilon$ is somewhat less pronounced. It is interesting to note that, at the low values of H_0, $\Delta\upsilon$ was smallest for $\theta = 55^{\circ}$, at which point $(3\cos^2\theta - 1) \simeq 0$. This is difficult to explain by the effect of dispersion in the demagnetization field, because the factor $(3\cos^2\theta - 1)$ appears in the dipolar term, but not in the demagnetization term of the spin Hamiltonian (Equation 64). At this angle, the proton linewidth of muscle water approached that of a spherical sample of

liquid water of comparable size when H_0 was decreased to the lowest values. These facts suggest, that whereas the dispersion of demagnetization is the main factor of the increased proton linewidth and its variation with θ for muscle water, there may also be a small contribution to line broadening from nonzero static dipolar interactions. The data in Table XVIII indicate that the broadening for $\theta = 0^{o}$ would be of the order of only a few hertz. This is much smaller than that suggested by the apparent splitting pattern shown by Fung (380). Packer has suggested (388) that there is a small residual quadrupolar splitting of several hertz for a fraction of D_2O (~20%) in muscle. Since neither of these estimations is highly accurate, it is not clear if the ratio $\Delta\upsilon_H/\Delta\upsilon_D$ for muscle water is comparable to that in other oriented heterogeneous systems (373, 374, 376, 381-383).

Multiple pulse experiments

The possible existence of a small static dipolar interaction in muscle water is further demonstrated in the results of the eight-pulse experiment (Table XIX). If the line broadening of the proton signal of muscle water is due to dispersion of the demagnetization field only, the ratio $\Delta\upsilon$ for the signal obtained under the MREV-8 sequence and that for a single pulse experiment will be $3/\sqrt{2} = 2.12$, or less.

If the proton signal under a single pulse is further broadened by nonzero static dipolar interactions, which vanish under the MREV-8, this ratio will be larger than 2.12. The data in Table XIX show that the latter was indeed the case, indicating the existence of dipolar broadening in the single pulse linewidth. It is to be noted, that for a perfectly aligned sample there would be no dipolar broadening at $\theta = 54.7^{o}$ for both the single pulse and the MREV-8 results. The fact that the linewidth ratio is larger than 2.12 at this angle is probably due to a lack of perfect alignment for the muscle sample. Considering that the uncertainties in the linewidths shown in Table XIX are ~5%, the dipolar broadening for the single pulse data would be of the order of a few hertz, consistent with the results of the varied H_0 experiments.

Magic-angle spinning

The magic-angle spectrum (Figure 56) also demonstrates the large contribution of anisotropic magnetic susceptibility to the proton linewidth of muscle water at high fields. On the other hand, proton T_2 did not change substantially with magic-angle spinning at a rate of 2 KHz. This implies that the longest correlation time of the motion of part (or all) of the water molecules must be less than 8×10^{-5} μsec, but tells nothing about other details of the molecular motion.

In a previous study by Fung (380), it was suggested that a nonzero static dipolar interaction in muscle water may have a large contribution to $1/T_2$ of the protons. However, since we have demonstrated that the dipolar interaction for muscle water is very small, this contribution to $1/T_2$ would not be substantial. Other explanations of the large ratio of T_1/T_2 for protons in muscle water have been offered recently (389, 390).

Summary

In summary, we conclude that the proton NMR spectra of muscle water in high magnetic fields are determined mainly by demagnetization field anisotropy and dispersion. The varied magnetic field and multiple pulse experiments demonstrated that a small static dipolar interaction of the order of a few hertz may be present and would have a small contribution to the proton linewidth.

REFERENCES

1. "Annual Review of Physical Chemistry," Annual Reviews: Palo Alto, 1950-1980; Vols. 1-31.

2. Purcell, E. M.; Torrey, H. C.; Pound, R. V. Phys. Rev. 1946, 69, 37.

3. Bloch, F.; Hansen, W. W.; Packard, M. Phys. Rev. 1946, 69, 127.

4. Abragam, A. "The Principles of Nuclear Magnetism," Oxford University Press: London, 1961.

5. Emsley, J. W.; Feeney, J.; Sutcliffe, L. H. "High Resolution NMR Spectroscopy," Pergamon: Oxford, 1965; Vols. 1 and 2.

6. Slichter, C. P. "Principles of Magnetic Resonance," Springer: New York, 1978.

7. Farrar, T. C.; Becker, E. D. "Pulse and Fourier Transform NMR," Academic: New York, 1971.

8. Shaw, D. "Fourier Transform NMR Spectroscopy," Elserier: London, 1976.

9. "NMR and The Periodic Table," Harris, R. K.; Mann, B. E., Eds.; Academic: New York, 1978.

10. Wüthrich, K. "NMR in Biological Research: Peptides and Proteins," North Holland: Amsterdam, 1976.

11. Dwek, R. A.; Cambell, I. D.; Richards, R. E. "NMR in Biology," Academic: London, 1977.

12. "NMR Spectroscopy in Molecular Biology," Pullman, B., Ed.; Reidel: Dordrecht, 1978.

13. Levy, G. C.; Lichter, R. L.; Nelson, G. L. "Carbon-13 Nuclear Magnetic Resonance Spectroscopy," John Wiley and Sons: New York, 1980.

14. Wehrli, F. W.; Wirthin, T. "Interpretation of Carbon-13 NMR Spectra," Heyden: London, 1976.

15. Randall, J. C. "Polymer Sequence Determination, Carbon-13 NMR Method," Academic: New York, 1977.

16. "Carbon-13 NMR in Polymer Science," Pasika, W. M., Ed.; Amer. Chem. Soc.: Washington, D. C., 1979.

17. Haeberlen, U. "High Resolution NMR in Solids, Selective Averaging," Academic: New York, 1976.

18. Mehring, M. "High Resolution NMR Spectroscopy in Solids," Springer: Berlin, 1976.

19. Vaughan, R. W. In "Annual Review of Physical Chemistry," Annual Reviews: Palo Alto, 1978; Vol. 29, p. 397.

20. Andrew, E. R. In "Progress in Nuclear Magnetic Resonance Spectroscopy," Emsley, J. W.; Feeney, J.; Sutcliffe, L. H., Eds.; Pergamon: Oxford, 1971; Vol. 8.

21. Gerstein, B. C.; Pembleton, R. G.; Wilson, R. C.; Ryan, L. M. J. Chem. Phys. 1977, 66, 361.

22. Vanderhart, D. L.; Retcofsky, H. L. Fuel 1976, 55, 202.

23. Bartuska, V. J.; Maciel, G. E.; Schaefer, J.; Stejskal, E. O. Fuel 1977, 56, 354.

24. Retcofsky, H. L.; Vanderhart, D. L. Fuel 1978, 57, 421.

25. Wemmer, D. E.; Pines, A. Amer. Chem. Soc. Div. of Fuel Chem. Preprints 1978, 23, 15.

26. Maciel, G. E.; Bartuska, V. J.; Miknis, F. P. Fuel 1978, 57, 505.

27. Resing, H. A.; Garroway, A. N.; Hazlett, R. N. Fuel 1978, 57, 450.

28. Maciel, G. E.; Bartuska, V. J.; Miknis, F. P. Fuel 1979, 58, 155.

29. Maciel, G. E.; Bartuska, V. J.; Miknis, F. P. Fuel 1979, 58, 391.

30. Miknis, F. P.; Maciel, G. E.; Bartuska, V. J. Org. Geochem. 1979, 1, 169.

31. Retcofsky, H. L.; Link, T. A. "High Resolution ^{1}H-, ^{2}H-, and ^{13}C- NMR in Coal Research: Applications to Whole Coals, Soluble Fractions, and Liquifaction Products," In "Analytical Methods for Coal and Coal Products," Karr, C., Jr., Ed; Academic: New York, 1978; Vol. II, Chapter 24.

32. Murphy, P. D. Ph. D. Dissertation, Iowa State University, Ames, Iowa, 1979.

33. Bloch, F. Phys. Rev. 1946, 70, 460.

34. Bloch, F,; Hansen, W. W.; Packard, M. Phys. Rev. 1946, 70, 474.

35. Pake, G. E. J. Chem. Phys. 1948, 16, 327.

36. Van Vleck, J. H. Phys. Rev. 1948, 74, 1168.

37. Andrew, E. R.; Bradbury, A.; Eades, R. G. Nature 1958, 182, 1659.

38. Andrew, E. R.; Bradbury, A.; Eades, R. G. Nature 1959, 183, 1802.

39. Lowe, I. J. Phys. Rev. Letters 1959, 2, 285.

40. Andrew, E. R.; Farnell, L. F.; Firth, M.; Gledhill, T. D.; Roberts, I. J. Mag. Res. 1969, 1, 27.

41. Zilm, K. W.; Alderman, D. W.; Grant, D. W. J. Mag. Res. 1978, 30, 563.

42. Andrew, E. R.; Bradbury, A.; Eades, R. G. Arch. Sci. (Geneva) 1958, 11, 223.

43. Andrew, E. R. Arch. Sci. (Geneva) 1959, 12, 103.

44. Andrew, E. R.; Eades, R. G. Discuss. Faraday Soc. 1962, 34, 38.

45. Andrew, E. R.; Eades, R. G. Mol. Phys. 1968, 15, 157.

46. Andrew, E. R.; Wynn, V. T. Proc. Roy. Soc. 1966, 291A, 257.

47. Andrew, E. R.; Jasinski, A. J. Phys. C 1970, 4, 391.

48. Andrew, E. R.; Firth, M. Jasinski, A.; Randall, P. J. Phys. Letters 1970, 31A, 446.

49. Andrew, E. R.; Carolan, J. L.; Randall, P. J. Phys. Letters 1971, 35A, 435.

50. Andrew, E. R.; Carolan, J. L.; Randall, P. J. Phys. Letters 37A, 125.

51. Andrew, E. R.; Carolan, J. L.; Randall, P. J. Chem. Phys. Letters 1971, 11, 298.

52. Doskocilova, D.; Schneider, B. Chem. Phys. Letters 1970, 6, 381.

53. Doehler, H.; Schnabel, B. Ann. Phys. (Leipzig) 1970, 25, 383.

54. Schneider, H.; Pivcova, H.; Doskocilova, D. Macromolecules 1972, 5, 125.

55. Chapman, D.; Oldfield, E.; Doskocilova, D.; Schneider, B. F. E. B. S. Letters 1972, 25, 1972.

56. Doskocilova, D.; Schneider, B. Macromolecules 1973, 6, 9.

57. Moritz, P.; Schnabel, B. Plaste Kautschuk 1972, 19, 281.

58. Andrew, E. R.; Hinshaw, W. S.; Jasinski, A. Chem. Phys. Letters 1974, 24, 399.

59. Pivcova, H.; Doskocilova, D.; Veksli, Z.; Schneider, B. J. Mag. Res. 1974, 14, 182.

60. Schnabel, B. Wiss. Z. Friedrich-Schiller Univ. Jena, Math.-Nat. R. 1973, 22, 335.

61. Rabii, M. Compt. rend. 1973, 277B, 269.

62. Benoit, H.; Rabii, M. Chem. Phys. Letters 1973, 21, 466.

63. Andrew, E. R. Prog. in NMR Spectroscopy 1971, 8, 1.

64. Waugh, J. S.; Huber, L. M.; Haeberlen, U. Phys. Rev. Letters 1968, 20, 180.

65. Haeberlen, U.; Waugh, J. S. Phys. Rev. 1968, 175, 453.

66. Mansfield, P. Phys. Letters 1970, 32A, 415.

67. Haeberlen, U.; Ellett, J. D.; Waugh, J. S. J. Chem. Phys. 1971, 55, 53.

68. Kessemeir, H.; Rhim, W. K. Phys. Rev. 1972, B5, 761.

69. Rhim, W. K.; Elleman, D. D.; Vaughan, R. W. J. Chem. Phys. 1973, 58, 1772.

70. Rhim, W. K.; Elleman, D. D.; Vaughan, R. W. J. Chem. Phys. 1973, 59, 3740.

71. Mansfield, P. J. Phys. C. 1971, 4, 1444.

72. Burum, D. P.; Rhim, W. K. J. Chem. Phys. 1979, 70, 3553.

73. Burum, D. P.; Rhim, W. K. J. Mag. Res. 1979, 34, 241.

74. Burum, D. P.; Rhim, W. K. J. Chem. Phys. 1979, 71, 944.

75. Pines, A.; Gibby, M. G.; Waugh, J. S. Chem. Phys. Letters 1972, 15, 373.

76. Pines, A.; Gibby, M. G.; Waugh, J. S. J. Chem. Phys. 1972, 56, 1776.

77. Pines, A.; Gibby, M. G.; Waugh, J. S. J. Chem. Phys. 1973, 59, 569.

78. Grannell, P. K.; Mansfield, P.; Whittaker, M. A. B. Phys. Rev. 1973, 8B, 4149.

79. Evans, W. A. B.; Poweles, J. G. Proc. Phys. Soc. (London) 1967, 92, 1046.

80. Waugh, J. S.; Wang, C. H. Phys. Rev. 1967, 162, 209.

81. Waugh, J. S.; Huber, L. M. J. Chem. Phys. 1967, 47, 1862.

82. Evans, W. A. B. Ann. Phys. (N.Y.) 1968, 48, 72.

83. Waugh, J. S.; Wang, C. H.; Huber, L. M.; Vold, R. L. J. Chem. Phys. 1968, 48, 662.

84. Waugh, J. S.; Haeberlen, U. Phys. Rev. 1969, 185, 420.

85. Rhim, W. K.; Elleman, D. D.; Schreiber, L. B.; Vaughan, R. W. J. Chem. Phys. 1974, 60, 4595.

86. Gerstein, B. C.; Dybowski, C. R. "An Introduction to the Theory and Practice of Pulse Techniques in Nuclear Magnetic Resonance" (in preparation).

87. Magnus, W. Commun. Pure Appl. Math. 1954, 7, 649.

88. Pople, J. A.; Schneider, W. G.; Bernstein, H. J. "High Resolution Nuclear Magnetic Resonance," McGraw-Hill: New York, 1959.

89. Müller, L.; Kumar, A.; Baumann, T.; Ernst, R. R. Phys. Rev. Letters 1974, 32, 1402.

90. Vanderhart, D. L. J. Chem. Phys. 1976, 64, 830.

91. Hester, R. K.; Ackermen, J. L.; Cross, V. R.; Waugh, J. S. Phys. Rev. Letters 1975, 34, 993.

92. Stoll, M. E.; Vega, A. J.; Vaughan, R. W. J. Chem. Phys. 1976, 65, 4093.

93. Bloembergen, N.; Rowland, T. J. Phys. Rev. 1955, 97 1679.

94. Schaefer, J.; Stejskal, E. O.; Buchdahl, R. Macromolecules 1975, 98, 1031.

95. Schaefer, J.; Stejskal, E. O. J. Amer. Chem. Soc. 1976, 98, 1031.

96. Schaefer, J.; Stejskal, E. O.; Buchdahl, R. Macromolecules 1977, 10, 384.

97. Maricq, M.; Waugh, J. S.; MacDiarmid, A. G.; Shirakawa, H.; Heeger, A. J. J. Amer. Chem. Soc. 1978, 100, 7729.

98. Lyerla, J. L.; Fyfe, C. A.; Yannoni, C. S. J. Amer. Chem. Soc. 1979, 101, 1351.

99. Dybowski, C. R.; Vaughan, R. W. Macromolecules 1975, 8, 50.

100. Lau, K. F.; Vaughan, R. W.; Satterthwaite, C. B. Phys. Rev. 1977, 15B, 2449.

101. Ellett, J. D.; Gibby, M. G.; Haeberlen, U.; Huber, L. M.; Mehring, M.; Pines, A.; Waugh, J. S. Adv. Mag. Res. 1971, 5, 117.

102. Vaughan, R. W.; Elleman, D. D,; Stacey, L. M.; Rhim, W. K.; Lee, J. W. Rev. Sci. Instr. 1972, 43, 1356.

103. Adduci, D. J.; Gerstein, B. C. Rev. Sci. Instr. 1979, 50, 1403.

104. Adduci, D. J. M. S. Dissertation, Iowa State University, Ames, Iowa, 1979.

105. Gerstein, B. C.; Chow, C.; Pembleton, R. G.; Wilson, R. C. J. Phys. Chem. 1977, 81, 565.

106. Motorola Semiconductor Products, Inc., Box 20912, Phoenix, Az. 85036.

107. Pembleton, R. G.; Ryan, L. M.; Gerstein, B. C. Rev. Sci. Instr. 1977, 48, 1286.

108. Pembleton, R. G. Ph.D. Dissertation, Iowa State University, Ames, Iowa 1978.

109. "Radio Amateur's Handbook," The American Radio Relay League, Inc.: Newington, 1972; p. 49.

110. Beams, J. W. Rev. Sci. Instr. 1930, 1, 667.

111. Beams, J. W.; Pickels, E. G. Rev. Sci. Instr. 1935, 6, 299.

112. Beams, J. W. J. Appl. Phys. 1937, 8, 795.

113. Apiezon Products Limited.

114. Sample decomposes in air within several hours, private communication, A. Cirillo, U. Wisconsin, Milwaukee.

115. Murphy, P. D.; Gerstein, B. C. Iowa State University, 1978, Report IS 4620.

116. Lorentzian lineshapes were used in all computer fittings to CRAMPS spectra in Chapter 4. Gaussian fits were also made, but those were found in poor agreement with the experimental results.

117. Fleisher, E. B.; Sung, N.; Hawkinson, S. J. Chem. Phys. 1968, 72, 4311.

118. Vul, E. B. Soviet Phys. Crystallog. 1969, 13, 856.

119. ApSimon, J. W.; DeMarco, P. V.; Mathieson, D. W.; Saunders, L. S.; Whalley, W. B. Tetrahedron 1970, 26, 119.

120. ApSimon, J. W.; Beirbeck, H. Can. J. Chem. 1971, 49, 1328.

121. Jackman, L. M.; Steinhell, S. "Applications of Nuclear Magnetic Resonance Spectroscopy in Organic Chemistry," Pergammon: Oxford, 1969.

122. Anca, R.; Carrera, S. M.; Bianco, S. G. Acta Cryst. 1967, 23, 1010.

123. Wheatley, P. J. J. Chem. Soc. 1964, 6036.

124. Fung, B. M.; Ryan, L. M.; Gerstein, B. C. Biophys J. 1980, 29, 229.

125. Buckingham, A. D.; Malm, S. M. Mol. Phys. 1971, 22, 1127.

126. Vaughan, R. W.; Elleman, D. D.; Rhim, W. K.; Stacey, L. M. J. Chem. Phys. 1972, 57, 5383.

127. Taylor, R. E.; Pembleton, R. G.; Ryan, L. M.; Gerstein, B. C. J. Chem. Phys. 1979, 71, 4541.

128. Taylor, R. E. Ph.D. Dissertation, Iowa State University, Ames, Iowa 1980.

129. Gerstein, B. C.; Ryan, L. M.; Murphy, P. D. American Chemical Society, Division of Fuel Chemistry Preprints 1979, 24, 90.

130. Cirillo, A. C., Jr.; Ryan, L. M.; Gerstein, B. C.; Fripiat, J. J. J. Chem. Phys. 1980, 73, 3060.

131. Taylor, R. E.; Ryan, L. M.; Tindall, P.; Gerstein, B. C. "Protonic Species in $H_{1.7}MoO_3$," J. Chem. Phys. (accepted for publication).

132. Solomon, P. R., Advanced Fuels Research, Inc., private communication.

133. Davidson, R. M. "Molecular Structure of Coal," London, January 1980, International Energy Agency Coal Research Report ICTIS/TRO8.

134. Berkowitz, N. "An Introduction to Coal Technology," Academic: New York, 1979.

135. Epstein, S. S.; Bulon, I.; Koplon, J.; Small, M.; Mantel, N. Nature (London) 1964, 204,750.

136. Huberman, E.; Sachs, L. Proc. Natl. Acad. Sci. U.S.A. 1976, 73, 188.

137. Freudenthal, R. I.; Lutz, G. A.; Mitchell, R. I. "Carcinogenic Potential of Coal and Coal Conversion Products," Columbus, February 1975, Battelle Energy Program Report.

138. van Krevelen, D. W. "Coal." Elsevier: Amsterdam, 1961.

139. Given, P. Fuel 1960, 39, 147.

140. "Advances in Chemistry Series 55 - Coal Science," Gould, R. F., Ed.; Amer. Chem. Soc.: Washington D.C., 1966; Sections 1 and 2.

141. Simon, J. A.; Hopkins, G. E. "Geology of Coal," In "Elements of Practical Coal Mining," Casidy, S. M., Ed.; AIME, Inc.: Baltimore, 1973.

142. Parks, B. C. "Origin, Petrography, and Classification of Coal," In "Chemistry of Coal Utilization," Lowry, H. H., Ed.; John Wiley and Sons: New York, 1963; Supplementary Volume, Chapter 1.

143. Dryden, I. G. C. J. Inst. Fuel 1957, 30, 193.

144. Howard, H. C. "Pyrolytic Reactions of Coal," In "Chemistry of Coal Utilization," Lowry, H. H., Ed.; John Wiley and Sons; New York, 1963; Supplementary Volume, Chapter 9.

145. Solomon, P. R. "Relation Between Coal Structure and Thermal Decomposition Products," Fuel, submitted for publication.

146. Solomon, P. R. "The Evolution of Pollutants During the Rapid Devolatilization of Pulverized Coal," NSF Report NSF/RA-770442, NTIS # PB278496/AS.

147. Horn, O. Brennst. Chemie 1929, 10, 369.

148. Fuchs, W. Fuel 1930, 9, 581.

149. Howard, H. C. "Chemical Constitution of Coal: As Determined by Oxidation Reactions," In "Chemistry of Coal Utilization," Lowry, H. H., Ed.; John Wiley and Sons: New York, 1945; Chapter 9.

150. Weiler, J. F. "Chemical Constitution of Coal: As Determined by Halogenation Reactions," In "Chemistry of Coal Utilization," Lowry, H. H., Ed.; John Wiley and Sons: New York, 1945; Chapter 8.

151. Weiler, J. F. "Chemical Constitution of Coal: As Determined by Reduction Reactions," In "Chemistry of Coal Utilization," Lowry, H. H., Ed.; John Wiley and Sons: New York, 1945; Chapter 10.

152. Dryden, I. G. C. "Chemical Constitution and Reactions of Coal," In "Chemistry of Coal Utilization," Lowry, H. H., Ed.; John Wiley and Sons: New York, 1963; Supplementary Volume, Chapter 6.

153. Studier, M. H.; Hayatsu, R.; Winans, R. E. "Analysis of Organic Compounds Trapped in Coal, and Coal Oxidation Products," In "Analytical Methods for Coal and Coal Products," Karr, C., Jr., Ed.; Academic: New York, 1978; Volume II, Chapter 21.

154. Tschamler, H.; de Ruiter, E. "Physical Properties of Coals," In "Chemistry of Coal Utilization," Lowry, H. H., Ed.; John Wiley and Sons: New York, 1963; Supplementary Volume, Chapter 2.

155. "Spectrometry of Fuels," Friedel, R. A., Ed.; Plenum: New York, 1970.

156. Speight, J. G. Appl. Spect. Rev. 1971, 5, 211.

157. Retcofsky, H. L. "Applications of Spectrometry in Studies of Coal Structure," In "Scientific Problems of Coal Utilization," CONF-770509, Oak Ridge, Tn. 1978, U. S. D. O. E. TIC, p. 79.

158. Speight, J. G. "Assessment of Structures in Coal by Spectroscopic Techniques," In "Analytical Methods for Coal and Coal Products," Karr, C., Jr., Ed.; Academic: New York, 1978; Volume II, Chapter 22.

159. Friedel, R. A.; Queiser, J. A. Fuel 1959, 38, 369.

160. Chakrabartty, S. K.; Berkowitz, N. Fuel 1959, 38, 240.

161. Schulze, T. Ber. deut. chem. Ges. 1871, 4, 802.

162. Giraud, V. Bull. Soc. chim. 1894, 11, 389.

163. Dickson, G.; Easterfield, T. H. Proc. Chem. Soc. 1898.

164. Picet, A.; Bouvier, M. Ber. 1913, 46, 3342.

165. Dimroth, O.; Kerkovious, B. Ann. 1913, 399, 120.

166a. Fischer, F. Ges. Abhandl. Kenntnis. Kohle 1919, 4, 802.

166b. Fischer, F.; Schrader, H. Ges. Abhandl. Kenntnis. Kohle 1919, 4, 342.

166c. Fischer, F.; Schrader, H. Ges. Abhandl. Kenntnis. Kohle 1920, 5, 200.

166d. Fischer, F.; Schrader, H.; Treibs, W. Ges. Abhandl. Kenntnis. Kohle 1920, 5, 267.

166e. Fischer, F.; Schrader, H. Ges. Abhandl. Kenntnis. Kohle 1921, 6, 1.

167. Fischer, F. Ges. Abhandl. Kenntnis. Kohle 1924, 8, 371.

168. Bone, W. A.; Pearson, A. R.; Quarendon, R. Proc. Roy. Soc. (London) 1924, 105A, 608.

169. Bone, W. A.; Quarendon, R. Proc. Roy. Soc. (London) 1926, 110A, 537.

170. Bone, W. A.; Horton, L.; Ward, A. Proc. Roy. Soc. (London) 1930, 127A, 480.

171. Bone, W. A.; Tei, L. J. Proc. Roy. Soc. (London) 1934, 147A, 58.

172. Bone, W. A.; Parsons, L. G. B.; Sapiro, R. H.; Groocock, C. M. Proc. Roy. Soc. (London) 1935, 148A, 492.

173. Bone, W. A.; Bard, B. J. A. Proc. Roy. Soc. (London) 1937, 162A, 495.

174. Bone, W. A.; Himus, G. W. "Coal, Its Constitution and Uses," Longmans, Green, and Co.: London, 1936; Chapters X and XI.

175. Francis, W.; Wheeler, R. V. J. Chem. Soc. 1925, 127, 2236.

176. Fuchs, W.; Stengel, W. Ann. 1930, 478, 267.

177. Juettner, B.; Smith, R. C.; Howard, H. C. J. Amer. Chem. Soc. 1935, 57, 2322.

178. Juettner, B. J. Amer. Chem. Soc. 1937, 59, 208.

179. Juettner, B.; Smith, R. C.; Howard, H. C. J. Amer. Chem. Soc. 1937, 59, 236.

180. Juettner, B. J. Amer. Chem. Soc. 1937, 59, 1472.

181. Smith, R. C.; Tomarelli, R. C.; Howard, H. C. J. Amer. Chem. Soc. 1939, 61, 2398.

182. Ward, J. J.; Kirner, W. R.; Howard, H. C. J. Amer. Chem. Soc. 1945, 67, 246.

183. Kent, C. R. Fuel 1940, 19, 119.

184. Franke, N. W.; Kiebler, M. W. Chem. Ind. 1946, 58, 580.

185. Ward, S. G. J. Inst. Fuel 1947, 21, 80.

186. Amed, M.; Kinney, C. R. J. Amer. Chem. Soc. 1950, 72, 559.

187. Ruof, C. H.; Savich, T. R.; Howard, H. C. J. Amer. Chem. Soc. 1951, 73, 3873.

188. Roy, A. N.; Howard, H. C. J. Amer. Chem. Soc. 1952, 74, 3239.

189. Kinney, C. R.; Friedman, W. D. J. Amer. Chem. Soc. 1952, 74, 3239.

190. Franke, N. W.; Kiebler, M. W.; Ruof, C. H.; Savich, T. R.; Howard, H. C. Ind. Eng. Chem. 1952, 44, 2784.

191. Holly, E. D.; Montgomery, R. S. Fuel 1956, 35, 49.

192. Holly, E. D.; Montgomery, R. S.; Gohlke, R. S. Fuel 1956, 35, 56.

193. Holly, E. D.; Montgomery, R. S.; Gohlke, R. S. Fuel 1956, 35, 60.

194. Biggs, B. S. J. Amer. Chem. Soc. 1936, 58, 484.

195. Biggs, B. S.; Weiler, J. F. J. Amer. Chem. Soc. 1936, 58, 1020.

196. Biggs, B. S.; Weiler, J. F. J. Amer. Chem. Soc. 1937, 59, 369.

197. LeClaire, C. D. J. Amer. Chem. Soc. 1941, 63, 343.

198. Kreulen, D. J. W. "Elements of Coal Chemistry," Nijgh and Van Ditmar: Rotterdam, 1954.

199. Francis, W. "Coal, Its Formation and Composition," Edward Arnold: London, 1954.

200. Randall, R. B.; Benger, M.; Groocock, G. M. Proc. Roy. Soc. (London) 1938, 165A, 432.

201. Howard, H. C. Ind. Chem. Eng. 1952, 44, 1083.

202. Mahadevan, C. Ind. J. Phys. 1929, 4, 79.

203. Mahadevan, C. Fuel 1929, 8, 462.

204. Mahadevan, C. Ind. J. Phys. 1930, 5, 525.

205. Mahadevan, C. Fuel 1930, 9, 574.

206. Turner, H. G.; Anderson, H. V. Ind. Eng. Chem. 1931, 23, 811.

207. Turner, H. G.; Anderson, H. V. Fuel 1932, 11, 262.

208. Coriez, P. C. R. Acad. Sci., Paris 1934, 199, 410.

209. Schoon, T. Z. agnew. Chem. 1941, 77, 609.

210. Brusset, H.; Devaux, J.; Guinier, A. C. R. Acad. Sci., Paris 1943, 216, 152.

211. Blayden, H. E.; Gibson, J.; Riley, H. L. "Proc. Conf. Ultrafine Struct. Coals Cokes," BCURA: London, 1944; p. 176.

212. Riley, D. P. "Proc. Conf. Ultrafine Struct. Coals Cokes," BCURA: London, 1944; p. 232.

213. Brusset, H. C. R. Acad. Sci., Paris 1947, 224, 1426.

214. Nelson, J. B. Research (London) 1952, 5, 489.

215. Mitra, G. B. Acta Cryst. 1953, 6, 101.

216. Ergun, S.; Tiensuu, V. H. Nature 1959, 183, 1669.

217. Ergun, S.; Tiensuu, B. H. Fuel 1959, 38, 64.

218. Ergun, S.; Tiensuu, V. H. Acta Cryst. 1959, 12, 1050.

219. Hirsch, P. B. Proc. Roy. Soc. (London) 1954, 226A, 143.

220. Brown, J. K.; Hirsch, P. B. Nature 1955, 175, 229.

221. Hirsch, P. B. "Proceedings of Conference on Science in the Use of Coal," The Institute of Fuel: London, 1958; p. A29.

222. Ergun, S.; Menster, M.; O'Donnell, H. J. Science 1960, 132, 1314.

223. Menster, M.; O'Donnell, H. J.; Ergun, S. Proc. Conf. Carbon, 5th 1961, 2 493.

224. Menster, M.; O'Donnell, H. J.; Ergun, S. Fuel 1962, 41, 153.

225. McCartney, J. T.; Ergun, S. Nature 1965, 205, 962.

226. Warren, B. E. Phys. Rev. 1941, 59, 693.

227. Biscoe, J.; Warren, B. E. J. Appl. Phys. 1942, 13, 364.

228. Nelson, J. B. Fuel 1954, 32, 153.

229. Nelson, J. B. Fuel 1954, 32, 381.

230. Diamond, R. Acta Cryst. 1957, 10, 359.

231. Diamond, R. Acta Cryst. 1958, 11, 129.

232. Diamond, R. Ph.D. Thesis, University of Cambridge, England, 1956.

233. Wilson, A. J. C. Acta Cryst. 1949, 2, 245.

234. Brindley, G. W.; Mering, J. Acta Cryst. 1951, 4, 441.

235. Franklin, R. E. Acta Cryst. 1950, 3, 107.

236. Cartz, L.; Hirsch, P. B. Phil. Trans. R. Soc. (London) 1960, 252A, 557.

237. van Krevelen, D. W. Brennst. Chemie. 1952, 33, 260.

238. van Krevelen, D. W. Brennst. Chemie. 1953, 34, 167.

239. van Krevelen, D. W.; Chermin, H. A. G. Fuel 1954, 33, 79.

240. van Krevelen, D. W.; Chermin, H. A. G. Fuel 1954, 33, 338.

241. van Krevelen, D. W. Brennst. Chemie. 1954, 35, 289.

242. Vlugter, J. C.; Waterman, H. I.; van Westen, H. A. J. Inst. Petrol. Technologists 1932, 18, 375.

243. Vlugter, J. C.; Waterman, H. I.; van Westen, H. A. J. Inst. Petrol. Technologists 1935, 21, 661.

244. Vlugter, J. C.; Waterman, H. I.; van Westen, H. A. J. Inst. Petrol. Technologists 1935, 21, 701.

245. van Krevelen, D. W.; Schuyer, J. "Coal Science," Elsevier: Amsterdam, 1957.

246. van Krevelen, D. W. Brennst. Chemie. 1952, 33, 260.

247. Schuyer, J.; van Krevelen, D. W. Trans. Faraday Soc. 1953, 49, 1391.

248. van Krevelen, D. W.; Blom, L.; Chermin, H. A. G. Nature 1953, 171, 1075.

249. Schuyer, J.; van Krevelen, D. W. Fuel 1954, 33, 176.

250. Huntjens, F. J.; van Krevelen, D. W. Fuel 1954, 33, 88.

251. Schuyer, J.; van Krevelen, D. W. Fuel 1954, 33, 348.

252. Schuyer, J.; Dijkstra, H.; van Krevelen, D. W. Fuel 1954, 33, 409.

253. van Krevelen, D. W.; Chermin, H. A. G.; Schuyer, J. Fuel 1957, 36, 313.

254. van Krevelen, D. W. Fuel 1959, 38, 245.

255. van Krevelen, D. W.; Chermin, H. A. G.; Schuyer, J. Fuel 1959, 38, 483.

256. van Krevelen, D. W.; Bigot, J. A.; Fortuin, J. M. N. Fuel 1959, 38, 535.

257. van Krevelen, D. W.; Wolfs, P. M. J.; Waterman, H. I. Brennst. Chemie. 1959, 40, 371.

258. Dryden, I. G. C.; Griffith, M. Fuel 1953, 32, 199.

259. Dryden, I. G. C. Fuel 1953, 32, 82.

260. Dryden, I. G. C. Fuel 1953, 32, 394.

261. Dryden, I. G. C.; Griffith, M. Fuel 1955, 34, S36.

262. Leicester, J. J. Appl. Chem. (London) 1956, 6, 96.

263. Schuyer, J. Naturwissenschaften 1955, 42, 388.

264. Honda, H.; Ouchi, K. Fuel 1957, 36, 159.

265. Franklin, R. E. Trans. Faraday Soc. 1949, 45, 274.

266. Dulhunty, J. A.; Penrose, R. E. Fuel 1951, 30, 109.

267. Retcofsky, H. L. Appl. Spect. 1977, 31, 116.

268. Bartle, K. D.; Jones, D. W. "Nuclear Magnetic Resonance Spectroscopy," In "Analytical Methods for Coal and Coal Products," Karr, C. Jr., Ed.; Academic: New York, 1978; Volume II; Chapter 23.

269. Gerstein, B. C. "Fingerprinting Solid Coals Using Pulse and Multiple Pulse Nuclear Magnetic Resonance," In "Analytical Methods for Coal and Coal Products," Karr, C. Jr., Ed.; Academic: New York, 1978.

270. Solomon, P. R. American Chemical Society, Division of Fuel Chemistry Preprints 1979, 24, 185.

271. Friedel, R. A. Brennst. Chemie. 1963, 44, 27.

272. Brown, J. K. J. Chem. Soc. 1955, 744.

273. Roy, M. M. Fuel 1957, 36, 249.

274. Kojima, K.; Sakashita, K.; Yoshimo, T. Nippon Kagaku Zasshi 1956, 77, 1432.

275. Cannon, C. G. Nature 1953, 171, 308.

276. Osawa, Y; Sugimara, H.; Fujji, S. Nenryo Kyokaishi 1969, 48, 694.

277. Brown, J. K.; Ladner, W. R. Fuel 1960, 39, 87.

278. Newman, P. C.; Pratt, L.; Richards, R. E. Nature 1955, 175, 645.

279. Bell, C. M. M.; Richards, R. E.; Yorke, R. W. Brennst. Chemie. 1958, 39, 530.

280. Schmidt, J.; van Raayen, W.; van Krevelen, D. W. Fuel 1959, 38, 540.

281. Richards, R. E.; Yorke, R. W. J. Chem. Soc. 1960, 2489.

282. Tschamler, H.; deRuiter, E. Brennst. Chemie 1962, 43, 212.

283. Ladner, W. R.; Stacey, A. E. Fuel 1964, 13.

284. Cunningham, A. C.; Ladner, W. R.; Wheatley, R.; Wyss, W. F. Fuel 1966, 45, 61.

285. Brown, J. K.; Ladner, W. R.; Sheppard, N. Fuel 1960, 39, 79.

286. Retcofsky, H. L.; Schweighart, F. K.; Hough, M. Analytical Chem. 1977, 44, 585.

287. Tingey, G. L.; Morrey, J. R. "Coal Structure and Reactivity," Richland, Wa., December 1973, Battelle Pacific Northwest Labs Report TID-26637.

288. Mazumdar, B. K. Fuel 1972, 51, 284.

289. van Krevelen, D. W.; Wolfs, P. M. J.; Waterman, H. I. Brennst. Chemie 1959, 40, 371.

290. Heredy, L. A.; Kostyo, A. E.; Neuworth, M. B. "Studies on the Structure of Coals of Different Rank, Hydrogen Distribution of Depolymerization Products," In "Advances in Chemistry Series 55 - Coal Science," Gould, R. F., Ed.; Amer. Chem. Soc.: Washington, D.C., 1966; p.493.

291. Takeya, G.; Itoh, M.; Suzuki, A.; Yokoyama, S. J. Fuel Soc. (Japan) 1964, 43, 837.

292. Durie, R. A.; Shewchyk, Y.; Sternhell, S. Fuel 1966, 45, 99.

293. Dryden, I. G. C. Fuel 1962, 41, 55.

294. Huston, J. L.; Scott, R. G.; Studier, M. H. Fuel 1976, 55, 281.

295. Huston, J. L.; Scott, R. G.; Studier, M. H. Org. Mass Spect. 1976, 11, 383.

296. de Ruiter, E.; Leutner, R.; Tschamler, H. Fuel 1962, 41, 118.

297. Ergun, S. Fuel 1958, 37, 365.

298. Friedel, R. A. Nature 1957, 179, 1237.

299. Chakrabartty, S. K.; Kretschmer, H. O. Fuel 1974, 53, 132.

300. van Krevelen, D. W.; Groenewege, M. D.; Rietweld, B. Nature 1958, 181, 640.

301. de Ruiter, E.; Tschamler, H. Brennst. Chemie 1958, 39, 362.

302. Shannon, J. S. Fuel 1958, 37, 352.

303. de Ruiter, E.; Tschamler, H. Fuel 1962, 41, 491.

304. Ergun, S.; McCartney, J. T.; Walline, R. E. Nature 1960, 187, 1014.

305. Ergun, S.; McCartney, J. T.; Walline, R. E. Fuel 1961, 40, 109.

306. Mayo, F. R. Fuel 1975, 54, 274.

307. Ghosh, G.; Banerjee, A.; Mazumdar, B. K. Fuel 1975, 54, 294.

308. Landolt, R. G. Fuel 1975, 54, 299.

309. Hayatsu, R.; Scott, R. G.; Moore, L. P.; Studier, M. H. Nature 1975, 257, 378.

310. Hayatsu, R.; Scott, R. G.; Moore, L. P.; Studier, M. H. Nature 1976, 261. 77.

311. Retcofsky, H. L.; Friedel, R. A. Fuel 1976, 55, 363.

312. Mayo, F. R.; Huntington, J. G.; Kirshen, N. A. "Chemistry of Coal Liquifaction," In "Organic Chemistry of Coal," Larsen, J. W., Ed.; Amer. Chem. Soc.: Washington, D.C., 1978; p. 126.

313. Mayo, R. R.; Kirshen, N. A. Fuel 1978, 57, 405.

314. Mayo, F. R.; Kirshen, N. A. Fuel 1979, 58, 698.

315. Whitehurst, D. D. "A Primer on the Chemistry and Constitution of Coal," In "Organic Chemistry of Coal," Larsen, J. W., Ed.; American Chemistry Society: Washington, D.C., 1978; p. 1.

316. Farcasiu, M. American Chemical Society, Division of Fuel Chemistry Preprints 1979, 24, 121.

317. Analysis made by B. Bauchman, Ames Laboratory, U.S.D.O.E., Iowa State University.

318. Pembleton, R. G.; Wilson, R. C.; Gerstein, B. C. J. Chem. Phys. 1977, 66, 5133.

319. Fits to Gaussian lineshapes were also attempted, but were found to produce even poorer results.

320. Retcofsky, H. L.; Friedel, R. A. "Spectra of Coals and Coal Extracts: Proton Magnetic Resonance Spectra of Pyridine and Carbon Disulfide Extracts," In "Spectrometry of Fuels," Friedel, R. A., Ed.; Plenum: New York, 1970.

321. Silva-Crawford, M.; Murphy, P. D.; Gerstein, B. C. Fuel, submitted for publication.

322. It was assumed that α^2 CH_2 groups are negligible in coal, as was found to be the case by Brown et. al. (285).

323. Deno, N. C.; Greigger, B. A.; Stroud, S. G. Fuel 1978, 57, 455.

324. Deno, N. C.; Greigger, B. A.; Stroud, S. G. American Chemical Society, Division of Fuel Chemistry Preprints 1978, 23, 54.

325. Sample provided by Dr. P. R. Solomon, Advanced Fuels Research, Inc.

326. Orning, A. A.; Greifer, B. Fuel 1956, 35, 381.

327. Sharkey, A. G., Jr.; Schultz, J. L.; Friedel, R. A. Fuel, 1961, 40, 423.

328. Brown, J. K. Fuel 1959, 38. 55.

329. Vahrman, M. Nature 1961, 189, 136.

330. Anthony, D. B.; Howard, J. B.; Hottel, H. C.; Meissner, H. P. Fuel 1976, 55, 121.

331. Anthony, D. B.; Howard, J. B.; Hottel, H. C.; Meissner, H. P. Rev. Sci. Inst. 1974, 45, 992.

332. Wilson, D. M., private communication.

333. Thomas, C. L. "Catalytic Processes and Proven Catalysts," Academic: New York, 1970.

334. Cirillo, A. C., Jr. Ph.D. Dissertation, University of Wisconsin at Milwaukee, Milwaukee, Wisconsin, 1979.

335. Abdo, S.; LoJacano, M.; Clarkson, R. B.; Hall, W. K. J. Catal. 1975, 36, 330.

336. Massoth, F. E. Adv. Catal. 1978, 27, 265.

337. Knötzinger, B. M. W.; Ratnasamy, P. Catal. Rev. 1978, 17, 31.

338. Cirillo, A. C.; Fripiat, J. J. J. Physique 1978, 39, 247.

339. Sermon, P. A.; Bond, G. C. Trans. 1976, 72, 730.

340. Krüger, G. J. Z. Naturforsch 1969, 24, 560.

341. Gatineau, L.; Keravis, D., private communication.

342. Birtill, J. J.; Dickens, P. G. Mat. Res. Bull. 1978, 13, 311.

343. Tinet, D.; Canesson, P.; Estrade, H.; Fripiat, J. J. J. Phys. Chem. Solids, submitted for publication.

344. Porter, V. R.; White, W. B.; Roy, R. J. Solid State Chem. 1972, 4, 250.

345. Dickens, P. G.; Birtill, J. J.; Wright, C. J.; J. Solid State Chem., accepted for publication.

346. Tinet, D.; Fripiat, J. J.; J. Chimie Physique, accepted for publication.

347. Wispenneuclx, M.; Poncelet, G.; Fripiat, J. J.; in preparation.

348. Goodenough, J. B. "Metallic Oxides," In "Progress in Solid State Chemistry," Pergamon Press: New York, 1971; Volume 5.

349. Norberg, R. E. Phys. Rev. 1952, 86, 745.

350. This bronze was prepared using a hydrogen plasma created by an r. f. discharge.

351. Ryan, L.; Wilson, R. C.; Gerstein, B. C. Chem. Phys. Lett. 1977, 52, 341.

352. Ditchfield, R. J. Chem. Phys. 1976, 65, 3123.

353. Lau, K. F.; Vaughan, R. W. Chem. Phys. Lett. 1975, 33, 550.

354. Torrey, H. C. Phys. Rev. 1954, 96, 690.

355. Resing, H. A.,; Torrey, H. C. Phys. Rev. 1963, 131, 1102.

356. Carr, H. Y.; Purcell, E. M. Phys. Rev. 1954, 94, 630.

357. Cirillo, A. C., Jr., Ph.D. Dissertation, University of Wisconsin at Milwaukee, Milwaukee, Wisconsin, 1979.

358. Taylor, R.; Silva-Crawford, M.; Gerstein, B. C. Second International Conference on Magnetic Resonance in Colloid and Interface Science, Menton, France. July 1979.

359. Thompson, R. J.; Kuispel, R. R.; Petch, H. E. Can. J. Phys. 1974, 52, 2164.

360. Knözinger, H. Adv. Catal. 1976, 25, 184.

361. Knözinger, H.; Ratnasamy, P. Catal. Rev. - Sci. Eng. 1978, 17, 31.

362. Peri, J. B.; Hannan, R. B. J. Phys. Chem. 1960, 64, 1526.

363. Peri, J. B. J. Phys. Chem. 1965, 69, 220.

364. Boehm, H. P. Adv. Catal. 1966, 16, 179.

365. Massoth, F. E. Adv. Catal. 1978, 27, 265.

366. Dabrowski, J. R.; Butt, J. B.; Bliss, H. J. Catal. 1970, 18, 297.

367. Zamora, M.; Cordoba, A. J. Phys. Chem. 1978, 82, 584.

368. Karlson, P. "Introduction to Modern Biochemistry," Academic: New York, 1968; Chapter XXI.

369. "Physiochemical State of Ions and Water in Living Tissues, and Model Systems," In "Annals of the New York Academy of Sciences," Hazelwood, C. F., Ed.; The New York Academy of Sciences: New York, 1973; Vol. 204.

370. Edzes, H. T.; Berendsen, H. J. C. Ann. Rev. Biophys. Bioeng. 1975, 4, 265.

371. "Magnetic Resonance in Colloid and Interface Science, A. C. S. Symposium, No. 34," Resing, H. A.; Wade, C. G., Eds.; American Chemical Society: Washington, D.C., 1976.

372. Shporer, M.; Civan, M. M. "The State of Water and Alkalai Cations Within the Intercellular Fluids: The Contribution of NMR Spectroscopy," In "Current Topics in Membranes and Transport," Bronner, F.; Kleinzeller, A., Eds.; Academic Press: New York, 1977; Vol. 9.

373. Berendsen, H. J. C. J. Chem. Phys. 1962, 35, 3297.

374. Migchelson, C.; Berendsen, H. J. C. "Deuteron Magnetic Resonance on Hydrated Collagen," In "Magnetic Resonance and Relaxation," Blinc, R., Ed.; North-Holland: Amsterdam, 1967; p. 761.

375. Berendsen, H. J. C.; Migchelson, C. "Hydrated Structures of Fibrous Macromolecules," In "Annals of the New York Academy of Sciences," Whipple, H. E., Ed.; The New York Academy of Sciences: New York, 1965; Vol. 125, No. 2.

376. Migchelson, C.; Berendsen, H. J. C.; Rupprecht, A. J. Mol. Biol. 1968, 37, 365.

377. Lynch, L. J.; Haly, A. R. Kolloid Z. Z. Polym. 1970, 239, 581.

378. Chapman, G. E.; McLauchlan, K. A. Nature (London) 1967, 215, 391.

379. Klein, M. P.; Phelps, D. E. Nature (London) 1969, 224, 70.

380. Fung, B. M. Science 1975, 190, 800.

381. Chapman, G. E.; McLauchlan, K. A. Proc. Roy. Soc. Lond. Biol. Sci. B 1969, 173, 223.

382. Woessner, D. E.; Snowden, B. S. J. Chem. Phys. 1969, 50, 1516.

383. Dehl, R. E. J. Chem. Phys. 1968, 48, 831.

384. Chapman, G. E.; Danyluk, S. S.; McLauchlan, K. A. Proc. Roy. Soc. (London) 1969, 178B, 465.

385. Dehl, R. E. Science 1970, 170, 738.

386. Fung, B. M.; Siegel, M. M. Biochim. Biophys. Acta. 1972, 278, 185.

387. Migchelson, C.; Berendsen, H. J. C. J. Chem. Phys. 1973, 59, 296.

388. Packer, K. J. Philos. Trans. Roy. Soc. London Biol. Sci. B 1977, 278, 59.

389. Civan, M. M.; Achlama, A. M.; Shporer, M. Biophys. J. 1978, 21, 127.

390. Fung, B. M.; McGaughy, T. W. Biophys. J. 1979, 28, 293.

ACKNOWLEDGEMENTS

I would first like to thank Dr. B. C. Gerstein for his enthusiastic guidance and friendship during my years as a graduate student.

There are many who contributed aid and advice in regards to this work. Besides Dr. Gerstein, among them are: Robert Taylor, Armin Paff, Bob Pembleton, Paul Murphy, and Peter Cheung. Their support is gratefully acknowledged.

Chuck Fry provided unparalleled leg-work and Sue Manley and Sue Musselman exceptional long-distance help in the nuts-and-bolts organization of this thesis after I had left Ames.

Finally, I wish to express my deep appreciation to Lynn for her support and forbearance.